The Pennsylvania State University

The Graduate School

College of Engineering

ON THE NATURE, REMEDIATION, AND QUANTIFICATION OF RADIUM IN HYDRAULIC FRACTURING CO-PRODUCTS

A Dissertation in

Environmental Engineering

by

Moses A. Ajemigbitse

Submitted in Partial Fulfilment

of the Requirements

for the Degree of

Doctor of Philosophy

August 2019

The dissertation of Moses A. Ajemigbitse was reviewed and approved* by the following:

Fred S. Cannon
Professor of Civil and Environmental Engineering
Dissertation Co-Advisor
Co-Chair of Committee

Nathaniel R. Warner
Assistant Professor of Civil and Environmental Engineering
Dissertation Co-Advisor
Co-Chair of Committee

Sridhar Komarneni
Distinguished Professor of Clay Mineralogy

Li Li
Associate Professor of Civil and Environmental Engineering

Patrick J. Fox
John A. and Harriette K. Shaw Professor
Chair of the Graduate Program

*Signatures are on file in the Graduate School

Abstract

Since its discovery by Marie and Pierre Curie in 1898, radium enjoyed a notorious celebrity throughout the 19th and 20th century. In the natural environment, radium is confined to exist in Uranium and Thorium bearing ores, deep within the earth' s crust. The practice of hydraulic fracturing for natural gas production provides a pathway for surface release from subsurface geologic reservoirs via liquid and solid co-products. The extensive application of this technology has led to large volumes of radium-bearing fluids and solid material, requiring specialized handling and management. In this work, the nature, remediation, and quantification of radium inthese co-products are considered.

In the first part of this dissertation, I address the distribution of radium in the solid and liquid co-products and speculate on novel treatment techniques that address the management of these radium-bearing materials with the goal of environmental sustainability. For the solid material, I evaluate a novel hydroacoustic cavitation system for separating the particle sizes and its effect on radium distribution. This hydroacoustic cavitation system enables the reclamation of marketable sand from the residual solid wastes worth $50,000 - $70,000/year, when sold at a fraction of the price of freshly mined silica sand. This reclaimed sand, along with reclaimable clay, could reduce waste volumes by 50%, which represents a yearly savings of $200,000 for facilities handling ~5,000 tons/year of residual solid waste. Additionally, treatment by hydroacoustic cavitation results in radium being concentrated in the finest particle sizes, presenting a new option for radioactivity management. Reclamation could result in the reduction of radioactivity disposed in landfills, mitigating the risk of radioactive exposure and contamination.

For the liquid material, I investigate the novel application of a synthetic clay with high Ra selectivity and high charge for radium removal. This synthetic clay, Na-4-mica, presents itself as an ideal candidate for radium removal as its interlayer can collapse upon complete substitution, hence sequestering radium and mitigating

release and environmental exposure. Na-4-mica can remove radium at every pH, and at high salinities, however, Ba, presents a significant competition for adsorption sites. Radium removal from real produced water samples by Na-4-mica requires pre-treatment to reduce the exchange competition of Ca, Mg, and Sr as their activities in the high total dissolved solids concentrations of produced waters overwhelm Ra's.

The second part of this dissertation addresses the quantification of radium in these co-products. More specifically, the nature of the radium-bearing media is considered. In the case of the solid materials, I probe the effect of sample density and volume on radium measurements; and with regard to the liquids, I probe the effect of the high salinity environment on radium measurements by gamma spectroscopy. I then suggest empirical methods to increase the accuracy of these measurements. Radium measurements of the solids can be inaccurate by up to ~50% when sample density and volume are ignored. The total dissolved solids concentrations of the liquids, as well as its composition, greatly influences radium measurements, and radium activities can be underestimated by up to 40% when they are not taken into account. Rapid and accurate measurements of radium in the solids and liquids can be achieved by performing direct analysis of radium at 186 keV following interference correction and by accounting for sample density and volume – in the case of the solids, or total dissolved solids concentration and composition – in the case of the liquids.

Finally, I describe a novel approach to rapid measurement performed by liquid scintillation counting by applying alpha/beta discrimination and spectrum deconvolution. This method utilizes a simple evaporative and acid-dissolution sample preparation protocol that is effective at removing the spectra interference of radium's daughters when combined with alpha/beta discrimination. The radium recovery of this sample preparation protocol is >90%. This novel method produces radium measurements with an R^2 of 0.92 when compared to high-accuracy gamma spectroscopy. The reduced sample preparation steps, low cost, and rapid analysis (four hour evaporation and one hour counting time) present this as a method ideal for rapid field appraisal prior to comprehensive radiochemical analysis.

Contents

List of Figures

List of Tables

Acknowledgements

Part of the journey is the end. And as my journey draws its conclusion, I am wont to reflect on the path that has led to my success. I am indebted to Dr. Fred Cannon, who was instrumental for the beginning of my journey. Without his belief in and commitment to me, I certainly could not have accomplished all that I have. Thank you for many hours of friendly conversation, for sharing your insight and wisdom, and for faithfully equipping me to be a responsible scientist. I am also indebted to Dr. Nathaniel Warner, for his role in getting me to the end. Thank you for adopting me into your research group and for teaching me all that I know about radium and gamma spectroscopy. It would not be an understatement to say that I couldn't have done this without the support of both of you. I am deeply grateful for your understanding and unwavering support, especially following the birth of my son.

I appreciate Dr. Sridhar Komarnmeni and Dr. Li Li for serving as members of my committee. Thank you, Dr. Komarneni, for introducing me to the world of clay science and Na-4-mica. Thank you, Dr. Li Li, for sharing your reactive transport modelling expertise with me. I am deeply grateful for your time and efforts.

Much of the work contained in this dissertation would not be completed without the assistance of several people. I would like to acknowledge Dr. Thomas Geeza and Shang Liu, for their help in running the hydroacoustic cavitation circuit; Dr. Mark Klima, for providing the lab space where the sample analyses occurred; Dr. Travis Tasker, for his help providing the produced water samples that were crucial to several chapters in this work; and Dr. Young Dong Noh for showing we how to

synthesize Na-4-mica. Several undergraduate students assisted me in the lab – Mitchell Ernest, Mohamed Almaimani, Olukorede Esan, Rafael Terreri, Huan Yi Low, Nicole Rella, and Austin Porter – thank you all.

I am also grateful to the people who became close friends and companions. The many wonderful students of Environmental Engineering – Carlos, Diana, Bonnie, Ben, Audrey, Alicia and other Sackett friends; the African students of PAN-APA; my church family of Unity Church of Jesus Christ; Dr. John Regan and the Saturday morning street hockey crew; and Josh Kerr.

I have been able to come so far because of the incredible support of my parents and sisters. Thank you, Rev. George and Dr. Adetutu, for teaching me the value of hard work, and for sacrificing yourselves for my education. Thank you, Misan, Alero and Jubilee, for supporting me in your own ways all through the years.

I reserve my final words for my darling wife, Ashley Rae. I am ever so grateful to have you in my life. Thank you for being my rock, a dutiful wife and wonderful mother.

All glory belongs to God my creator, Jesus my friend, and the Holy Spirit my companion.

This work was funded by a Fellowship from the Pennsylvania State University's College of Engineering and by the U.S. National Science Foundation Division of Industrial Innovation and Partnerships (PFI: AIR-TT #1640634). Any opinions, findings, and conclusions or recommendations expressed in this work are those of the author and do not necessarily reflect the views of the Pennsylvania State University or the U.S. National Science Foundation.

Moses A. Ajemigbitse

2019

"I must confess that I have in the course of this research made myself more and more familiar with this thought, and venture to put the opinion forward, while I am quite conscious that the hypothesis advanced still requires a more solid foundation."

> Wilhelm Konrad Röntgen on his ground-breaking discovery of X-rays in *On a New Kind of Rays, 1896*.

This dissertation is dedicated to my son, Malachi, whose birth hastened its timely completion.

Chapter 1

Introduction

Pitchblende Ore. Radium was discovered and isolated from Pitchblende, a Uranium rich ore, by Marie and Pierre Curie in December 1898.

1.1 Radioactivity and Radium †

The atom as the building block of all matter and life enraptured the minds of the great thinkers since before the discovery and study of nuclear radiation in the late 19th and early 20th century. From the alchemists of the middle ages, to the Greek philosophers, and eventually the early scientists, the existence of ultimate smallness has been hotly debated. The history of radioactivity is linked to the history of modern science and the development of our understanding of smallness and the structure of the atom.

Following the discovery of cathode rays in 1869, Wilhelm Röntgen began probing the nature of these rays. In November of 1895, Röntgen discovered a new form of radiation, which he coined "*x*-rays" , denoting their mysterious, unknown origins [13]. Henri Becquerel began his study on the nature of this new radiation, believing it to be a property of luminescent materials. He hypothesized that *x*-rays were released by phosphorescent bodies. While working with potassium-uranyl sulfate, he discovered that the sulfate salt affected a photographic plate, though it had been kept in the dark away from the sun. This unexpected discovery suggested that the potassium-uranyl sulfate emitted spontaneous radiation. He later concluded that this radiation could be attributed to neither *x*-rays nor phosphorescence, as it did not require an external energy source such as the sun, but it was in fact produced by the emitting body; and this new radiation persisted longer than any phosphorescence previously observed. His further study on this phenomenon

† The historical information in this section has been gathered from several magazine articles, essays and reports cited as References [1 - 12]. In order to minimize the occurrence of citation numbers, direct references have been omitted, except in cases where supplemental references were available.

led him to realize that uranium was responsible for this new radiation, earning them the name "uranic rays". However, in 1897, Henri Becquerel concluded his study of uranic rays.

Around the same time, a young PhD student named Marie Curie was in the search of a dissertation topic. Upon learning about uranic rays, Marie Curie was fascinated by this and chose this new radiation as her PhD inquiry. Using an electrometer (an early ionization chamber) that was designed by her husband Pierre, Marie could study the phenomenon of uranic rays in more quantitative measures than Becquerel could – Becquerel used photographic plates so his work was qualitative. Marie identified other substances that could emit these Becquerel rays (so named since uranium was not the only element to emit them) by studying their effect on the electrical conductivity of air. This led her to discover that Thorium also emitted Becquerel rays. Using her quantitative approach, Marie was able to determine that Pitchblende, an ore of Uranium, emitted more radiation than could be attributed to its uranium content. She hypothesized that there must be another element, or elements, more active in emitting this radiation than uranium. Marie and Pierre began searching for these elements. In July, and later in December, of 1898, they discovered two new elements, Polonium and Radium. In presenting their findings, they coined the word "*radioactive*" to describe this incredible phenomena whereby substances spontaneously produce radiation without external stimuli. Marie and Pierre later discovered that the intensity of the radiation was a function of the amount of matter present, and not a function of its state or mineral composition, establishing the atom as the origin of radiation.

Just as a young scientist in Marie Curie had built on the foundation laid by Henri Becquerel, another young scientist would build on her work. In 1899 Ernest

Rutherford investigated the penetrating power of uranium radiation by using aluminum sheets of increasing thickness. Through this research, Rutherford discovered that uranium radiation consisted of multiple types of radiation, as evidenced by his findings where the uranic rays were greatly reduced by a few sheets of aluminum, but then levelled off after multiple sheets [14]. This laid the foundation for the discovery of alpha and beta radiation. Further investigations, using magnetic fields, led to the discovery that the alpha rays were heavy, positively charged particles, while the beta rays were lighter, negatively charged particles. Paul Villard, in 1900, identified yet a third radiation, which became known as gamma rays. The nature of these radiation would later be identified to be the helium nuclei (alpha), electrons (beta), and high energy photons (gamma).

Up till this point, the scientific community believed the atom to be unchanging and indivisible. However, Rutherford and Soddy would oversee a paradigm shift with their conclusion that the emission of radiation should result in the natural transmutation of the element through radioactive decay. In 1902, they introduced the concept of the radioactive series – the idea that a radioactive element transforms into another radioactive element, which itself decays to yet another radioactive element, as so on until a stable element is formed. This discovery would lead to the law of radioactive decay:

$$N = N_0 e^{-\lambda t} \tag{1.1}$$

Where N is the number of radioactive atoms present at time t; N_0 is the # of atoms present at $t = 0$; and λ is the probability for any particular atom to decay per unit time.

The discovery of radiation allowed scientists to probe the structure of the atom. Rutherford's famous gold foil experiment in 1911 (in conjunction with Geiger and Marsden) and its surprising finding, wherein a beam of alpha particles passed through the gold mostly unaffected, led to the realization that the atom was mostly empty space. After observing the scattering pattern of the alpha particles, Rutherford concluded that the center of the atom was positively charged; and he mathematically approximated it to have a radius that was orders of magnitude smaller than the known size of the atom, 10^{-14} m compared to 10^{-10} m. He then coined the term nucleus to describe the dense, positively charged center of the atom. Further work by Rutherford and his team led to the discovery of the proton in 1920, and in 1932, Chadwick discovered the neutron. These discoveries, with the discovery of isotopes in 1913 by Soddy [15], established our modern understanding of the atomic structure.

Today, we now know that radiation occurs because of an imbalance in the number of protons and neutrons, leading to an unstable nucleus where electrostatic repulsion overcomes the strong nuclear force. We also know that radiation results in the release of energy, from the conversion of mass as predicted by Einstein's special theory of relativity.

Alpha radiation being the release of a helium atom results in the loss of two protons and two neutrons from the nucleus of the emitting atom. The alpha particle being of relative high atomic mass, and of high kinetic energy, interacts strongly with matter (through ionization) over very short distances. In this manner, alpha particles are highly damaging to the local environment in which they are emitted. It is therefore relatively easy to terminate alpha radiation, a thin piece of paper is sufficient. This property of alpha radiation renders it most dangerous to living

tissue when the source of alpha radiation is ingested, as the alpha particles dissipate high energy in the short distances they travel in the surrounding tissue. Beta decay involves a neutron being transformed into a proton and an electron. The electron is emitted from the nucleus, resulting in the new element with one more proton. The radiated electron, being relatively lightweight, interacts with matter to a less degree (also through ionization), thereby penetrating further than alpha radiation. Whenever the emission of an alpha or beta particle results in an excited nucleus (i.e. one in which the protons or neutrons are above the ground state) a gamma ray is also emitted. Gamma rays are short wavelength, high energy photons (and are a form of electromagnetic radiation) that interact very sparsely with matter and thus penetrate much farther than beta radiation. Gamma radiation, being electromagnetic in nature, reacts with matter through three processes namely: the Photoelectric Effect, the Compton Effect, and Pair Production. These process involve the absorption of the gamma ray energy by an electron in the affected atom. This adsorption can be complete (photoelectric and pair production), or partial (Compton Effect). These processes cause the intensity of the gamma radiation to decrease with penetration depth, and is found to be directly proportional to the depth. This is now well understood as the attenuation of gamma rays by matter [16–18].

With the basis of nuclear radiation introduced, we can now focus our attention on a most important element, radium. After its discovery and isolation by Marie Curie and her colleagues, radium was thrust into the spotlight, quickly gaining a cult following with many uses, ranging from the truly groundbreaking – as in early cancer treatment – to the fantastical – radium charged water as the fountain of youth [4]. However, it soon became clear that exposure to radium was not without consequence. Marie would later pass way in 1934 from pernicious anemia, which

she most certainly developed following prolonged exposure to radium and radiation. Nevertheless, our understanding of nuclear radiation allows us to continue to reap the benefits of radiation without the deadly consequences, when applied in an altruistic manner. Modern applications of radium are limited to use by the medical practitioner and the scientific inquirer.

Radium, Ra, is an alkaline earth metal with thermochemical properties similar to those of barium, exhibits one aqueous oxidation state (+2), and is not easily complexed [19]. Radium forms soluble chloride, bromide and nitrate salts, while its sulfate, carbonate and phosphate salts are insoluble. Radium co-precipitates easily with barium salts [19]. The low hydration energy, and thus low hydrated radius, of radium result in high selectivity for ion exchange processes [9]. Radium is not vital to living organisms, and its radioactivity, primarily its alpha decay, creates adverse health effects when incorporated into biochemical processes [19].

While there are several isotopes of radium, two are of relevance to this work: ^{226}Ra and ^{228}Ra, both occurring naturally. These isotopes occur by radioactive decay from either primordial ^{238}U (^{226}Ra) or primordial ^{232}Th (^{228}Ra) [9]. Radium-226 is converted to ^{222}Rn by alpha decay (Eq. 1.2), with a half-life of 1600 years. This decay also releases a characteristic gamma ray. Radon-222 is in turn radioactive and giving rise to the ^{226}Ra series illustrated in Figure 1.1 (part of the ^{238}U series). Radium-226 and ^{222}Rn are hazardous, particularly when ingested – ^{226}Ra can replace calcium in bones, while ^{222}Rn being gaseous, can be deposited in the lungs [20].

$$^{226}_{88}\mathrm{Ra} \rightarrow {}^{222}_{86}\mathrm{Rn} + {}^{4}_{2}\mathrm{He}^{2+} + \gamma + \mathrm{hv} \tag{1.2}$$

Radium-228, on the other hand, decays by beta decay to ^{228}Ac (Eq. 1.3) with a half-life of 5.75 years. Gamma radiation is also released, but of much less energy

than the ^{226}Ra decay. Actinium-228 is also radioactive, producing a decay chain for ^{228}Ra illustrated in Figure 1.1 (part of the ^{232}Th series).

$$^{228}_{88}\mathrm{Ra} \rightarrow ^{228}_{89}\mathrm{Ac} + \mathrm{e}^{-} + \gamma + \mathrm{h}\nu \tag{1.3}$$

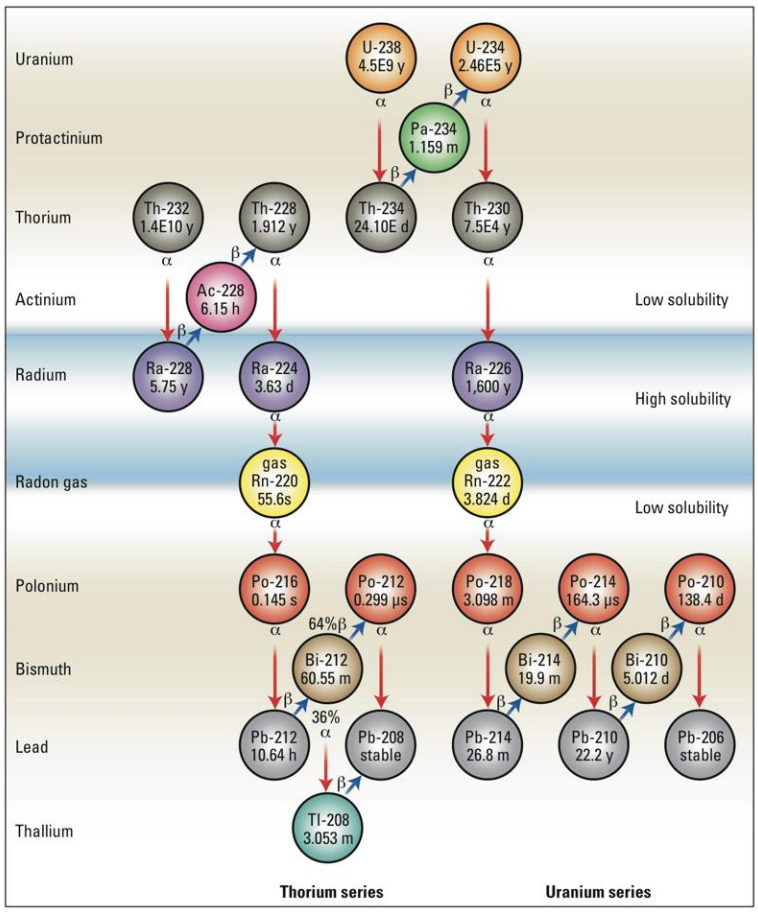

Figure 1.1: ^{226}Ra and ^{228}Ra decay chains showing the primordial parent nuclides, ^{238}U and ^{232}Th. Figure reproduced with permission from Nelson et al. [21]

The relatively short half-lives of ^{226}Ra and ^{228}Ra render their existence tied to the persistent formation by their primordial parent nuclides ^{238}U and ^{232}Th, whose half-

lives are on the order of billions of years. Owing to this, much of radium exists with the occurrence of uranium and thorium ores and deposits. However, deviations in the secular equilibrium between the parent and daughter nuclide indicate that radium possesses its own distinct pathway, separate from its parents. Nevertheless, the occurrence of radium should always be preceded with the occurrence of its parents, and this relationship cannot be ignored when discussing radium..

The decay series for ^{226}Ra and ^{228}Ra introduces a complexity when handling material that contains these elements, even when they have been separated from their parent material. In measuring the radioactivity present, one must consider the additional radiation given off by the radioactive daughter nuclides. Following the law of radioactive decay given by Rutherford and Soddy (Eq. 1.1), Harry Bateman in 1908 presented a solution to a series of differential equations that allows us to calculate the activity of each daughter in a given decay series, with great precision and accuracy, provided enough detail is known about the nature of the decay [22].

These equations have come to be known as the Bateman equations and are fundamental to understanding and predicting the behavior of radioactive decay chains. The equations can be summarized in the following manner:

$$A_n = \lambda_n N_n \tag{1.4}$$

$$N_n = c_1 e^{-\lambda_1 t} + c_2 e^{-\lambda_2 t} + c_3 e^{-\lambda_3 t} + \cdots + c_n e^{-\lambda_n t} \tag{1.5}$$

$$c_1 = \frac{\lambda_1 \lambda_2 \ldots \lambda_{n-1}}{(\lambda_2 - \lambda_1)(\lambda_3 - \lambda_1)(\lambda_n - \lambda_1)} N_1^0 \tag{1.6}$$

$$c_2 = \frac{\lambda_1 \lambda_2 \ldots \lambda_{n-1}}{(\lambda_1 - \lambda_2)(\lambda_3 - \lambda_2)(\lambda_n - \lambda_2)} N_1^0 \tag{1.7}$$

$$c_n = \frac{\lambda_1 \lambda_2 \dots \lambda_{n-1}}{(\lambda_1 - \lambda_n)(\lambda_2 - \lambda_n)(\lambda_{n-1} - \lambda_n)} N_1^0 \tag{1.8}$$

Where A_n is the activity of the nth element in the decay series, λ_n is the probability of an atom of the nth element to decay per unit time and N_n is the number of radioactive atoms of the nth element present at time t; N_1^0 is the number of atoms of the first element in the decay series present at $t = 0$.

1.2 Energy Production and Hydraulic Fracturing

The industrial revolution of the 18th Century forever changed human history, ushering in a new epoch, the Anthropocene – the age of man [23]. The discovery of new sources of energy in coal, and then crude oil, advanced the human species at an astonishing pace, hitherto unknown. Energy exploration and production continues to be a driving force of human evolution. However, as the effects of the industrial revolution are being felt and addressed, it behooves us to work towards a future where our appetite for energy is satiated. As we move away from inefficiency and carbon-rich fuels towards renewable energy sources, a transition period wherein the supply of renewable energy is supplemented by an efficient, yet carbon-low fuel is most desirable. Natural gas being of lower carbon than coal and crude oil [24], presents itself as such a fuel.

Prior to natural gas, crude oil had been the crux fuel. Crude oil, being a mineral, requires mining from its source rock. In many cases, crude oil is deposited in sandstone, carbonate or limestone reservoirs having migrated from a deeper source rock. To produce crude oil, wells were drilled vertically to the sandstone reservoirs. Given the permeable nature of sandstone, pressure overburden and Darcy flow were suf-

ficient to sustain the production of the crude oil. In time, this form of well development and production would come to be known as conventional exploration – describing the scenario of a vertical well intersecting a hydrocarbon-bearing confined reservoir, having migrated from its source rock [25]. Given the nature of crude oil and the migration from its source rock, it is uncommon for natural gas to be in plentiful quantities in the oil-bearing sandstone reservoirs. Although, physical laws dictate that some crude oil will transition its phase from the liquid to the gas following changes in the pressure and temperature regime [26]. Developing wells for vast amounts of natural gas production would require that we go to the point where crude oil was being formed first as natural gas before it could mature to its richer liquid state. This would require probing the very source rock, usually a shale, which lay deeper in the earths crust, and of much lower permeability than a sandstone. Thus was born the technology we know as hydraulic fracturing [25].

Hydraulic fracturing, in its modern application, is a process whereby water, sand, and chemicals are pumped into tight oil and gas-bearing source rocks in order to augment the natural fractures, or to propagate new fractures, for the enhanced production of natural gas. Because the wells are drilled directly to a source rock, this form of production is termed unconventional. Over time, the process of hydraulic fracturing and unconventional production has developed to include directional drilling – whereby a single well bore consists of both vertical and horizontal sections. The horizontal sections allow for greater contact with the low permeability source rock – while minimizing surface disturbance – in turn allowing for far greater production and profits than with vertical wells alone [25,27].

First developed in the late 19th and early 20th century, hydraulic fracturing evolved from the process of treating shallow formations with napalm, to the more sophisticated, computer model driven process it is today [27]. Hydraulic fracturing

has increased US recoverable gas reserves by an estimated 90% [27]. Since the early 2010s, hydraulic fracturing has been widely implemented in the United States to tap the resources of the shale plays. Advancements in hydraulic fracturing, together with directional drilling, allowed for the economic development of natural gas, affording the U.S. energy independence and more importantly, vast and cheap energy in the form of that transition fuel, natural gas [24,28]. The hydraulic fracturing of a well requires great amounts of water (as much as $10 - 25$ million liters), large amounts of the fracturing agent, usually silica sand (as much as 5,000 tons), and chemical additives (e.g. biocides, acids, gelling agents, and friction reducers usually at 0.1% - 1% by weight) [11]. During the early production of the well, a portion of the water used in the fracturing process returns as *flowback*, but greater volumes of formation water are produced during the life of the well, termed *produced water*. Hydraulically fractured wells produced an estimated 1.7 to 1.3 million liters of flowback and produced water over their producing life [29]. This produced water, together with the drilling solids, form the hydraulic fracturing co-products pertinent to this dissertation study.

The formation pertinent to this study is the Marcellus Shale. The Marcellus Shale is an organic, and clay-rich Middle Devonian age shale in the Appalachian Basin, underlying ~95,000 sq. miles of the northeastern US states of New York, Pennsylvania, Ohio, and West Virginia [30]. It is estimated that the Marcellus Shale contains 84 trillion cubic feet of natural gas [31], placing it as the largest in the United States [32]. As such, rapid development has been ongoing. Developing the Marcellus Shale resulted in an estimated $3.9 billion in revenue, and created ~44,000 jobs to Pennsylvania in 2012 [33]. The produced water of the Marcellus Shale are typical of

the Appalachian basin – being dominated by the chloride and rich in metal content, primarily Na and Ca; and yielding high salinities, up to 400,000 mg/L, among the highest in mineral waters [34,35]. This high salinity is thought to originate from formation water that evaporated beyond halite precipitation [35,36].

1.3 Occurrence of Radium in Hydraulic Fracturing Co-products

Radium concentrations in the produced water can be explained by the U/Th content of the source rock [35]. The Marcellus Shale having higher U content yields ^{226}Ra at higher concentrations than ^{228}Ra [37]. Radium is relatively soluble over a wide range of pH and redox conditions. Radium is thought to be liberated from the U or Th bearing source rock into the formation water, and thus into produced water by three mechanisms.

Firstly, the solubility of radium being higher than U or Th suggests that the mineral-water interface plays a significant role in the concentrations of radium in the formation water. This, coupled with the reducing conditions, results in a situation wherein radium is preferentially concentrated in the aqueous phase.

Secondly, the continuous production of the produced water encourages mineral dissolution and leaching of radium from the mineral phases. Although a large fraction is adsorbed at the surface of mineral grains, cations, such as Ba, Sr, Na, and K, desorb Ra from the surface of these minerals [37]. Radium is also mobilized in the presence of anions [38]. Radium can also adsorb to organic matter [39–42], but the increasing salinity increasingly desorbs radium [43]. Precipitation as Ra-Ba-SO_4 is the major mechanism controlling radium transport in natural systems, however, the

produced waters are reducing in nature, and therefore barite precipitation does not control radium transport from the subsurface [38, 44, 45].

Thirdly, radium is transferred to the aqueous phase via alpha recoil. Alpha recoil is a phenomenon wherein the transfer of kinetic energy of a nuclei following alpha decay is great enough to cause crystal damage, and to create a path for liquid infiltration through which the soluble radium escapes from the rock and into the formation water [38,46,47]. All these processes lend to median ^{226}Ra concentrations of ~148 Bq/L (4,000 pCi/L) and ^{228}Ra of ~37 Bq/L (1000 pCi/L) [37] in Marcellus Shale produced waters. Because ^{226}Ra far outlives ^{228}Ra, and because of its higher concentrations, ^{226}Ra is generally the isotope of major concern. The combination of high ^{226}Ra activities – typically >74 Bq/L (2,000 pCi/L) – and low ^{228}Ra/^{226}Ra values – less than 0.3 – serve as tools for identifying the Marcellus shale formation waters in the natural environment.

The solid fraction of the co-products comprises the drill cuttings from the vertical and horizontal portions of the wellbore (itself comprising the bedrock shale), the spent proppant, and spent drilling mud [48]. Among these, the radium activities of the vertical drill cuttings and drilling mud are very low, typically ~104 Bq/kg (2.8 pCi/g) ^{226}Ra and ~37 Bq/kg (1 pCi/g) ^{228}Ra, being of low U/Th content [49,50]. The spent proppant contain more radium than their pristine counterparts [50], but the activities are also low, with ^{226}Ra activities ranging from 6 Bq/kg (0.17pCi/g) – 13.2 Bq/kg (0.358 pCi/g) [50]. It is the horizontal, clay and organic-rich shale fragments that have considerable radium content, averaging ~185 Bq/kg (5 pCi/g) ^{226}Ra and 23.3 Bq/kg (0.63 pCi/g) ^{228}Ra, owing to their higher U/Th content [37,49,50].

1.4 Opportunities for Novel Treatment and Measurement Techniques for Radium in Hydraulic Fracturing Co-products

The rapid development of the Marcellus Shale for natural gas production quickly brought with it the need for a new type of industry to manage the vast quantities of co-products. For instance, in Pennsylvania, over 2 billion liters of flowback and produced water was generated in 2011, along with ~800,000 tons of drill cuttings, and ~15,000 tons of flowback fracturing sands [30]. The management and disposal of these co-products continues to be a concern, with regards to their high salts, metals, and NORM content. Current management and disposal of the liquid co-products have included disposal via Class II Underground Injection Control (UIC) wells, surface disposal via industrial/municipal waste treatment plants, recycling in other hydraulic fracturing jobs, and beneficial reuse (i.e. use outside the industry). The solid co-products have typically been landfilled in Subtitle D RCRA hazardous waste landfills. [30,51–53]

While disposal via Class II UIC wells is commonly practiced, it continues to be under scrutiny due to reports of injection-induced seismicity [54]. In some states, such as Pennsylvania, the number of Class II UIC wells have been limited by regulatory bodies (in 2016 PA had 8 active wells while OH had over 200) [55], for such states, produced water must be transported to other states for disposal via injection incurring high transportation costs, necessitating the need for a different management and disposal practice in those areas [30]. Disposal via surface discharges from centralized treatment plants is permitted by the National Pollutant Discharge Elimination System (NPDES) under the Clean Water Act of 1972 [52]. The effluent limits for these discharges are permitted based on either the technology available in these plants or the water quality of the receiving water bodies [52]. However, these

facilities were unable to sufficiently treat contaminant concentrations to nontoxic levels. As a result, surface waters have been exposed to radium, metals, chloride, bromide, and organic compounds, threatening the health of the receiving streams and their wildlife through increased salinization of the streams and radium accumulation in the stream sediments [56–61]. The health of human populations downstream of these discharges were also at risk due to the generation of carcinogenic disinfection byproducts during when these streams were sourced for drinking water [62,63]. Additionally, the treatment solids from these plants contained high levels of NORM [50], requiring specialized disposal in a low-level radioactive waste facility in Utah, incurring high transportation and disposal costs [64]. Recycling the produced water to hydraulically fracture other wells is a highly desired management practice as this can reduced the need for freshwater use, as well as the disposal volumes [52]. However, the high-total dissolved solids (TDS) concentrations of the produced water, along with the increased sulfate concentrations and dissolved oxygen, creates problems in recycle including downhole scale generation [65]and increased, undesirable microbial activity [66], resulting in reduced well performance. Recycling the produced waters will also result in higher TDS concentrations, which can in turn result in increased radium activities in the produced waters. Reuse outside the industry has included road spreading for dust suppression [30,51,67,68], and agricultural irrigation [52,69], although these practices have only utilized produced water from conventional production. However, research shows that these practices resulted in radium and metals being released to the environment, thereby threatening water quality and human health [70,71]. Finally, the disposal of the solids in hazardous waste landfills has largely gone without scrutiny. A study by the PA DEP reported that there was no significant difference in the chemical compositions of leachate from a landfill accepting oil and gas waste solids when compared to one that had not accepted

any such material, suggesting that this practice is without additional environmental concern borne from the origin of the solids [50].

Environmental sustainability continues to be a theme of growing importance, and the oil and gas industry is responding [72,73]. As such, efforts are being taken to consider beneficial reuse of these co-products, specifically from the produced water, by resource recovery [51,52]. The high Na and Cl content of these waters lends them as a feed stock for NaCl salt generation. This is already underway as NaCl is commercially available for road deicing in winter months and for pool maintenance [74]. Lithium recovery from the produced water is also of interest, being in high demand for the manufacture of batteries [75–80]. In light of these efforts, it is surprising that there has been little effort documented to recover the resources in the solid co-products, despite their high volume and presence of potentially useful materials like fracturing proppant and clay minerals [30].

In light of the issues surrounding the current management and treatment practices, and the desire for beneficial reuse of the co-products through resource recovery, is it evident that there is a need for new treatment techniques for the produced water that are specific to radium, even in the presence of high-TDS concentrations. Such techniques would reduce the high volumes of radioactive treatment solids requiring specialized disposal. In addition, a new treatment protocol for the solid co-products that recovers a portion of the raw materials and ultimately diminishes the volume of landfill waste is highly desirable.

The management of these wastes being tied to their radium concentrations necessitates the need for accurate and reliable radium measurements. While there are many methods to quantify radium in the liquids, these methods have been shown to be unreliable when performed on produced waters [81,82]. This is exacerbated by the fact that the recommended EPA methods for measuring radium are based on

freshwater methods and do not consider the high-TDS concentrations of the produced waters, or require pre-concentration steps that have been shown to have poor radium recovery [64,81,83]. While gamma spectroscopy remains the recommended method for measuring radium, radium measurements of the produced waters and oil and gas solids have been shown to be have high variability, even when the same samples are measured by different labs using similar methods [82]. There has been little attempt made to address the causes of such high variability, or to propose methods to account for and correct for these variance, especially in the context of these oil and gas products.

While gamma spectroscopy is the recommended method, it remains expensive, inaccessible for many oil and gas operators, and in many cases, the analysis requires long waiting times. There is therefore a need for new rapid and accurate methods for quantifying radium in the co-products (prior to and after treatment), beneficially recovered resources, and any treatment wastes generated as a result of these efforts.

1.5 Dissertation Outline

This dissertation, composed of two parts, presents research that addresses radium's occurrence in hydraulic fracturing solid and liquid co-products. The first part of this dissertation is dedicated to the nature and remediation of radium in the co-products, with the goal of developing novel treatment techniques for the co-products that allow for sustainable, beneficial reuse of these co-products.

I begin in Chapter 2 by appraising the potential for a hydroacoustic cavitation system to separate out and recover marketable raw materials from the would-

be landfilled solids. Sequential extractions and leaching experiments provided insights into radium's association with the solid fractions, and its potential migration or transformation during treatment and landfill disposal. This work presents itself as one of the firsts to perform detailed analysis of radium associations in these solids, attempt the recovery of raw materials, speculate on the marketability of the process, and the evaluate the effect of such a process on radium during disposal.

With the solids addressed, Chapter 3 turns the focus towards the liquid co-products by investigating a novel radium-specific treatment for the high-TDS produced waters. Specifically, I appraise a synthetic clay, Na-4-mica, that possesses high affinity for radium. I evaluate several syntheses protocols for Na-4-mica and characterize the synthesized Na-4-mica for its purity and efficacy for radium removal. Then, I explored the fundamental principles that can affect radium removal by Na-4-mica. As such, it is of an exploratory nature.

Following the investigations into the design of new treatment techniques, it became clear that there existed knowledge gaps in the quantification of ra-dium, particularly as applied to hydraulic fracturing co-products. The second part of this dissertation addresses these gaps by detailed analyses on the quantification of radium by gamma spectroscopy and by liquid scintillation. I propose new considerations for rapid and accurate analysis of radium, by addressing the nature of the co-products and the incurred attenuation of the gamma decay, and I propose a new method for quantifying radium in the liquid co-products.

Chapter 4 addresses the problem of quantifying radium in the solid co-products. The chapter evaluates the effect of varying sample density and sample volume on the attenuation of gamma rays and their effect on radium measurements. I ad-

dress this problem by performing radioactive analyses on mixed sediments of varying densities with certified radium activities. I present a technique to account for the self-attenuation of the solids that occur due to sample density and volume. Then I applied these corrections to sediments from oil and gas operations and provide recommendations for rapid and accurate radium measurements of the solids.

In Chapter 5, I explore the effect of the high-TDS environment on radium measurement by gamma spectroscopy. I present an empirical approach to correct for the self-attenuation incurred by the high-TDS concentrations and its ionic compositions. These investigation were performed using synthetic brines that were either NaCl-only or a mixed Na-Ca-Ba-Sr-Mg-Cl. I then evaluated these corrections for real produced waters and provide recommendations for rapid and accurate radium measurements of the high-TDS produced waters.

Finally, in Chapter 6, I present a rapid method for quantifying radium in produced water through the application of alpha-beta discrimination coupled with spectrum analysis in liquid scintillation. I provide detailed descriptions of this novel method and using real produced waters, provide comparisons with gamma spectroscopy for the sake of accuracy. I highlight the relative simplicity of this method, its reasonable cost and provide recommendations to industry persons to whom this could be very useful.

1.6 References

(1) Wolke, R. L. Marie Curie's Doctoral Thesis: Prelude to a Nobel Prize. *J. Chem. Educ.* 1988, *65* (7), 561. https://doi.org/10.1021/ed065p561.

(2) Radiochemical Methods Group. Discovery of Radioactivity. *The Royal Society of Chemistry*. London.

(3) Maloney, J. A. Radium-Nature's Oddest Child Pt. 3. 1937, *157* (3), 148–150. https://doi.org/10.2307/24997474.

(4) Maloney, J. A. Radium-Nature's Oddest Child Pt. 4. 1937, *157* (4), 212–215. https://doi.org/10.2307/26070913.

(5) Radiochemical Methods Group. Discovery of the Neutron. *The Royal Society of Chemistry*. London.

(6) Radiochemical Methods Group. Alpha, Beta and Gamma Radioactivity. *The Royal Society of Chemistry*. London.

(7) Radvanyi, P.; Villain, J. The Discovery of Radioactivity. *Comptes Rendus Phys.* 2017, *18* (9–10), 544–550. https://doi.org/10.1016/J.CRHY.2017.10.008.

(8) Reed, A. B. The History of Radiation Use in Medicine. *J. Vasc. Surg.* 2011, *53* (1), 3S-5S. https://doi.org/10.1016/j.jvs.2010.07.024.

(9) International Atomic Energy Agency (IAEA). *The Environmental Behaviour of Radium: Revised Edition. Technical Report Series No. 476*; Vienna, 2014.

(10) Langevin-Joliot, H. Radium, Marie Curie and Modern Science. *Radiat. Res.* 1998, *150* (5), S3. https://doi.org/10.2307/3579803.

(11) Maloney, J. A. Radium-Nature's Oddest Child. 1937, *157* (1), 18–20. https://doi.org/10.2307/24997429.

(12) Maloney, J. A. Radium-Nature's Oddest Child. Pt 2. 1937, *157* (2), 83–85. https://doi.org/10.2307/24997452.

(13) Rontgen, W. C. *On a New Kind of Rays. By W.C. Rontgen. Translated by Arthur Stanton from the Sitzungsberichte Der Wü rzburger Physic-Medic. Gesellschaft, 1895. Nature, January 23, 1896.*; 1970; Vol. 36, pp 185–188.

(14) Rutherford, E. VIII. Uranium Radiation and the Electrical Conduction Produced by It. *London, Edinburgh, Dublin Philos. Mag. J. Sci.* 1899, *47* (284), 109–163. https://doi.org/10.1080/14786449908621245.

(15) Soddy, F. Intra-Atomic Charge. *Nature* 1913, *92*, 399–400.

(16) Gilmore, G. R. *Practical Gamma-Ray Spectrometry*; John Wiley & Sons, Ltd: Chichester, UK, 2008. https://doi.org/10.1002/9780470861981.

(17) Bolivar, J. P.; Garcí a-Leó n, M.; Garcí a-Tenorio, R. On Self-Attenuation Corrections in Gamma-Ray Spectrometry. *Appl. Radiat. Isot.* 1997, *48* (8), 1125– 1126. https://doi.org/10.1016/S0969-8043(97)00034-1.

(18) Hubbell, J. H. Photon Mass Attenuation and Energy-Absorption Coefficients. *Int. J. Appl. Radiat. Isot.* 1982, *33* (11), 1269– 1290. https://doi.org/10.1016/0020-708X(82)90248-4.

(19) Kirby, H. W.; Salutsky, M. L. The Radiochemistry of Radium. *NAS-NRC Nucl. Sci. Ser.* 1964.

(20) IAEA. Radiation Protection and the Management of Radioactive Waste in the Oil and Gas Industry. *Environ. Health Perspect.* 2014, *122* (2), A50-5.

(21) Nelson, A. W.; Eitrheim, E. S.; Knight, A. W.; May, D.; Mehrhoff, M. A.; Shannon, R.; Litman, R.; Burnett, W. C.; Forbes, T. Z.; Schultz, M. K. Understanding the Radioactive Ingrowth and Decay of Naturally Occurring Radioactive Materials in the Environment: An Analysis of Produced Fluids from the Marcellus Shale. *Environ. Health Perspect.* 2015, *123* (7), 689– 696. https://doi.org/10.1289/ehp.1408855.

(22) Bateman, H. The Solution of a System of Differential Equations Occuring in the Theory of Radio-Acive Transformations. *Cambridge Philos. Soc.* 1910, *15* (1908– 10), 423– 427.

(23) Stromberg, J. What Is the Anthropocene and Are We in It? *Smithsonian Magazine*. January 2013.

(24) Kerr, R. A. Energy. Natural Gas from Shale Bursts onto the Scene. *Science* 2010, *328* (5986), 1624– 1626. https://doi.org/10.1126/science.328.5986.1624.

(25) Lyons, W. C.; Pilsga, G. J.; Lorenz, M. D. *Standard Handbook of Petroleum and Natural Gas Engineering*; Gulf Professional Publishing, 2016.

(26) Pedersen, K. S. (Karen S.; Christensen, P. L. (Peter L.; Shaikh, J. A. *Phase Behavior of Petroleum Reservoir Fluids.*

(27) Montgomery, C. T.; Smith, M. B. Hydraulic Fracturing: History of an Enduring Technology. *J. Pet. Technol.* 2010, *62* (12), 26–40. https://doi.org/10.2118/1210-0026-JPT.

(28) U.S. Energy Information Administration. *Annual Energy Outlook*; Washington, DC, 2018.

(29) Kondash, A. J.; Albright, E.; Vengosh, A. Quantity of Flowback and Produced Waters from Unconventional Oil and Gas Exploration. *Sci. Total Environ.* 2017, *574*, 314–321. https://doi.org/10.1016/j.scitotenv.2016.09.069.

(30) Maloney, K. O.; Yoxtheimer, D. A. Production and Disposal of Waste Materials from Gas and Oil Extraction from the Marcellus Shale Play in Pennsylvania. *Environ. Pract.* 2012, *14* (December), 278–287. https://doi.org/10.1017/S146604661200035X.

(31) Coleman, J. L.; Milici, R. C.; Cook, T. A.; Charpentier, R. R.; Kirschbaum, M.; Klett, T. R.; Pollastro, R. M.; Schenk, C. J. *Assessment of Undiscovered Oil and Gas Resources of the Devonian Marcellus Shale of the Appalachian Basin Province, 2011*; 2011.

(32) Wells; Peggy. *Top 100 U.S. Oil and Gas Fields*; 2015.

(33) Considine, T.; D Robert Watson, P.; E Seth Blumsack, P. *The Economic Impacts of the Pennsylvania Marcellus Shale Natural Gas Play: An Update*; 2010.

(34) Dresel, P.; Rose, A. Chemistry and Origin of Oil and Gas Well Brines in Western Pennsylvania. *Pennsylvania Geol. Surv., 4th Ser. Open …*2010, 48. https://doi.org/Open-File Report OFOG 1001.0.

(35) Rowan, E. L.; Engle, M. A.; Kraemer, T. F.; Schroeder, K. T.; Hammack, R. W.; Doughten, M. W. Geochemical and Isotopic Evolution of Water Produced from Middle Devonian Marcellus Shale Gas Wells, Appalachian Basin, Pennsylvania. *Am. Assoc. Pet. Geol. Bull.* 2015, *99* (2), 181–206. https://doi.org/10.1306/07071413146.

(36) Stewart, B. W.; Chapman, E. C.; Capo, R. C.; Johnson, J. D.; Graney, J.

R.; Kirby, C. S.; Schroeder, K. T. Origin of Brines, Salts and Carbonate from Shales of the Marcellus Formation: Evidence from Geochemical and Sr Isotope Study of Sequentially Extracted Fluids. *Appl. Geochemistry* 2015, *60*, 78–88. https://doi.org/10.1016/j.apgeochem.2015.01.004.

(37) Rowan, E. L.; Engle, M. a.; Kirby, C. S.; Kraemer, T. F. Radium Content of Oil- and Gas-Field Produced Waters in the Northern Appalachian Basin (USA): Summary and Discussion of Data. *USGS Sci. Investig. Rep.* 2011, 38 pp.

(38) Wiegand, J. W.; Sebastian, F. Origin of Radium in High-Mineralised Waters. *Technol. Enhanc. Nat. Radiat. (TENR II) - Proc. an Int. Symp. Held Rio Janeiro; IAEA - TECDOC - 1271* 2002, 107–111.

(39) Alhajji, E.; Al-Masri, M. S.; Khalily, H.; Naoum, B. E.; Khalil, H. S.; Nashawati, A. A Study on Sorption of 226Ra on Different Clay Matrices. *Bull. Environ. Contam. Toxicol.* 2016, *97* (2), 255–260. https://doi.org/10.1007/s00128-016-1852-1.

(40) Nathwani, J. S.; Phillips, C. R. Adsorption of 226Ra by Soils in the Presence of Ca2+ Ions. Specific Adsorption (II). *Chemosphere* 1979, *8* (5), 293–299. https://doi.org/10.1016/0045-6535(79)90112-7.

(41) Krishnaswami, S.; Graustein, W. C.; Turekian, K. K.; Dowd, J. F. Radium, Thorium and Radioactive Lead Isotopes in Groundwaters: Application to the in Situ Determination of Adsorption- desorption Rate Constants and Retardation Factors. *Water Resour. Res.* 1982, *18* (6), 1663–1675. https://doi.org/10.1029/WR018i006p01663.

(42) Shao, H.; Kulik, D. A.; Berner, U.; Kosakowski, G.; Kolditz, O. Modeling the Competition between Solid Solution Formation and Cation Exchange on the Retardation of Aqueous Radium in an Idealized Bentonite Column. *Geochem. J.* 2009, *43* (6). https://doi.org/10.2343/geochemj.1.0069.

(43) Webster, I. T.; Hancock, G. J.; Murray, A. S. Modelling the Effect of Salinity on Radium Desorption from Sediments. *Geochim. Cosmochim. Acta* 1995, *59* (12), 2469–2476. https://doi.org/10.1016/0016-7037(95)00141-7.

(44) Bloch, S.; Key, R. M. Modes of Formation of Anomalously High Radioactivity in Oil-Field Brines. 1953, pp 154–159.

(45) Lowson, R. T. The Thermochemistry of Radium. *Thermochim. Acta* 1985, *91* (C), 185–212. https://doi.org/10.1016/0040-6031(85)85214-X.

(46) Kraemer, T. F.; Reid, D. F. The Occurrence and Behavior of Radium in Saline Formation Water of the U.S. Gulf Coast Region. *Chem. Geol.* 1984, *46* (2), 153–174. https://doi.org/10.1016/0009-2541(84)90186-4.

(47) Fleischer, R. L.; Raabe, O. G. Recoiling Alpha-Emitting Nuclei. Mechanisms for Uranium-Series Disequilibrium. *Geochim. Cosmochim. Acta* 1978, *42* (7), 973–978. https://doi.org/10.1016/0016-7037(78)90286-7.

(48) Barry, B.; Klima, M. S. Characterization of Marcellus Shale Natural Gas Well Drill Cuttings. *J. Unconv. Oil Gas Resour.* 2013, *1–2*, 9–17. https://doi.org/10.1016/J.JUOGR.2013.05.003.

(49) Eitrheim, E. S.; May, D.; Forbes, T. Z.; Nelson, A. W. Disequilibrium of Naturally Occurring Radioactive Materials (NORM) in Drill Cuttings from a Horizontal Drilling Operation. *Environ. Sci. Technol. Lett.* 2016, *3* (12), 425–429. https://doi.org/10.1021/acs.estlett.6b00439.

(50) Pennsylvania Department of Environmental Protection (PA DEP). Technologically Enhanced Naturally Occurring Radioactive Materials (TENORM) Study Report http://www.depgreenport.state.pa.us/elibrary/getdocument?docid=5815&docname=01 pennsylvania department of environmental protection tenorm study report rev 1.pdf (accessed Feb 8, 2018).

(51) U.S. Environmental Protection Agency. *Detailed Study of the Centralized Waste Treatment Point Source Category for Facilities Managing Oil and Gas Extraction Wastes*; Washington, D.C., 2018.

(52) U.S. Environmental Protection Agency. *Study of Oil and Gas Extraction Wastewater Management Under the Clean Water Act EPA-821-R19-001*; Washington, D.C., 2019.

(53) Veil, J. *U.S. Produced Water Volumes and Management Practices in 2012*;

2015.

(54) Ellsworth, W. L. Injection-Induced Earthquakes. *Science (80-.).* 2013, *341* (6142), 1225942. https://doi.org/10.1126/SCIENCE.1225942.

(55) Pennsylvania Department of Environmental Protection (PA DEP). *2016 Oil and Gas Annual Report*; 2016.

(56) Geeza, T. J.; Gillikin, D. P.; McDevitt, B.; Van Sice, K.; Warner, N. R. Accumulation of Marcellus Formation Oil and Gas Wastewater Metals in Freshwater Mussel Shells. *Environ. Sci. Technol.* 2018, *52* (18), 10883–10892. https://doi.org/10.1021/acs.est.8b02727.

(57) Van Sice, K.; Cravotta, C. A.; McDevitt, B.; Tasker, T. L.; Landis, J. D.; Puhr, J.; Warner, N. R. Radium Attenuation and Mobilization in Stream Sediments Following Oil and Gas Wastewater Disposal in Western Pennsylvania. *Appl. Geochemistry* 2018, *98*, 393–403. https://doi.org/10.1016/j.apgeochem.2018.10.011.

(58) Vengosh, A.; Jackson, R. B.; Warner, N. R.; Darrah, T. H.; Kondash, A. A Critical Review of the Risks to Water Resources from Unconventional Shale Gas Development and Hydraulic Fracturing in the United States. *Environ. Sci. Technol.* 2014, *48* (15), 8334–8348. https://doi.org/10.1021/es405118y.

(59) Burgos, W. D.; Castillo-Meza, L.; Tasker, T. L.; Geeza, T. J.; Drohan, P. J.; Liu, X.; Landis, J. D.; Blotevogel, J.; McLaughlin, M.; Borch, T.; et al. Watershed-Scale Impacts from Surface Water Disposal of Oil and Gas Wastewater in Western Pennsylvania. *Environ. Sci. Technol.* 2017, *51* (15), 8851–8860. https://doi.org/10.1021/acs.est.7b01696.

(60) Lauer, N. E.; Warner, N. R.; Vengosh, A. Sources of Radium Accumulation in Stream Sediments near Disposal Sites in Pennsylvania: Implications for Disposal of Conventional Oil and Gas Wastewater. *Environ. Sci. Technol.* 2018. https://doi.org/10.1021/acs.est.7b04952.

(61) Warner, N. R.; Christie, C. A.; Jackson, R. B.; Vengosh, A. Impacts of Shale Gas Wastewater Disposal on Water Quality in Western Pennsylvania. *Environ. Sci. Technol.* 2013, *47*, 11849–11857. https://doi.org/10.1021

/es402165b.

(62) Harkness, J. S.; Dwyer, G. S.; Warner, N. R.; Parker, K. M.; Mitch, W. A.; Vengosh, A. Iodide, Bromide, and Ammonium in Hydraulic Fracturing and Oil and Gas Wastewaters: Environmental Implications. *Environ. Sci. Technol.* 2015, *49* (3), 1955−1963. https://doi.org/10.1021/es504654n.

(63) Parker, K. M.; Zeng, T.; Harkness, J.; Vengosh, A.; Mitch, W. A. Enhanced Formation of Disinfection Byproducts in Shale Gas Wastewater-Impacted Drinking Water Supplies. *Environ. Sci. Technol.* 2014, *48* (19), 11161−11169. https://doi.org/10.1021/es5028184.

(64) U.S. EPA. A System's Guide to the Management of Radioactive Residuals from Drinking Water. *Epa 816-R-05-004* 2005.

(65) Paukert Vankeuren, A. N.; Hakala, J. A.; Jarvis, K.; Moore, J. E. Mineral Reactions in Shale Gas Reservoirs: Barite Scale Formation from Reusing Produced Water As Hydraulic Fracturing Fluid. *Environ. Sci. Technol.* 2017, *51* (16), 9391−9402. https://doi.org/10.1021/acs.est.7b01979.

(66) He, C.; Zhang, T.; Vidic, R. D. Use of Abandoned Mine Drainage for the Development of Unconventional Gas Resources. *Disruptive Sci. Technol.* 2013, *1* (4), 169−176. https://doi.org/10.1089/dst.2013.0014.

(67) Lutz, B. D.; Lewis, A. N.; Doyle, M. W. Generation, Transport, and Disposal of Wastewater Associated with Marcellus Shale Gas Development. *Water Resour. Res.* 2013, *49* (October 2012), 647−656. https://doi.org/10.1002/wrcr.20096.

(68) Dunne, E. J. *Flowback and Produced Waters*; Dunne, E. J., Ed.; National Academies Press: Washington, D.C., 2017. https://doi.org/10.17226/24620.

(69) Pichtel, J.; John. Oil and Gas Production Wastewater: Soil Contamination and Pollution Prevention. *Appl. Environ. Soil Sci.* 2016, *2016*, 1−24. https://doi.org/10.1155/2016/2707989.

(70) McDevitt, B.; McLaughlin, M.; Cravotta, C. A.; Ajemigbitse, M. A.; Van Sice, K. J.; Blotevogel, J.; Borch, T.; Warner, N. R. Emerging Investigator Series: Radium Accumulation in Carbonate River Sediments at Oil and Gas

Produced Water Discharges: Implications for Beneficial Use as Disposal Management. *Environ. Sci. Process. Impacts* 2019, *21* (2), 324–338. https://doi.org/10.1039/C8EM00336J.

(71) Tasker, T. L.; Burgos, W. D.; Piotrowski, P.; Castillo-Meza, L.; Blewett, T. A.; Ganow, K. B.; Stallworth, A.; Delompré , P. L. M.; Goss, G. G.; Fowler, L. B.; et al. Environmental and Human Health Impacts of Spreading Oil and Gas Wastewater on Roads. *Environ. Sci. Technol.* 2018, *52* (12), 7081–7091. https://doi.org/10.1021/acs.est.8b00716.

(72) Alnuaim, S. What Does Sustainability Mean for Oil and Gas? *Society of Petroleum Engineers*. 2018.

(73) Sekhran, N.; Sheahan, B.; Sullivan, B. *Mapping the Oil and Gas Industry to the SDGs: An Atlas*; New York, 2017.

(74) Dorich, A. Eureka Resources Recovers Vital Resources from Flowback and Production Wastewater. *Energy & Mining International*. 2017.

(75) MGX Minerals Inc. (Press Release). MGX Minerals and Eureka Resources Announce Joint Venture to Recover Lithium from Produced Water in Eastern United States https://www.prnewswire.com/news-releases/mgx-minerals-and-eureka-resources-announce-joint-venture-to-recover-lithium-from-produced-water-in-eastern-united-states-300806407.html (accessed May 13, 2019).

(76) Paranthaman, M. P.; Li, L.; Luo, J.; Hoke, T.; Ucar, H.; Moyer, B. A.; Harrison, S. Recovery of Lithium from Geothermal Brine with Lithium–Aluminum Layered Double Hydroxide Chloride Sorbents. *Environ. Sci. Technol.* 2017, *51* (22), 13481–13486. https://doi.org/10.1021/acs.est.7b03464.

(77) Schaller, J.; Headley, T.; Prigent, S.; Breuer, R. Potential Mining of Lithium, Beryllium and Strontium from Oilfield Wastewater after Enrichment in Constructed Wetlands and Ponds. 2014. https://doi.org/10.1016/j.scitotenv.2014.06.097.

(78) Swain, B. Recovery and Recycling of Lithium: A Review. *Sep. Purif. Technol.*

2017, *172*, 388–403. https://doi.org/10.1016/j.seppur.2016.08.031.

(79) Jang, Y.; Chung, E. Adsorption of Lithium from Shale Gas Produced Water Using Titanium Based Adsorbent. *Ind. Eng. Chem. Res.* 2018, *57* (25), 8381–8387. https://doi.org/10.1021/acs.iecr.8b00805.

(80) Flexer, V.; Fernando Baspineiro, C.; Galli, C. I. Lithium Recovery from Brines: A Vital Raw Material for Green Energies with a Potential Environmental Impact in Its Mining and Processing. *Sci. Total Environ.* 2018, *639*, 1188–1204. https://doi.org/10.1016/j.scitotenv.2018.05.223.

(81) Nelson, A. W.; May, D.; Knight, A. W.; Eitrheim, E. S.; Mehrhoff, M.; Shannon, R.; Litman, R.; Schultz, M. K. Matrix Complications in the Determination of Radium Levels in Hydraulic Fracturing Flowback Water from Marcellus Shale. *Environ. Sci. Technol. Lett.* 2014, *1* (3), 204–208. https://doi.org/10.1021/ez5000379.

(82) Tasker, T. L.; Burgos, W. D.; Ajemigbitse, M. A.; Lauer, N. E.; Gusa, A. V.; Kuatbek, M.; May, D.; Landis, J. D.; Alessi, D. S.; Johnsen, A. M.; et al. Accuracy of Methods for Reporting Inorganic Element Concentrations and Radioactivity in Oil and Gas Wastewaters from the Appalachian Basin, U.S. Based on an Inter-Laboratory Comparison. *Environ. Sci. Process. Impacts* 2019, *21* (2), 224–241. https://doi.org/10.1039/C8EM00359A.

(83) Zhang, T.; Bain, D.; Hammack, R.; Vidic, R. D. Analysis of Radium-226 in High Salinity Wastewater from Unconventional Gas Extraction by Inductively Coupled Plasma-Mass Spectrometry. *Environ. Sci. Technol.* 2015, *49* (5), 2969–2976. https://doi.org/10.1021/es504656q.

Part I

Novel Treatment Techniques for Radium in Hydraulic Fracturing Co-Products

Chapter 2

Raw Material Recovery from Hydraulic Fracturing Residual Solid Waste with Implications for Sustainability and Radioactive Waste Disposal

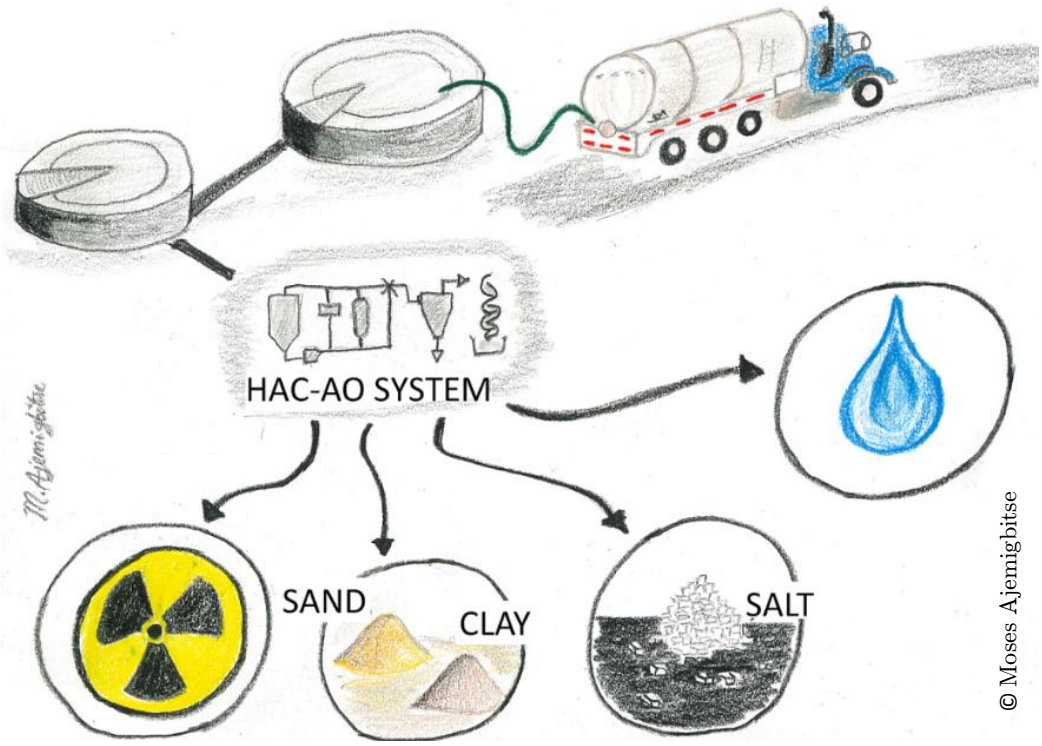

Ajemigbitse MA, Cannon FS, Klima M, Furness JC, and Warner NR. "Raw Material Recovery from Oil and Gas Residual Waste with Implications for Sustainability and Radioactive Waste Disposal." *Environ Sci.: Processes Impacts.* 2018, 21(2): 308-323.

2.1 Abstract

Unconventional oil and gas residual solid wastes are generally disposed in municipal waste landfills (RCRA Subtitle D), but they contain valuable raw materials such as proppant sands. A novel process for recovering raw materials from hydraulic fracturing residual waste is presented. Specifically, a novel hydroacoustic cavitation system, combined with physical separation devices, can create a distinct stream of highly concentrated sand, and another distinct stream of clay from the residual solid waste by the dispersive energy of cavitation conjoined with ultrasonics, ozone and hydrogen peroxide. This combination cleaned the sand grains, by removing previously aggregated clays and residues from the sand surfaces. When these unit operations were followed by a hydrocyclone and spiral, the solids could be separated by particle size, yielding primarily cleaned sand in one flow stream; clays and fine particles in another; and silts in yet a third stream. Consequently, the separation of particle sizes also affected radium distribution – the sand grains had low radium activities, as lows as 0.207 Bq/g (5.6 pCi/g). In contrast, the clays had elevated radium activities, as high as 1.85 – 3.7 Bq/g (50 – 100 pCi/g) – and much of this radium was affiliated with organics and salts that could be separated from the clays. We propose that the reclaimed sand could be reused as hydraulic fracturing proppant. The separation of sand from silt and clay could reduce the volume and radium masses of wastes that are disposed in landfills. This could represent a significant savings to facilities handling oil and gas waste, as much as \$100,000 – \$300,000 per year. Disposing the radium-enriched salts and organics downhole will mitigate radium release to the surface. Additionally, the reclaimed sand could have market value, and this could represent as much as a third of the cost savings. Tests

that employed the toxicity characteristic leaching protocol (TCLP) on these separated solids streams determined that this novel treatment diminished the risk of radium mobility for the reclaimed sand, clays or disposed material, rendering them better suited for landfilling.

2.2 Introduction

Environmental sustainability is one of eight millennium development goals put forward by the United Nations; and it remains one of the biggest challenges for the current generation. Now, more than ever before, engineered solutions must be assessed through the lens of environmental sustainability. Solutions to meet the increasing energy demand of a growing population must be economically and environmentally sustainable. As our society transitions from fossil fuels to cleaner and greener energy sources, natural gas has served as an important bridge fuel toward sustainably renewable energy and a low-carbon future. This is because the burning of natural gas yields about half to two-thirds as much carbon dioxide per unit of energy generated, when compared to gasoline or coal [1].

Hydraulic fracturing has allowed for the extraction of natural gas from previously uneconomic, low-permeability formations; and this opportunity has sparked an energy revolution that is rapidly moving America towards energy independence [2]. However, this energy revolution has not proceeded without controversy regarding issues around the relationship between hydraulic fracturing and potential environmental impacts such as: waste solids landfilling, and potential radioactivity exposure [3], elevated methane concentrations and leakage along natural gas distribution lines in urban centers [4,5], greenhouse gas emissions of methane [6–9], elevated salt impacts on streams [10–15], surface water impacts [15–18], and associated health impacts

[19,20]. Groundwater methane contamination from oil and gas activities has been investigated with conflicting results: Osborn *et al.* [21] and Vengosh *et al.* [18] support this claim, while Molofsky *et al.* [22] and Siegel *et al.* [23] attribute this to natural geography. Herein, we address the first of these issues, namely, waste solids handling and management of radioactivity from hydraulic fracturing.

The handling and treatment of hydraulic fracturing waste is challenging because the liquid and solid wastes can contain elevated levels of naturally occurring radioactive material (NORM) and high concentrations of salts [24,25]. Surface discharge of partially treated liquid wastes, including flowback and produced water, has led to increased levels of metals, chloride, bromide and radioactivity in the receiving waters and sediments, as well as posing risks to aquatic and human health [10–12]. These discharges are also linked with the possibility of generating disinfectant by-products, which are possible carcinogens, in the drinking water treatment facilities that are located further downstream [14,15,26]. Studies on the treatment of produced water for NORM removal have included sulfate precipitation (as barium or strontium sulfate) by sodium sulfate addition [27–29], or by blending with acid mine drainage [30–32]; and ion exchange using strong acid resins [33]. Sulfate precipitation remains a very effective treatment for NORM removal from produced waters, however, sulfate addition results in the generation of sludge enriched with NORM. Moreover, the dose of sulfate needed to precipitate barium (and co-precipitated radium) is far greater with such high levels of salts – and consequently suppressed activity coefficients – than would be needed if such precipitation was occurring in freshwater that contained low salt levels [29]. Additionally, sulfate addition can result in scale formation [34] and increased activity of sulfate reducing bacteria [30] when the fluid is reused for hydraulic fracturing. While ion exchange can provide targeted radium

removal, this process would require pre-treatment to reduce the competition for exchange sites offered by other divalent cations.

The authors herein are not aware of published research on reclaiming the solid materials used in hydraulic fracturing, such as sand and clay, despite the considerable amounts of pristine solids consumed by this industry. A sustainable energy future includes efforts to reduce wastes that are landfilled, and strategies to recover valuable raw materials from wastes prior to disposal. Silica sand is utilized as a proppant for extending the natural fractures and maintaining higher permeability following hydraulic fracturing. The hydraulic fracturing of a single well can consume as much as 5,000 tons of sand as proppant [35]. Currently, in Pennsylvania, fracturing sands that return to the surface with flowback fluids and produced waters are disposed in landfills. In 2011, about 15,000 tons of fracturing sand were reported disposed in landfills, second after drill cuttings in disposal volume [36]. In that same year, 290 million liters (2.4 million barrels) of drilling fluids, 1 billion liters (9 million barrels) of produced water, and 940 million liters (7.9 million barrels) of flowback fluid were generated in Pennsylvania. Of that liquid waste, 70% of drilling fluids were reused and 72% of the flowback fluid and brine were reused/recycled in subsequent wells. However, we found no reported reuse/recycle of the fracturing sands [36].

The hydraulic fracturing industry has increased the demand for silica sand, and consequently, sand's price has likewise increased from about \$40/ton to \$87/ton in a mere 10 years (dollar values adjusted to avg. 2017 USD)[35]. Most of the fracturing sand comes from the Upper Midwest, especially Wisconsin – which in 2014 supplied almost 50% of all silica sand used for hydraulic fracturing [35]. In 2013, silica sand accounted for 85% of all proppants (by weight). This demand for sand affects other

sand-using industries notably glass makers and iron foundries, who extensively use the same fine-grained silica sand from the Upper Midwest [35,37,38] (see Figure A1). Between 2003 and 2012, there was a 32% compound annual growth rate for silica sand used for hydraulic fracturing, in that same period, the amount of sand used for other non-fracturing uses dropped by an annual rate of 2.2%, further illustrating how the hydraulic fracturing industry is a strong market force for silica sand [35].

Economic, societal, and environmental issues related to sand mining and sand resources are growing; and these pressures have been documented in reports on the diminishing sand supply [39], land disputes [40], erosion caused by mining and transportation [35], damage to local ecosystems, increased risk of flooding [41–43], and activist protests [41,44,45]. The Appalachian Basin, of which the Marcellus Shale is a part, is the second most sand-consuming US basin[46] (following the Eagle Ford and Woodbine Formation in the East Texas Basin.) The demand for sand is expected to increase with the increased focus on developing the Marcellus Shale for natural gas and gas liquids, as well as the anticipated increased drilling of an underlying Utica Shale Formation [35].

The increased drilling activity will not only lead to greater raw material use but also greater waste volume generation. In Pennsylvania, as shown in Figure A2, landfills accepted almost 7,000 tons of sludge from oil and gas wastewater treatment facilities in 2017. This sludge contains radioactive material with typical ^{226}Ra activities ranging from 0.111 Bq/g to 17.8 Bq/g (3 pCi/g to 480 pCi/g) [47,48]. Research on the treatment of such technologically enhanced naturally occurring radioactive materials (TENORM) sludge is limited [48–50]. Therefore, there is an opportunity to evaluate raw material recovery and solid waste radioactive management for the unconventional oil and gas industry.

Herein we propose to facilitate raw material recovery from unconventional oil and gas residual solid wastes by employing a novel hydroacoustic cavitation system that can also include advanced oxidation (HAC-AO). The HAC-AO system has been applied to the foundry and coal industries for raw material recovery and waste reduction; and this has pointed the way to diminished raw material use and significant savings to operating costs in both industries [52–64]. Specifically, foundries that have implemented HAC-AO have been able to save tens of millions of dollars over several decades, due to diminished sand, clay, and coal consumptions, lower air pollution, and lower scrap metal use [55,58,64]. The system (Figure 2.1) utilizes cavitation to generate localized cavities, which then collapse under ultrasonic inducement, resulting in high pressure – reported to be as high as 172 MPa (1700 atm) – and temperature – as high as 4000-5000 °K, at the nanoscale [65–67]. When the cavities are formed at the sand-clay-residue interfaces, this intense collapse causes surface debris to be pried and sheared away from such solid surfaces as sand grains, thus cleaning the sands [68]. At these localized regions, hydroxyl radicals are generated, which react aggressively with organic compounds that are present on the solid surfaces or in solution. Advanced oxidants, such as hydrogen peroxide and ozone, can be added into solution so as to increase hydroxyl radicals generation [69]. HAC-AO technology causes disaggregation of the waste particles by the dispersive energy released at bubble collapse, as well as the reactive effects of the advanced oxidants. This HAC-AO system, which consists of a cavitation-inducing chamber and ultrasonic generator, can be coupled with a hydrocyclone and a spiral concentrator to first disaggregate sands from clays and silts, and then separate these three from one another (Figure 2.1).

In a recent publication, the underlying mechanism for HAC-AO was studied by nanoscale Surface Imaging Spectroscopy (SIS) [68]. The SIS technique provided evidence for the separation mechanism of HAC-AO, as the microscopic cleaning process for the removal of asphalt from a glass surface was observed. This study demonstrated the principles that caused the separation of sand grains from spent foundry residues.

The goal of this work was to reclaim hydraulic fracturing raw materials, while reducing landfill wastes and mitigating possible exposure to natural radium in the wastes. There were three objectives of this research. 1) To appraise a novel approach for reclaiming sand from hydraulic fracturing waste using HAC or HAC-AO, so as to reduce the volume of solid material that is disposed in landfills; 2) to evaluate the resulting radioactivity of the sands and clays that have been separated out of the waste materials following HAC or HAC-AO treatment, including leachability in a simulated landfill environment; and 3) to explore the radium affiliation within hydraulic fracturing solid materials. The hypothesis was that hydroacoustic cavitation (and/or HAC-AO) would disaggregate fine material (clays) from large grain material (sand); and following this disaggregation, physical separation devices could then create a distinct stream of recoverable, cleaned sand. As a consequence of this particle separation, we expected that higher radium activities would become affiliated with the clay-sized fractions (including dried salts and organic surfactants that could be separated from the clays); whereas lower radium activities would become affiliated with sand-sized fractions.

2.3 Materials and Methods

2.3.1 Sample Collection

Representative dewatered residual solid waste was collected in ~20 liters (5 gal) buckets from a hydraulic fracturing, residual waste-processing facility located in Pennsylvania. The buckets were transferred to laboratories at the Pennsylvania State University and stored at room temperature prior to testing. The water content of the residual waste was 53% by weight as determined gravimetrically and in triplicate from multiple well-mixed buckets.

2.3.2 Size Classification

Size classification was determined using USA standard testing sieve ASTM E-11 specification by WS Tyler Incorporated. The solids were size-classified by wet sieving through US sieve mesh #70 through #230 (212 μm to 63 μm), and immediately dried overnight in a 105 °C convection oven, after which the dry weights were recorded. All grains smaller than 63 μm, along with the wet-sieving water, were dried in the bottom pan; and this fraction thus contained some dissolved salts and organics. The samples were put into three bins based on size: +70 mesh, i.e. material retained on the #70 sieve; -70+230 mesh, i.e. material that passed through the #70 sieve but not the #230 sieve; and -230 mesh, i.e. material that passed through the #230 sieve. For simplification in discussion, material greater than sieve size #70 (+70 mesh i.e. > 212 μm) is referred to as "sand", and material less than sieve size #230 (-230 mesh i.e. <63 μm) is referred to as "clay" per ASTM D6913-04 [62]. Material between those two size fractions is referred to here as "silt".

2.3.3 Hydroacoustic Cavitation System

We employed a pilot-scale system that included hydroacoustic cavitation, which could be coupled with advanced oxidation (herein identified as "HAC-AO"). This system was developed by Furness-Newburge, Inc. (Versailles, KY). Its components are scaled to pilot size and are similar to those used in industrial and sand reclaim systems as adapted under the registered trademark names of Sonoperoxoneff and Pneucol®; and these modular components can be put in parallel to treat greater masses, up to 2 tons per hour. The system circuit was as shown in Figure 2.1. The system has been used by previous Penn State researchers: Liu *et al.* (2017) [61] and Barry *et al.* (2015 and 2017) [62,63]. The hydrocyclone and spiral used in these tests had been previously used by Benusa and Klima (2009) [70]. The HAC-AO system consists of a 227 L (60 gal) polyethylene conical "*feed*" tank (61 cm diameter and 107 cm height [24" diameter and 42" height]), a 5 HP centrifugal pump (3450 RPM) with Bluffon fixed-speed motor, a 11.43 cm to 15.24 cm (4.5 in by 6 in) ID and 16.51 cm (6.5 in) OD stainless steel ultrasonic chamber controlled by an ultrasonic generator operating nominally at 25 kHz with an automatic frequency control unit, and a cavitation chamber designed to cause hydrodynamic cavitation within the flow field of passing fluid. The circuit was piped with 3.81 cm (1.5 in) diameter PVC schedule 80 piping. Three way valves along the circuit enabled flow to be in the recirculation mode (without cavitation or ultrasonics) or in operation mode (with cavitation and ultrasonics).

The hydroacoustic cavitation circuit was then connected to a Krebs urethane hydrocyclone (MOD U4-in-10°) with inlet pressure of 103 kPa (15 psi). The hydrocyclone is a device used for size separations on a slurry stream. The slurry was fed

tangentially via the inlet. As the slurry flowed through the hydrocyclone, centrifugal forces caused coarse particles to migrate to the wall of the hydrocyclone and out through the bottom. This material was classified as the "*underflow*". Meanwhile, a counter vortex pushed finer particles along with the bulk of the water up through the top vortex. This material was classified as the "*overflow*". By the principles of the hydrocyclone, the overflow will host a lower percent of solids, smaller particle sizes, and larger flow rates, while the underflow will have a high solids percent, larger particle sizes, and lower flow rates. After separation by the hydrocyclone, the spiral concentrator was deployed to further separate the solids. A Multotec SX7 single-start two-stage seven-turn spiral concentrator was used. The spiral was operated as a closed-circuit consisting of a 5.08 cm by 3.81 cm (2 in by 1.5 in) centrifugal pump (Ash, MOD 5 ME), 15 HP motor (Westinghouse, 460 V, 1760 rpm) with variable frequency controller (ABB), and 378 L (100 gal) stainless steel sump. The spiral concentrator operated by gravity separation as the slurry flowed along the descending spiral trough. Low density particles were forced to migrate to the outer perimeter, while high-density particles migrated to the inner perimeter. After four turns, the most-dense materials were diverted into the center column, while the remaining slurry continued to flow down the trough. The splitter box, located at the end of the trough, partitioned the slurry into six streams or ports. Samples were collected at this point from each of the spiral "*ports*". For these tests, fines were concentrated to the inner ports (1-3), while coarse-grained material was at the outer ports (4-6). The densest particles, were rejected from the first stage through the center column (port 7).

2.3.4 Pilot Scale Experimental Methods

The residual solids were mixed with University Park municipal tap water to prepare a 5% solids slurry, and then this slurry was sieved through US #16 mesh (1.2 mm). This tap water source was used because of its convenience at our pilot plant, and hosted negligible radium. The sieving removed grains that could otherwise clog the pump impellers; and few grains were found larger than 1.2mm. This slurry was introduced into the 50-gallon "*feed*" tank (Figure 2.1). The HAC-AO system was run as a pseudo-batch reactor: flow was recirculated from the feed tank, bypassing the cavitation box through the hydroacoustic chamber and back to the feed tank to homogenize the material. This recirculation was done with hydroacoustic cavitation turned off. After about 2 minutes of homogenizing the material, the components of interest for each run were turned on and the system operated for 10 minutes. After this 10 minute operation, the flow was diverted to the hydroclone, where the "*underflow*" and "*overflow*" were collected in ~20 L (5 gal) buckets and a ~200 L (55 gal) drum. The overflow and underflow material were separately processed through the spiral concentrator. For each run, samples were collected from the feed tank, underflow, overflow and spiral outlet ports (see Figure 2.1). These samples were then size-classified as described above. The following experimental conditions were chosen to test the hypothesis:

1. No HAC Control: This was the Control run. The slurry was not sent through the cavitation box and the ultrasonics unit was not operating. Recirculation proceeded for 10 minutes before passing the slurry through the

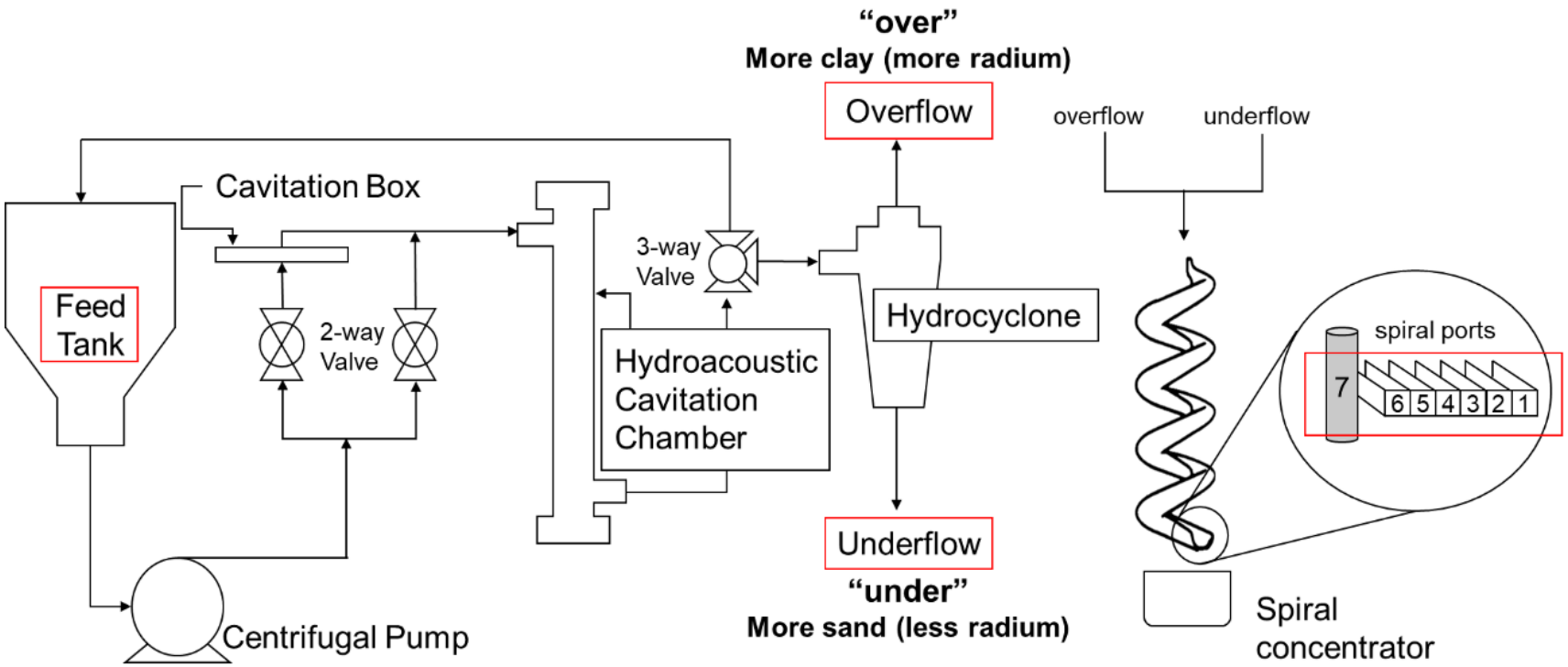

Figure 2.1: The Furness Newburge hydroacoustic cavitation circuit showing process flow and components (not to scale). Slurry from the *feed tank* was circulated through the cavitation box and hydroacoustic cavitation chamber for treatment. Following treatment, the slurry was pumped to the *hydroclone*: slurry came in through the inlet and two outflow streams were created: the underflow – with larger grains and higher solids concentration; and the overflow – with smaller grains and lower solids concentration. The hydrocyclone separated particles by size – fines were diverted to the overflow while coarser particles were diverted to the underflow. Next was the *spiral concentrator*: the underflow or overflow slurry was pumped upward from the sump to the top of the stack. Separation by gravity occurred as the slurry flowed downward through the spiral trough. The repulper at the end of the first stage (after 4 turns) rejected very coarse material into the central column (port 7). The remaining slurry passed over the final 4 turns and discharged through the spiral ports. The spiral separated particles primarily by density – low-density particles were diverted to ports 1 & 2, while high-density particles were diverted to ports 3-7. Red boxes denote sampling points. After [62] and [70].

hydrocyclone.

2. HAC: Hydroacoustic cavitation was implemented (without ozone or hydrogen peroxide). The slurry was sent through the cavitation box and the ultrasonic unit was operating at 100% frequency power. Recirculation proceeded for 10 minutes before passing the slurry through the hydrocyclone.

Additionally, two conditions were included for further analysis to evaluate the redistribution of radium. These were:

3. HAC-AO: Hydroacoustic cavitation coupled with advanced oxidation (AO - hydrogen peroxide, at a dose of 0.1% (1,000 mg/L), and near-saturated ozone (at a rate of 566 L/m (20 SCFM) from an oxygen-to-ozone system). Based on prior trials, this H_2O_2 plus ozone dose in freshwater was found to generate about $0.5 - 1$ mg/L of OH* radical [71].
4. HAC-LR: Hydroacoustic cavitation (no AO) for a longer run (LR) of 30 minutes operation as opposed to 10 minutes. We conducted limited tests with HAC-LR.

Representative samples from these additional runs provided further insight into the effect of HAC-AO or HAC-LR on radium management and will be further discussed.

We also collected an "As received" solid sample, which was directly sampled from multiple representative and well mixed ~20 L (5 gal) buckets. To collect a "feed" sample, we passed the 5% slurry around the recirculation loop (without HAC or AO) for 2 minutes, to achieve a uniform mix, and then collected the slurry sample from the recirculation outlet at the feed tank.

2.3.5 Toxicity Characteristic Leaching Procedure

The EPA Method 1311 Toxicity Characteristic Leaching Procedure (TCLP) [72] evaluated the mobility of ^{226}Ra and inorganic cations from the treated solids after HAC-AO, HAC, or the Control treatment. The TCLP is intended to mimic the chemical conditions of a landfill environment. The extraction fluid (fluid #2 – 5.7 mL glacial acetic acid diluted to a volume of 1 L using reagent water) was mixed with solid samples at a 20:1 fluid-solid mass ratio in 250 mL Nalgeneff polypropylene flat bottom centrifuge tubes. After mixing for 18 hours, the suspension was centrifuged on an Eppendorf 5810R centrifuge at 3,000 RPM for 10 minutes. The supernatant was filtered through a 0.7 μm TCLP glass fiber filter (Pall Laboratory) and then transferred to a 50 mL test tube, acidified to <pH 2 with concentrated nitric acid, and stored at 4 °C until analyses using inductively coupled plasma atomic emission spectrophotometry (ICP-AES). The solid residue was then dried and the ^{226}Ra activity of this solid was determined by gamma spectroscopy (see description below).

2.3.6 Sequential Extractions

Radium (and major metal) association in the size-classified solids was determined by a four step sequential extraction procedure that we modified from [73] and [74]. The extractions were performed at a 20:1 fluid-to-solid mass ratio in which the extraction fluids were chosen to determine radium association with salts/evaporated pore water (Step 1: distilled–deionized water for 24 hours); with surface sites (Step 2: 1M ammonium acetate for 12 hours); with carbonate minerals (Step 3: 9% acetic acid for 12 hours); and with metal oxides (Step 4: 0.1M hydrochloric acid for 12

hours) (see Table 2.1). The initial ^{226}Ra activity, prior to Step 1 extraction, of the "As received" solids, or wet sieved, size-classified treated solids was classified as Step 0. It is noted that none of these extraction steps would dissolve barium sulfate.

The sequential extractions were carried out in 250 mL Nalgene® polypropylene flat bottom centrifuge tubes. After each extraction, the suspensions were centrifuged on an Eppendorf 5810R centrifuge at 3,000 RPM for 10 minutes, and then decanted. The pelletized solids were then rinsed with distilled-deionized water at about two-thirds the volume of the extraction fluid. All rinsates and supernatants were combined, filtered through a 0.7 μm TCLP glass fiber filter (Pall Laboratory), transferred to 50 mL test tubes, acidified to <pH 2 with concentrated nitric acid, and then refrigerated at 4 °C until ICP-AES analyses. The resulting pellets were oven-dried and ^{226}Ra activity in the solid was determined by gamma spectroscopy (as described below).

2.3.7 Major Metals Analyses

Elemental compositions of the acidified supernatants (Li, Na, K, Mg, Ca, Sr, Ba, Mn, Fe, and Al) were determined using ICP-AES on a Perkin-Elmer Optima 5300DV optical Emission Spectrometer per EPA standard 200.7.

2.3.8 Radium Analysis

Radium-226 activities of all solid samples were determined by gamma spectroscopy on a Canberra ultra-low background small anode germanium (SAGe) well detector, after the incubation period of three weeks. The reported ^{226}Ra activity was the average of the daughter products activities (^{214}Pb at 295.2 keV and 351.9 keV, ^{214}Bi

Table 2.1: A four step sequential extraction was designed to investigate radium associations in the HAC-treated residual waste. After [73] and [74]. Extractions performed with 20:1 fluid-to-solid ratio. After extraction, solids were separated by centrifugation, rinsed with DI water, and dried. Radium-226 activities of the dried solids were determined by gamma spectroscopy.

Step	*Description*	*Extraction Targets*	*Target Examples*
0	Oven dried "As Recvd" and wet sieved, size-classified solids (includes TDS)	No extraction	All soluble and insoluble solids
1	Distilled-deionized (DI) Water for 24 hours	Soluble salts/evaporated pore water	$NaCl$, $BaCl_2$, $CaCl_2$, & $SrCl_2$
2	1M Ammonium Acetate for 12 hours	Surface exchangeable/ low-charge interlayer	From surface of sand and silt grains; from illite clay interlayer
3	9% Acetic Acid for 12 hours	Carbonate minerals	$CaCO_3$, $MgCO_3$, $Al_2(CO_3)_3$ & $Fe_2(CO_3)_3$
4	0.1 M Hydrochloric Acid for 12 hours	High-charge interlayer/partial silicate/oxides	MnO_x, FeO_x

at 609.3 keV). The standard error was reported and the error calculation is included in Appendix A.2. The sample geometry used was a Wheaton 24 mL poly seal cone-lined urea capped HDPE liquid scintillation vial with counting efficiencies determined using the certified UTS-2 uranium tailings provided by the Canadian Certified Reference Materials Project (CCRMP). The efficiencies of the samples were corrected for height and density, as these factors could otherwise cause a 5-40% affect in apparent ^{226}Ra activities. We monitored ^{226}Ra because it is the prominent radioactive parent in unconventional oil and gas wastes and its long half-life (1600 years) makes it persistent in the environment. Because radium's isotopes are chemically identical, the results presented for ^{226}Ra should be consistent for ^{228}Ra [75,76].

Sample masses ranged from 5 g to 35 g. To control for mass, we counted our standards within similar masses of 8g to 40 g, and develop a regression for the efficiencies at the varying masses we encountered. Counting time ranged from a few hours to a few days, because data collection was terminated either when the counting error was lower than 5% or counting time had exceeded 48 hrs. with insignificant counts. Most samples were counted once. Representative samples were tested in triplicate, and found to be within $1 - 3\%$ of one another.

2.3.9 Materials

All analytical chemicals were reagent grade and supplied by VWR. Distilled deionized water was provided by the ThermoScientific Barnstead Nanopure water system with resistivity at $18.2\, m\Omega$. The extraction fluids for the toxicity characteristic leaching procedure and sequential extractions were stored in glass Pyrex bottles at room temperature. Optical light microscope images were acquired on a Zeiss Axiophot microscope.

2.4 Results

2.4.1 Pilot Scale Trials for Raw Material Recovery

We conducted grain size analysis of the treated solids that were recovered at the "*feed*" tank, "o*verflow*", "*underflow*", and the "*spiral ports*" (Figures 2.2A – 2.2F). In this figure, fine particle streams will plot high and to the left, while coarse particle streams will plot low and to the right. In the No HAC Control run (Figure 2.2D), the overflow and underflow overlap – showing that the two streams had very similar particle sizes because no disaggregation had occurred. When HAC was

applied (Figure 2.2A), particle disaggregation occurred – the clays were separated from the sand and the hydrocyclone successfully created two distinct streams of clay versus sand. The material collected from the overflow has plotted higher than the material collected from the underflow, indicating finer grain size in the overflow than the underflow, with both streams having distinct particle sizes from the feed material that entered the system.

In our Control run (No HAC), there was no particle disaggregation, and thus no subsequent physical separation was observed in the spiral effluents (ports 1 and 2) when processing the overflow (Figure 2.2E). Likewise, there was little physical separation observed in the spiral port 7 when processing the underflow (Figure 2.2F). In contrast, when the solids were treated with HAC, the physical separation devices successfully separated the disaggregated solids into a clay-rich stream that discharged from the overflow versus a sand-rich stream that discharged from the underflow (Figure 2.2A). Moreover, when the overflow was passed through the spiral, a clay-rich stream could be gleaned from ports 1 and 2 (Figure 2.2B), and when the underflow was passed through the spiral, a sand-rich stream could be gleaned from ports 3 and 7 (Figure 2.2C). Indeed, HAC treatment (even without AO) resulted in a particle stream from the overflow that was 82% – 88% "clays" ($<$ 63 μm) through ports 1 and 2; and these ports constituted about 90% of all the overflow solids. Furthermore, the particle stream following HAC from the underflow was as high as 76% "sand" ($>$ 210 μm) through port 7 and 51% though port 3 (Figure A3); and these ports constituted about 72% of all underflow solids. Thus, the HAC-hydrocyclone-spiral unit operations could offer a means for recovering these raw materials.

With HAC-AO, the sand recovery from port 7 was 61%. Without HAC, the control offered only slight separation of sizes (Figure A3).

The mass balance-normalized recovery of raw materials is shown in Table 2.2. The recovery of sand through ports 3 and 7 was ~38% when treated with HAC versus only 3% for the Control – No HAC. The recovery of clays through ports 1 and 2 was ~15% when treated with HAC versus ~10% for the Control – No HAC. Without HAC treatment, the underflow contained 36% clay; compared to only 20% when treated with HAC.

Table 2.2: Summary of the mass-balance normalized raw material recovery for control (No HAC) and treatment (HAC). Up to 15% of the residual solid waste can be reclaimed as clays and 38% as sand.

Sampling point	*No HAC*		*HAC*	
	Clay	*Sand*	*Clay*	*Sand*
Feed	24%	35%	47%	23%
Overflow	8%	1%	11%	0%
Spiral Port 1	8%	1%	10%	0%
Spiral Port 2	2%	0%	5%	0%
Underflow	36%	7%	20%	14%
Spiral Port 3	5%	1%	2%	3%
Spiral Port 7	6%	2%	3%	35%

The percentage represents how much of the material sampled was clay (< 63 μm i.e. #230 mesh), or sand (>210 μm i.e #70 mesh), relative to the starting mass of the "As Received" material.

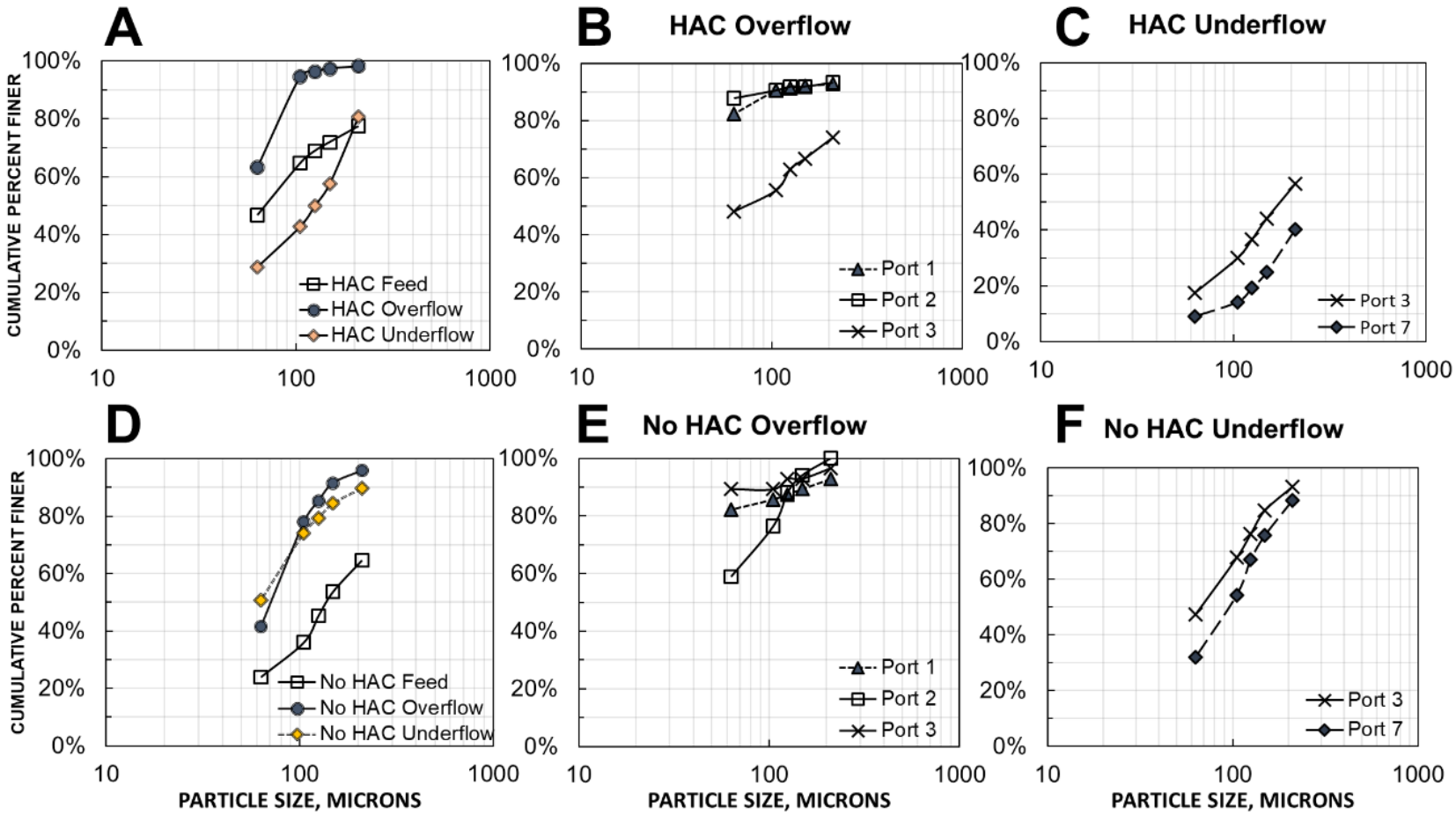

Figure 2.2: Grain size analysis of HAC treatment (without AO – panels **A**, **B**, & **C**) and Control (No HAC – panels **D**, **E** & **F**) of solids collected at sampling points downstream of the treatment system. Fine particles will plot high and to the left, while coarse particles will plot low and to the right. Grain size analysis performed using US mesh sieves per ASTM D6913-04 from < 63 μm (#230 mesh i.e. clay) to >210 μm (#70 mesh i.e. sand). HAC causes disaggregation of homogenized solids when processing dewatered residual solids in 5% slurry with municipal tap water (for HAC treatment (panel **A**) compared to the No HAC Control (panel **D**). Fine particles go to the overflow and large particles go to the underflow. Disaggregated solids can be further separated by the cyclone and spiral – with HAC, the process achieved higher concentration of clay (panel **B** vs **E**) and sand (panel **C** vs **F**). HAC treatment results in a distinct particle size distribution.

Optical microscope images provided a visual assessment of the performance of these treatments. Figure 2.3 shows the HAC-treated reclaimed sand (underflow port 7) as compared to the untreated, as-received material. As shown, the disaggregating effect of HAC treatment removed the adhered/aggregated clay particles, and yielded clean, clear sand grains.

The control, without HAC, yielded grains that looked much like the "As received" material (photo not shown herein).

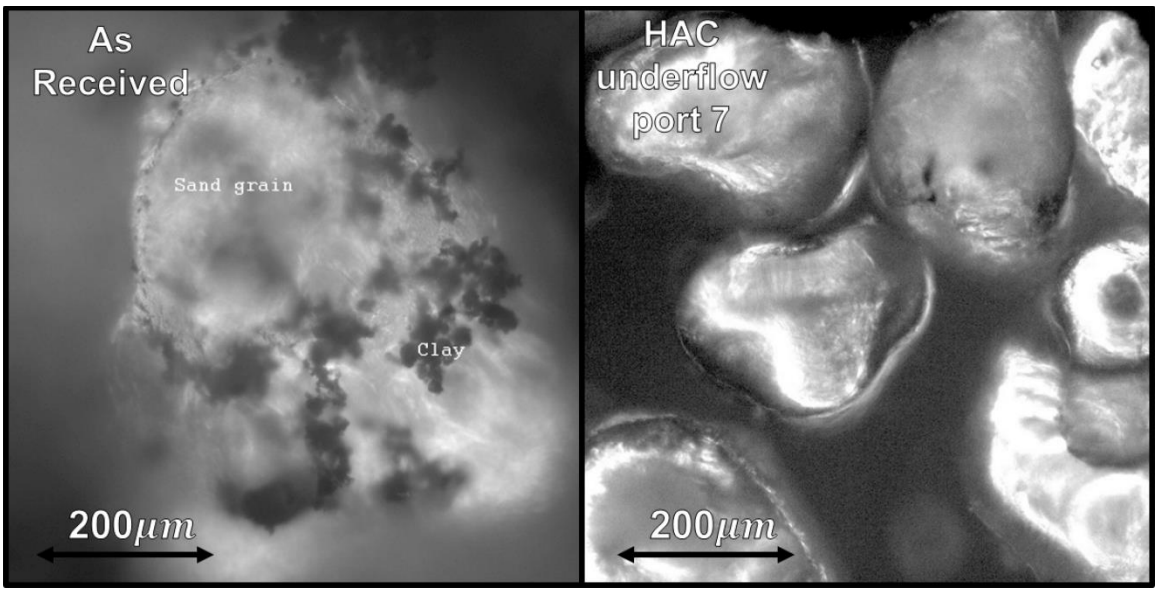

Figure 2.3: Optical light microscopy (Zeiss Axiophot microscope) provided visual assessment of the "As received" sand grains aggregated with clays and fines on their surfaces (left panel), compared to the HAC treatment (right panel), which was effective at disaggregating the clay fines off the sand. Further physical separation devices resulted in reclaimed sand that was free of clays and silts.

2.4.2 Toxicity Characteristic Leaching Protocol (TCLP)

The mobility of major elements and radioactivity of the selected size-classified solid waste samples was assessed using the TCLP to investigate whether HAC treatment increased the leachability of these elements from the residual solid waste material (Figures 2.4 & 2.5). These results showed that radium did not leach from any of the samples, except for the "As received" clays (Figure 2.4). For all other cases, radium activities of the treated solids remained the same before and after the TCLP extraction. This indicated that there would be less risk of radium leaching from solids following treatment by HAC or HAC-AO than for solid materials that received no treatment.

We also monitored the mobility of several major elements (Li, Na, K, Mg, Ca, Sr, Ba, and Mn) that could be leached from these solids during the TCLP extraction (Figure 2.5). Although iron and aluminum were also monitored, their concentrations were always below detection. Barium leached extensively from the "As received" material, and especially from the "As received" clays, but it did not leach significantly from any of the treated solid samples. Strontium, sodium, lithium and potassium leached the most from the "As received" and "feed" samples, and from the No HAC overflow. Calcium and magnesium leached from many of the treated samples.

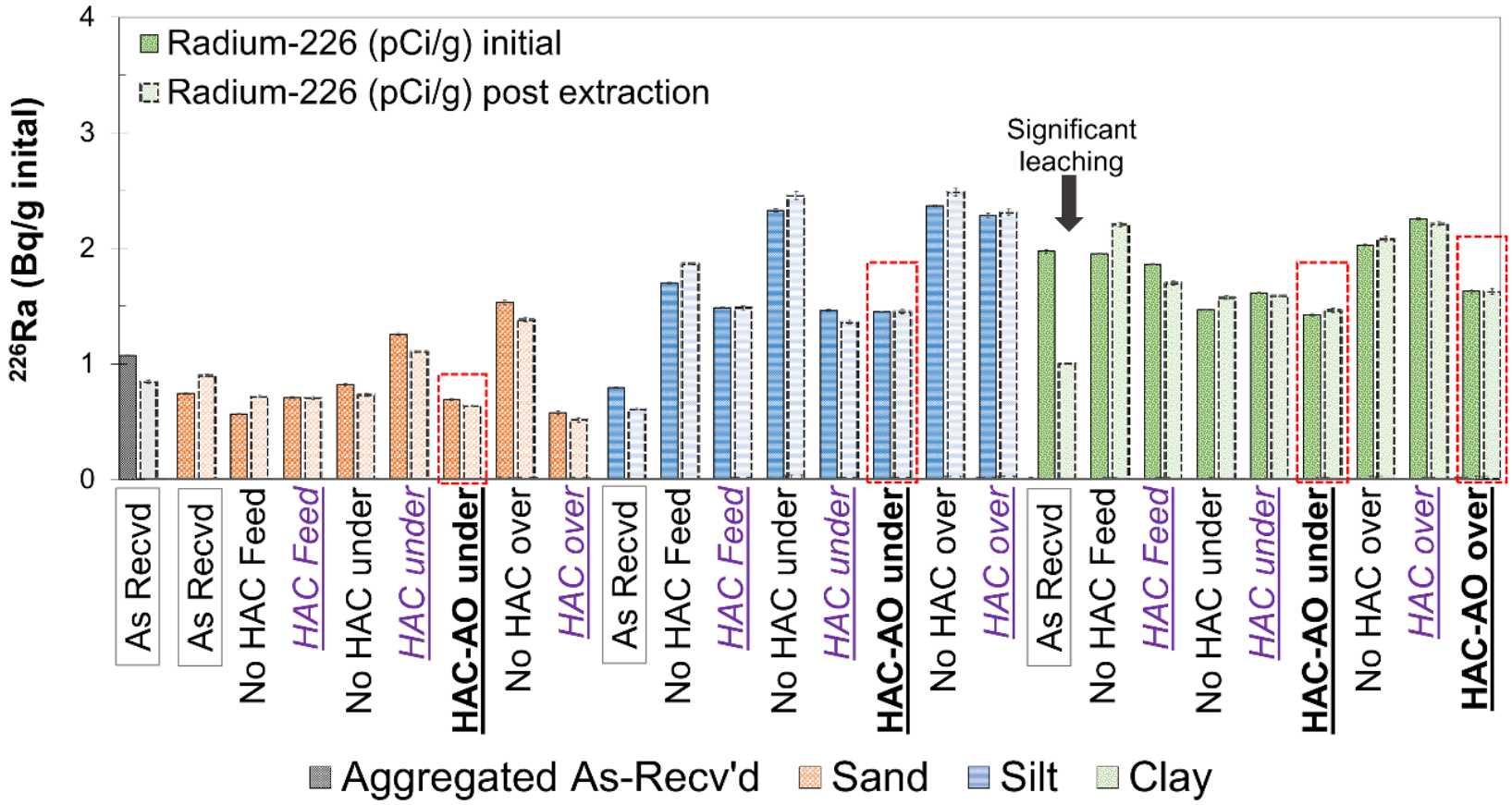

Figure 2.4: Radium-226 activities on the size-classified solids from various sample ports: initial and post TCLP extraction. Radium-226 activities (Bq) have been normalized to initial mass (g) of the solid prior to extraction. Error bars denote combined standard error in radium measurements and mass measurements. Samples were taken from the feed, hydrocyclone, underflow (under), and overflow (over). Red boxes highlight HAC-AO treatment. Size classification using US mesh sieves per ASTM D6913-04: < 63 μm is clay (#230 mesh), >210 μm is sand (#70 mesh), and in-between is silt. Radium leached significantly from the "As Received" clay sized solids. These results indicated that treatment diminished the risk of radium leaching out in the landfill.

When comparing Figure 2.4 with Figure 2.5, we observed that radium mobility strongly followed barium mobility. Specifically, the TCLP extracted both radium and barium from the "As received" clays; but following treatment, the TCLP extracted minimal amounts of radium or barium.

Following any of these HAC or HAC-AO treatments, the barium concentration in the extractants was 0.8 mg/L to 2 mg/L (Table A1), compared to levels of 2 to 13.5 mg/L for the No-HAC Control. Notably, all these extractant levels following treatment were far below the TCLP regulatory limit of 500 mg/L. The concentrations of the other metals in the extractants from the treated solids were all less than 5 mg/L, indicating that there was little potential for leaching from HAC-treated materials.

2.4.3 Sequential Extractions

Radium and major metal associations in the size-classified solids were determined by a four step sequential extraction procedure modified from [73,77] and [74] (Figures 2.6 & 2.7). These samples were selected to represent recoverable sand (sand fraction from underflow port 7), recoverable clay (clay fraction from overflow port 1), and the intermediate silts that would be disposed (silt fraction from underflow).

For all size fractions, considerable radium was leached during step 4 – and to a lesser extent during step 3 (Figure 2.6). The cations that leached most during step 4 were Ba, Sr, Fe, and Al (Figure 2.7), indicating that radium was likely associated with their oxides. During step 3, it was the Ca, Mg, and Fe-carbonates that could be extracted – along with some radium that was associated with these carbonates. For the "As received" samples from each size-classification, the barium leached far

more during steps 2, 3, and 4 than barium leached from the treated samples (Figure 2.7).

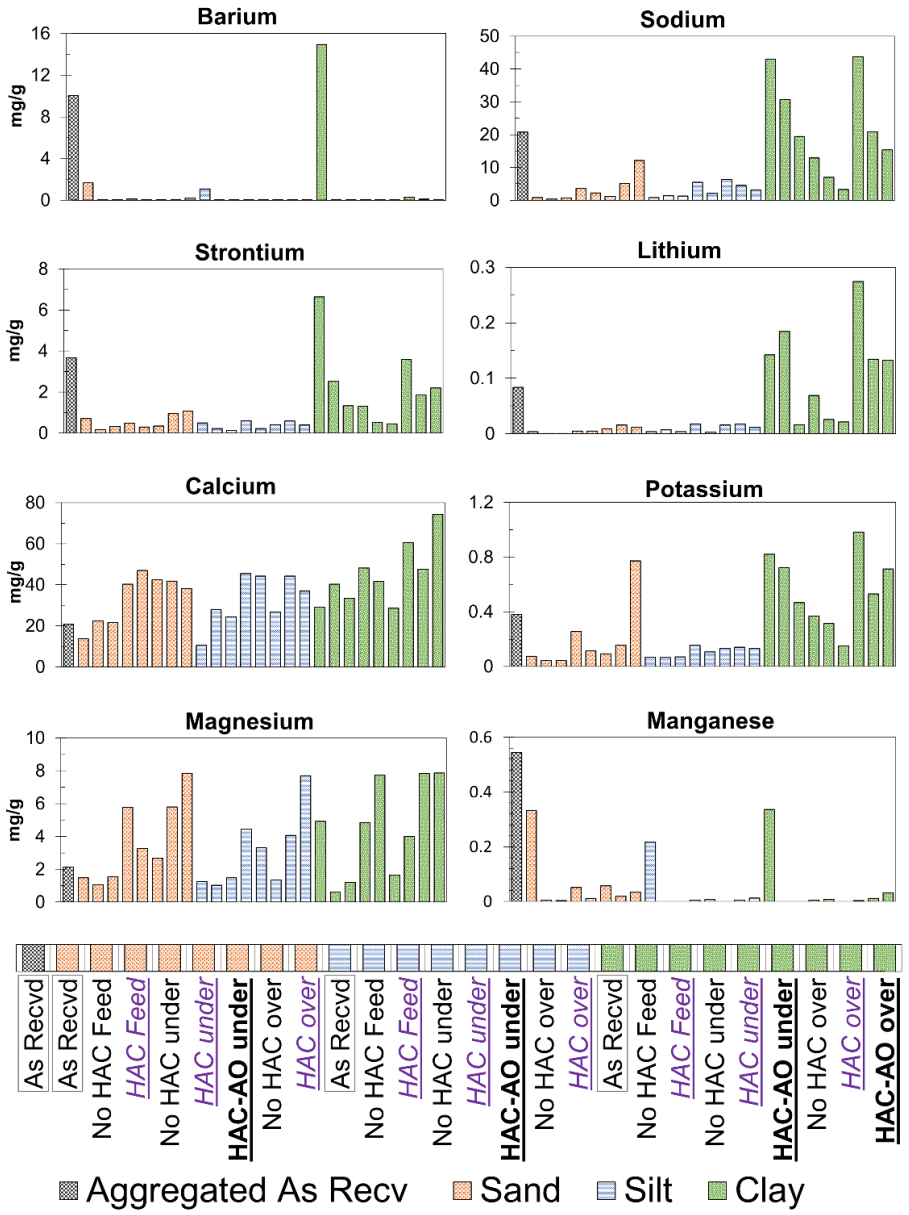

Figure 2.5: Major metal mobility of the size-classified samples following TCLP extraction, in mg metal extracted per initial g of solids. Samples were taken from the feed, hydrocyclone, underflow (under), and overflow (over). Radium mobility strongly followed barium mobility. Leaching did not result in concentrations above regulatory limits for TCLP and landfill disposal.

Sequential extractions of the reclaimable sand (underflow port 7), revealed minimal radium leaching during steps 1 and 2 when HAC or HAC-AO was applied; and more radium leached during steps 3 and 4 – indicating that in the sand matrix, radium was associated with carbonate and oxide minerals (Figure 2.6). When HAC or HAC-AO was employed, the reclaimable sands had ^{226}Ra activities of ~0.74 Bq/g (20 pCi/g). Parenthetically, when HAC was operated for an extended time of 30 minutes (i.e. HAC-LR), the sand from this underflow had ^{226}Ra activities of 0.207 Bq/g (5.6 pCi/g) (Figure A4). Thus, the HAC-LR process could yield a reclaimable sand that hosted low radium levels. Major metal mobility showed that calcium, magnesium, and iron were also greatly leached by step 3 (Figure 2.7). This infers that there could be some carbonate minerals in the sand-size particles leaching calcium, magnesium, iron, and aluminum. Step 4 leached barium, iron, and aluminum – inferring the presence of these oxides (Figure 2.7).

For all the clay fractions, the first extraction step (DI water) diminished radium activity, indicating that a substantial portion of the radium in these clay-sized fractions was affiliated with dissolvable salts and/or organic surfactants (Figure 2.6). Particularly, relative to the overflow port 1 "clays", organic surfactants, with their 0.85 – 0.95 mg/L density, would be expected to congregate at port 1. When the sequential extraction results (Figure 2.6) are overlapped with the major metals leached (Figure 2.7), it appears that radium was associated (at least in part) with strontium, lithium, sodium, and potassium salts (step 1); with calcium, magnesium, iron, and aluminum carbonates (step 3); and with strontium and iron oxides (step 4). Amongst these clay-rich samples, there was limited radium leaching after step 2, indicating again that radium was not associated with surface sites or low-charge clay interlayer sites.

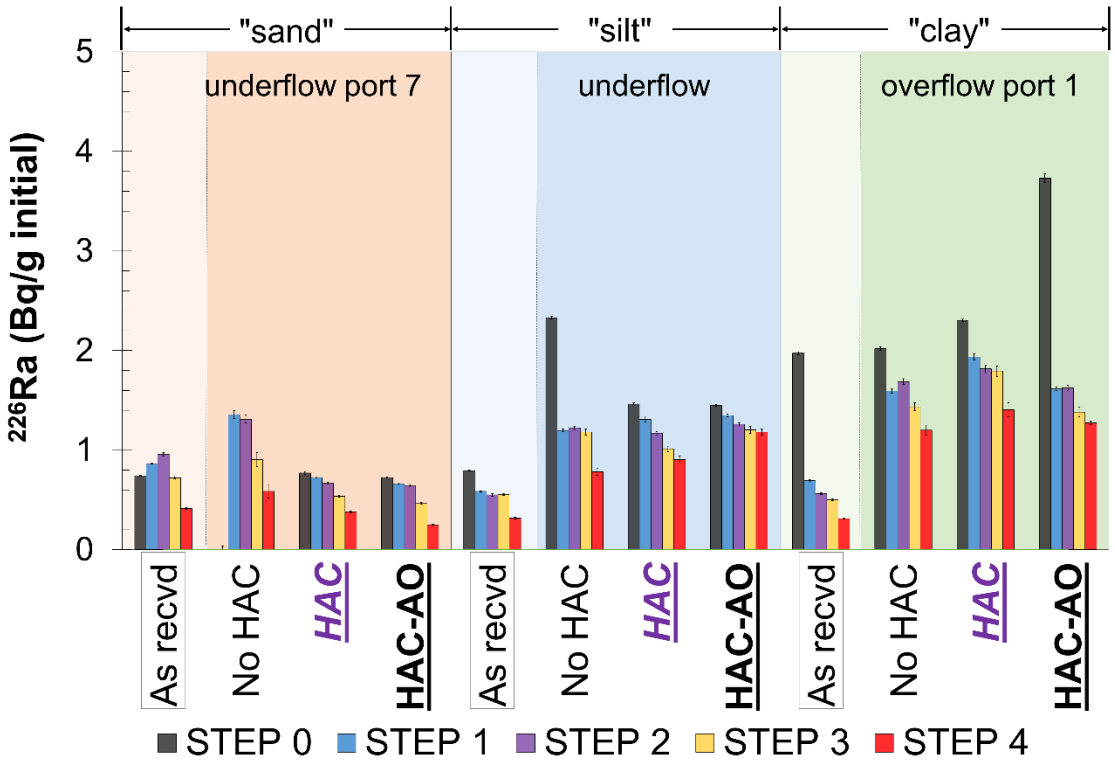

Figure 2.6: Radium-226 activities of the sequentially extracted, size-classified, treated solids. Radium-226 activities (Bq) have been normalized to initial mass (g) of the solid prior to extraction. Error bars denote combined standard error in radium measurements and mass measurements. Step 0 (■): Initial solid; Step 1 (■): DI water rinse for soluble salts; Step 2 (■): 1M ammonium acetate for surface sites; Step 3 (■): 9% acetic acid for carbonates; Step 4 (■): 0.1 M hydrochloric acid for oxides. shading for sand, for silt, and for clay. The "As received" samples are demarcated with a lighter shade.

We also monitored the mass loss that occurred during each extraction (Figure 2.8). While the dissolution of carbonate minerals during step 3 accounted for the greatest mass loss (Figure 2.8), radium did not follow this trend, as step 1 accounted for the greatest radium leaching. This is suggestive that radium association with the

clays was not by interlayer adsorption but instead, radium was associated with the dried salts that had precipitated out of solution during the drying process after wet sieving – and also possibly with organic surfactants.

Finally, for the silts (underflow) that we presume will be disposed, sequential extractions showed that radium was not made more mobile following HAC-AO treatment compared to the Control samples. Although a greater portion of this HAC-AO silt fraction contained oxides (step 4) (Figure 2.8) – possibly strontium, iron, and aluminum oxides (Figure 2.7) – radium was not released during their dissolution. Metal mobility also showed the presence of calcium, magnesium, iron, and aluminum carbonates (step 3) (Figure 2.7). However, none of the treatments rendered radium more readily leachable from the silts.

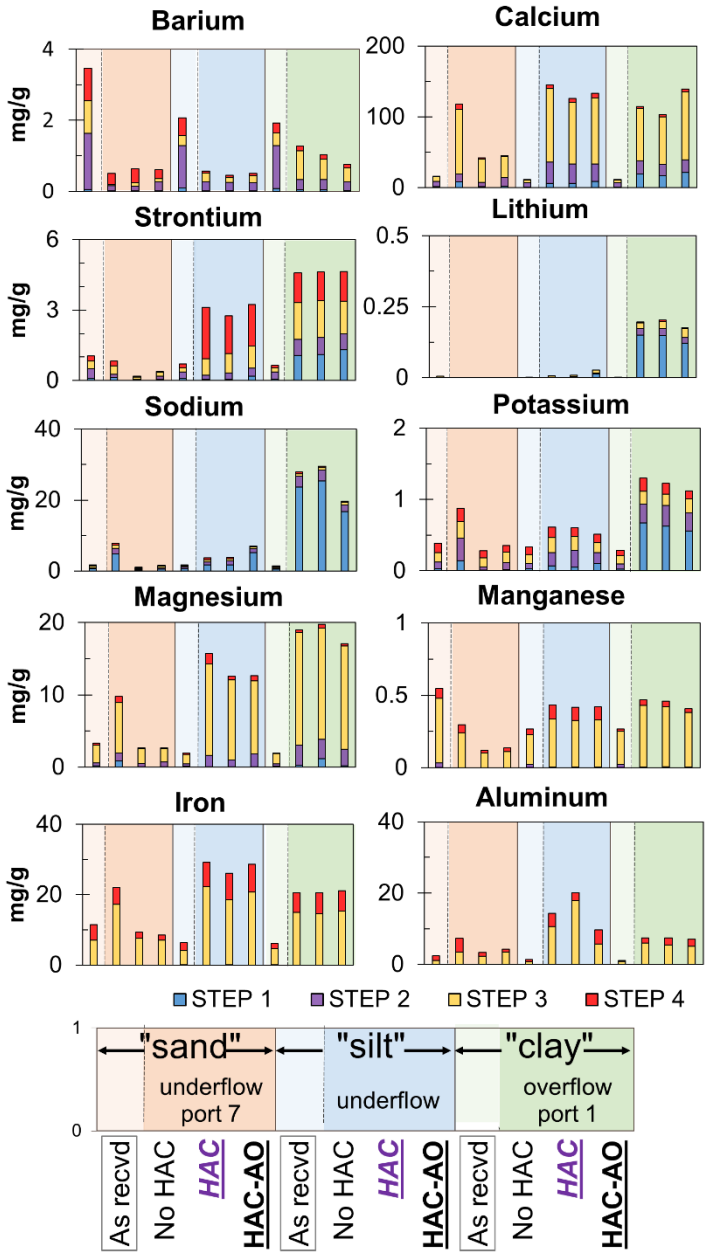

Figure 2.7: Major metal mobility of the size-classified, sequentially extracted samples in mg metal extracted per g of solids prior to each extraction step. Step 1 (■): DI water rinse for soluble salts; Step 2 (■): 1M ammonium acetate for surface sites; Step 3 (■): 9% acetic acid for carbonates; Step 4 (■): 0.1 M hydrochloric acid for oxides. shading for sand, for silt, and for clay. The "As received" samples are demarcated with a lighter shade.

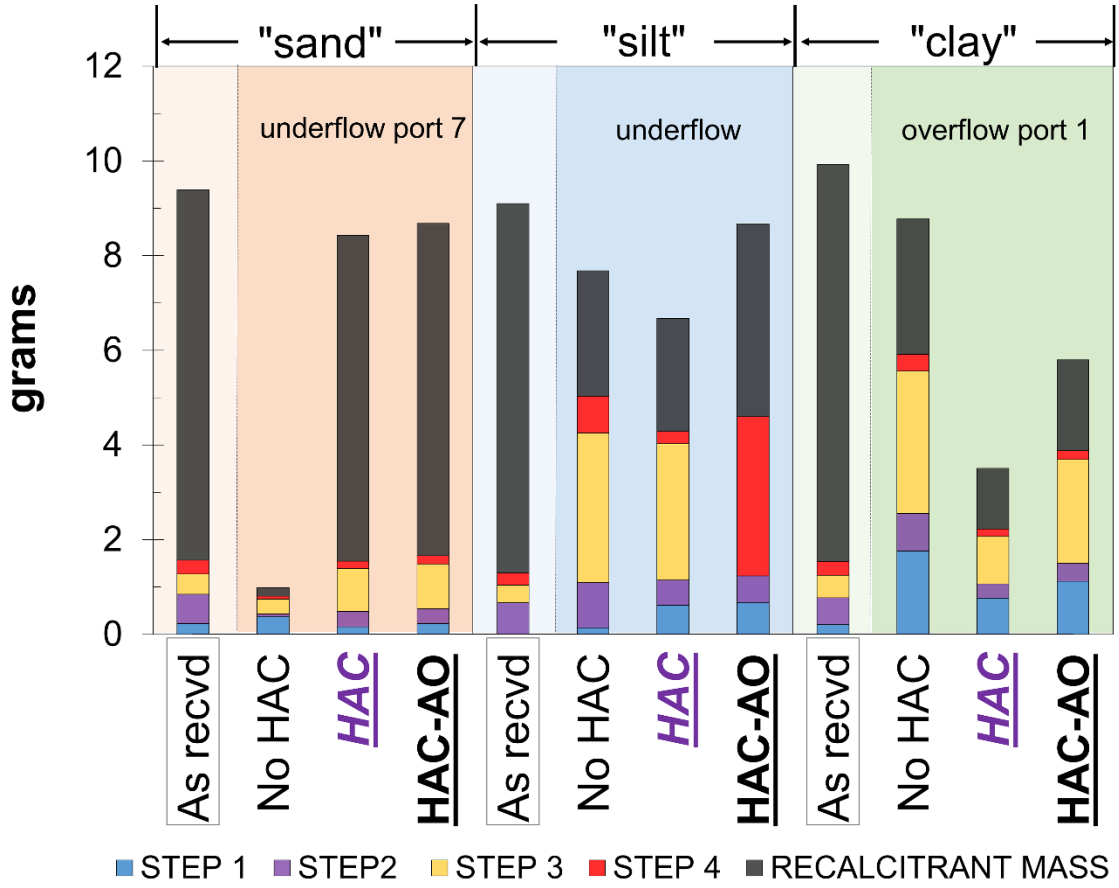

Figure 2.8: Mass lost from the size-classified solids following sequential extractions. Step 1 (■): DI water rinse for soluble salts; Step 2 (■): 1M ammonium acetate for surface sites; Step 3 (■): 9% acetic acid for carbonates; Step 4 (■): 0.1 M hydrochloric acid for oxides; and Recalcitrant mass (■) following steps 1-4. shading for sand, for silt, and for clay. The "As received" samples are demarcated with a lighter shade.

2.5 Discussion

2.5.1 Raw material recovery: HAC treatment resulted in the disaggregation of residual solids, allowing for sand and clay separation

The market for hydraulic fracturing sand continues to grow as increased drilling activity, greater sand demand and a globally diminishing supply of suitable sand drive prices higher. It is becoming necessary to seek out alternative sources for raw materials. The quality of sand used as hydraulic fracturing proppant is specified by the API RP 19C/ISO 13503-2 standard [78]. The standard includes specifications for particle size, roundness and sphericity, among others. The HAC treatment herein resulted in the recovery of sand particles that had properties consistent with those required by the API standard. The reclaimed sand grains herein were all retained on the US #70 sieve sizes and hence could be utilized as 40/70 proppant (i.e. sand between #40 and #70 sieves). Optical microscope images revealed that these sand grains also had similar roundness and sphericity as required by the API standard. In addition, when HAC treatment was applied for 30 minutes, the radium activity on the sand grains could be as low as 0.207 Bq/g (5.6 pCi/g), which offers a reduced risk for worker exposure to radioactivity. The HAC treatment of the residual waste also resulted in the concentration of fine clays. These clays (and dried salts/organic surfactants) were found to have high radium activities, as high as $1.85 - 3.7$ Bq/g ($50 - 100$ pCi/g). However, more than half of the radium in these dried solids was associated with salts or organic surfactants, and was mobilized when the dried solids were suspended in DI water. These salts and surfactants could be returned back downhole with the hydraulic stimulation fluid; and they would thus not end up with landfilled solids.

We anticipate that by passing the underflow material through the HAC or HAC-AO systems a second time, we could achieve even more sand and clay recovery, as the underflow following one pass still contained 20% clays by mass when size fractioned (Table 2.2). While these clays are not presently of market value, the accumulation of radium presents an opportunity to revise the current management practices for radioactive residual waste.

Assuming a waste generation of 5,000 tons per year from such a facility as encountered by this work, HAC treatment can result in the generation of marketable source sand that could be valued around $40,000 to $80,000 per year, when sold at a fraction of the price of freshly mined sand (Table 2.3). This value can be 3 to 5 times greater if resin coated sands or ceramic proppant have been used [79]. In 2017, 6,700 tons of residual sludge waste from facilities treating oil and gas wastewater was recorded as being disposed in PA landfills (Figure A2). The reduction in sludge waste volume as a result of sand and clay reclamation with treatment via HAC could reduce landfill costs by about $100,000 to $300,000 per year in Pennsylvania. This is a significant cost savings for waste management operations.

Table 2.3: Summary of the raw material recovery and market opportunity from HAC-treated residual waste assuming a disposal volume of 5,000 tons/y.

	Recovery	*Price of pristine material*	*Estimated benefit assuming 5,000 tons/y of residual solid*
Silica Sand	~37%	$84/ton [35]	Resell at $30/ton = $50,000 - $60,000/y
Resin coated/ Ceramic proppant	~37%*	$200 - $500/ton [79]	Resell at $70 - $150/ton = $130,000 - $280,000/y
Wasted Material	~63%	-$76/ton [80]	Potential cost savings of $140,000/y

* Assuming similar recovery of resin coated sand or ceramic proppant as for silica sand.

2.5.2 Radium associations in the residual solids: HAC treatment diminished radium and barium mobility

The combination of the modified TCLP and sequential extractions gave insights into radium mobility and radium association in the HAC-treated residual waste solids. Firstly, without treatment, the clay-sized particles (<63μm) showed unfavorably high potential for losing radium and barium through leaching in the landfill. After HAC-treatment, this potential was dramatically and consistently reduced for both radium and barium. Additionally, the silt-sized (between 63μm and 210μm) and sand-sized particles (>210μm), did not show potential for leaching radium or barium following HAC or HAC-AO treatments. Radium associations in the residual waste before treatment indicated that radium was most mobile from the particle sizes less than 63μm and should be further evaluated prior to disposal.

An interesting finding was that radium was removed during step 1 of the sequential extractions, and thus perceived as being associated with dried salts or organic surfactants in this residual waste. This residual waste was collected from a facility that does not treat the wastewater with sulfate addition for radium control. There are a number of such facilities with similar operations that handle oil and gas waste. The residual solids coming from such facilities are likely to have similar radium associations.

It is possible that radium was complexed with organic compounds in this material. Such compounds could be surfactants, acetate, and EDTA. These (and especially surfactants) are used during hydraulic fracturing; and they have been detected in flowback and produced water [25,81,82]. We observed the presence of organics (enough to form a surface sheen) in the waste and slurry used in the HAC treatment; and this would be indicative that surfactants are present. Moreover, the combination of cavitation and bubbled ozone resulted in dissolved air that accumulated in the ultrasonic chamber, and apparently created a similar phenomenon as for a small-scale dissolved-air flotation unit. This resulted in the agglomeration of an organic-rich clay in samples collected from HAC and especially HAC-AO treatments. As these samples dried, we infer that the radium that had been complexed by these organic compounds became associated with the clays. The operation of the HAC system would have caused these organic-rich clays to be concentrated in the overflow and subsequently in spiral ports 1 and 2. This could be an explanation of the very high radium activity found in the clays from HAC-AO overflow port 1. The sequential extraction of these clays showed radium mobility following the first step (DI water). Our prior research with foundry green sand indicated that HAC-AO released organic residues from solid surfaces [56,68]. Thus, such radium-rich organic compounds, as well as salts, could be separated from the

clays, and returned back downhole with hydraulic stimulation fluids. We note that the chemical oxygen demand (COD) of the extractant following this step was determined to be 1,300 mg/L; indicating that indeed anionic organic surfactants, which are known to complex cationic radium [83], could in part explain the mobility of radium. In overview, the combination of radium association with salts and organics presents an opportunity for the development of new radium management practices of such residual solids.

2.5.3 Implications for disposal

The Pennsylvania Department of Environmental Protection (PA DEP) commissioned a study to investigate exposure and contamination risks from TENORM at facilities impacted by oil and gas operations [47]. The average radium activity reported by this PA DEP study for proppant sand prior to hydraulic fracturing was 8.99 Bq/kg $\pm$ 2.18 (243 pCi/kg $\pm$ 59), and after was 128 Bq/kg $\pm$ 110 (3460 pCi/kg $\pm$ 2990); while the filter cake (i.e., sludge) of nine zero liquid discharge facilities had activities that ranged from 0.111 Bq/g to 17.8 Bq/g (3 pCi/g to 480 pCi/g) [47]. The reclaimed sand from our work had radium activity as low as 0.207 Bq/g (5.6 pCi/g), with little risk for leaching of this radium; while the reclaimed clays (including salts and organics) could be as high as 3.7 Bq/g (100 pCi/g). The activity of the eventually disposed material ranged from 0.74 Bq/g to 1.48 Bq/g (20 pCi/g to 40 pCi/g). The disposed material will thus contain lower net radium mass and lower volume, thereby reducing TENORM waste disposal and landfill costs. Alternative treatment for solid waste management with elevated radioactivity can be proposed following the findings from the TCLP and sequential extractions. Radium

in the residual solids was associated with salts, carbonates, oxides, and possibly surfactants at this study site.

2.5.4 Limitations of this study

In this work, municipal tap water was used to make the slurries prior to experimental runs on the HAC system. This protocol was an inherent artefact of conducting these pilot-scale tests at Penn State, miles from the residual waste-processing facility. We acknowledge that such intentional dilution would be impractical for a full-scale operation. Instead high-TDS produced and flowback water would be present in any on-site slurries.

The fate of several heavy metals was not evaluated; however, non-heavy metal concentrations of Fe, Al, and Mn in extraction fluids following the TCLP and sequential extractions suggest that heavy metal concentration will be relatively low. Reported heavy metal concentration in Marcellus Shale produced fluids are <1mg/L, compared to barium, calcium, and magnesium at $50 - 30{,}000$ mg/L [25,84]. The concentrations of these metals (Ba, Ca, and Mg) in the extractants did not exceed 5 mg/L, therefore it is not expected that the heavy metals will have significant concentrations. Additionally, we did not attempt to quantify the effect of treatment or the leaching potential of these solids for other radionuclides such as Uranium (U). Eitrheim *et al.*[85] found that U was mobile from Appalachian drilling wastes when the TCLP was applied. U could also have been released by these solids given the sonication, cavitation, and oxidation processes involved herein.

2.6 Conclusions and Recommendations

A novel process for recovering raw material from oil and gas residual waste was presented using hydroacoustic cavitation and advanced oxidants, combined with physical separation devices to create distinct streams of highly concentrated sand and clay. The separation of particles sizes affected radium distribution – the sand grains had low radium activities, as low as 0.185 – 0.74 Bq/g (5 – 20 pCi/g); whereas the clays (along with their associated salts and organics) had elevated radium activities, as high as 1.85 – 3.7 Bq/g (50 – 100 pCi/g). We propose that the sand grains can be reused as recycled hydraulic fracturing proppant. The separation of sand from clay and silt could reduce the volume of radium-containing wastes that are disposed in landfills, and also reduce the radium mass to landfills. This could represent a significant savings to facilities handling unconventional oil and gas waste. Additionally, the reclaimed sand could have market value in hydraulic fracturing drilling, or in other silica sand-using industries. Although the clays (and associated salts and organics) are currently of little market value, their elevated radium activity presents an opportunity to revise current waste handling practices for radioactive management. Disposing these radium-enriched salts and dislodged organic compounds downhole with hydraulic fracturing fluid will lower radium exposure and therefore risk to human health and the environment. Extractions performed on the residual waste indicated that in facilities that do not perform sulfate precipitation, radium is likely to be associated with dried salts and organic compounds.

The continued development of the Marcellus Shale and the underlying Utica Shale will result in greater use of raw materials and greater volume of solid and liquid waste. The Utica Shale is estimated to produce 2.5 times more produced

water per unit gas than the Marcellus Shale [86]. These produced waters will contain NORM that could otherwise end up in impoundment sludge or water treatment sludge. If not mitigated, the continued recycling of produced water for hydraulic fracturing could cause an increase in TDS and radium activities [48], potentially increasing the radioactivity and volume of sludge generated during treatment. This work provides evidence that when these solids (sands, suspended solids, and sludge) are collected in a waste handling facility, hydroacoustic cavitation with advanced oxidation followed by physical separation devices can be applied to (a) reclaim the sands with lowered radioactivity; (b) separate the clays, salts and organics with high activity, and (c) reduce the potential of radium leaching from the solids that require disposal.

2.7 Acknowledgments

This research was funded by a National Science Foundation PFI: AIR-TT #1640634. Further support originated from a Penn State College of Engineering Graduate Excellence Fellowship. We acknowledge Hydro Recovery LP for providing the samples used in this study.

2.8 References

(1) R. A. Kerr, Energy. Natural gas from shale bursts onto the scene., *Science*, 2010, 328, 1624–6.

(2) U.S. Energy Information Administration, *Annual Energy Outlook*, Washington, DC, 2018.

(3) D. M. Kargbo, R. G. Wilhelm and D. J. Campbell, Natural Gas Plays in the Marcellus Shale: Challenges and Potential Opportunities, *Environ. Sci. Technol.*, 2010, 44, 5679–5684.

(4) M. E. Gallagher, A. Down, R. C. Ackley, K. Zhao, N. Phillips and R. B. Jackson, Natural Gas Pipeline Replacement Programs Reduce Methane Leaks and Improve Consumer Safety, *Environ. Sci. Technol. Lett.*, 2015, 2, 286–291.

(5) K. McKain, A. Down, S. M. Raciti, J. Budney, L. R. Hutyra, C. Floerchinger, S. C. Herndon, T. Nehrkorn, M. S. Zahniser, R. B. Jackson, N. Phillips and S. C. Wofsy, Methane emissions from natural gas infrastructure and use in the urban region of Boston, Massachusetts., *Proc. Natl. Acad. Sci. U. S. A.*, 2015, 112, 1941–6.

(6) G. Heath, J. Meldrum, N. Fisher, D. Arent and M. Bazilian, Life cycle greenhouse gas emissions from Barnett Shale gas used to generate electricity, *J. Unconv. Oil Gas Resour.*, 2014, 8, 46–55.

(7) R. W. Howarth, R. Santoro and A. Ingraffea, Methane and the greenhouse-gas footprint of natural gas from shale formations, *Clim. Change*, 2011, 106, 679–690.

(8) R. W. Howarth, A. Ingraffea and T. Engelder, Should fracking stop?, *Nature*, 2011, 477, 271–275.

(9) M. Jiang, W. Michael Griffin, C. Hendrickson, P. Jaramillo, J. VanBriesen and A. Venkatesh, Life cycle greenhouse gas emissions of Marcellus shale gas, *Environ. Res. Lett.*, 2011, 6, 34014.

(10) N. R. Warner, C. A. Christie, R. B. Jackson and A. Vengosh, Impacts of shale gas wastewater disposal on water quality in Western Pennsylvania, *Environ. Sci. Technol.*, 2013, 47, 11849–11857.

(11) K. J. Ferrar, D. R. Michanowicz, C. L. Christen, N. Mulcahy, S. L. Malone and R. K. Sharma, Assessment of effluent contaminants from three facilities discharging marcellus shale wastewater to surface waters in Pennsylvania, *Environ. Sci. Technol.*, 2013, 47, 3472–3481.

(12) J. M. Wilson and J. M. Van Briesen, Source Water Changes and Energy Extraction Activities in the Monongahela River, 2009–2012, *Environ. Sci. Technol.*, 2013, 47, 12575–12582.

(13) J. M. Wilson, Y. Wang and J. M. VanBriesen, Sources of High Total Dissolved Solids to Drinking Water Supply in Southwestern Pennsylvania, *J. Environ. Eng.*, 2014, 140, B4014003-1-B4014003-10.

(14) J. M. Wilson and J. M. VanBriesen, Oil and Gas Produced Water Management and Surface Drinking Water Sources in Pennsylvania, *Environ. Pract.*, 2012, 14, 288–300.

(15) K. M. Parker, T. Zeng, J. Harkness, A. Vengosh and W. A. Mitch, Enhanced Formation of Disinfection Byproducts in Shale Gas Wastewater-Impacted Drinking Water Supplies, *Environ. Sci. Technol.*, 2014, 48, 11161–11169.

(16) W. D. Burgos, L. Castillo-Meza, T. L. Tasker, T. J. Geeza, P. J. Drohan, X. Liu, J. D. Landis, J. Blotevogel, M. McLaughlin, T. Borch and N. R. Warner, Watershed-Scale Impacts from Surface Water Disposal of Oil and Gas Wastewater in Western Pennsylvania, *Environ. Sci. Technol.*, 2017, 51, 8851–8860.

(17) J. S. Harkness, G. S. Dwyer, N. R. Warner, K. M. Parker, W. A. Mitch and A. Vengosh, Iodide, bromide, and ammonium in hydraulic fracturing and oil and gas wastewaters: Environmental implications, *Environ. Sci. Technol.*, 2015, 49, 1955–1963.

(18) A. Vengosh, R. B. Jackson, N. R. Warner, T. H. Darrah and A. Kondash, A Critical Review of the Risks to Water Resources from Unconventional Shale Gas Development and Hydraulic Fracturing in the United States, *Environ. Sci. Technol.*, 2014, 48, 8334–8348.

(19) J. Kravchenko, T. H. Darrah, R. K. Miller, H. K. Lyerly and A. Vengosh, A review of the health impacts of barium from natural and anthropogenic exposure, *Environ. Geochem. Health*, 2014, 36, 797–814.

(20) L. Konkel, Salting the Earth: The Environmental Impact of Oil and Gas Wastewater Spills, *Environ. Health Perspect.*, 2016, 124, A230–A235.

(21) S. G. Osborn, A. Vengosh, N. R. Warner and R. B. Jackson, Methane contamination of drinking water accompanying gas-well drilling and hydraulic fracturing., *Proc. Natl. Acad. Sci. U. S. A.*, 2011, 108, 8172–6.

(22) L. J. Molofsky, J. A. Connor, A. S. Wylie, T. Wagner and S. K. Farhat, Evaluation of Methane Sources in Groundwater in Northeastern Pennsylvania, *Groundwater*, 2013, 51, 333–349.

(23) D. I. Siegel, N. A. Azzolina, B. J. Smith, A. E. Perry and R. L. Bothun, Methane Concentrations in Water Wells Unrelated to Proximity to Existing Oil and Gas Wells in Northeastern Pennsylvania, *Environ. Sci. Technol.*, 2015, 49, 4106–4112.

(24) E. L. Rowan, M. A. Engle, T. F. Kraemer, K. T. Schroeder, R. W. Hammack and M. W. Doughten, Geochemical and isotopic evolution of water produced from Middle Devonian Marcellus shale gas wells, Appalachian basin, Pennsylvania, *Am. Assoc. Pet. Geol. Bull.*, 2015, 99, 181–206.

(25) T. Hayes, *Sampling and Analysis of Water Streams Associated with the Development of Marcellus Shale Gas*, Marcellus Shale Coalition Final Report, Des Plaines, 2009.

(26) K. D. Good and J. M. VanBriesen, Current and Potential Future Bromide Loads from Coal-Fired Power Plants in the Allegheny River Basin and Their Effects on Downstream Concentrations, *Environ. Sci. Technol.*, 2016, 50, 9078–9088.

(27) C. He, M. Li, W. Liu, E. Barbot and R. D. Vidic, Kinetics and Equilibrium of Barium and Strontium Sulfate Formation in Marcellus Shale Flowback Water, *J. Environ. Eng.*, 2014, 140, B4014001-1-B4014001-9.

(28) T. Zhang, K. Gregory, R. W. Hammack and R. D. Vidic, Co-precipitation of radium with barium and strontium sulfate and its impact on the fate of

radium during treatment of produced water from unconventional gas extraction, *Environ. Sci. Technol.*, 2014, 48, 4596–4603.

(29) M. I. Zermeno-Motante, C. Nieto-Delgado, F. S. Cannon, C. C. Cash and C. C. Wunz, Chemical modeling for precipitation from hypersaline hydrofracturing brines, *Water Res.*, 2016, 103, 233–244.

(30) C. He, T. Zhang and R. D. Vidic, Use of Abandoned Mine Drainage for the Development of Unconventional Gas Resources, *Disruptive Sci. Technol.*, 2013, 1, 169–176.

(31) C. He, T. Zhang and R. D. Vidic, Co-treatment of abandoned mine drainage and Marcellus Shale flowback water for use in hydraulic fracturing, *Water Res.*, 2016, 104, 425–431.

(32) C. He, T. Zhang, X. Zheng, Y. Li and R. D. Vidic, Management of Marcellus Shale Produced Water in Pennsylvania: A Review of Current Strategies and Perspectives, *Energy Technol.*, 2014, 2, 968–976.

(33) Y. Bi, H. Zhang, B. R. Ellis and K. F. Hayes, Removal of Radium from Synthetic Shale Gas Brines by Ion Exchange Resin, *Environ. Eng. Sci.*, 2016, 33, 791–798.

(34) A. N. Paukert Vankeuren, J. A. Hakala, K. Jarvis and J. E. Moore, Mineral Reactions in Shale Gas Reservoirs: Barite Scale Formation from Reusing Produced Water As Hydraulic Fracturing Fluid, *Environ. Sci. Technol.*, 2017, 51, 9391–9402.

(35) M. E. Benson and A. B. Wilson, *Frac Sand in the United States—A Geological and Industry Overview*, U.S. Geological Survey Open-File Report 2015–1107, DOI: 10.3133/ofr20151107, 2015.

(36) K. O. Maloney and D. A. Yoxtheimer, Production and Disposal of Waste Materials from Gas and Oil Extraction from the Marcellus Shale Play in Pennsylvania, *Environ. Pract.*, 2012, 14, 278–287.

(37) U.S. Geological Survey (USGS), Industrial sand and gravel, in Metals and minerals: U.S. Geological Survey Minerals Yearbooks 1991–2017, various pagination, http://minerals.usgs.gov/ minerals/pubs/usbmmyb.html and http://minerals.usgs.gov/ minerals/pubs/commodity/silica/, (accessed 17 February 2018).

(38) Baker-Hughes Inc, Baker-Hughes Rig count: North America Rig Count, http://phx.corporate-ir.net/phoenix.zhtml?c=79687&p=irol-reportsother, (accessed 20 February 2018).

(39) V. Beiser, The World's Disappearing Sand

https://www.nytimes.com/2016/06/23/opinion/the-worlds-disappearing-sand.html, (accessed 17 February 2018).

(40) T. W. Pearson, Frac Sand Mining in Wisconsin: Understanding Emerging Conflicts and Community Organizing, *Cult. Agric. Food Environ.*, 2013, 35, 30–40.

(41) V. Beiser, The Deadly Global War for Sand, https://pulitzercenter.org/reporting/india-deadly-global-war-sand, (accessed 17 February 2018).

(42) V. Beiser, How Sand Mining Helped Flood Houston, https://pulitzercenter.org/reporting/how-sand-mining-helped-flood-houston, (accessed 17 February 2018).

(43) V. Beiser, Sand mining: the global environmental crisis you've never heard of, https://www.theguardian.com/cities/2017/feb/27/sand-mining-global-environmental-crisis-never-heard, (accessed 17 February 2018).

(44) V. Beiser, India: The Deadly Global War for Sand, https://pulitzercenter.org/reporting/india-deadly-global-war-sand, (accessed 17 February 2018).

(45) V. Beiser, He who controls the sand: the mining 'mafias' killing each other to build cities, https://www.theguardian.com/cities/2017/feb/28/sand-mafias-killing-each-other-build-cities, (accessed 17 February 2018).

(46) D. Bleiwas, Estimates of hydraulic fracturing (Frac) sand production, consumption, and reserves in the United States., https://www.thefreelibrary.com/Estimates+of+hydraulic+fracturing+(Frac)+sand+production%2C...-a0418603320, (accessed 20 February 2018).

(47) Pennsylvania Department of Environmental Protection (PA DEP), Technologically Enhanced Naturally Occurring Radioactive Materials (TENORM) Study Report, http://www.depgreenport.state.pa.us/elibrary/getdocument?docid=5815&docname=01 pennsylvania department of environmental protection tenorm study report rev 1.pdf, (accessed 8 February 2018).

(48) T. Zhang, R. W. Hammack and R. D. Vidic, Fate of Radium in Marcellus Shale Flowback Water Impoundments and Assessment of Associated Health Risks, *Environ. Sci. Technol.*, 2015, 49, 9347–9354.

(49) M. F. Attallah, M. M. Hamed, E. M. El Afifi and H. F. Aly, Removal of226Ra and228Ra from TENORM sludge waste using surfactants solutions, *J. Environ. Radioact.*, 2015, 139, 78–84.

(50) W. M. Kappel, J. H. Williams and Z. Szabo, *Water Resources and Shale Gas/Oil Production in the Appalachian Basin—Critical Issues and Evolving Developments*, U.S. Geological Survey Open-File Report 2013–1137, 2013.

(51) Pennsylvania Department of Environmental Protection (PA DEP), PA DEP Oil and Gas Reporting Website: Statewide Data Downloads by Reporting Period, https://www.paoilandgasreporting.state.pa.us/publicreports/Modules/Welcome/ProdWasteReports.aspx, (accessed 20 February 2018).

(52) J. T. Fox, F. S. Cannon, R. C. Voigt, P. B. Smith, S. E. Lewallen and J. E. Goudzwaard, Simultaneous Sand , Clay and Coal Reclamation Using Induced Particle Collision , Discretionary Settling and Advanced Oxidation, *Trans. Am. Foundry Soc.*, 2007, 115, 1–16.

(53) J. T. Fox, F. S. Cannon, R. C. Voigt, J. C. Furness, F. Headington, D. Coan and S. Lewallen, Waste Green Sand to Core Sand Reclamation, Demonstration via Casting Study with Simultaneous Clay Recovery via a Novel Ultrasonic-Cavitation System, *Trans. Am. Foundry 116*, 2008, 116, 523–538.

(54) J. T. Fox, F. S. Cannon, R. C. Voigt, J. E. Goudzwaard, M. Wosoba and P. B. Smith, Decreased Bond Consumption by Processing Baghouse Dust through Ultrasonic-Cavitation-Settling Coupled to Advanced Oxidation, *Trans. Am. Foundry Soc.*, 2008, 116, 539–546.

(55) J. E. Goudzwaard, C. M. Kurtti, J. H. Andrews, F. S. Cannon, R. C. Voigt, J. E. Firebaugh, J. C. Furness and D. L. Sipple, Foundry Emissions Effects with an Advanced Oxidation Blackwater System, *Trans. Am. Foundry Soc.*, 2003, 111, 1191–1211.

(56) Y. Wang, F. S. Cannon, S. Komarneni, R. C. Voigt and J. C. Furness, Mechanisms of advanced oxidation processing on bentonite consumption reduction in foundry, *Environ. Sci. Technol.*, 2005, 39, 7712–7718.

(57) C. R. Glowacki, G. R. Crandell, F. S. Cannon, J. K. Clobes, R. C. Voigt, J. C. Furness, B. A. McComb and S. M. Knight, Emissions Studies at a Test Foundry using an Advanced Oxidation-Clear Water System, *Trans. Am. Foundry Soc.*, 2003, 111, 579–598.

(58) D. A. Neill, F. S. Cannon, R. C. Voigt, J. C. Furness and R. H. Bigge, Effects of Advanced Oxidants on Green Sand System in a Black Water System, *Trans. Am. Foundry Soc.*, 2001, 109, 1–19.

(59) J. D. Land, R. C. Voigt, F. S. Cannon, J. C. Furness, J. Goudzwaard and H. Luebben, Performance and Control of a Green Sand System During the Installation and Operation of an Advanced Oxidation System., *Trans. Am. Foundry Soc.*, 2002, 110, 705–713.

(60) J. Andrews, R. Bigge, F. S. Cannon, G. R. Crandell, Furness J.C., M. Redmann and R. C. Voigt, Advanced oxidants offer opportunities to improve mold properties, emissions, *Mod. Cast.*, 2000, 90, 40.

(61) S. Liu, T. Geeza, F. S. Cannon, M. S. Klima, J. C. Furness and J. Pagnotti, Hydroacoustic Cavitation for Recovering Anthracite Fines from Waste Silt Slurry, *J. Min. World Express*, 2017, 6, 10.

(62) B. Barry, M. S. Klima and F. S. Cannon, Effect of hydroacoustic cavitation treatment on the spiral processing of bituminous coal, *Int. J. Coal Prep. Util.*, 2015, 35, 76–87.

(63) B. Barry, M. S. Klima and F. S. Cannon, Effects of Desliming and Hydroacoustic Cavitation Treatment on the Flotation of Ultrafine Bituminous Coal, *Int. J. Coal Prep. Util.*, 2017, 37, 213–224.

(64) R. M. Torielli, F. S. Cannon, R. C. Voigt, T. J. Considine, J. C. Furness, J. T. Fox, J. E. Goudzwaard and H. Huang, The Environmental Performance and Cost of Innovative Technologies for Ductile Iron Foundry Production, *Int. J. Met.*, 2014, 8, 37–48.

(65) E. B. Flint and K. S. Suslick, The temperature of cavitation., *Science*, 1991, 253, 1397–1399.

(66) Y. T. Didenko, W. B. McNamara and K. S. Suslick, Temperature of multibubble sonoluminescence in water, *J. Phys. Chem. A*, 1999, 103, 10783–10788.

(67) T. J. Mason and D. Peters, in *Practical Sonochemistry*, Horwood Publishing Limited, Chichester, 2nd edn., 2002, vol. 1, ch. 1, pp. 12.

(68) X. Y. S. Zhang, M. A. Ajemigbitse, F. S. Cannon, A. E. Hooper, D. L. Allara, P. D. Paulsen and J. C. Furness, Hydrogen Peroxide-Generated Gases at Asphalt-Glass Interface: Effect on Surface Cleaning and Analysis by Nanoscale Surface Imaging Spectroscopy, *Environ. Eng. Sci.*, 2018, 35, 300–310.

(69) T. J. Mason and J. P. Lorimer, in *Applied Sonochemistry*, Wiley-VCH, Weinheim, 1st edn., 2002, vol. 1, ch. 2, pp. 36-38.

(70) M. D. Benusa and M. S. Klima, An Evaluation of a Two-Stage Spiral Processing Fine Anthracite Refuse, *Int. J. Coal Prep. Util.*, 2009, 29, 49–67.

(71) N. Milan-Segovia, Y. Wang, F. S. Cannon, R. C. Voigt and J. C. Furness, Comparison of Hydroxyl Radical Generation for Various Advanced Oxidation Combinations as Applied to Foundries, *Ozone Sci. Eng.*, 2007, 29, 461–471.

(72) Environmental Protection Agency (EPA), EPA Test Method 1311 - Toxicity Characteristic Leaching Procedure (TCLP) https://www.epa.gov/sites/production/files/2015-12/documents/1311.pdf, (accessed 5 September 2017).

(73) T. L. Tasker, P. K. Piotrowski, F. L. Dorman and W. D. Burgos, Metal Associations in Marcellus Shale and Fate of Synthetic Hydraulic Fracturing Fluids Reacted at High Pressure and Temperature, *Environ. Eng. Sci.*, 2016, 33, 753–765.

(74) B. W. Stewart, E. C. Chapman, R. C. Capo, J. D. Johnson, J. R. Graney, C. S. Kirby and K. T. Schroeder, Origin of brines, salts and carbonate from shales of the Marcellus Formation: Evidence from geochemical and Sr isotope study of sequentially extracted fluids, *Appl. Geochemistry*, 2015, 60, 78–88.

(75) International Atomic Energy Agency (IAEA), *The Environmental Behaviour of Radium: Revised Edition. Technical Report Series no. 476*, Vienna, 2014.

(76) A. W. Nelson, E. S. Eitrheim, A. W. Knight, D. May, M. A. Mehrhoff, R. Shannon, R. Litman, W. C. Burnett, T. Z. Forbes and M. K. Schultz, Understanding the Radioactive Ingrowth and Decay of Naturally Occurring Radioactive Materials in the Environment : An Analysis of Produced Fluids from the Marcellus Shale, *Environ. Health Perspect.*, 2015, 123, 689–696.

(77) A. W. Nelson, A. J. Johns, E. S. Eitrheim, A. W. Knight, M. Basile, E. A. Bettis III, M. K. Schultz and T. Z. Forbes, Partitioning of naturally-occurring radionuclides (NORM) in Marcellus Shale produced fluids influenced by chemical matrix, *Environ. Sci. Process. Impacts*, 2016, 18, 456–463.

(78) American Petroleum Institute, *API RP 19C/ISO 13503-2: "Recommended Practice for Measurement of Properties of Proppants Used in Hydraulic Fracturing and Gravel-packing Operations"*, American Petroleum Institute (API), Washington DC, 1st edn., 2008.

(79) Carbo Ceramics, personal communication.

(80) D. Shin, M.S. Thesis, Columbia University, 2014.

(81) J. L. Luek and M. Gonsior, Organic compounds in hydraulic fracturing fluids and wastewaters: A review, *Water Res.*, 2017, 123, 536–548.

(82) D. M. Akob, I. M. Cozzarelli, D. S. Dunlap, E. L. Rowan and M. M. Lorah, Organic and inorganic composition and microbiology of produced waters from Pennsylvania shale gas wells, *Appl. Geochemistry*, 2015, 60, 116–125.

(83) A. V. Matyskin, N. L. Hansson, P. L. Brown and C. Ekberg, Barium and Radium Complexation with Ethylenediaminetetraacetic Acid in Aqueous Alkaline Sodium Chloride Media, *J. Solution Chem.*, 2017, 46, 1951–1969.

(84) N. Abualfaraj, P. L. Gurian and M. S. Olson, Characterization of Marcellus Shale Flowback Water, *Environ. Eng. Sci.*, 2014, 31, 514–524.

(85) E. S. Eitrheim, D. May, T. Z. Forbes and A. W. Nelson, Disequilibrium of Naturally Occurring Radioactive Materials (NORM) in Drill Cuttings from a Horizontal Drilling Operation, *Environ. Sci. Technol. Lett.*, 2016, 3, 425–429.

(86) R. D. Vidic and D. Yoxtheimer, presented in part at the 2017 Shale Network Workshop, State College, May, 2017.

Chapter 3

Removing Radium from Produced Waters with Tailored Clays

Ajemigbitse MA, Sridhar K, Cannon FS, and Warner NR. "Removing Radium from Produced Waters with Tailored Clays." Manuscript in Preparation.

3.1 Abstract

Oil and gas production results in large volumes of co-produced formation water commonly referred to as produced water. Among the many constituents of interest found in produced water, radium, a radioactive element, presents a great challenge because of its possible impact on human and wildlife health. Radium-226 has a half-life of 1600 years, which presents a lasting and persistent environmental challenge. The current treatment and handling of radium in produced water results in the generation of hundreds of tons of low-level radioactive sludge that requires substantial transport and disposal costs. The development of novel treatment processes that reduce sludge production will also reduce waste management costs.

This work evaluated a new process for radium removal from produced water with a synthetic clay mineral that is highly selective for radium. Interlayer adsorption of radium by the synthetic clay leads to preferential radium removal even in the presence of high salinity (1.5 M NaCl). Batch experiments of clay-synthetic water suspensions with increasing complexity provided an insight into the key mechanisms driving radium adsorption onto the clay. In a synthetic produced water, radium removal by the synthetic clay was greater than a Na-montmorillonite Bentonite. In addition, these experiments led to the identification of the following controls on treatment with clay adsorption: radium removal was pH independent but dependent on the solution salinity, competing ions and dissolved organic compounds content.

3.2 Introduction

High volumes of water co-produced with oil and gas contains naturally occurring radioactive materials (NORM) [1,2]. Radium is the primary radionuclide of interest and its isotopes, ^{226}Ra (half-life 1600 years) and ^{228}Ra (half-life 5.75 years), are monitored during the treatment, disposal and discharge of oil and gas waste. Due to the limited availability of freshwater sources in some regions, and a lack of easy disposal options in others, the recycling and reuse of produced water has become an attractive shale gas wastewater management strategy [3,4]. However, improper handling of this produced water can result in exposure risk for human health [5,6] and environmental contamination [7–11].

Several studies on the treatment of produced water for NORM removal have included sulfate precipitation by sodium sulfate addition [12,13], by blending with acid mine drainage [14–16], and ion exchange using strong acid resin [17]. Sulfate precipitation remains a very effective treatment for NORM removal from produced waters, however, sulfate addition is a non-targeted radium treatment and results in the generation of radioactive sludge. However, sulfate addition can result in scale formation [18] and increased activity of sulfate reducing bacteria [16] when the fluid is reused for hydraulic fracturing. While ion exchange can provide targeted radium removal, pretreatment to reduce the competition from other divalent cations is necessary [17]. In addition, the lack of radium specific treatment results in the loss of valuable feedstock for crystallization of marketable salts ($CaCl_2$, NaCl and $BaSO_4$). The development of radium-specific treatment processes will reduce radioactive sludge production, increase the potential for salt recovery, and continue to provide a freshwater alternative for hydraulic fracturing.

Clays have been used as adsorbents for remediation of contaminated soils and waters [19–22] and radium sorption onto clays has been studied [23,24]. Consequently,

this work is investigating radium removal from highly saline produced water with a synthetic clay (Na-4-mica, $Na_4Mg_6Al_4Si_4O_{20}F_4{*}xH_2O$) that is highly selective for radium [25] (see Figure 3.1).

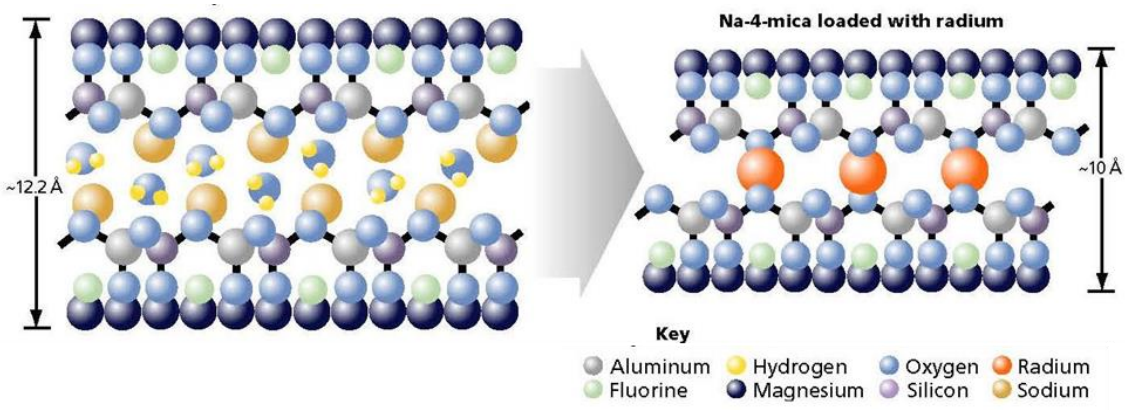

Figure 3.1: Na-4-mica showing hydrated 12 Å basal spacing (left). Ion exchange of sodium for radium occurs after adsorption from solution. Upon adsorption, a strong electrostatic bond is formed which collapses the basal spacing to 10 Å (right). Figure reproduced with permission from Frazer 2002, *Environ. Health Persp.* [26].

Gregorkiewitz and Rausell-Colom [27] first synthesized Na-4-mica from the reaction of augite in NaF-MgF_2 melts at approximately 900 °C. They identified a 2:1 layer silicate with unusually high charge, due to four sodium ions in the interlayer. This layered silicate possessed the ability to readily hydrate to an expanded lattice, making Na-4-mica a candidate for interlayer ion exchange. The structure and chemical composition of the phases of Na-4-mica were later identified as presented in Figures 3.2 and 3.3. Further research has led to the development of new synthesis protocols for pure crystals of Na-4-mica, with different precursor materials under different conditions [25,28–33]. Significant among these are the methods by Komarneni

et al. [31,34], which utilizes kaolinite after calcination (metakaolin), and by Park *et al.* [32], which uses stoichiometric powder mixtures of fumed silica, aluminum oxide, magnesium fluoride and sodium chloride. This method was further modified to become a mixture of silicic acid, boehmite, magnesium fluoride, and sodium chloride.

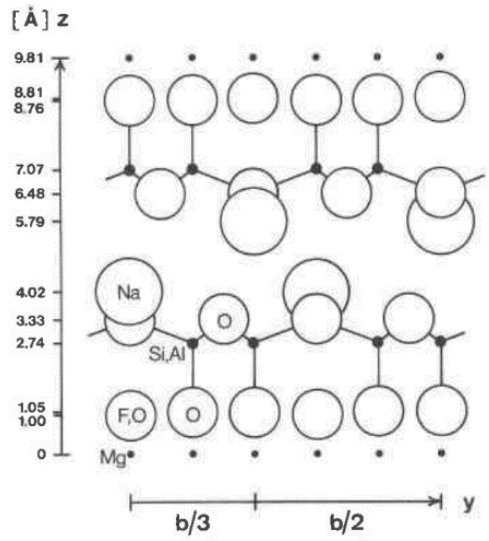

Figure 3.2: Proposed model for anhydrous Na-4-mica as projected on plane perpendicular to a. The displacement of the upper layer with respect to the lower one is +b/3. Figure reproduced with permission from Gregorkiewitz *et al.* 1987*, Am. Mineral* [27].

First deployed for the decontamination and disposal of nuclear waste, Na-4-mica has also served as a sorbent for remediation of metal contaminated soils [33–35]. Na-4-mica is selective for ions of low hydration, especially radium, due to its high charge density and offset layer-stacking [25,36]. Upon radium uptake, electrostatic bonding could result in the collapse of the interlayer (see Figure 3.1), resulting in the entrapment of radium in the crystal lattice.

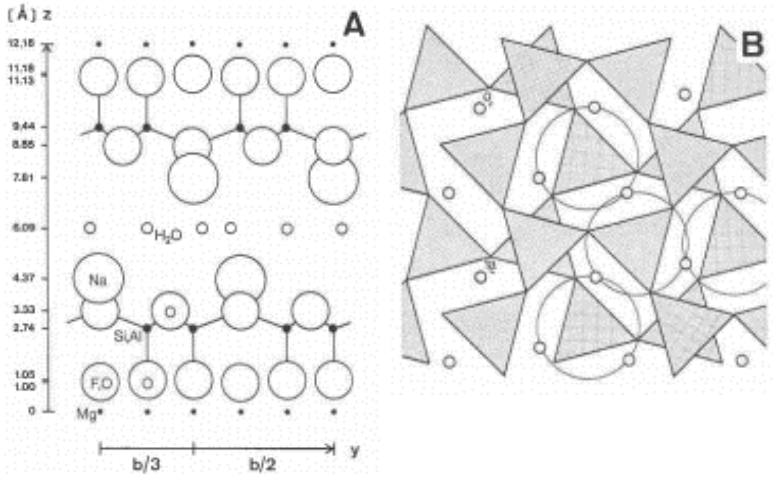

Figure 3.3: Proposed model for hydrated Na-4-mica. The displacement between adjacent layers is +b/3. The model shows 4 Na and 6 H_2O sites per unit cell. Only 3.2 and 4.3 are actually occupied. (**A**) Projection on plane perpendicular to a; (**B**) projection on (001). Figure reproduced with permission from Gregorkiewitz *et al.* 1987*, Am. Mineral*[27].

The application of Na-4-mica for high TDS water treatment, such as hydraulic fracturing produced waters, has never been attempted. This study is motivated by the need to effectively separate radium from shale gas produced water to reduce the volume of Ra-contaminated phases during treatment steps. Solid-phase partitioning provides an opportunity to concentrate radium in a lower volume solid waste form and, in some cases, could allow subsequent separation steps (e.g., co-precipitation) to produce solid phases that are almost Ra-free, with potential commercial value (e.g., barite and $CaCl_2$ salts).

The work herein focuses on the synthesis and characterization of Na-4-mica; its application for radium removal from the high TDS produced waters; and investigates the mechanisms – *pH, salinity and competing ions* – that can control radium adsorption by Na-4-mica in highly saline waters.

3.3 Materials and Methods

3.3.1 Materials

Na-4-mica was synthesized from dry mixtures of stoichiometric amounts of silica and aluminum in 1:1 ratio from silicic acid (J.T. Baker), boehm-ite (by Condea Chemie), magnesium fluoride (Aldrich Chemical Co), and sodiumchloride (VWR), or from kaolinite (Georgia Kaolin Company). Barium chloride,used in the competing ion test, was from VWR. All chemicals were reagent grade. Corundum (nano-aluminum oxide) was supplied by Inframat Advanced Materials.

Radium was provided by NIST, and radium stock solutions (in 5% nitric acid) were created at 20,000 pCi/L and stored in glass bottles to reduced wall adsorption. Radium-226 activities in the liquid were determined by gamma spectroscopy on a Canberra ultra-low background small anode germanium (SAGe) well detector after the incubation period of three weeks. The reported ^{226}Ra activity was the direct measurement of ^{226}Ra determined at 186 keV after peak deconvolution to correct for ^{235}U interference. The sample geometry used was a 24mL urea capped HDPE liquid scintillation vial.

Distilled de-ionized (DDI) water was provided by the ThermoScientific Barnstead Nanopure water system with resistivity at 18.2$m\Omega$. Batch experiments were performed in 50 mL Nalgene Oak Ridge Teflon centrifuge tubes. The clay-water

suspensions were separated by centrifugation on an Eppendorf 5810R centrifuge at 3,000 RPM for 10 minutes.

X-ray diffraction (XRD) for phase purity was performed on dry powders on a PANalytical Empryean X-Ray Diffractometer with a Cu source. Scanning electron microscopy (SEM) for morphology was performed on a ThermoFisher FEI Q250 Environmental SEM with a Tungsten emitter.

3.3.2 Synthesis of Na-4-mica

Na-4-mica, $Na_4Si_4Al_4Mg_6O_{20}F_4.xH_2O$, was synthesized from a dry mixture of stoichiometric amounts of silica and aluminum in 1:1 ratio. This was done by providing stoichiometric amounts of compounds containing silica and alumina or by using a base that already has Si to Al molar ratio of 1:1. In the first case, silicic acid and boehmite were used, while metakaolin was used in the second case. Metakaolin is the dehydrated, amorphous product formed from heating kaolinite at 700 °C for 10 hours. Magnesium fluoride was the source of magnesium and fluoride, while excess sodium chloride was the source of sodium. The two synthesis methods for Na-4-mica are outlined below, with further details provided in Appendix B.1:

i) Method I – Silicic acid, + Boehmite, AlO(OH) + Magnesium Fluoride, MgF_2 + 12 M Sodium Chloride, NaCl.

ii) Method II – Metakaolin, $Si_2Al_2O_7$ + Magnesium Fluoride, MgF_2 + 12 M Sodium Chloride, NaCl.

The constituent chemicals were gently mixed and homogenized with an agate mortar and pestle. The mixture was then transferred to a crucible (alumina or platinum), which was heated in a muffle furnace at 900 °C for 5 or 10 hours. After

cooling to room temperature, the resulting solid was transferred to a 50 ml test tube using distilled deionized (DDI) water and filled to about the 45 ml mark. The solid was re-suspended using a test tube vortexer then centrifuged at 3000 RPM for 10 minutes, after which the supernatant was decanted off. This washing process was repeated for a total of 3 rinses. The solid was then dried in an oven at 60 °C for 2 days. XRD and SEM characterization of the dried solids were then performed.

3.3.3 Characterization of Na-4-mica

The dried samples were characterized for phase purity and crystallinity by XRD. The diffraction patterns were analyzed by JADE (Materials Data). Particle size and shape was determined by SEM. Cation exchange capacity (CEC) was determined by the ammonium acetate method (see Appendix B.2). The point of zero charge of the synthesized clays was determined by both the mass titration (MT) method [37] and the drift method [38].

3.3.4 Radium Adsorption Tests

Adsorption of ^{226}Ra onto Na-4-mica was studied through batch reactions. A solution of 20,000 pCi/L ^{226}Ra standard was made by diluting a 0.10 mCi ^{226}Ra standard solution with DDI water in 1L Pyrex bottles. The standard was acidified with nitric acid to <pH 2 to reduce adsorption to the walls of the bottle. Thirty (30) mL of the radium solution was transferred to Teflon centrifuge tubes and the clays were added to make various solid concentrations ranging from 0.1 g/L to 2 g/L for Na-4-mica, or 5 g/L for Bentonite. The water chemistry was made more complex to investigate the key mechanisms driving radium adsorption onto the clay – pH,

solution ionic strength, and competing ion concentration. The simplest water chemistry was the radium solution at pH 2.5 with no added salt (Experiment #1). For pH effect, the pH was adjusted to 10 (Experiment #2). For ionic strength effect, the ionic strength was adjusted to 1.5 M using NaCl (Experiment #3). For competing ion effect, barium was added to a concentration of ~0.01 M using barium chloride (Experiment #4). Finally, two additional experiments were performed using real produced water samples (Experiments # 5 and #6). The centrifuge tubes were mixed on a horizontal rotary mixer for 60 minutes, after which the solid and liquid fractions were separated by centrifugation. Radium-226 activities in the liquid portion was determined by gamma spectroscopy. XRD was performed on select solids to investigate the effect of adsorption on the basal spacing of Na-4-mica. A sodium rich Bentonite with high cation exchange capacity was used to compare the adsorption performance of Na-4-mica.

3.3.5 Major Metals Analyses

Following the adsorption tests, the compositions of the major metals, Ba, Ca, Sr, Na, and Mg in the supernatants were determined by a Perkin Elmer Optima 5300 Inductively Coupled Plasma Emission Spectrometer (ICP-AES) per EPA Method 200.7.

3.4 Results and Discussion

3.4.1 Characterization of Synthesized Na-4-mica

Na-4-mica has a characteristic peak at ~7° (Degrees 2θ) from the (001) reflection with basal spacing of 12.2 Å. Another characteristic peak often appears at ~9°

(Degrees 2θ) due to basal spacing of 9.81 Å [32]. The basal spacing of 12.2 Å represents the hydrated and expandable phase of Na-4-mica. In this form, Na-4-mica is more suitable for radium adsorption. The basal spacing of 9.81 Å represents the anhydrous phase of Na-4-mica, with a dehydrated and collapsed interlayer, making it unsuitable for radium adsorption. The synthesis protocol of Na-4-mica often results in the formation of mineral impurities namely, neighborite and sodalite [31,35], hence these two minerals are often present when XRD analyses are performed.

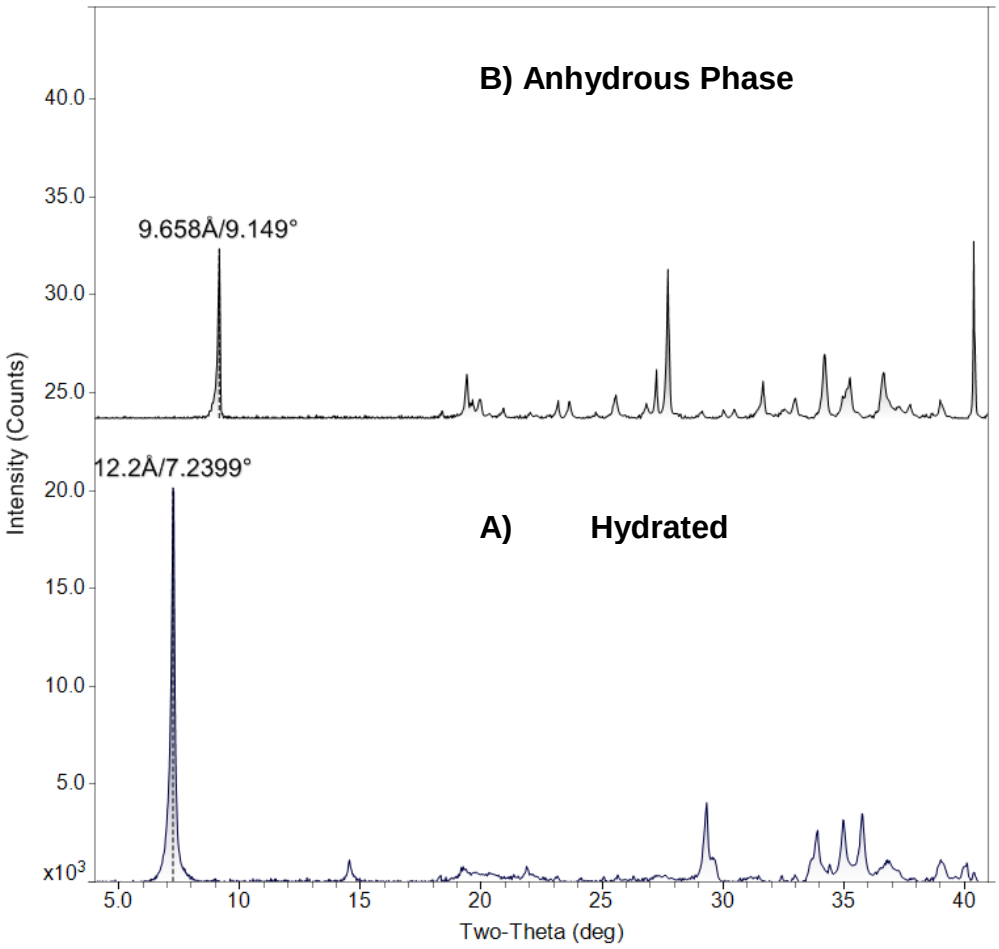

Figure 3.4: XRD patterns of Na-4-mica showing syntheses of Na-4-mica dominated by the hydrated phase (A) or by the anhydrous phase (B).

Shown in Figure 3.3 are representative XRD patterns for hydrated and anhydrous Na-4-mica. Figure 3A showed that the prepared Na-4-mica showed the characteristic basal spacing of 12.2 Å, indicating its suitability for these adsorption experiments. When the synthesis protocol attempted to create larger masses of Na-4-mica (6 g or more), the synthesized clay was often dominated by the anhydrous phase. Additional XRD patterns for several syntheses are provided in Appendix B.3.

SEM micrographs of representative anhydrous and hydrated Na-4-mica are provided in Figures 3.4 and 3.5. Figure 3.4 showed that the hydrated Na-4-mica had particles size of individual flakes at around 2 μm and this small particle size was ideal for adsorption. The anhydrous Na-4-mica exhibited larger particle sizes. In addition, the collapsed nature of the clay particles resulted in large aggregates with the suggestion of a "glassy" phase. The SEM micrographs showed that the anhydrous phase was not suitable for adsorption. Additional SEM micrographs for several syntheses are provided in Appendix B.4.

Theoretical calculations estimate the maximum CEC for hydrated Na-4-mica at 4.68 meq/g, although synthesized Na-4-mica often does not achieve this due to interlayer collapse as a result of electrostatic attraction [34]. The CEC of several synthesized samples showed a maximum of 1.5 meq/g (Table 3.1); this CEC was achieved with method I, i.e. using the solid mixture of silicic acid, boehmite, magnesium fluoride and sodium chloride, in an alumina crucible heated at 900 °C for 5 hours.

Solution pH plays a role in the adsorption of charged species onto solids [39]. The pH can affect the speciation and oxidative state of dissolved species, as well as the surface charge of the solid. The surface charge of a solid can go from positive to

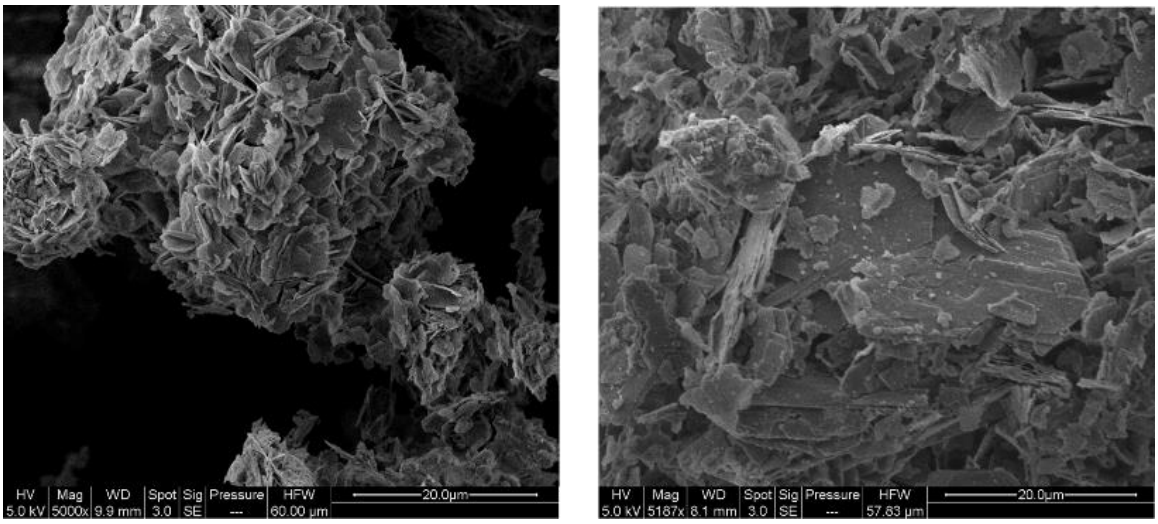

Figure 3.5: Scanning electron microscopy micrographs of hydrated phase Na-4-mica showed the flaky nature of the clay. Small particle size with high surface area makes this clay suitable for adsorption and sequestration of metal contaminants such as radium.

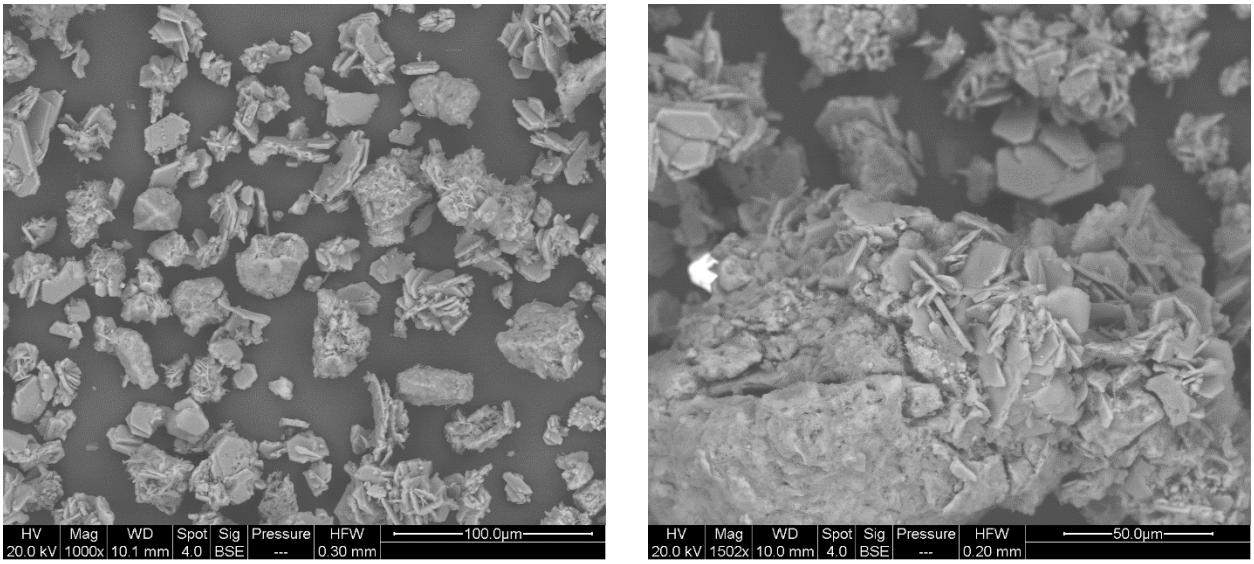

Figure 3.6: Scanning electron microscopy micrographs of anhydrous phase Na-4-mica showed large, aggregated particles as a result of the collapsed interlayer nature of the clay, making it unsuitable for radium adsorption.

Table 3.1: Cation Exchange Capacity (CEC) of several Na-4-mica samples.

Sample	CEC (meq/g)
Na-4-mica (Method I) made in platinum crucible at 900 °C for 10 hours	1.03
Na-4-mica (Method I) made in platinum crucible at 900 °C for 5 hours	1.28
Na-4-mica (Method I) made in alumina crucible at 900 °C for 10 hours	0.78
Na-4-mica (Method I) made in alumina crucible at 900 °C for 5 hours	1.50
Na-4-mica (Method II) made from meta-Kaolinite in platinum crucible at 900 °C for 5 hours	1.48
Na-4-mica (Method II) made from meta-Kaolinite in alumina crucible at 900 °C for 5 hours	1.28

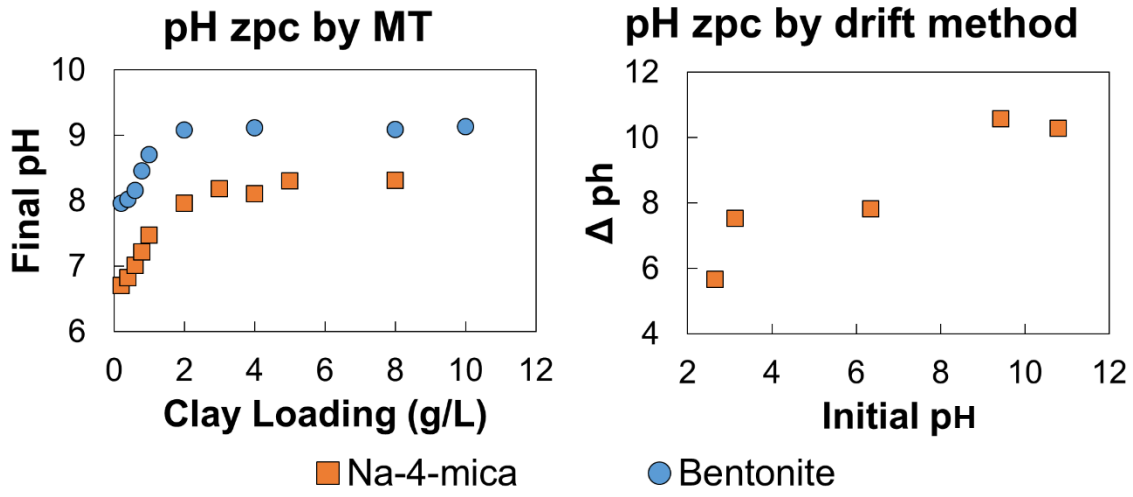

Figure 3.7: Point of zero charge of Na-mica and Bentonite as determined by the mass titration (MT) and drift methods.

negative depending on solution pH. The pH at which the surface transitions from positive to negative is known as the pH_{zpc}, 'zero point charge'. Below this pH, the surface is positively charged; above it the charge is negative [19]. The pH_{zpc} of Na-4-mica was determined to be between 8 and 8.5 by both the mass titration and the drift methods (Figure 3.6).

3.4.2 Quantitative Description of Na-4-mica Purity

So far, Na-4-mica has been qualitatively, or semi-quantitatively described by the XRD diffraction patterns, SEM micrographs, CEC, and pH_{zpc}. However, a thorough quantitative descriptor has yet to be developed. Considering that Na-4-mica often exists as both its hydrated and anhydrous phases, a measure to describe the quantity of the Na-4-mica that is in the hydrated phase is salient.

One approach to this measure is quantitative phase analysis by XRD (or quantitative XRD). In order to perform quantitative XRD, the relative integrated intensity of the strongest line of the mineral phase of interest to the relative integrated intensity of a reference standard must be known, this ratio of intensities is known as the Reference Intensity Ratio (RIR) [40]. The strongest line for Na-4-mica is the (001) reflection that appears at 7° (12.2 Å basal spacing) for the hydrated phase, or at 9° (9.81 Å basal spacing) for the anhydrous phase. Corundum (α-Al_2O_3) is often the reference standard.

The RIR of the hydrated and anhydrous phases of Na-4-mica were determined as follows. First, samples were selected to represent pure phases of the hydrated and anhydrous Na-4-mica. The XRD patterns of these samples is shown in Figure 3.3. Then, a 50:50 by mass mixture of the hydrated/anhydrous Na-4-mica was

created. These solid solutions were mixed with an agate mortar and pestle to minimize mineral contamination. After mixing, the XRD patterns of the solid were collected. The diffraction patterns were analyzed in JADE for the integrated intensity of the strongest lines. This analysis was repeated in triplicate samples and triplicate XRD scans in order to minimize issues that could arise from inhomogeneous mixing or preferred sample orientation during XRD scans. The experimentally determined RIRs for the Na-4-mica phases are presented in Table 3.2.

Table 3.2: The Relative Intensity Ratios (RIRs) for the hydrated and anhydrous phases of Na-4-mica as determined by the internal standard method using Corundum (α-Al_2O_3).

Na-4-mica phase	**RIR**
Hydrated Phase	1.071
Anhydrous Phase	1.857

Following the development of the RIRs, quantitative analysis of the synthesized Na-4-mica samples was performed. By comparing the integrated intensities for each characteristic peak (at 7° for the hydrated phase, or at 9° for the anhydrous phase), the mass fraction of each phase can be determined by equation (3.1) [40]:

$$\frac{X_\alpha}{X_\beta} = \frac{I_{i\alpha}}{I_{j\beta}} \times \frac{I_{j\beta}^{rel}}{I_{i\alpha}^{rel}} \times \frac{RIR_{\beta,c}}{RIR_{\alpha,c}} \tag{3.1}$$

where

X_α, X_β are the mass fractions of the two phases

$I_{i\alpha}, I_{j\beta}$ are the integrated intensities of each phases characteristic line

$I_{j\beta}^{rel}, I_{i\alpha}^{rel}$ are the line intensities, which is 100% for the (001) reflections

$RIR_{\alpha,c}, RIR_{\beta,c}$ are the relative intensity ratios for the two faces relative to corundum

The purity of different Na-4-mica samples, described here as the mass fraction of hydrated Na-4-mica, is presented in Table 3.3.

Table 3.3: Purity of Na-4-mica from several synthesis protocols. Purity is defined as the mass fraction of the synthesized Na-4-mica that is the hydrated phase.

Sample	**Purity (%)**
Na-4-mica (Method I) made in platinum crucible at 900 °C for 5 hours	100
Na-4-mica (Method I) made in alumina crucible at 900 °C for 5 hours	89.7
Na-4-mica (Method I) made in alumina crucible at 900 °C for 5 hours with controlled heating and cooling rate	96.2
Na-4-mica (Method II) made from meta-Kaolinite in platinum crucible at 900 °C for 5 hours	100
Na-4-mica (Method II) made from meta-Kaolinite in alumina crucible at 900 °C for 5 hours	88.8
Na-4-mica (Method II) made from meta-Kaolinite in platinum crucible at 900 °C for 5 hours but at 3 g instead of 2 g	98.1
Na-4-mica (Method I) made in alumina crucible at 900 °C for 5 hours but at 4 g instead of 2 g	65.6
Na-4-mica (Method II) made from meta-Kaolinite in platinum crucible at 900 °C for 5 hours but at 6 g instead of 2 g	2.3
Na-4-mica (Method I) made in platinum crucible at 900 °C for 5 hours but at 8 g instead of 2 g	0

Na-4-mica of high purity was consistently produced when the synthesis was done with the platinum crucible and at low synthesis mass of 2 g. High purity Na-4-mica can be synthesized from both methods set of constituent chemicals. Therefore, for environmental remediation purposes, readily available natural kaolinite clay can be adapted for the synthesis of high purity Na-4-mica. The synthesis protocol failed to produce high quality of Na-4-mica at masses higher than 3 g. One reason for this could be that at higher mass loadings, the temperature gradient created within the solid solution cannot sufficiently transform the chemicals to Na-4-mica in 5 hours. Further work is required to investigate and improve the protocols for higher throughput.

3.4.3 Interlayer Behavior due to Radium Adsorption

Adsorption by clays can occur by different mechanisms, such as surface attachment, edge attachment, inter-lamellar spaces, and inter-particle spaces, as illustrated in Figure 3.7. For the purpose of radium removal, inter-lamellar or interlayer adsorption is the desired mechanism. Interlayer adsorption in Na-4-mica is highly specific for radium, and could result in the entrapment of radium due to edge collapse caused by electrostatic attraction between the positively charged ions and the negatively charged clay layers [35].

Interlayer adsorption can be observed as a change in the basal spacing, which can be observed as shifts in the peak position in the diffraction patterns. Figure 3.8 (B − G) shows the basal spacing of Na-4-mica after radium adsorption. The experiments were performed with the same starting radium concentration (20,000 pCi/L) but with increasing clay concentration, from 0.4 g/L to 10 g/L. At a clay

loading of 0.4 g/L, the basal spacing increased to 14.6 Å. As the clay loading was increased, the basal spacing decreased and returned to the original value of 12.2 Å.

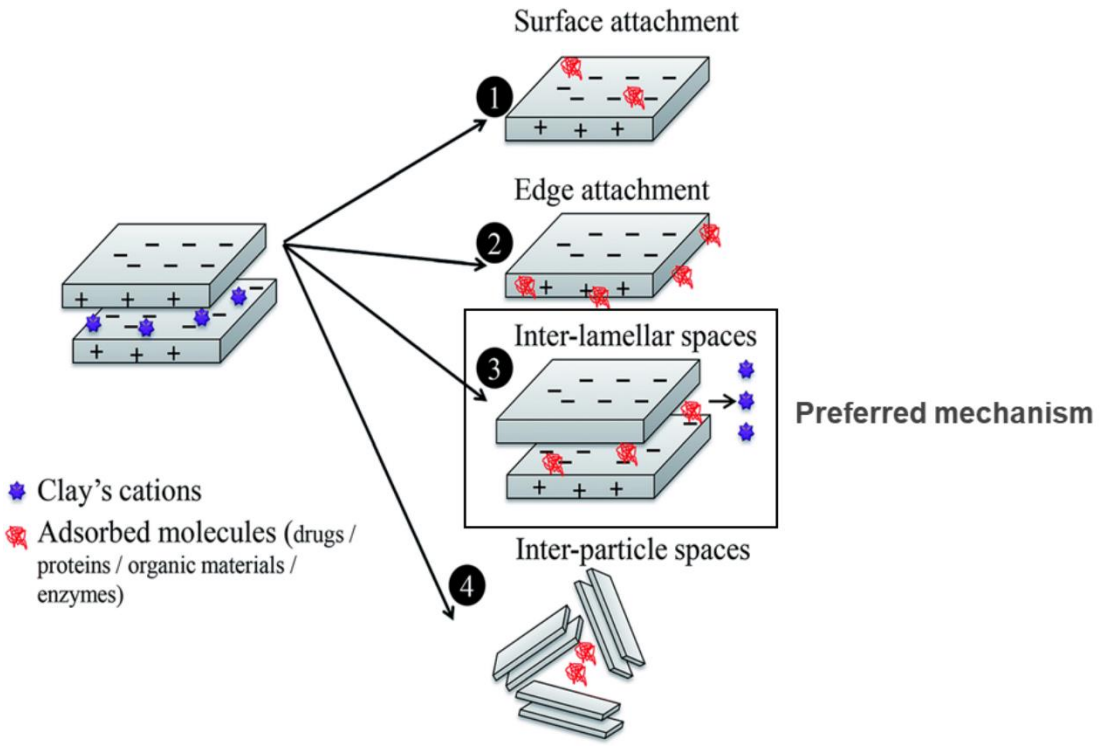

Figure 3.8: The adsorption mechanism for cations onto clay minerals can take many forms. Cations can be adsorbed to the outer surface of the clays as in (**1**) resulting in a surface attachment. They can adsorb to the edge sites as in (**2**). When clay minerals are delaminated, the interlayer sites become available as in (**3**), and finally, adsorption sites are made available when the crystal lattice is broken off as in (**4**). Figure adapted with permission from Ghadiri *et al.* 2015, *RSC Adv.* [20].

This result strongly suggested that ^{226}Ra adsorption by Na-4-mica has occurred via interlayer adsorption.

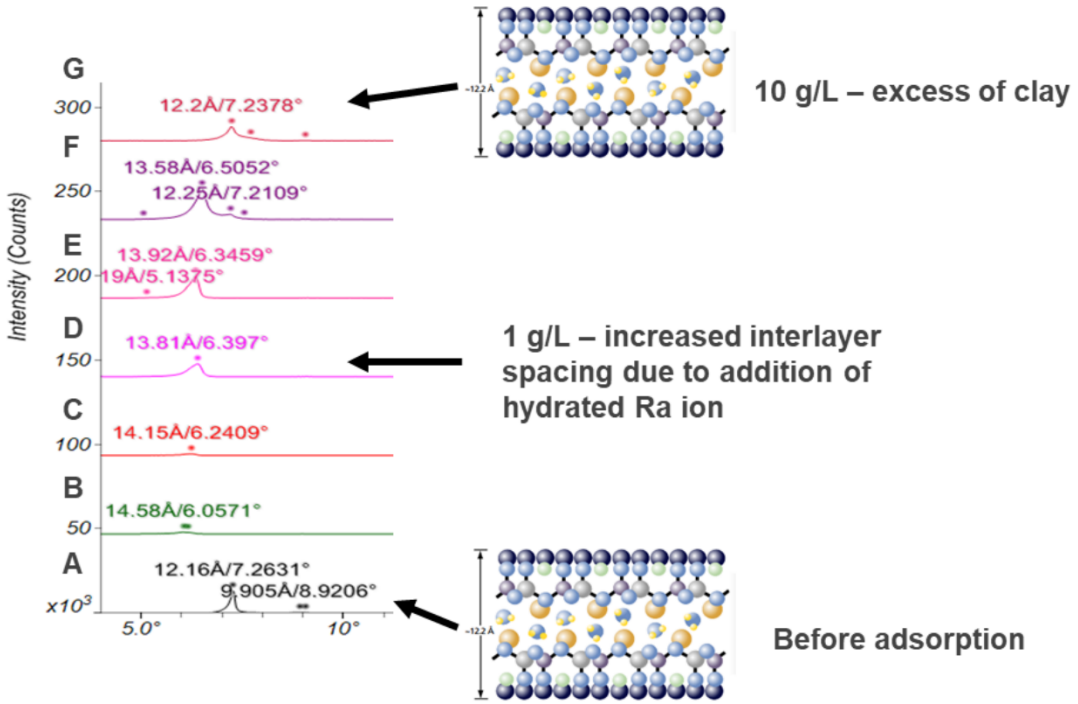

Figure 3.9: X-ray diffraction patterns of Na-4-mica before and after radium adsorption at different solid loadings **A**) before adsorption, **B**) – **G**) 0.4 g/L to 10 g/L Na-4-mica in radium solution. At low solid loading (0.4 g/L) the basal spacing expanded, while with increasing solids loading, the basal spacing decreased until it returned to the original spacing of 12 Å. X-ray diffraction allows us to look into the interlayer. X-ray diffraction patterns of Na-4-mica before adsorption and after adsorption at different solid loadings (0.4 g/L to 10 g/L). At low solid loading, 0.4 g/L, the basal spacing expanded while with increasing solids loading, the basal spacing decreased until it returned to the original spacing of 12 Å.

3.4.4 Effect of pH on Radium Adsorption

Radium (and most metals) exist as positive ions in solution. For effective removal by solid phase adsorption, the solid surface should be negative. Na-4-mica, like many clays, has permanent negative charge due to isomorphic substitutions in the clay lattice [35]. However, edge and surface charges can be derived by imperfections

in the clay lattice. Edge charges will be affected at low pH because of proton equilibrium. Solution pH will have an effect on the abundance of such non-permanent charge, therefore, it is important to understand the extent of these pH-derived charges.

Panels A and B in Figures 3.9 show the effect of pH on radium adsorption by Na-4-mica. At low pH (Figure 3.9A), radium is completely removed by 0.5 g/L clay. Low pH will represent a condition in which surface and edge sites are saturated by protons, thereby reducing radium adsorption at these sites. At high pH (Figure 3.9B), radium removal is still high >90%. (The reduced efficiency is attributed to the effect of high pH solution interacting with the plastic measuring vials during sampling.) These results suggests that radium removal by Na-4-mica is independent of solution pH. This finding is further supported by the result that Na-4-mica adsorbed radium in the interlayer sites, not the surface or edge sites, (see previous section and Figure 3.8.)

3.4.5 Effect of Ionic Strength on Radium Adsoprtion

Ionic strength affects the activity coefficient of dissolved species. For inorganic compounds, higher salinity reduces the activity coefficient [41]. Increased salinity also compresses the Debye length, or the effective region in which a charged surface can attract an oppositely charged particle [41]. Therefore increasing salinity will have a negative effect on radium removal but it is important to evaluate the extent of this effect.

The effect of salinity is observed in Figure 3.9C. At low clay loading, radium removal is negligible. As the amount of clay is increased, radium removal is also increased. Increasing the amount of clay is analogous to increasing the number of

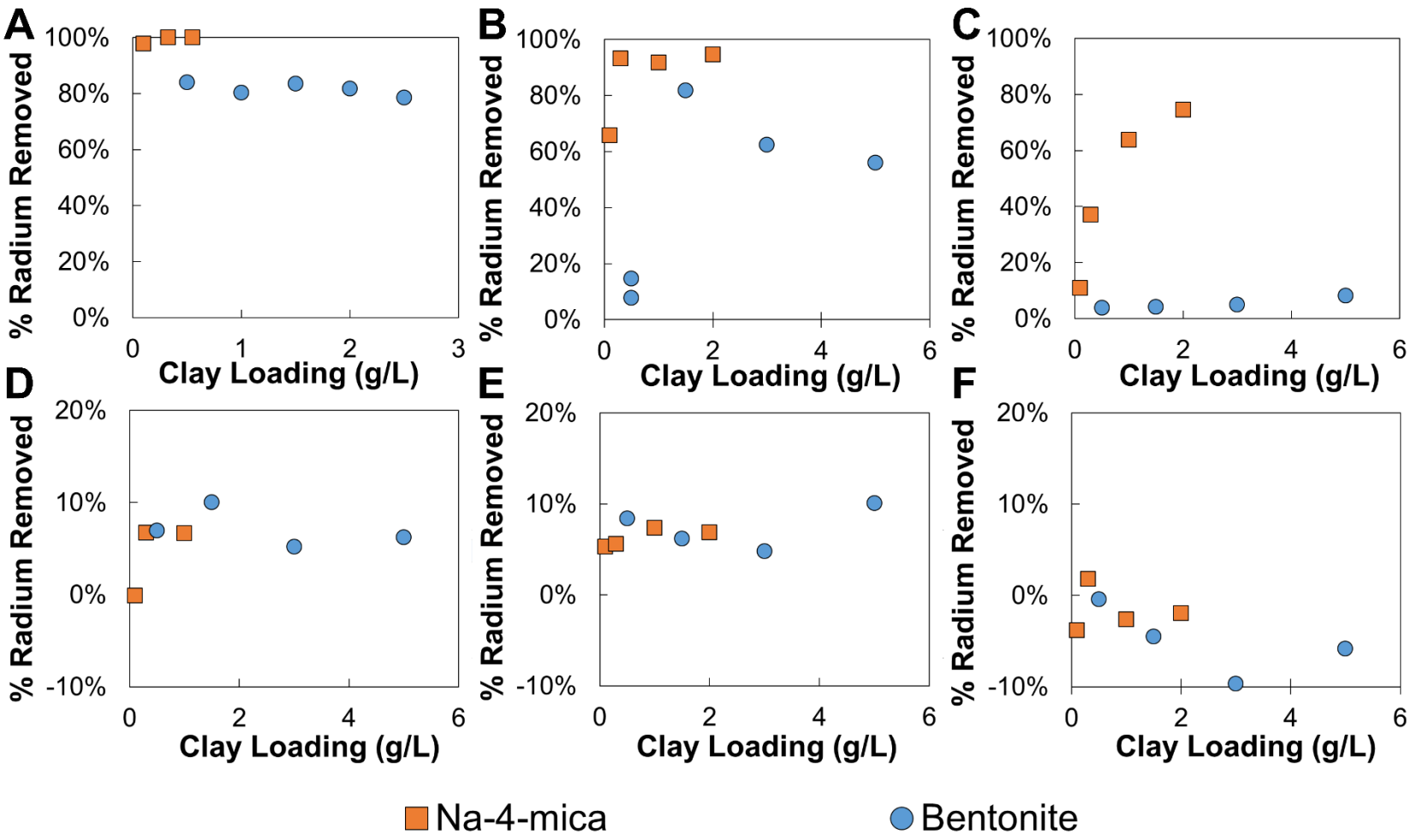

Figure 3.10: Removal efficiency for ^{226}Ra (c_0 = 20,000 pCi/L) by Na-4-mica and Bentonite in batch experiments after a mixing time of 60 minutes. Batch reactors were not buffered. **A**) Initial solution pH = 2.5, no added salt. **B**) Initial solution pH = 10, no added salt. **C**) 1.5 M NaCl and pH = 7. **D**) 1.5M NaCl, 0.01M Ba^{2+}, and pH = 7. **E**) Produced Water Sample #1, ^{226}Ra = 8,950 pCi/L. **F**) Produced Water Sample #2, ^{226}Ra = 11,550 pCi/L.

available sites. Increasing salinity has the effect of reducing the effective charged area " volume" , thereby reducing the effective number of adsorption sites. By increasing the total number of sites, i.e. adding more clay to the system, it is possible to overcome the negative effect of high salinity.

3.4.6 Effect of Competing Ions on Radium Adsoprtion

For ion exchange processes at low salinity, selectivity of metal cations is known to follow the following order of preference: H > Ra > Ba > Ca > Mg > Na [42]. When the salinity is high, the selectivity can become reversed. Ion-exchange is a thermodynamic process that involves displacement of an adsorbed ion by the desorbing ion. The activity (concentration) and selectivity of the adsorbed and desorbed ions are important in deciding the direction of ion-exchange. In oil and gas co-produced waters, Ba, Ca, Mg and Sr are on the order of 10^6 greater concentrations than Ra [1]. Barium is most similar to radium in its selectivity, and as such, it was expected to provide the strongest competition for radium. For this study, the effect of barium was evaluated.

The effect of the competing ion is observed in Figure 3.9D. Barium greatly inhibits radium removal by Na-4-mica. For these experiments, barium was dosed at a concentration of ~0.01M, which is the mean concentration found in Marcellus Shale produced waters [1]. Even though radium is thermodynamically preferred to barium, the preferences is overcome by the activity difference of the two ions. Additionally, it is suggestible that the uptake kinetics will be altered by the high salinity and high barium concentration, such that ion exchange is incomplete after 60 minutes. Further study is required to evaluate this possible complication.

3.4.7 Radium Removal from Produced Water Samples by Na-4-mica

In addition to radium, the concentration of barium, calcium, strontium, sodium, and magnesium were monitored in the supernatants following the adsorption experiments (these results are presented in Table 3.4). The change in the concentrations of these cations during the experiments provided further insight to the adsorption behavior that resulted in radium removal. It was expected that radium was removed by sodium displacement from the clay interlayer. This mechanism could be verified by monitoring the concentration of sodium in the supernatant for increased levels following the adsorption experiments.

For experiments $\#1 - \#3$ where radium removal was high, sodium was desorbed in orders of magnitude higher than radium, or indeed any of the other elements, was adsorbed (on a meq basis). More sodium was desorbed at higher clay loading. More sodium was also released at low to circumneutral pH (i.e. below the pH_{zpc}), when considered on a massic basis (meq per g of added clay). For experiment #4, which included barium, the results indicated that significant barium adsorption occurred, which resulted in little radium removal. For experiments $\#5 - \#6$ with the real produced waters, adsorption of barium, calcium, strontium outperformed radium, resulting in little to no radium removal.

Oil and gas produced waters are characterized by high concentrations of Na, Ba, Ca, and Mg, at levels ~10^6 times that of radium. The adsorption experiments provided evidence that Na-4-mica can remove radium in high-TDS environment, when the composition of TDS is Na and Cl-. However, the presence of barium, even at concentrations of 0.01 M, was enough to have a significant negative impact on radium removal. When the radium removal by Na-4-mica was tested in real produced waters, the additional competition provided by barium, calcium,

magnesium, and strontium overpowered any capacity for radium. Although Na-4-mica is selective for radium, the high ionic strength environment changes the aqueous behavior of the cations. This effect is expressed in illustrated in Figure 3.10A. At high ionic strengths, the activity coefficients of Mg, Ca, and Sr, are elevated high above the activity coefficient of Ra, and even Ba. Therefore, their competition is greatly increased at the high-TDS and high ionic strengths of oil and gas produced waters. As with other ion exchange processes, one approach to overcoming the competing ions is a precipitation or complexation pretreatment that reduces the active concentrations of Mg, Ca, and Sr. One such approach would be metal complexation by EDTA. EDTA forms metal complexes selectively with Mg, Ca, and Sr, before Ra [17]. Additionally, the metal complexes are more strongly formed at high ionic strengths as evidenced by the formation constants (Figure 3.10B). This phenomenon can be exploited in designing a pre-treatment step. In further studies of radium removal by Na-4-mica, the effectiveness of an EDTA-metal complex pre-treatment can be evaluated.

In addition to the competition offered by Mg, Ca, and Sr, further competition could be presented by dissolved organic matter. It is possible that radium is complexed with organic compounds present in the produced waters. Such compounds could be acetate, surfactants, and EDTA routinely used during the process of hydraulic fracturing [1,43,44]. An exploratory Reactive Transport Model (RTM) was developed to investigate the effect of dissolved organic compounds on radium removal by clays. The model simulated a batch reactor, with a volume of 500ml and 12-hour reaction time. Competition for adsorption was simulated through complexation with organic matter. Additional details of the RTM have been provided in Appendix B.5.

Table 3.4: Concentration of barium, calcium, strontium, sodium, magnesium, and radium in the supernatants following the adsorption experiments.

		Clay added (g)	Barium		Calcium		Strontium		Sodium		Magnesium		Radium							
			C (mg/L)	Amount desorbed (meq)	C (mg/L)	Amount desorbed (meq)	C (mg/L)	Amount desorbed (meq)	C (mg/L)	Amount desorbed (meq)	C (mg/L)	Amount desorbed (meq)	C (pCi/L)	Amount desorbed (meq)	% removal	Desorbed Na (meq/g)	Total meq desorbed	Total meq absorbed	Total meq/g desorbed	Total meq/g absorbed
Exp 1: No salt & pH 2.5	Control		0.079		0.513629		0.021		0.6		0.126272		23934	6.35E-09						
	0.1 g/L Na-4-mica	0.003	0.011	2.94E-05	0.500806	-1.92E-05	0.0055	-1.1E-05	3.7	0.004	1.077178	2.35E-03	517	6.22E-09	98%	1.320	0.006	2.98E-05	0.063	9.94E-03
	0.55 g/L Na-4-mica	0.017	0.010	2.99E-05	0.127115	-5.79E-04	0.0077	-9.1E-06	31.2	0.040	1.874108	4.31E-03	0	6.35E-09	100%	2.415	0.044	5.88E-04	0.080	3.56E-02
	0.5 g/L Bentonite	0.015	0.032	2.04E-05	2.395449	2.82E-03	0.0483	1.87E-05	6.7	0.008	0.742636	1.52E-03	3822	5.34E-09	84%	0.523	0.012	5.34E-09	0.024	3.56E-07
	2.5 g/L Bentonite	0.075	0.034	1.94E-05	3.803424	4.93E-03	0.0885	4.62E-05	26.8	0.034	1.165276	2.56E-03	5129	4.99E-09	79%	0.455	0.042	4.99E-09	0.017	6.66E-08
Exp 2: No salt & pH 10	Control		0.028		0.23		0.009		113.9		0.08		5337	1.42E-09						
	0.1 g/L Na-4-mica	0.003	0.008	8.91E-06	0.31	1.20E-04	0.014	3.08E-06	120.4	0.008	0.09	3.96E-05	1824	9.33E-10	66%	2.811	0.009	9.33E-10	0.086	3.11E-07
	2 g/L Na-4-mica	0.06	0.007	9.18E-06	0.17	-9.10E-05	0.009	-2.7E-07	130.5	0.022	0.74	1.64E-03	288	1.34E-09	95%	0.360	0.023	9.13E-05	0.012	1.52E-03
	0.5 g/L Bentonite	0.015	0.025	1.09E-06	0.62	5.89E-04	0.027	1.21E-05	115.9	0.003	0.10	6.08E-05	4700	1.69E-10	12%	0.171	0.003	1.69E-10	0.006	1.13E-08
	5 g/L Bentonite	0.15	0.028	1.31E-07	2.44	3.31E-03	0.084	5.12E-05	132.0	0.024	1.10	2.53E-03	2351	7.93E-10	56%	0.157	0.029	7.93E-10	0.006	5.28E-09
Exp 3: 1.5M Na & pH 7	Control		0.070		2.69		0.081		28229		0.19		19383	5.15E-09						
	0.1 g/L Na-4-mica	0.003	0.053	-7.5E-06	3.34	9.70E-04	0.077	-2.9E-06	29302	1.399	0.89	1.74E-03	17271	5.61E-10	11%	466.340	1.402	1.04E-05	14.017	3.47E-03
	2 g/L Na-4-mica	0.06	0.030	-1.7E-05	2.70	7.93E-06	0.041	-2.7E-05	30365	2.786	6.94	1.67E-02	4926	3.84E-09	75%	46.433	2.803	4.44E-05	1.401	7.40E-04
	0.5 g/L Bentonite	0.015	0.096	1.15E-05	5.74	4.56E-03	0.168	5.95E-05	28769	0.704	0.55	8.90E-04	18638	1.98E-10	4%	46.913	0.709	1.98E-10	1.418	1.32E-08
	5 g/L Bentonite	0.15	0.395	0.000142	28.86	3.92E-02	0.984	6.18E-04	28241	0.015	2.70	6.19E-03	17794	4.22E-10	8%	0.102	0.061	4.22E-10	0.012	2.81E-09
Exp 4: 1.5M Na, 0.015M Ba & pH 7	Control		1008.2		3.23		0.08		32112		0.15		23464	6.23E-09						
	0.1 g/L Na-4-mica	0.003	906.1	-0.045	2.34	-1.33E-03	0.07	-7.87E-06	28721	-4.42	0.2156	1.69E-04	24004	-1.4E-10	-2%	-1474.46	0.0002	4.47	0.002	1.49E+03
	2 g/L Na-4-mica	0.06	918.4	-0.039	5.94	4.05E-03	0.12	2.43E-05	29415	-3.52	1.3712	3.02E-03	47654	-6.4E-09	-103%	-58.632	0.007	3.56	0.004	5.93E+01
	0.5 g/L Bentonite	0.015	971.1	-0.016	5.37	3.21E-03	0.15	4.75E-05	29766	-3.06	0.3976	6.18E-04	22305	3.08E-10	5%	-204.028	0.004	3.08	0.008	2.05E+02
	5 g/L Bentonite	0.15	893.4	-0.050	26.74	3.52E-02	0.80	4.93E-04	28925	-4.16	2.2554	5.20E-03	22480	2.61E-10	4%	-27.715	0.041	4.21	0.008	2.80E+01
Exp 5: Produced Water Sample #1	Control		4908.4		9503.7		2758.7		23648		724.2		8951	2.38E-09						
	0.1 g/L Na-4-mica	0.003	4761.2	-0.064	9326.3	-2.66E-01	2684.9	-5.05E-02	21798	-2.413	711.4	-3.17E-02	9294	-9.1E-11	-4%	-804.387	0	2.83	0	9.42E+02
	2 g/L Na-4-mica	0.06	4777.6	-0.057	9275.9	-3.41E-01	2695.8	-4.3E-02	22437	-1.579	723.8	-9.32E-04	9126	-4.6E-11	-2%	-26.325	0	2.02	0	3.37E+01
	0.5 g/L Bentonite	0.015	4723.6	-0.081	9232.9	-4.05E-01	2663.4	-6.53E-02	22331	-1.718	720.8	-8.36E-03	8988	-9.8E-12	0%	-114.528	0	2.28	0	1.52E+02
	5 g/L Bentonite	0.15	4712.5	-0.086	9367.5	-2.04E-01	2648.0	-7.58E-02	22131	-1.979	720.8	-8.32E-03	9476	-1.4E-10	-6%	-13.192	0	2.35	0	1.57E+01
Exp 6: Produced Water Sample #2	Control		5954.0		10645.1		3280.8		27296		912.7		11548	3.07E-09					0	
	0.1 g/L Na-4-mica	0.003	5726.2	-0.100	10309.0	-5.03E-01	3107.8	-1.2E-01	26871	-0.554	854.4	-1.44E-01	10937	1.62E-10	5%	-184.657	0	1.42	0	4.73E+02
	2 g/L Na-4-mica	0.06	5583.3	-0.162	10058.3	-8.79E-01	3093.1	-1.3E-01	25605	-2.205	867.1	-1.12E-01	10753	2.11E-10	7%	-36.753	0	3.49	0	5.81E+01
	0.5 g/L Bentonite	0.015	5704.4	-0.109	10167.6	-7.15E-01	3107.5	-1.19E-01	25634	-2.167	872.3	-9.96E-02	10580	2.57E-10	8%	-144.458	0	3.21	0	2.14E+02
	5 g/L Bentonite	0.15	5655.0	-0.131	10176.3	-7.02E-01	3075.4	-1.41E-01	25911	-1.806	863.2	-1.22E-01	10385	3.09E-10	10%	-12.041	0	2.90	0	1.93E+01

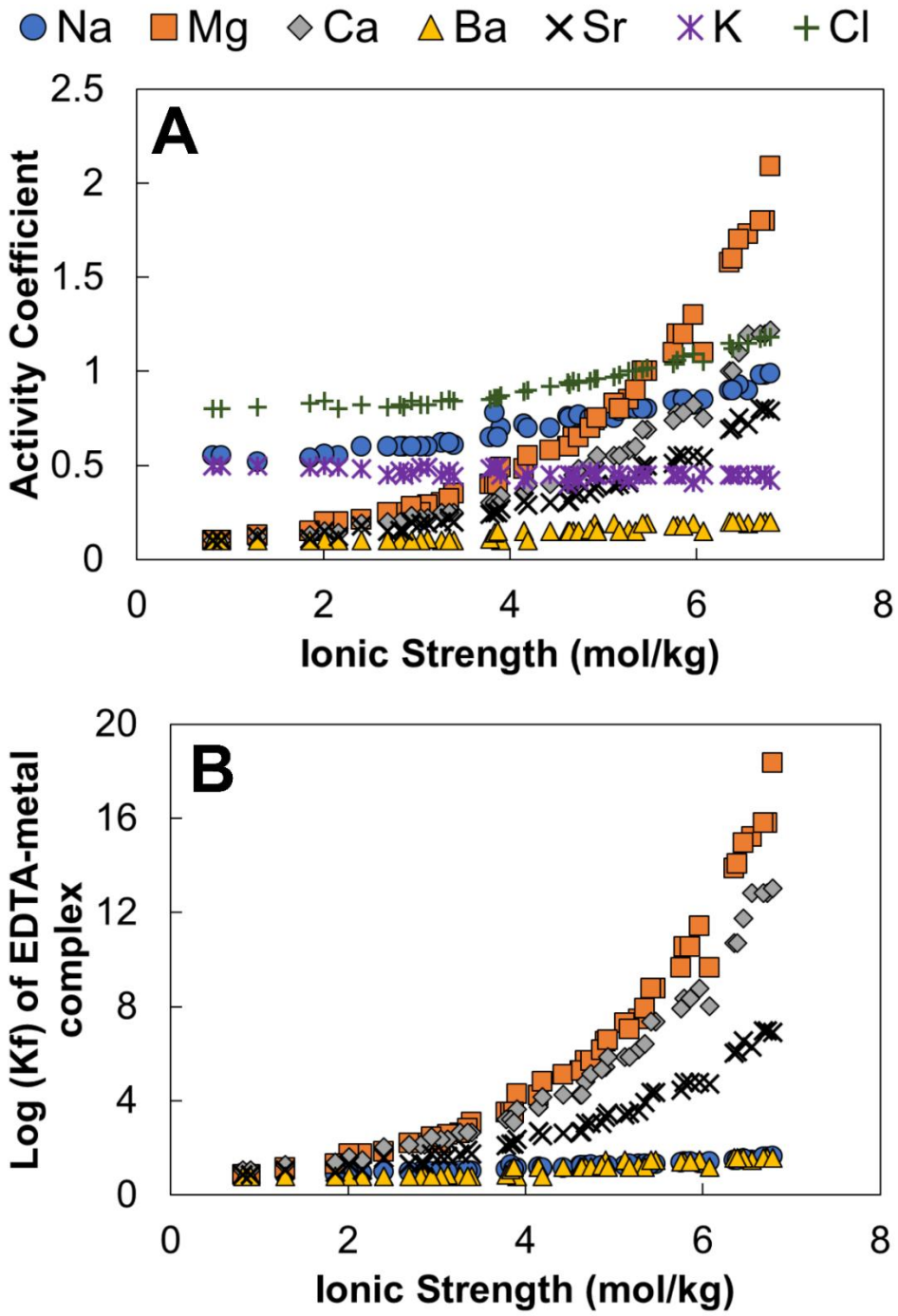

Figure 3.11: (**A**) Activity coefficients and (**B**) log of the EDTA-Metal complex formation constants over the range of ionic strength encountered in high-TDS oil and gas produced waters.

The model was able to highlight that organic matter (or surface complexation) serves as a radium sink; and in fact this competition serves to diminish radium removal from solution (Figure 3.11). Therefore, the presence of dissolved organic compounds that can complex radium most likely reduces radium removal by Na-4-mica.

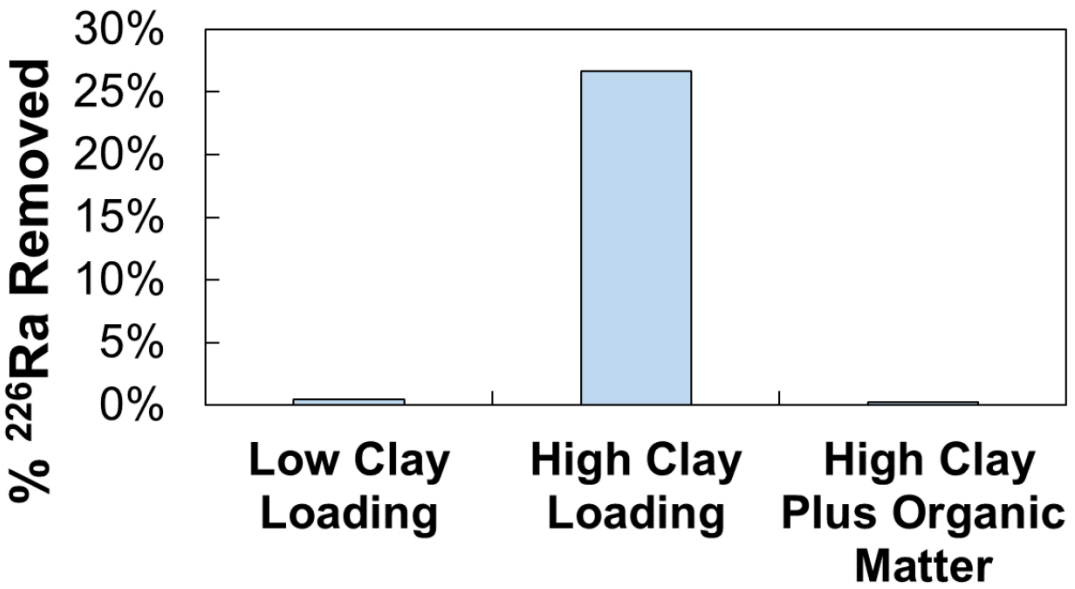

Figure 3.12: Reactive Transport Modelling of organic matter complexation of ^{226}Ra and the effect on radium removal by ion exchange. Organic matter serves as a radium sink, diminishing radium removal by clays.

3.5 Conclusions

This work fundamentally asks the question, " Is Na-4-mica a viable treatment option for Ra in high TDS waters?" Batch experiments of clay with synthetic produced water provided valuable insights into the key mechanisms driving radium removal by Na-4-mica. Interlayer adsorption of radium led to preferential radium

removal even in the presence of 1.5 M NaCl; however, this is negatively impacted by the presence of barium. When real produced waters were tested, radium was not preferentially removed by Na-4-mica. The presence of calcium, magnesium and strontium, at concentrations many orders of magnitude above radium, presupposes the need for a pretreatment step that reduces the competition from these species. Furthermore, the presence of dissolved organic compounds in produced water presents additional competition for radium. The effect of these organic compounds on radium removal by Na-4-mica was not determined experimentally, but an exploratory model suggested that dissolved organic compounds that can form metal complexes will greatly reduce radium removal by Na-4-mica.

3.6 Acknowledgments

This research was funded by a National Science Foundation (NSF) PFI: AIR-TT #1640634. Further support originated from a Penn State College of Engineering Graduate Excellence Fellowship and a Penn State SEED Grant. We thank Nichole Wonderling from the Penn State Materials Research Institute for her assistance with Quantitative X-ray diffraction.

3.7 References

(1) Hayes, T. *Sampling and Analysis of Water Streams Associated with the Development of Marcellus Shale Gas*; Des Plaines, 2009.

(2) Pennsylvania Department of Environmental Protection (PA DEP). Technologically Enhanced Naturally Occurring Radioactive Materials (TENORM) Study Report http://www.depgreenport.state.pa.us/elibrary/getdocument?docid=5815&docname=01 pennsylvania department of environmental protection tenorm study report rev 1.pdf (accessed Feb 8, 2018).

(3) Gregory, K. B.; Vidic, R. D.; Dzombak, D. A. Water Management Challenges Associated with the Production of Shale Gas by Hydraulic Fracturing. *Elements* 2011, *7* (3), 181–186.

(4) Rahm, B. G.; Bates, J. T.; Bertoia, L. R.; Galford, A. E.; Yoxtheimer, D. A.; Riha, S. J. Wastewater Management and Marcellus Shale Gas Development: Trends, Drivers, and Planning Implications. *J. Environ. Manage.* 2013, *120*, 105–113.

(5) Kravchenko, J.; Darrah, T. H.; Miller, R. K.; Lyerly, H. K.; Vengosh, A. A Review of the Health Impacts of Barium from Natural and Anthropogenic Exposure. *Environ. Geochem. Health* 2014, *36* (4), 797–814.

(6) Tasker, T. L.; Burgos, W. D.; Piotrowski, P.; Castillo-Meza, L.; Blewett, T. A.; Ganow, K. B.; Stallworth, A.; Delompré , P. L. M.; Goss, G. G.; Fowler, L. B.; et al. Environmental and Human Health Impacts of Spreading Oil and Gas Wastewater on Roads. *Environ. Sci. Technol.* 2018, *52* (12), 7081–7091.

(7) Geeza, T. J.; Gillikin, D. P.; McDevitt, B.; Van Sice, K.; Warner, N. R. Accumulation of Marcellus Formation Oil and Gas Wastewater Metals in Freshwater Mussel Shells. *Environ. Sci. Technol.* 2018, *52* (18), 10883–10892.

(8) Burgos, W. D.; Castillo-Meza, L.; Tasker, T. L.; Geeza, T. J.; Drohan, P. J.; Liu, X.; Landis, J. D.; Blotevogel, J.; McLaughlin, M.; Borch, T.; et al. Watershed-Scale Impacts from Surface Water Disposal of Oil and Gas Wastewater in Western Pennsylvania. *Environ. Sci. Technol.* 2017, *51* (15), 8851–8860.

(9) Lauer, N. E.; Warner, N. R.; Vengosh, A. Sources of Radium Accumulation in Stream Sediments near Disposal Sites in Pennsylvania: Implications for Disposal of Conventional Oil and Gas Wastewater. *Environ. Sci. Technol.* 2018.

(10) McDevitt, B.; McLaughlin, M.; Cravotta, C. A.; Ajemigbitse, M. A.; Van Sice, K. J.; Blotevogel, J.; Borch, T.; Warner, N. R. Emerging Investigator Series: Radium Accumulation in Carbonate River Sediments at Oil and Gas

Produced Water Discharges: Implications for Beneficial Use as Disposal Management. *Environ. Sci. Process. Impacts* 2019, *21* (2), 324– 338.

(11) Warner, N. R.; Christie, C. A.; Jackson, R. B.; Vengosh, A. Impacts of Shale Gas Wastewater Disposal on Water Quality in Western Pennsylvania. *Environ. Sci. Technol.* 2013, *47*, 11849– 11857.

(12) He, C.; Li, M.; Liu, W.; Barbot, E.; Vidic, R. D. Kinetics and Equilibrium of Barium and Strontium Sulfate Formation in Marcellus Shale Flowback Water. *J. Environ. Eng.* 2014, *140* (5), B4014001– 1 – B4014001– B4014009.

(13) Zhang, T.; Gregory, K.; Hammack, R. W.; Vidic, R. D. Co-Precipitation of Radium with Barium and Strontium Sulfate and Its Impact on the Fate of Radium during Treatment of Produced Water from Unconventional Gas Extraction. *Environ. Sci. Technol.* 2014, *48* (8), 4596– 4603.

(14) He, C.; Zhang, T.; Vidic, R. D. Co-Treatment of Abandoned Mine Drainage and Marcellus Shale Flowback Water for Use in Hydraulic Fracturing. *Water Res.* 2016, *104*, 425– 431.

(15) He, C.; Zhang, T.; Zheng, X.; Li, Y.; Vidic, R. D. Management of Marcellus Shale Produced Water in Pennsylvania: A Review of Current Strategies and Perspectives. *Energy Technol.* 2014, *2* (12), 968– 976.

(16) He, C.; Zhang, T.; Vidic, R. D. Use of Abandoned Mine Drainage for the Development of Unconventional Gas Resources. *Disruptive Sci. Technol.* 2013, *1* (4), 169– 176.

(17) Bi, Y.; Zhang, H.; Ellis, B. R.; Hayes, K. F. Removal of Radium from Synthetic Shale Gas Brines by Ion Exchange Resin. *Environ. Eng. Sci.* 2016, *33* (10), 791– 798.

(18) Paukert Vankeuren, A. N.; Hakala, J. A.; Jarvis, K.; Moore, J. E. Mineral Reactions in Shale Gas Reservoirs: Barite Scale Formation from Reusing Produced Water As Hydraulic Fracturing Fluid. *Environ. Sci. Technol.* 2017, *51* (16), 9391– 9402.

(19) Ammann, L. Cation Exchange and Adsorption on Clays and Clay Minerals. 2003, 1– 113.

(20) Ghadiri, M.; Chrzanowski, W.; Rohanizadeh, R. Biomedical Applications of Cationic Clay Minerals. *RSC Adv.* 2015, *5* (37), 29467– 29481.

(21) Adeyemo, A. A.; Adeoye, I. O.; Bello, O. S. Adsorption of Dyes Using Different Types of Clay: A Review. *Appl. Water Sci.* 2017, *7* (2), 543– 568.

(22) Uddin, M. K. A Review on the Adsorption of Heavy Metals by Clay Minerals, with Special Focus on the Past Decade. *Chem. Eng. J.* 2017, *308*, 438– 462.

(23) Alhajji, E.; Al-Masri, M. S.; Khalily, H.; Naoum, B. E.; Khalil, H. S.; Nashawati, A. A Study on Sorption of 226Ra on Different Clay Matrices. *Bull. Environ. Contam. Toxicol.* 2016, *97* (2), 255– 260.

(24) Ames, L. L.; Mcgarrah, J. E.; Walker, B. A. Sorption of Trace Constituents from Aqueous Solutions onto Secondary Minerals. II. Radium. *Clays Clay Miner.* 1983, *31* (5), 335– 342.

(25) Komarneni, S.; Kozai, N.; Paulus, W. J. Superselective Clay for Radium Uptake. *Nature* 2001, *410* (6830), 771– 771.

(26) Frazer, L. Mighty Mica: Synthetic Clay Remediates Radium. *Environ. Health Perspect.* 2002, *110* (9), A528– 8.

(27) Gregorkiewitz, M.; Rausell-Colom, J. A. Characterization and Properties of a New Synthetic Silicate with Highly Charged Mica-Type Layers. *Am. Mineral.* 1987, *72* (5-6), 515– 527.

(28) Ravella, R.; Submitted. Swelling Mica-Type Clays of Variable Charge: Synthesis, Characterization and Ion Exchange Studies. 2006, No. August.

(29) Kodama, T.; Komarneni, S. Simplified Synthesis of Na-4-Mica from Kaolinite and Cation- Exchange Properties. *Sep. Sci. Technol.* 2000, *35* (8), 1133– 1152.

(30) Franklin, K. R.; Lee, E. Synthesis and Ion-Exchange Properties of Na-4-Mica. 1996, *6*, 109– 115.

(31) Komarneni, S.; Pidugu, R.; Amonette, J. E. Synthesis of Na-4-Mica from Metakaolinite and MgO: Characterization and Sr 2 + Uptake Kinetics. *J.*

Mater. Chem. 1998, *8* (1), 205– 208.

(32) Park, M.; Lee, D. H.; Choi, C. L.; Kim, S. S.; Kim, K. S.; Choi, J. Pure Na-4-Mica : Synthesis and Characterization. 2002, No. 14, 2582– 2589.

(33) Ravella, R.; Komarneni, S. Synthesis of Swelling Micas with Stoichiometric Amount of Fluorine, Characterization and Ion Exchange Studies. *Appl. Clay Sci.* 2008, *39* (3-4), 180– 185.

(34) Kodama, T.; Komarncni, S. Alkali Metal and Alkaline Earth Metal Ion Exchange with Na-4-Mica Prepared by a New Synthetic Route from Kaolinite. *J. Mater. Chem.* 1999, *9* (10), 2475– 2480.

(35) Kodama, T.; Harada, Y.; Ueda, M.; Shimizu, K. I.; Shuto, K.; Komarneni, S. Selective Exchange and Fixation of Strontium Ions with Ultrafine Na-4-Mica. *Langmuir* 2001, *17* (16), 4881– 4886.

(36) Paulus, W. J.; Komarneni, S.; Roy, R. Bulk Synthesis and Selective Exchange of Strontium Ions in Na4Mg6Al4Si4O20F4 Mica. *Nature* 1992, *357* (6379), 571– 573.

(37) Fiol, N.; Villaescusa, I. Determination of Sorbent Point Zero Charge: Usefulness in Sorption Studies. *Environ. Chem. Lett.* 2009, *7* (1), 79– 84.

(38) Nasiruddin Khan, M.; Sarwar, A. Determination of Points of Zero Charge of Natural and Treated Adsorbents. *Surf. Rev. Lett.* 2007, *14* (03), 461– 469.

(39) Yan, N.; Masliyah, J. H. Effect of pH on Adsorption and Desorption of Clay Particles at Oil– Water Interface. *J. Colloid Interface Sci.* 1996, *181* (1), 20– 27.

(40) Hubbard, C. R.; Snyder, R. L. RIR - Measurement and Use in Quantitative XRD. *Powder Diffr.* 1988, *3* (02), 74– 77.

(41) Zermeno-Motante, M. I.; Nieto-Delgado, C.; Cannon, F. S.; Cash, C. C.; Wunz, C. C. Chemical Modeling for Precipitation from Hypersaline Hydrofracturing Brines. *Water Res.* 2016, *103*, 233– 244.

(42) Beneš , P.; Borovec, Z.; Strejc, P. Interaction of Radium with Freshwater

Sediments and Their Mineral Components - III. Muscovite and Feldspar. *J. Radioanal. Nucl. Chem. Artic.* 1986, *98* (1), 91– 103.

(43) Luek, J. L.; Gonsior, M. Organic Compounds in Hydraulic Fracturing Fluids and Wastewaters: A Review. *Water Res.* 2017, *123*, 536– 548.

(44) Akob, D. M.; Cozzarelli, I. M.; Dunlap, D. S.; Rowan, E. L.; Lorah, M. M. Organic and Inorganic Composition and Microbiology of Produced Waters from Pennsylvania Shale Gas Wells. *Appl. Geochemistry* 2015, *60*, 116– 125.

Part II

Novel Measurement Techniques for Radium in Hydraulic Fracturing Co-Products

Chapter 4

Self-Attenuation Corrections for Radium Measurements of Oil and Gas Solids by Gamma Spectroscopy

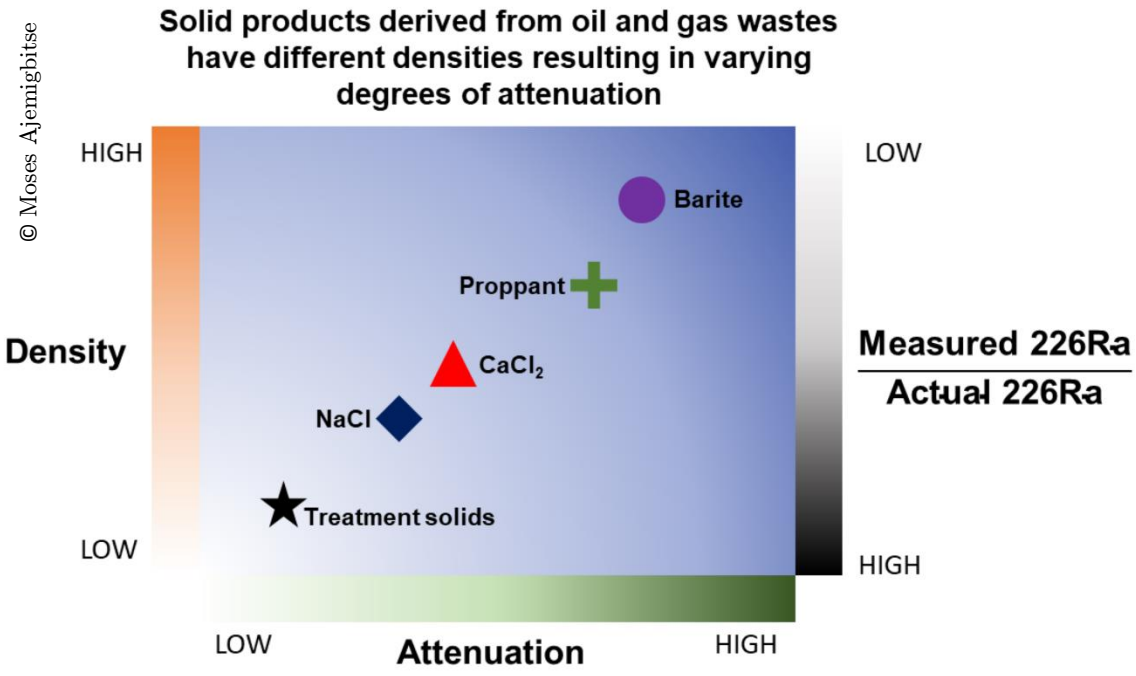

Ajemigbitse MA, Cheng Y, Cannon FS, and Warner NR. "Self-Attenuation Corrections for Radium Measurements of Oil and Gas Solids by Gamma Spectroscopy." Manuscript in Preparation.

4.1 Abstract

Beneficial reuse and resource recovery from produced water often requires treatment to remove radium before valuable products are extracted. The radium content of the treatment waste solids and beneficial products must be accurately determined when evaluating the efficacy and social validity of such treatments. While gamma spectroscopy remains the recommended method for radium measurements, these measurements can be impacted by the composition/mineralogy of the solids, which influence the attenuation of the gamma decay energy − with denser sediments incurring greater degrees of attenuation. This self-attenuation must be accounted for when accurately measuring radium, otherwise radium measurements are found to be inaccurate, sometimes by as much as 50%. To meet industry needs, measurements should be both accurate and rapid, even for small sample sizes. Consequently, we propose a rapid method for accurate radium measurements with an empirical technique to account for sample attenuation in well-detector gamma spectroscopy. This technique utilizes the sample density and sample volume in the measuring vial. These corrections are relevant to a wide range of solid samples and sediment densities that may be encountered during treatment and management of oil and gas solids, including clays, environmental sediment samples, sand grains, and precipitated salts. These corrections can also be applied for situations were low volumes of material are present, as in bench scale studies, thereby rendering this technique applicable to a wider range of scenarios.

4.2 Introduction

Radionuclides play critical roles in the environmental sciences as they serve as geochemical tracers for both natural and anthropogenic processes [1–6]. The shale gas revolution brought rapid application of hydraulic fracturing and extensive extraction of natural gas from unconventional shale reservoirs; but it also created large volumes of produced water that contain high levels of total dissolved solids, heavy metals, and naturally occurring radioactive material (NORM) [7–10]. Moreover, NORM is present in bedrock or drill cuttings, spent hydraulic fracturing proppant sand, drilling sediments, and formation clays [11–13]. Current treatment and management practices for the produced water often generate secondary solids in the form of precipitates or filter cake from fluid processing plants [14], or stream sediments from surface disposal [6,15–17]. These solids have been found to contain high levels of NORM; and when these are derived during treatment, they are classified as technologically enhanced NORM (TENORM) [18]. The appropriate management and plausible treatment options for the produced water, primary solids, and secondary solids is often dictated by their radioactivity [14,19,20]. Indeed, the ecological impact from recent extraction of natural gas from unconventional formations [21–30], including radioactive contamination [6,30–34] has drawn attention and led to exploration of alternative management options for solids associated with oil and gas wastes. Likewise, the increased emphasis on alternative beneficial uses of produced water – through reuse, recycling and resource recovery [35–37]– necessitates accurate accounting of radium in the co-products and the final waste streams to ensure health and safety of workers and consumers.

High purity germanium (HPGe) γ spectroscopy (γ-spec) remains one of the most widely accepted methods for radium measurements [38]. However, research has shown

that activities reported from these measurements can still be widely variable. For example, an inter-lab comparison study revealed that the reported radium activities of sediments had ±30% difference among labs, possibly due to calibration inconsistencies, radon leakage, or failure to correct for sample self-attenuation [39]. Self-attenuation of γ-rays is greatly dependent on the mineralogy and density of the sample [40–42], and must be accounted for during measurements. Otherwise, recurring under-reporting of radium activities could occur. With a coaxial and planar detector configuration of the γ-spec, and specified sample geometry, a point source method can be used to account for sample self-attenuation, such as the Cutshall Method [43,44]. However, in well-detector γ-spec, it is difficult to account for self-attenuation using a point source. This is because the 2-π geometry results in a non-uniform signal being transmitted from the point source through the sample to the detector [40]. Furthermore, when dealing with engineered, environmental, and laboratory-scale samples – where minimal masses of samples are available – the low mass can produce varying efficiency performance due to the fill height in the chosen sample geometry. As γ-spec remains one of the most widely applied techniques for radium measurement, this research aimed to conduct a study on well-detector γ-spec, so as to account for self-attenuation on solid samples over varying densities and varying fill heights. This study is aimed to aid researchers and entrepreneurs during studies on the beneficial use of co-products of oil and gas extraction, such as for lithium recovery [45–51] and commercial salt recovery [52] or surface water disposal, where sample volume could be low (e.g., bench-scale studies) and sample densities can vary (e.g., precipitates NaCl, $CaCl_2$ or $BaSO_4$).

The objectives of this study were to i) account and correct for self-attenuation in the γ-spec measurements of solids where a point source correction is impractical, ii) investigate and describe the effect of varying sample sizes and sediment densities on the reported radioactivity, and iii) provide recommendations for generating rapid and accurate radium measurements in solids derived from oil and gas waste management.

4.3 Materials and Methods

4.3.1 Materials

Inframat® Advanced Materials provided ultrapure alpha-aluminum oxide nano-powder, which hosted a tamped density of 1.110 g/mL (with tamping per the density-packed protocol below). Sigma Aldrich supplied bentonite (Na-Montmorillonite), with a tamped density of 0.998 g/mL. The certified reference materials (CRM) UTS-2, UTS-3, and UTS-4 uranium tailings were provided by the Canadian Certified Reference Materials Project (CCRMP). These had tamped densities of 1.809 g/mL, 1.830 g/mL, and 1.422 g/mL; and certified ^{226}Ra activities of 5.6 Bq/g, 13.3 Bq/g, and 22.9 Bq/g. Certified elemental compositions of the CRMs are presented in Table C1. The sample vial geometry was a Wheaton 24 mL poly seal cone-lined urea capped high density poly ethylene (HDPE) scintillation vial, with cylindrical dimensions of 2.8 cm diameter by 6.1 cm height.

4.3.2 Density and Height Distribution

The certified CRM UTS-2 was mixed with either bentonite or alpha-aluminum oxide, while UTS-3 was mixed with the alpha-aluminum oxide using an agate mortar and pestle. These mixtures varied in their proportions of CRM-to-bentonite or

CRM-to-aluminum oxide, with the CRM portion listed first. These proportions were 0:100, 10:90, 40:60, 70:30, or 80:20. After mixing, the sediments were packed into the 24 mL scintillation vials. We ensured that the vials were densely packed by tamping using a rubber nib to compress the sediment. Into this 2.8 cm diameter vial, we applied about 30 kPa (4.35 psi) of pressure about $20 - 50$ times for each lift of sediment until the sediment could not be compressed further. This protocol required about $8 - 10$ lifts of ~$3 - 5$ g of sediment for each lift in order to fully fill a vial. The density of each sample, at each mix ratio, was determined as the mass used to fully fill the vial (after tamped-dense packing) divided by a nominal volume of 24 mL. The corresponding densities of these blended sediments ranged from 0.998 g/mL to 1.83 g/mL, with detailed results as presented in Table C2. The caps of the vials were then sealed shut by wrapping with several layers of Parafilm M®.

In order to compare detector efficiency versus fill height, the UTS-2 and UTS-3 samples were filled and tamped per the same protocol above. These vials were filled to 6 cm (fully filled vial), 3.5 cm or 3 cm, 2 cm, and 1 cm. The caps of the vials were then sealed shut by wrapping with several layers of Parafilm M®.

4.3.3 Radium Analysis of the Sediments

Radium-226 activities of all sediment samples were determined by γ-spec on a Canberra ultra-low background small anode germanium (SAGe) well detector, after the incubation period of about 30 days, so as to reach secular equilibrium between radium and its progeny. These included 19 conditions of varying sediment proportions and sample fill heights. Each sample was counted twice for twelve hours. The variance-weighted average of the two counts was then used for efficiency determination. The detector efficiency was determined at the following energy levels: 186.2

keV (^{226}Ra), 295.2 keV (^{214}Pb), 351.9 keV (^{214}Pb), and 609.3 keV (^{214}Bi). The standard error was reported and the error propagation has been included in Appendix A.2.

The alpha-aluminum oxide had no measurable radium activity. Bentonite contained some measurable radium, and the activity was accounted for by using the efficiency determined from the UTS-2 certified sediment at full height. Thus, for samples that contained bentonite, the total radium activities were additive of both that of bentonite and the CRM. Detailed information on the total radium activities of the mixed sediments is presented in Table C3.

4.3.4 Interference Correction for Radium-226 at 186 keV Energy Level by Peak Deconvolution

When radium measurements are made from the direct analysis of the decay at the 186.2 keV, they must be corrected for interference caused by ^{235}U at the 185.7 keV energy level [40] that causes a broader, larger peak in total counts centered around 186 keV. Uranium could be present in many natural sediments, and it was certainly present in the CRMs UTS-2 and UTS-3, as exhibited by Table C1.

An empirical interference correction can be performed by assuming secular equilibrium between ^{234}Th and ^{238}U. Then, the activity of ^{235}U can be estimated by multiplying the activity of ^{234}Th (measured at 63 keV) by the mean natural abundance ratio of the uranium isotopes ^{235}U and ^{238}U. The activity of ^{235}U can then be subtracted from the total activity at the 186 keV peak, leaving the activity of ^{226}Ra. The detector efficiency for ^{226}Ra can then be determined as given in Eq. (4.1) [53].

$$\gamma_{yield}^{186}\epsilon^{186} = \frac{R_{bkg-corr}^{186\,KeV} - \left(\frac{R_{bkg-corr}^{63\,KeV} \times 0.04605 \times 0.571}{0.0375}\right)}{A^{Ra-226}} \tag{4.1}$$

where,

$\gamma_{yield}^{186}\epsilon^{186}$ is the nuclear yield of ^{226}Ra gamma decay at 186 keV multiplied by the detector efficiency at 186.2 keV energy level

$R_{bkg-corr}^{186\,KeV}$ is the count rate at 186.2 keV corrected for the background count rate attributed to radium-226 and uranium-235, sec^{-1}

$R_{bkg-corr}^{63\,KeV}$ is the count rate at 63 keV corrected for the background count rate attributed to thorium-234, sec^{-1}

0.04605 is the mean natural activity ratio of ^{235}U/^{238}U [53]

0.571 is the nuclear yield of ^{235}U gamma decay at 185.7 keV [40]

0.0375 is the nuclear yield of ^{234Th} gamma decay at 63 keV [40], and

A^{Ra-226} is the certified radium-226 activity in Bq

When this interference correction was applied, measured radium activities were within 5% of the certified value, compared to 10 − 45% when the interference correction was not applied (Table C6).

4.3.5 Statistical Analyses

Statistical analyses were performed using Minitab® 18; including linear regressions of the efficiency versus the sample heights and sediment densities. Data analyses were performed in MATLAB® and Microsoft® Excel.

4.4 Results and Discussion

4.4.1 Influence of Sample Size and Density on Radium Efficiency

For a given source material, densities were generally proportional to fill height. Moreover, for mixtures of certified sediments and either bentonite or aluminum oxide, densities were generally quite close to the value that would be anticipated by mass/volume balance of the proportions of each component. The density determination protocol is presented in the SI, as well as the densities and heights of the mixed sediments (Table C2).

In order to ensure that the CRMs were similar/representative of the mineralogy of the sediments where this method would be applicable, we compared the compositions of the CRMs with sediment cores from a river impacted by disposal of oil and gas produced water [6]. We found that the CRMs were within the range of mineralogy (Al, Fe, Ti, S, Ba and Ca) of the river sediments (Table C1 and C5). Additionally, the CRMs are Feldspar/Quartz sediments, which are similar to the sediments that could be encountered when using this activity correction.

The self-attenuation of the mixed sediments can be glimpsed by observing the change in the detector efficiency at the varying density and height values. The efficiency at 186 keV is calculated by Eq. (4.1). For the other energy levels – 295.2 keV (^{214}Pb), 351.9 keV (^{214}Pb), and 609.3 keV (^{214}Bi) – the efficiency is determined by the following equation:

$$\gamma_{yield}^{E}\epsilon^{E} = \frac{R_{bkg-corr}^{E\,KeV}}{A^{Ra}} \tag{4.2}$$

where,

ϵ^{E} is detector efficiency at the given energy level, $E\,keV$

$R_{bkg-corr}^{E\,KeV}$ is the count rate at E keV corrected for the background count rate, cps

γ_{yield}^{E} is the nuclear yield of the isotope gamma decay at the given E keV, and

A^{Ra} is the certified Ra-226 activity added of the mixed sediments, Bq

Illustrated in Figure 4.1 is the influence of density and height on the detector efficiency. First, we observe the change in efficiency when the density is varied but the fill height is kept constant (Figure 4.1A). Next, we observe the change in efficiency when the sample fill height is varied for a sediment at constant density (Figure 4.1B). Clearly shown is the mass-dependent attenuation, as the mixed sediments with higher density report lower detector efficiencies. Additionally, when the vial is not fully filled, the efficiency values are higher. Increasing the mass of the sediment either by increasing the density or the fill height resulted in a reduced efficiency. This mass dependence of self-attenuation is expected [41,42]. We can define a relationship between the attenuated and un-attenuated efficiencies as follows:

$$\epsilon_A^E = \epsilon^E + \alpha_{height}H + \alpha_{density}D \tag{4.3}$$

where

ϵ_A^E is the attenuated efficiency at any given energy level

α_{height} is the height-influenced attenuation factor

$\alpha_{density}$ is the density-influenced attenuation factor

H is the sample fill height, cm, and

D is the sediment density, g/mL

The attenuation factors can be determined empirically by performing a linear regression of the detector efficiency against the fill height and density.

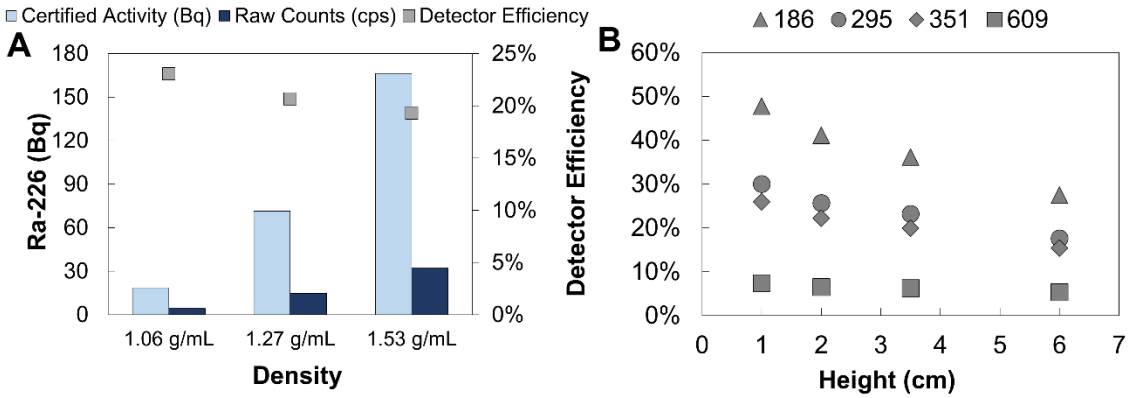

Figure 4.1: **A.** The certified activity compared to the raw instrument counts (cps) of UTS-2 blended with bentonite to three density values. The ratio of raw counts to the certified activity gives the detector efficiency. **B.** The detector efficiencies at the different energy levels plotted against the different sample fill heights.

The detector efficiencies at each energy level were linearly regressed against density and height. The coefficients of the regression were tested for statistical significance on a two-sided 95% confidence interval and all coefficients were found to be statistically significant (Table 4.1).

Statistical analyses showed that about 85% of the regression was explained by the height variation, while 15% was explained by the density variation. A MATLAB code (included in Appendix C.2) performed the density determination based on mass and fill height, and the corresponding efficiency correction based on the derived density and fill height.

The linear regression showed that the attenuation factors of height and density were both slightly negative, meaning that greater height or greater density correlated to lesser gamma energy detection (Table 4.1). As most measurements are performed at full vial height, we can take the efficiency at full height as a reference point. For comparison, measurements of samples that do not fill the vial will result in a higher efficiency, and thus a lower reported activity. That is to say, for the same sample measured at full height and at partial height, the activity determined at partial height will be less than the activity determined at full height − if the height-influenced attenuation is ignored; and thus the partial height γ-spec analysis would be inaccurately biased low.

Table 4.1: Linear Regression Results. The detector efficiency at each energy level, regressed against the fill height and sample density provided estimates of the height- and density-influenced attenuation factors. P-values of the estimates shown in parenthesis. All estimates were statistically significant (two-sided 95% confidence interval).

$\epsilon^{E\,keV}$ = Constant + α_{height} × Height + $\alpha_{density}$ × Density	R^2
ϵ^{186} = 0.0242 - 0.00135 × Height (p = 0.00) - 0.00348 × Density (p = 0.00)	95.2%
ϵ^{295} = 0.0816 - 0.00437 × Height (p = 0.00) - 0.0122 × Density (p = 0.00)	93.4%
ϵ^{351} = 0.136 - 0.00720 × Height (p = 0.00) - 0.0203 × Density (p = 0.00)	93.1%
ϵ^{609} = 0.0465 - 0.00167 × Height (p = 0.00) - 0.00618 × Density (p = 0.016)	72.5%

The same analysis was applied to measurements at various densities; however, in this case, we did not define the reference point for measurements based on density. Nevertheless, if we can assume a reference sediment density that is high, and that

there are natural or anthropogenic processes that result in a lower density due to mineralogical changes, but with no associated mass or radium loss, then measurements performed on the final sediment will have lower activities (on a mass basis), than the starting sediment, even though there has been no change in the radium activity.

4.4.2 Error Analysis

The sources of error for the γ-spec radium activity after correcting for density and height include the following: i) mass measurement as determined by a balance, ii) height measurement, as determined by a ruler, iii) standard counting error, as reported from the instrument, iv) standard error of the calculated density, v) standard error of the γ-spec efficiency due to height, and vi) standard error of the γ-spec efficiency due to density.

The standard error of the balance was 0.05%, the standard error of the ruler was 5%, and the standard error of the calculated density was 0.6%. With sufficient counting time (i.e. 12 hours), the standard error of the instrument measurement can be <5%. The standard error of the γ-spec efficiency value based on the height and density was between 2-6% (Figure 4.3).

For ^{226}Ra, the lowest standard error could be obtained by direct measurement at the 186 keV energy level. Measurements performed at this energy level typically require longer counting times to achieve a satisfactory counting error (typically <5%) as the nuclear yield of ^{226}Ra is low at this energy level [40]. When the measurements are performed at the other energy levels i.e. using the daughter products at 295 keV, 351 keV, and 609 keV, the counting time required to reach <5% error is

greatly reduced since the daughters have higher nuclear yields. However, this requires an incubation period of ~30 days to allow for secular equilibrium between ^{226}Ra and its short-lived daughters ^{214}Pb and ^{214}Bi [40]. Radium characterizations that are inferred by the daughter products are likely to have higher standard errors than when obtained by direct analysis at 186 keV, as shown by the statistical analyses (Figure 4.2). The analyses also showed that the standard error was greater at the lowest density, then decreased as the density approached ~1.55 g/mL. Relative to height, errors were higher than at shorter sample heights. The 609 keV energy level exhibited the greatest standard error − up to 5 − 6 % at low density or short sample height.

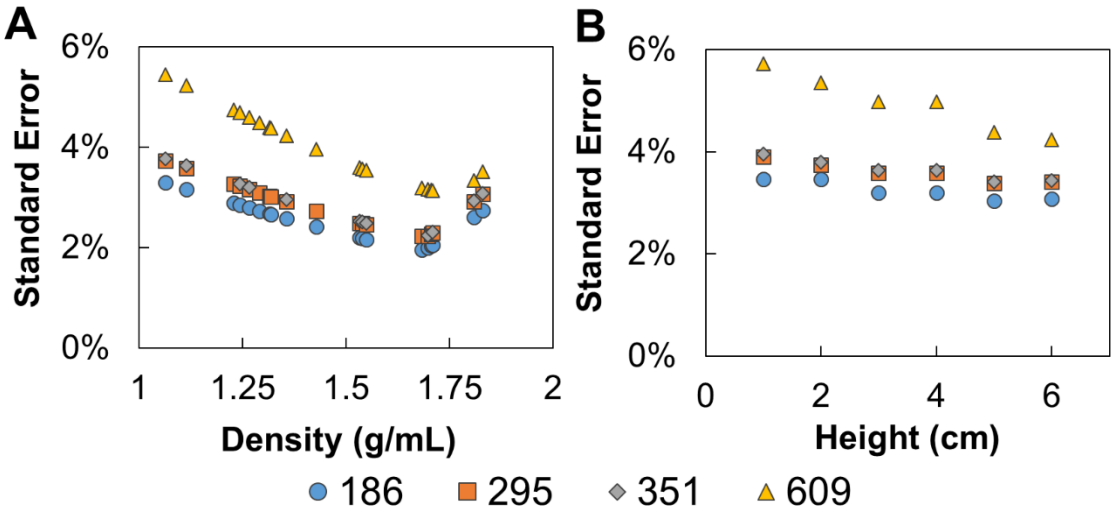

Figure 4.2: 95% confidence interval standard errors expressed as percentages, as obtained from the linear regressions when γ-spec efficiency is regressed against Density (panel **A**), and Height (panel **B**).

4.4.3 Method Validation

To check the validity of the γ-spec efficiency regression on height and density, the γ-spec efficiencies of the CRMs UTS-2 and UTS-3, were derived using the densities, fill heights and the regression equations from Table 1. The derived γ-spec efficiency values were then compared to the measured γ-spec efficiency. This validation showed that the γ-spec efficiency was within 9.7% (95% confidence interval) (Figure 4.3) of the actual γ-spec efficiencies.

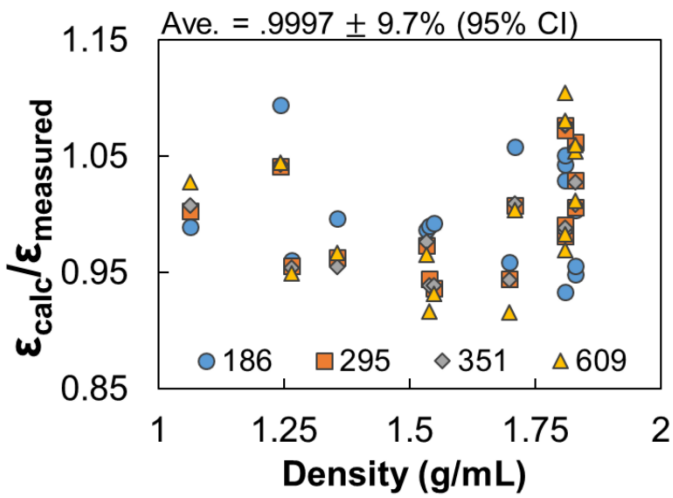

Figure 4.3: Validation of the γ-spec efficiency derived from the linear regression, showing that for all the energy levels and densities, the regression was within 9.7% (95% confidence interval) of the actual γ-spec efficiency values. Data includes results from energy levels 186 keV 609 keV.

When the density and height attenuation corrections were applied to the CRMs UTS-2 and UTS-3, we found that the corrected activities more closely reflected the

certified activities, than when the corrections were not applied (Figure 3.4A). Although this was the same dataset used to develop the linear regressions, we performed this analysis as a means to explore the conditions when the correction produced favorable results. We observed that for the CRMs UTS-2 and UTS-3, the corrections served to reduce the reported activities; and this efficiency had a greater effect when the vials were not fully filled, highlighting again that the corrections are most pertinent when there is low sample volume/mass.

We evaluated the robustness of our proposed attenuation correction by applying it to the CRM UTS-4 at various fill heights. UTS-4 was not employed in developing the linear regressions and thus could be treated as a new, unknown sample. Notably, the ^{226}Ra activity of UTS-4 was twice as high as for UTS-3, and six-times higher than for UTS-2 (compare Figure 4.4A to 4.4B). We compared the calculated ^{226}Ra activities based on the density and height attenuation correction to the certified activities (Figure 4.4B). UTS-4 had a measured density of 1.42 g/mL (Table C1). We note that the density of UTS-4 was much less than the starting densities of UTS-2 and UTS-3, but the blended sediments of UTS-2, UTS-3, and bentonite or aluminum oxide had densities that ranged from 0.998 to 1.83 g/mL. The densities of the CRMs correlated somewhat to their total Fe content, although owing to the small sample size (n = 3) this was only a qualitative correlation (Table C1). The corrected radium activities of UTS-4 were most similar to the certified activities at the 3 cm fill height. At 6 cm, the correction underestimated the activity by 15%; and at 1.2 cm, the correction underestimated the activity by 57%. It is common for linear regressions to have high accuracy at the center of the regression, and low accuracy at the extremes, for example as illustrated in Figure 4.2A. However, with the low density of UTS-4, only 5.87 g was required to fill the vial to a height of 1.2 cm. UTS-4 also possessed a higher ^{226}Ra content, perhaps the sample

mass at this fill height is too small compared to the radium content for the corrections to produce tight results.

4.4.4 Implications on Radium Measurements of Shale-Gas Associated Solids

Tasker *et al.* [39] performed an inter-lab study were the radium activities of oil and gas impacted sediments were measured by ten labs. We evaluated these sediments and performed the density and height attenuation corrections on the radium activities. We compared the ^{226}Ra activities reported by the study (the most probable value, MPV, following statistical analyses of all reported values) to the activities we calculated based on our corrections. We found that our corrections increased the calculated ^{226}Ra activities by 20 - 50 % higher than the MPVs(Figure 4.4C). Several of the labs that participated in the inter-lab study evaluated ^{226}Ra based on its daughter products without reported attenuation corrections. Problems can arise from using the daughter products, because radon gas can leak out of the sample, rendering measurements inaccurate if the sample and standard do not retain identical percentages of the radon generated. When radon gas leaks through the sample, the equilibrium is broken, and the reported activities would be underestimating the true activity.

The management and disposal of shale-gas associated solids continues to be an important issue. A study by the Pennsylvania Department of Environmental Protection (PADEP) on TENORM showed that there was a wide range in the mineralogy of impacted solid materials– from fine clays and bedrock, to silica sand. There was also a broad range of the radium activities of these solids – from < 0.1 Bq/g

^{226}Ra to as high as 18 Bq/g ^{226}Ra [18]. However, the uncertainty in these measurements can be quite high, with standard errors as high as 85%.

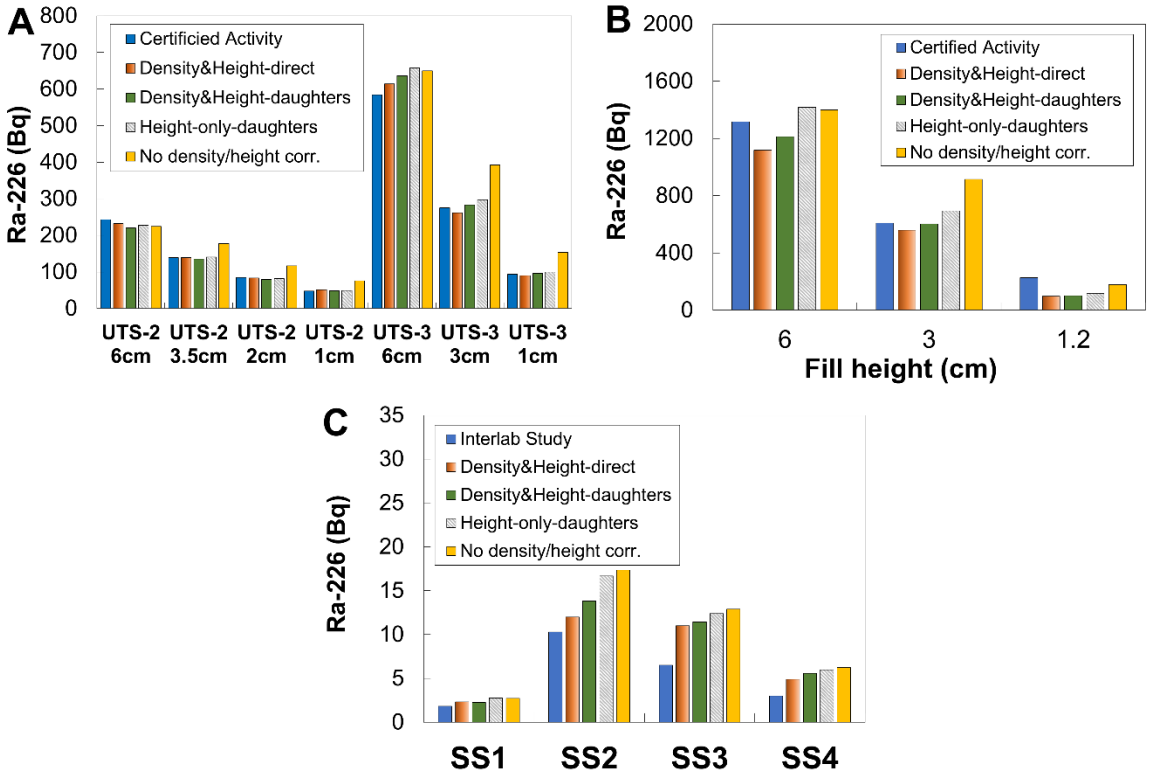

Figure 4.4: **A**. The certified ^{226}Ra activities (Bq) of seven UTS-2 and UTS-3 certified reference materials (CRMs) compared to the activities calculated when the density and height influenced attenuation correction was applied, and when it was not applied. **B**. The certified ^{226}Ra activities (Bq) of three UTS-4 samples compared to the activities calculated when the density and height influenced attenuation correction was applied, and when it was not applied. **C**. The most probable value (MPV) of ^{226}Ra activities of samples from the inter-lab by Tasker *et al.*[39] compared to our calculations with and without attenuation correction. For each panel, the UTS-2 CRM at full height was used to determine the activity for the case of 'No density/height corr.' Radium-226 activities were determined either by direct measurement at 186.2 keV ('direct') or by the daughter products ('daughters').

Clays, sands, and silt sediments can have greatly varying densities, which will influence the reported activities. In a previous study [37] conducted by this research team wherein this density and height influenced self-attenuation corrections were applied to clays, silts and sands that came from shale gas extraction, we found that when they had not been corrected for density and fill height, the reported activities of the solids could be inaccurately low by as much as 40%.

Efforts towards beneficial reuse and resource recovery from produced water are underway [36,47,51]. The radium content of the generated treatment solids and co-products must be accurately quantified before these efforts can be deemed socially and environmentally responsible. For example, NaCl extracted from produced water have become commercially available for swimming pool maintenance and for road deicing [52]. Given that both applications provide a contaminant exposure pathway for radium to humans and/or animals, it is of the utmost importance that the radium content of the salt is accurately determined. A common technique to remove radium from produced water is through co-precipitation with barium to form barite [54]. Assuming that this treatment technique is employed prior to NaCl crystallization, the radium content of the NaCl and barite would need to be determined. Based on our protocol, the packed density of a NaCl standard used in this study was ~1.4 g/mL, while lab grade barite ($BaSO_4$) had a packed density of ~2 g/mL. This disparity in density values highlights the need for a method that considers and addresses the composition of the solid samples.

Radium-226 measurements of oil and gas impacted solids are usually determined by the daughter products. This analysis requires a 30 day incubation period to allow for secular equilibrium between radium and its daughters. However, our results suggest that measurements can be performed rapidly and accurately by direct

analysis of ^{226}Ra, without the need to wait for secular equilibrium. Produced waters typically have low U content [13], therefore the interference by ^{235}U at 186 keV is minimal, and we provide a means to account for this interference. The increased benefit of rapid radium measurements could enable entrepreneurs, operators, and scientists to more quickly and efficiently evaluate the solid products (~1 day compared to >21 days). This would help facilitate development of new techniques for deriving alternate uses of produced water.

4.5 Acknowledgments

This research was funded by a National Science Foundation PFI: AIR-TT #1640634. Further support originated from a Penn State College of Engineering Graduate Excellence Fellowship.

4.6 References

(1) Perrier, F.; Girault, F.; Bouquerel, H.; Bollinger, L. Effective Radium Concentration in Agricultural versus Forest Topsoils. *J. Environ. Radioact.* 2016, *160*, 123–134.

(2) Engle, M. A.; Rowan, E. L. Geochemical Evolution of Produced Waters from Hydraulic Fracturing of the Marcellus Shale, Northern Appalachian Basin: A Multivariate Compositional Data Analysis Approach. *Int. J. Coal Geol.* 2014, *126*, 45–56.

(3) Warner, N. R.; Jackson, R. B.; Darrah, T. H.; Osborn, S. G.; Down, A.; Zhao, K.; White, A.; Vengosh, A. Geochemical Evidence for Possible Natural Migration of Marcellus Formation Brine to Shallow Aquifers in Pennsylvania. *Proc. Natl. Acad. Sci.* 2012, *109* (30), 11961–11966.

(4) Hou, X.; Roos, P. Critical Comparison of Radiometric and Mass Spectrometric Methods for the Determination of Radionuclides in

Environmental, Biological and Nuclear Waste Samples. *Anal. Chim. Acta* 2008, *608* (2), 105–139.

(5) Vinson, D. S.; Tagma, T.; Bouchaou, L.; Dwyer, G. S.; Warner, N. R.; Vengosh, A. Occurrence and Mobilization of Radium in Fresh to Saline Coastal Groundwater Inferred from Geochemical and Isotopic Tracers (Sr, S, O, H, Ra, Rn). *Appl. Geochemistry* 2013, *38*, 161–175.

(6) Burgos, W. D.; Castillo-Meza, L.; Tasker, T. L.; Geeza, T. J.; Drohan, P. J.; Liu, X.; Landis, J. D.; Blotevogel, J.; McLaughlin, M.; Borch, T.; et al. Watershed-Scale Impacts from Surface Water Disposal of Oil and Gas Wastewater in Western Pennsylvania. *Environ. Sci. Technol.* 2017, *51* (15), 8851–8860.

(7) Zhang, T.; Bain, D.; Hammack, R.; Vidic, R. D. Analysis of Radium-226 in High Salinity Wastewater from Unconventional Gas Extraction by Inductively Coupled Plasma-Mass Spectrometry. *Environ. Sci. Technol.* 2015, *49* (5), 2969–2976.

(8) Kargbo, D. M.; Wilhelm, R. G.; Campbell, D. J. Natural Gas Plays in the Marcellus Shale: Challenges and Potential Opportunities. *Environ. Sci. Technol.* 2010, *44* (15), 5679–5684.

(9) Rowan, E. L.; Engle, M. A.; Kraemer, T. F.; Schroeder, K. T.; Hammack, R. W.; Doughten, M. W. Geochemical and Isotopic Evolution of Water Produced from Middle Devonian Marcellus Shale Gas Wells, Appalachian Basin, Pennsylvania. *Am. Assoc. Pet. Geol. Bull.* 2015, *99* (2), 181–206.

(10) Hayes, T. *Sampling and Analysis of Water Streams Associated with the Development of Marcellus Shale Gas*; Des Plaines, 2009.

(11) Benson, M. E.; Wilson, A. B. *Frac Sand in the United States—A Geological and Industry Overview*; 2015.

(12) Maloney, K. O.; Yoxtheimer, D. A. Production and Disposal of Waste Materials from Gas and Oil Extraction from the Marcellus Shale Play in Pennsylvania. *Environ. Pract.* 2012, *14* (December), 278–287.

(13) Eitrheim, E. S.; May, D.; Forbes, T. Z.; Nelson, A. W. Disequilibrium of

Naturally Occurring Radioactive Materials (NORM) in Drill Cuttings from a Horizontal Drilling Operation. *Environ. Sci. Technol. Lett.* 2016, *3* (12), 425– 429.

(14) Zhang, T.; Hammack, R. W.; Vidic, R. D. Fate of Radium in Marcellus Shale Flowback Water Impoundments and Assessment of Associated Health Risks. *Environ. Sci. Technol.* 2015, *49* (15), 9347– 9354.

(15) Van Sice, K.; Cravotta, C. A.; McDevitt, B.; Tasker, T. L.; Landis, J. D.; Puhr, J.; Warner, N. R. Radium Attenuation and Mobilization in Stream Sediments Following Oil and Gas Wastewater Disposal in Western Pennsylvania. *Appl. Geochemistry* 2018, *98*, 393– 403.

(16) Lauer, N. E.; Warner, N. R.; Vengosh, A. Sources of Radium Accumulation in Stream Sediments near Disposal Sites in Pennsylvania: Implications for Disposal of Conventional Oil and Gas Wastewater. *Environ. Sci. Technol.* 2018, *52* (3).

(17) McDevitt, B.; McLaughlin, M.; Cravotta, C. A.; Ajemigbitse, M. A.; Van Sice, K. J.; Blotevogel, J.; Borch, T.; Warner, N. R. Emerging Investigator Series: Radium Accumulation in Carbonate River Sediments at Oil and Gas Produced Water Discharges: Implications for Beneficial Use as Disposal Management. *Environ. Sci. Process. Impacts* 2019, *21* (2), 324– 338.

(18) Pennsylvania Department of Environmental Protection (PA DEP). Technologically Enhanced Naturally Occurring Radioactive Materials (TENORM) Study Report http://www.depgreenport.state.pa.us/elibrary/getdocument?docid=5815&docname=01 pennsylvania department of environmental protection tenorm study report rev 1.pdf (accessed Feb 8, 2018).

(19) Attallah, M. F.; Hamed, M. M.; El Afifi, E. M.; Aly, H. F. Removal of 226 Ra and 228 Ra from TENORM Sludge Waste Using Surfactants Solutions. *J. Environ. Radioact.* 2015, *139* (412), 78– 84.

(20) Kappel, W. M.; Williams, J. H.; Szabo, Z. *Water Resources and Shale Gas/Oil Production in the Appalachian Basin—Critical Issues and Evolving Developments*; 2013.

(21) Gallagher, M. E.; Down, A.; Ackley, R. C.; Zhao, K.; Phillips, N.; Jackson, R. B. Natural Gas Pipeline Replacement Programs Reduce Methane Leaks and Improve Consumer Safety. *Environ. Sci. Technol. Lett.* 2015, *2* (10), 286–291.

(22) McKain, K.; Down, A.; Raciti, S. M.; Budney, J.; Hutyra, L. R.; Floerchinger, C.; Herndon, S. C.; Nehrkorn, T.; Zahniser, M. S.; Jackson, R. B.; et al. Methane Emissions from Natural Gas Infrastructure and Use in the Urban Region of Boston, Massachusetts. *Proc. Natl. Acad. Sci. U. S. A.* 2015, *112* (7), 1941–1946.

(23) Howarth, R. W.; Santoro, R.; Ingraffea, A. Methane and the Greenhouse-Gas Footprint of Natural Gas from Shale Formations. *Clim. Change* 2011, *106* (4), 679–690.

(24) Jiang, M.; Michael Griffin, W.; Hendrickson, C.; Jaramillo, P.; VanBriesen, J.; Venkatesh, A. Life Cycle Greenhouse Gas Emissions of Marcellus Shale Gas. *Environ. Res. Lett.* 2011, *6* (3), 034014.

(25) Warner, N. R.; Christie, C. A.; Jackson, R. B.; Vengosh, A. Impacts of Shale Gas Wastewater Disposal on Water Quality in Western Pennsylvania. *Environ. Sci. Technol.* 2013, *47*, 11849–11857.

(26) Ferrar, K. J.; Michanowicz, D. R.; Christen, C. L.; Mulcahy, N.; Malone, S. L.; Sharma, R. K. Assessment of Effluent Contaminants from Three Facilities Discharging Marcellus Shale Wastewater to Surface Waters in Pennsylvania. *Environ. Sci. Technol.* 2013, *47*, 3472–3481.

(27) Wilson, J. M.; Van Briesen, J. M. Source Water Changes and Energy Extraction Activities in the Monongahela River, 2009–2012. *Environ. Sci. Technol.* 2013, *47* (21), 12575–12582.

(28) Wilson, J. M.; Wang, Y.; VanBriesen, J. M. Sources of High Total Dissolved Solids to Drinking Water Supply in Southwestern Pennsylvania. *J. Environ. Eng.* 2014, *140* (5), B4014003–1 – B4014003–B4014010.

(29) Wilson, J. M.; VanBriesen, J. M. Oil and Gas Produced Water Management and Surface Drinking Water Sources in Pennsylvania. *Environ. Pract.* 2012,

14 (4), 288– 300.

(30) Parker, K. M.; Zeng, T.; Harkness, J.; Vengosh, A.; Mitch, W. A. Enhanced Formation of Disinfection Byproducts in Shale Gas Wastewater-Impacted Drinking Water Supplies. *Environ. Sci. Technol.* 2014, *48* (19), 11161– 11169.

(31) Harkness, J. S.; Dwyer, G. S.; Warner, N. R.; Parker, K. M.; Mitch, W. A.; Vengosh, A. Iodide, Bromide, and Ammonium in Hydraulic Fracturing and Oil and Gas Wastewaters: Environmental Implications. *Environ. Sci. Technol.* 2015, *49* (3), 1955– 1963.

(32) Vengosh, A.; Jackson, R. B.; Warner, N. R.; Darrah, T. H.; Kondash, A. A Critical Review of the Risks to Water Resources from Unconventional Shale Gas Development and Hydraulic Fracturing in the United States. *Environ. Sci. Technol.* 2014, *48* (15), 8334– 8348.

(33) Kravchenko, J.; Darrah, T. H.; Miller, R. K.; Lyerly, H. K.; Vengosh, A. A Review of the Health Impacts of Barium from Natural and Anthropogenic Exposure. *Environ. Geochem. Health* 2014, *36* (4), 797– 814.

(34) Konkel, L. Salting the Earth: The Environmental Impact of Oil and Gas Wastewater Spills. *Environ. Health Perspect.* 2016, *124* (12), A230– A235.

(35) U.S. Environmental Protection Agency. *Detailed Study of the Centralized Waste Treatment Point Source Category for Facilities Managing Oil and Gas Extraction Wastes*; Washington, D.C., 2018.

(36) U.S. Environmental Protection Agency. *Study of Oil and Gas Extraction Wastewater Management Under the Clean Water Act EPA-821-R19-001*; Washington, D.C., 2019.

(37) Ajemigbitse, M. A.; Cannon, F. S.; Klima, M. S.; Furness, J. C.; Wunz, C.; Warner, N. R. Raw Material Recovery from Hydraulic Fracturing Residual Solid Waste with Implications for Sustainability and Radioactive Waste Disposal. *Environ. Sci. Process. Impacts* 2019, *21* (2), 308– 323.

(38) Nelson, A. W.; May, D.; Knight, A. W.; Eitrheim, E. S.; Mehrhoff, M.; Shannon, R.; Litman, R.; Schultz, M. K. Matrix Complications in the Determination of Radium Levels in Hydraulic Fracturing Flowback Water

from Marcellus Shale. *Environ. Sci. Technol. Lett.* 2014, *1* (3), 204–208.

(39) Tasker, T. L.; Burgos, W. D.; Ajemigbitse, M. A.; Lauer, N. E.; Gusa, A. V.; Kuatbek, M.; May, D.; Landis, J. D.; Alessi, D. S.; Johnsen, A. M.; et al. Accuracy of Methods for Reporting Inorganic Element Concentrations and Radioactivity in Oil and Gas Wastewaters from the Appalachian Basin, U.S. Based on an Inter-Laboratory Comparison. *Environ. Sci. Process. Impacts* 2019, *21* (2), 224–241.

(40) Gilmore, G. R. *Practical Gamma-Ray Spectrometry*; John Wiley & Sons, Ltd: Chichester, UK, 2008.

(41) Appleby, P. G.; Richardson, N.; Nolan, P. J. Self-Absorption Corrections for Well-Type Germanium Detectors. *Nucl. Instruments Methods Phys. Res. Sect. B Beam Interact. with Mater. Atoms* 1992, *71* (2), 228–233.

(42) Hubbell, J. H. Photon Mass Attenuation and Energy-Absorption Coefficients. *Int. J. Appl. Radiat. Isot.* 1982, *33* (11), 1269–1290.

(43) Cutshall, N. H.; Larsen, I. L.; Olsen, C. R. Direct Analysis of 210Pb in Sediment Samples: Self-Absorption Corrections. *Nucl. Instruments Andm.* 1983, *206*, 309–312.

(44) Bolivar, J. P.; Garcí a-Leó n, M.; Garcí a-Tenorio, R. On Self-Attenuation Corrections in Gamma-Ray Spectrometry. *Appl. Radiat. Isot.* 1997, *48* (8), 1125–1126.

(45) Schaller, J.; Headley, T.; Prigent, S.; Breuer, R. Potential Mining of Lithium, Beryllium and Strontium from Oilfield Wastewater after Enrichment in Constructed Wetlands and Ponds. 2014.

(46) Flexer, V.; Fernando Baspineiro, C.; Galli, C. I. Lithium Recovery from Brines: A Vital Raw Material for Green Energies with a Potential Environmental Impact in Its Mining and Processing. *Sci. Total Environ.* 2018, *639*, 1188–1204.

(47) Jang, Y.; Chung, E. Adsorption of Lithium from Shale Gas Produced Water Using Titanium Based Adsorbent. *Ind. Eng. Chem. Res.* 2018, *57* (25), 8381–8387.

(48) Jang, Y.; Chung, E. Lithium Adsorptive Properties of H2TiO3 Adsorbent from Shale Gas Produced Water Containing Organic Compounds. *Chemosphere* 2019, *221*, 75–80.

(49) Paranthaman, M. P.; Li, L.; Luo, J.; Hoke, T.; Ucar, H.; Moyer, B. A.; Harrison, S. Recovery of Lithium from Geothermal Brine with Lithium–Aluminum Layered Double Hydroxide Chloride Sorbents. *Environ. Sci. Technol.* 2017, *51* (22), 13481–13486.

(50) Swain, B. Recovery and Recycling of Lithium: A Review. *Sep. Purif. Technol.* 2017, *172*, 388–403.

(51) MGX Minerals Inc. (Press Release). MGX Minerals and Eureka Resources Announce Joint Venture to Recover Lithium from Produced Water in Eastern United States https://www.prnewswire.com/news-releases/mgx-minerals-and-eureka-resources-announce-joint-venture-to-recover-lithium-from-produced-water-in-eastern-united-states-300806407.html (accessed May 13, 2019).

(52) Dorich, A. Eureka Resources Recovers Vital Resources from Flowback and Production Wastewater. *Energy & Mining International*. 2017.

(53) Landis, J. D.; Renshaw, C. E.; Kaste, J. M. Measurement of 7Be in Soils and Sediments by Gamma Spectroscopy. *Chem. Geol.* 2012, *291*, 175–185. https://doi.org/10.1016/j.chemgeo.2011.10.007.

(54) Köhler, M.; Preuße, W.; Gleisberg, B.; Schäfer, I.; Heinrich, T.; Knobus, B. Comparison of Methods for the Analysis of 226Ra in Water Samples. *Appl. Radiat. Isot.* 2002, *56* (1–2), 387–392. https://doi.org/10.1016/S0969-8043(01)00219-6.

(55) He, C.; Zhang, T.; Zheng, X.; Li, Y.; Vidic, R. D. Management of Marcellus Shale Produced Water in Pennsylvania: A Review of Current Strategies and Perspectives. *Energy Technol.* 2014, *2* (12), 968–976. https://doi.org/10.1002/ente.201402060.

Chapter 5

Influence of High Total Dissolved Solids Concentration and Ionic Composition on Gamma Spectroscopy Radium Measurements of Oil And Gas Produced Water

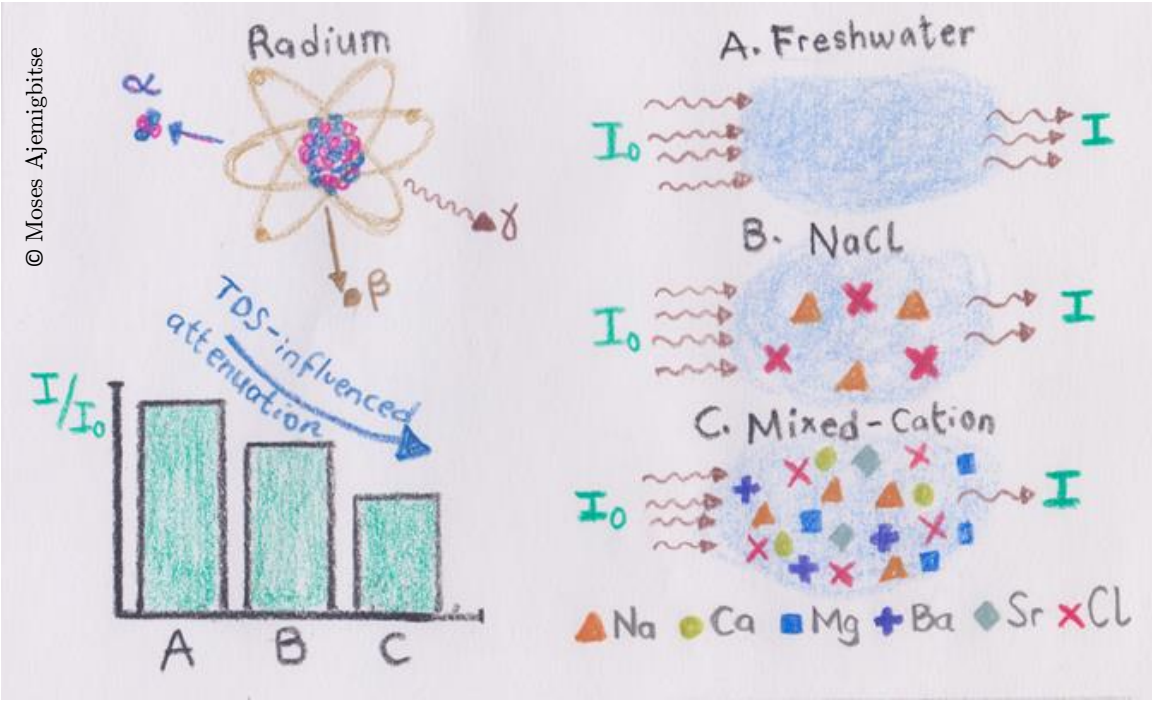

Ajemigbitse MA, Tasker TL, Cannon FS, and Warner NR. "Influence of High Total Dissolved Solids Concentration and Ionic Composition on Gamma Spectroscopy Radium Measurements of Oil and Gas Produced Water." Submitted to *Environmental Science & Technology*.

5.1 Abstract

Radium measurements in high total dissolved solids (TDS) fluids from oil and gas extraction can have low precision and accuracy. Gamma spectroscopy is often recommended for determining radium activities in these fluids, but even this method can produce a range of reported activities for the same sample. In order to reduce measurement duration and to maintain or improve accuracy, we propose a method to rapidly assess both ^{226}Ra and ^{228}Ra and to account for the self-attenuation of gamma rays in high-TDS oil and gas fluids when they are monitored by a well-detector. In this work, comparisons between a NaCl-only and a multi-cation-chloride synthetic brine spiked with known amounts of ^{226}Ra and ^{228}Ra indicated that both the TDS concentration and the type of TDS (i.e. Na only vs. Na-Mg-Ba-Ca-Sr) influenced self-attenuation in well-detector gamma spectroscopy; thus highlighting the need to correct for this TDS influenced self-attenuation. Radium activities can be underestimated if the correction is not applied. For instance, ^{226}Ra activities could be ~40% lower in a sample when measured directly at the 186 keV energy level if the attenuation of the high TDS of the fluid is not considered. We also showed that using a NaCl-only brine to match the matrix of high-TDS oil and gas brines is inadequate to produce accurate measurements– rather, the full set of cation should be included.

5.2 Introduction

Oil and gas (O&G) production, specifically shale gas production (e.g. the Marcellus and Utica shale plays) generates produced water with high total dissolved solids (TDS) concentrations [1–6] and measurable activities of radium (^{226}Ra and ^{228}Ra) [7–9]. Radium presents a challenge for the management of the associated waste streams

from O&G development [10–12]. Many reports show that prior (and sometimes poor) practice, management, or treatment of these wastes has resulted in radium release to the environment [6,13–15], which can persist over long periods of time [1,13,16,17]. Typically, produced water generated from wells are disposed through underground injection control permits [18]. However, O&G fields in states such as OK, TX, OH,PA, AK, CO, and NM are generating larger volumes of produced water than historically [18,19] and associated disposal through deep well injection has lead, in some cases, to induced seismicity [20]. This has led to a growing interest in developing alternative beneficial uses of O&G produced water [21–23]. In addition, the high concentration of some resources make O&G produced water possible targets for resource recovery, such as lithium [24–29] and NaCl [30]. In cases of beneficial use, the quantification of radium pre- and post-treatment, or prior to commercial use, is vital to assuage concerns of exposure to humans and wildlife. Therefore, accurate and rapid measurement of radium in a range of TDS concentrations is necessary to allow operators to assess the efficacy of their treatments. Analytical measurement techniques exist for measuring radioactivity in freshwaters [31,32], but specific methods for the fluids with high-TDS concentrations found in produced waters from shale gas production are few [31].

Many of the techniques for measuring radium generate inconsistent and variable results in high-TDS O&G produced waters. An inter-lab study [33] showed that labs analyzing O&G produced waters for radium activity often differed from one another by $\pm 40\%$, even when the participating labs used similar methods. Gamma spectroscopy (γ-spec) has been recommended for measuring radium activities in O&G wastewater, since wet chemical methods are often ineffective at recovering

radium from high-TDS produced water [31]. The degree of attenuation of the gamma decay energy by the high density of O&G fluids has not been discussed in the refereed literature, relative to how this attenuation skews the radioactivity analyses of these produced waters. This is despite fluid density (and parenthetically TDS) being a known source of attenuation [34–36]. One technique that accounts for this attenuation uses a radioactive multi-isotope point source, as per the Cutshall method [37,38]. However, this requires a geometry that allows for the point source to be properly placed on the detector, as well as a uniform sample matrix. Among gamma spectrometers, a well-type detector offers the highest counting efficiencies. Point source attenuation correction is not achievable for a well-detector gamma spec, due to the 2-π geometry, resulting in an uneven signal transmission of the point source gamma rays through the sample matrix [34]. As self-attenuation is an intrinsic property of the mass and atomic number of the components [36], the dissolved solids, as well as their composition, have a salient impact. To illustrate, a 100 g/L NaCl brine does not have the same specific gravity (fluid density) as a 100g/L $CaCl_2$ or $BaCl_2$ brine (See Figure D1). Although certified labs often use NaCl to matrix-match calibration standards to sample salinity [33], it was yet to be seen whether a NaCl-only brine produced the same attenuation as the shale gas brines which are typically dominated by Cl, Na, Ca, Mg, and other alkaline earth metals. With the increased emphasis on resource recovery and beneficial reuse of produced water, this study aimed to conduct an in-depth study on the nature of the attenuation of high-TDS, multi-cation brines, and to compare it to the attenuation of a mere NaCl brine. Herein, we found that NaCl did not generate the same

levels of attenuation. This study has been aimed to benefit operators and researchers who wish to accurately quantify radium activities during studies on alternative uses of O&G produced water.

The objectives of this paper were to i) derive a multi-cation brine that possesses a similar degree of self-attenuation as do field-sourced high-TDS brines, ii) investigate the effect of TDS on the self-attenuation of high-TDS brines in a well-detector γ-spec, and ii) present an accurate and rapid method for measuring radium in high-TDS brines by well-detector γ-spec.

5.3 Materials and Methods

5.3.1 Materials

Radioactivity analyses were performed in 24 mL Wheaton high density polyethylene (HDPE) scintillation vials (2.8 cm diameter by 6.1 cm height) with poly seal cone-lined urea caps. The caps of the vials were then sealed shut by wrapping with several layers of Parafilm M® to reduce radon leakage. The analytical chemicals were VWR reagent grade. Ultrapure distilled de-ionized water (18.2 $m\Omega$) was provided by a ThermoScientific Barnstead Nanopure water system.

5.3.2 Appalachian Basin Produced Water Chemistry

Forty (40) produced water samples were collected from various conventional and shale gas wells in the Appalachian Basin of Pennsylvania and Ohio. The solution chemistry of some of these samples have been previously reported.[17] The TDS of the samples were determined gravimetrically by EPA Method 160.1. Elemental compositions of the brine cations (Na, Mg, Ca, Ba, Sr, and K) were determined

using Inductively Coupled Plasma-Optical Emission Spectroscopy (ICP-OES) on a Thermo Scientific iCAP 6000 optical Emission Spectrometer per EPA Method 200.7. Prior to analyses, 100 mL of each sample was digested with 6 mL of aqua regia for 4 hours at 70 °C. Thereafter, samples were filtered and diluted 2000 times in 2% nitric acid for ICP-OES analysis. The anions Cl and Br, were determined with a Dionex ICS-1100 ion chromatograph (IC) with an AS18 column for Cl and Br. In Appalachian conventional and shale gas produced waters, it has been found that sulfate and bicarbonate generally represent less than 0.1 % of the anions [39], and so their compositions were not determined. Radium activities were determined by γ-spec on a Canberra ultra-low background small anode high purity germanium (HPGe) well detector, after incubating the samples for ~30 days. Each sample was counted twice for at least twelve hours. The reported activity was the weighted average of the two counts. The ^{226}Ra activities were determined at the following energy levels: 186.2 keV (^{226}Ra), 295.2 keV (^{214}Pb), 351.9 keV (^{214}Pb), and 609.3 keV (^{214}Bi). The ^{228}Ra activities were determined at 911.2 keV (^{228}Ac). The standard error was reported (which was < 5%) and the error propagation has been included in Appendix A.2.

The specific gravity and TDS were calculated gravimetrically. We calculated the composition of each element as molality (mol/kg) by multiplying the specific gravity of the produced water sample by the molarity (mol/L) of each element. Then, for the cations (Na, Mg, Ca, Ba, Sr, and K), each element was expressed as a percent of the total cation molality; and for the anions (Cl and Br), each was expressed as percent of the total anion molality present. The ionic strength, *IS*, of these samples was determined by the Lewis-Randall ionic strength equation for non-ideal solutions [40]:

$$IS = \frac{1}{2}\sum_{i} m_i z_i^2 \tag{5.1}$$

where m_i and z_i are the molality (mol/kg) and the charge of the *ith* ion in solution.

5.3.3 Radium Standards with Various TDS Concentrations

Radium standards (^{226}Ra and ^{228}Ra) were supplied by the National Institute of Standards and Technology (NIST) Gaithersburg, MD. From these standards, stock solutions were created at 185 Bq/L (5,000 pCi/L) in ultrapure distilled de-ionized water with 5% nitric acid. The stock solutions were stored in Pyrex glass bottles to minimize wall adsorption. In addition, we created two types of synthetic brines (i.e. a NaCl-only brine and a multi-cation brine) at five TDS concentrations (0 g/L, 50 g/L, 100 g/L, 200 g/L, and 300 g/L) to encompass the TDS range of shale gas produced waters. The distribution of the multi-cation brine reflected a representative elemental compositions of the 40 sampled shale gas produced waters. For example, the 100 g/L TDS synthetic brine hosted 57.36 g/L NaCl, 21.78 g/L $CaCl_2$, 10.9 g/L $BaCl_2$, 3.4 g/L $MgCl_2$, and 6.22 g/L $SrCl_2$ (see Table S1 for the composition of all the synthetic brines).

The NaCl-only and the multi-cation synthetic brines contained ~124 pCi (4.6 Bq) of ^{226}Ra and ^{228}Ra. Radium activity of the salts used to create the brines contributed to less than 1% of the total radium activity. We determined this by measuring the massic activity (pCi/g) of the dry salts by γ-spec and then multiplying by the quantity of added salt. Using the following equation, we determined detector efficiencies at the following energy levels: 186.2 keV (^{226}Ra), 295.2 keV (^{214}Pb), 351.9 keV (^{214}Pb), 609.3 keV (^{214}Bi), 1120.3 (^{214}Bi), and 1764.5 keV (^{214}Bi) for ^{226}Ra; 911.2 keV (^{228}Ac) for ^{228}Ra:

$$\epsilon^{E} = \frac{R_{bkg-corr}^{E\,KeV}}{\gamma_{yield}^{E} \times A^{Ra}} \tag{5.2}$$

where,

ϵ^{E} is detector efficiency at the given energy level, $E\,keV$

$R_{bkg-corr}^{E\,KeV}$ is the count rate at E keV corrected for the background count rate, cps

γ_{yield}^{E} is the nuclear yield of the isotope gamma decay at the given E keV, and

A^{Ra} is the Ra-226 or Ra-228 activity added to the brines from the stock solution, Bq

5.4 Results and Discussion

5.4.1 Elemental Composition, SG, TDS, and IS of Produced Water Samples

The elemental composition of the produced water samples have been summarized in Figure 5.1. The TDS of these brines ranged from ~50 g/L to almost 400 g/L, the specific gravity ranged from 1.05 to 1.2, and the ionic strength ranged from 1 mol/kg to 7 mol/kg. These results were consistent with the reported range for Appalachian Basin brines (Table D2).

As shown schematically in Figure 5.1A, the following elemental composition describes the mean of these Appalachian Basin produced water brines (by mole %): Cations: 75% Na, 15% Ca, 4% Ba, 3% Mg, 3% Sr; and Anions: 100% Cl. Thus, in

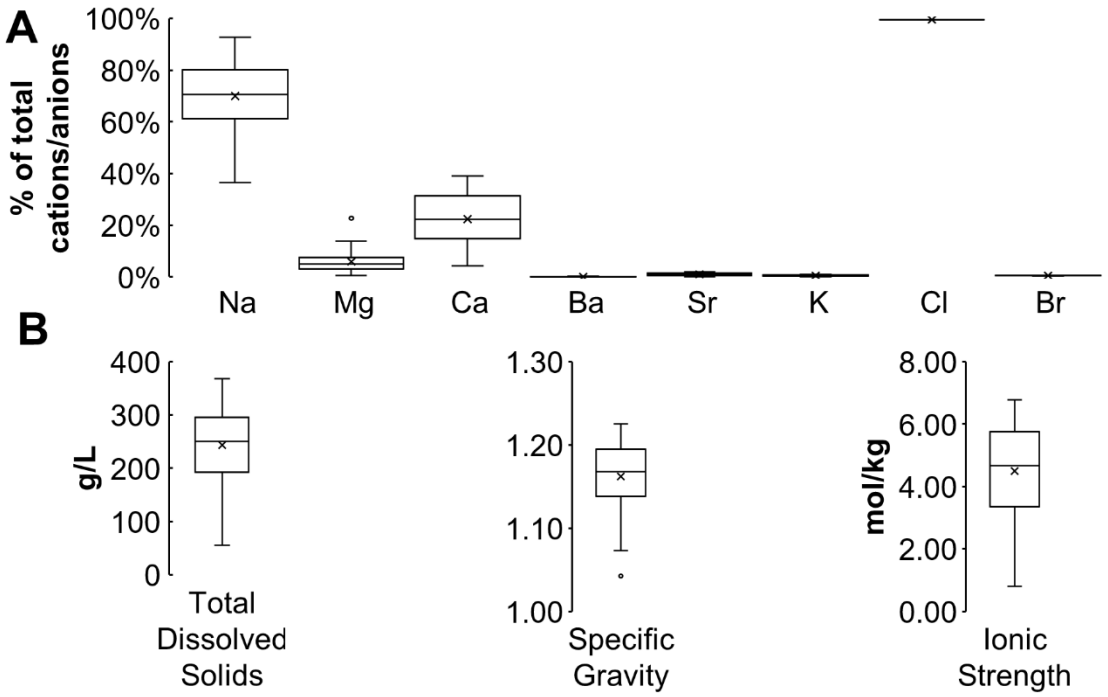

Figure 5.1: **A**. Elemental composition of produced water samples (n=40) expressed as a percent of the total cation or anion molality. **B**. Box plots of the total dissolved solids (TDS), ionic strength, and specific gravity of 40 Appalachian Basin brine samples. Boxes are 1st and 3rd quartile, the whiskers are minimum and maximum values.

preparing the synthetic multi-cation brine, we maintained these cationic proportions while varying the TDS from 50 to 300 g/L.

5.4.2 Influence of TDS on Radium Efficiency for Synthetic Brines

The TDS concentration and composition influenced attenuation; and we evaluate this by observing its effect on the detector efficiencies. First, we determined the detector efficiency for a freshwater (0 g/L) radium standard (Figure 5.2A). Since

we do not perform a point-source attenuation correction, this efficiency incorporates the attenuation due to water alone. We describe this as an *attenuated efficiency,* ϵ_A^E. Thereafter, we determined the detector efficiencies for each of the two synthetic brine sets at each TDS concentration. These detector efficiencies are also *attenuated efficiencies*; however, we can glimpse the attenuation effect of the dissolved solids by performing a regression of the efficiency against the TDS for each brine and at each energy level (Figure 5.2B). We define the relationship between the TDS-influenced attenuation factor, α_{TDS}, the *attenuated efficiency*, ϵ_A^E, and the *un-attenuated efficiency*, ϵ^E, as follows:

$$\epsilon_A^E = \epsilon^E + \alpha_{TDS} \times TDS \tag{5.3}$$

Linear regressions of the efficiency versus TDS was performed using Minitab 18. The five TDS concentrations, five energy levels, and two synthetic brines resulted in fifty data points for analysis. Table D3 summarizes the results of the linear regressions. The slope, herein identified as the TDS-influenced attenuation factor, α_{TDS}, for each energy level with its 95% confidence interval (CI), and corresponding p-value are presented in these tables. For ^{226}Ra, the estimates of α_{TDS} were statistically significant (p-value <0.05) for both the NaCl-only and mixed-cation brines at 186 keV, 295 keV, 351 keV and 609 keV; but not at 1764 keV. The estimate of α_{TDS} was also not statistically significant at 1120 keV for the NaCl-only brine. For ^{228}Ra, the estimates of α_{TDS} were not statistically significant, i.e. at 911 keV (Table D3). When the estimates of α_{TDS} were not statistically significant, they were set to zero, and in fact were very close to zero. We performed a similar comparison of freshwater-to-high TDS mixed-cation synthetic brine, but with ^{226}Ra activities at 5 pCi/mL and at 20 pCi/mL (Figure 5.2C). This comparison showed that the

observed changes in the efficiencies, i.e. α_{TDS}, were independent of the ^{226}Ra activity.

This α_{TDS} represents the change in the detector efficiency as the TDS concentration changes. Therefore, a negative value indicates that as the TDS increases, the efficiency decreases, reflecting the effect of increased attenuation at higher TDS concentrations. More negative values correspond to greater attenuation of the gamma decay energy. This α_{TDS} was more negative at the lower energy levels and reduced in negative magnitude as the energy level increased. Figure 5.2D graphically depicts α_{TDS} versus energy level, and showed that the two types of brines have different curves; indicating that when a NaCl-only brine is used as a reference standard for real produced waters, the measured radium activities will be inferred incorrectly as less attenuated than when a multi-cation brine is used - where the array of cations representatively reflect the composition of produced waters. This result indicated that the other aqueous cation species (mainly Ca, Ba, Sr, and Mg) provide significant additional mass, and therefore additional attenuation, which should not be ignored.

These results indicated that, especially for ^{226}Ra measurements, 1) it is necessary to create a reference standard that is compositionally similar to shale gas produced waters; and this composition should include Ca, Mg, and Ba; 2) NaCl alone does not accurately represent these produced waters, as shown by Figure 5.2D and Table D3. We propose that reference standards for shale gas produced waters should match the composition of this mixed-cation brine. This will improve the accuracy of ^{226}Ra measurements, and it will be better than when a mere NaCl brine is used instead. Using merely a freshwater reference standard when analyzing shale brines would yield radioactivity results that are improperly too low.

For ^{228}Ra, we inferred α_{TDS} to be zero (p-values were >0.05) which indicated that the high TDS environment does not attenuate the high-energy gamma decay of ^{228}Ac at 911.2 keV, the proxy for determining ^{228}Ra activity. We expect this result, as higher energy gamma decays are less susceptible to attenuation [34]. Conversely, we expect greater attenuation at the lower energy levels, and this is indeed what we observed. Thus, when monitoring ^{228}Ra (as ^{228}Ac), we need not consider a TDS-influenced attenuation correction.

5.4.3 Error Analyses

The sources of error for the radium activity include the following: i) the standard error of mass measurements from an analytical balance (which includes TDS and specific gravity determination), ii) the standard error of counting from the HPGe gamma spec, and iii) the standard error of the efficiency determination by the linear regression of efficiency and TDS.

The standard error of the analytical balance was 0.05%. With sufficiently long counting times (for our brines, we found 12 hours was sufficient), the standard error of the γ-spec can be <5%. The standard error of the efficiency value based on the regression with TDS was between $1 - 12\%$ for energy levels 295, 351, 609 and 911 keV, and less than 1% for 186 keV (Figure 5.3).

For ^{226}Ra, the lowest standard error could be obtained by using the 186 keV energy level (i.e. direct measurement of ^{226}Ra). This would require longer counting times (e.g. 12 hours) to achieve a low counting error, since the ^{226}Ra nuclear yield is lower at this energy level [34]. Using the other energy levels, 295, 351, and 690 keV (i.e. the daughter products), would result in faster counting times (e.g. $2 - 4$ hours)

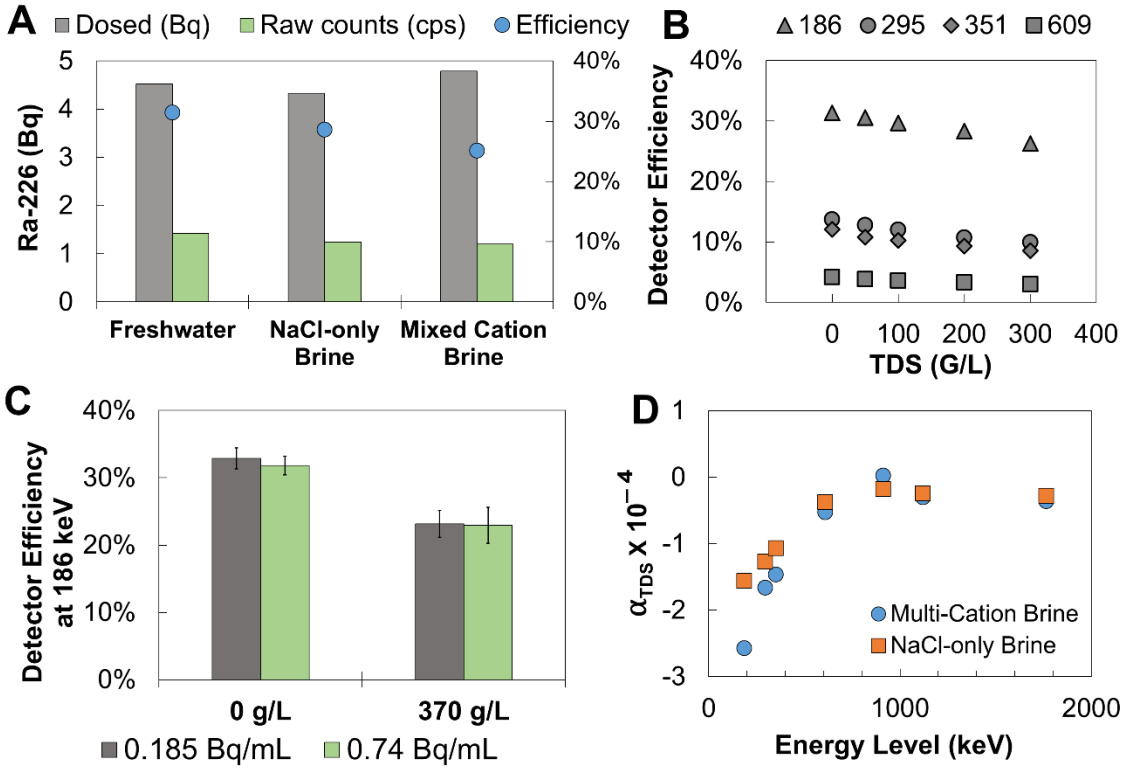

Figure 5.2: **A**. The dosed Ra-226 activity (Bq) compared to the raw instrument counts (cps) for a freshwater standard and the two synthetic brine standards at 300 g/L. The ratio of raw counts to dosed activity gives the detector efficiency. **B**. The detector efficiencies at the different energy levels plotted against the TDS concentration of the NaCl-only synthetic brine provided insight into the TDS-influenced attenuation. **C**. The detector efficiencies at 186 keV for a 5 pCi/mL and a 20 pCi/mL mixed-cation synthetic brine at 0 g/L and 370 g/L showed that attenuation was independent of radium activity. **D**. The TDS-influenced attenuation factor, α_{TDS}, at each energy level showed a profile for the NaCl-only synthetic brine that was distinct from the multi-cation synthetic brine, particularly at the lowest energy levels.

due to higher gamma decay nuclear yield, but would require an incubation period of about 30 days for secular equilibrium between ^{226}Ra and its short-lived daughters

^{214}Pb and ^{214}Bi [41]. However, measurements based on the daughter products would result in higher standard error, as shown by the statistical analyses (Figure 5.3). Finally, the analyses also showed that the standard error increases sharply as the TDS increased over ~200 g/L.

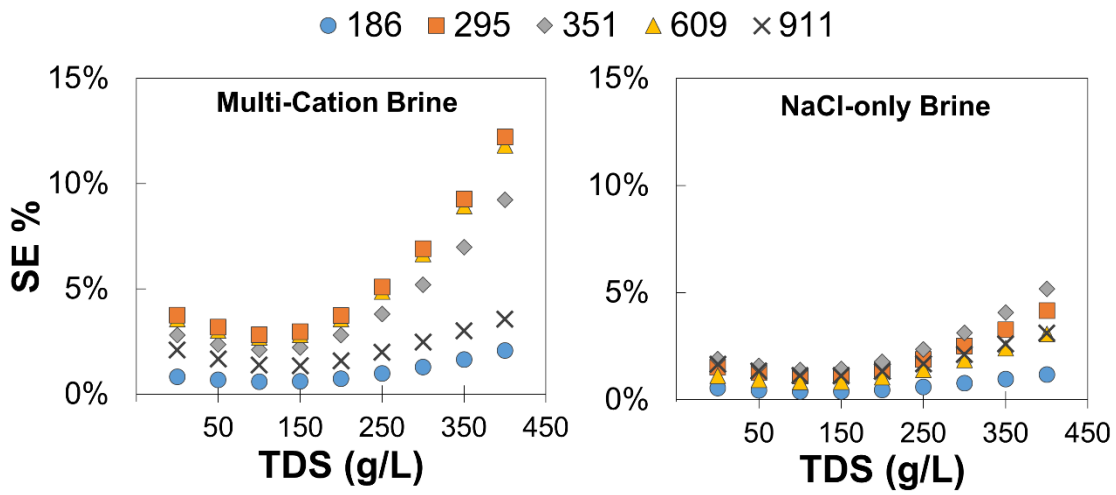

Figure 5.3: The standard error, expressed as a percentage (SE %), from the linear regression of efficiency against TDS for the multi-cation synthetic brine and for NaCl-only synthetic brine.

5.4.4 Validation of the Linear Regression Analyses

We compared the actual measured efficiencies with the predicted efficiencies to validate the linear regression. For the matrix-matched synthetic brines, the regression predicted the efficiencies to within 7% (95% CI) of actual values on average. The regression based on the NaCl-only brine predicted the efficiencies to within 5% of actual values on average (Table D5).

Appleby *et al.* [35] derived an empirical formula to determine the self-adsorption corrections in a well detector based on sample mass attenuation coefficients, determined by Hubbell's [36] approximations, and a geometrical parameter based on the dimension of the cylindrical well. This method requires that the elemental composition of the sample be fully known. We applied this correction to the 300 g/L mixed-cation brine and calculated an attenuation of $20 - 22$ % between 150 keV and 200 keV, based on the theoretical derivation of the geometric parameter. When we applied our TDS corrections, the attenuation for the same brine was ~23 % at 186 keV. This, thus showed good agreement between the TDS correction derived here and Appleby's method (Tables D3, D5 – D7).

5.4.5 Implications on Radium Measurement of High-TDS Produced Water

This work has investigated the effect of ion distribution on the self-attenuation of high-TDS brines in well-detector γ-spec. As part of this work, we present a method and new considerations for more accurate radium measurements of oil and gas produced waters. To this effect, we have shown that the TDS concentration, as well as its composition, has a marked effect on self-attenuation in high-TDS brines, and thus, accurate measurements of ^{226}Ra must include a self-attenuation correction. This is most applicable to chloride dominated brines, such as Appalachian Basin brines studied herein, but extends to other high-TDS, and high Cl brines including the Permian (133 g/L TDS and 81 g/L Cl), Antrim (140 g/L TDS and 85 g/L Cl), and Williston Basins (150 g/L TDS and 92 g/L Cl) (per representative data from the USGS produced water database v2.3n). It is yet to be seen if this analysis applies to non-Cl brines, such as from the Western US Basins that are

SO_4-dominated [42]. For these high-TDS, high Cl brines, we observed that radium data was sparse (the USGS produced water database reported radium data only for the Appalachian Basin brines). While radium activities in these brines might be low, it should be noted that the disposal and surface discharge of these brines can still lead to significant radium accumulation, such as in river sediments [43]. Other practices of produced water management, such as road spreading or agricultural irrigation, should be evaluated with consideration for radium.

The robustness of our proposed attenuation correction was tested by applying it to real produced waters. We evaluated radium activities of the produced waters based on a freshwater standard, a NaCl-only standard set, and a multi-cation standard set of varying TDS concentrations. Then, we compared the radium activities calculated based on the brines, which included TDS-influenced attenuation corrections, to the freshwater. Thereafter, we computed the percentage difference between these activities. These results are summarized in Figure 5.4A and 5B. Additionally, we evaluated the radium activities of three oil and gas samples that were characterized in a recent inter-laboratory study conducted by Tasker *et al.* [33] We compared the activities reported from the inter-lab study to the activities determined using the methods proposed in this study (Figure 5.4C).

We found that the self-attenuation correction based on the multi-cation brine was more sensitive to changes in TDS than was the mere NaCl brine. In all cases, the activities reported based on the brine standards were higher than those reported based on mere freshwater standards; and this disparity increased with increasing TDS (Figure 5.4A and 5.4B). That is to say, the impact of the dissolved solids incurred greater attenuation with increasingly higher TDS concentrations, and would result in erroneous radium activities if not corrected. Whenever radium

measurements of high-TDS fluids are reported without a reported attenuation correction, it is very likely that the reported activities have been underestimated because the higher attenuation caused by other sources of TDS (Ba, Mg, Ca, Sr) have not been taken into account

We were however surprised to discover that the percentage difference in activity between the brine standard and freshwater standard was higher when the radium activities were determined from the daughter products (Figure 5.4B). This result was unexpected as α_{TDS} is less negative at the higher energy levels of the radium daughters' decay (i.e. at 295, 351, and 609 keV- see Table D3). We probed the reason for this by observing the ratio between the activity determined by direct measurement and by the daughters for all three cases. We found that the ratio was often higher for the freshwater standard than for either the NaCl-only or multi-cation brine, i.e. radium activities determined by the daughter differed more when they were determined by the freshwater standard. In effect, this almost doubled the difference between the activities that were determined by the brine standards, when compared to the mere freshwater standard. One possible explanation for this is the reduced solubility and subsequently, increased radon leakage that occurs at higher salinity [44–46]. When we compared our results to those of the inter-lab study, we found that our corrected activities were higher than those reported by other labs, and this disparity was correlated to the TDS concentration of the fluids (Figure 5.4C), i.e. higher TDS correlated to greater disparity. Given the above discussion, we wonder whether this difference could be attributed to the difference in measurement techniques and standardization techniques employed by labs that

participated in that study – standardization techniques that have not been forwarded to the authors herein. Apparently, radium measurements were often determined by daughter products and without a self-attenuation correction reported.

Radium-226 activities can be determined either directly at 186.2 keV or indirectly (daughter products after ~21 day incubation). It should be noted that there are drawbacks to either approach. When ^{226}Ra is determined directly, TDS has a greater effect on the attenuation, as reflected in the α_{TDS} value (Figure 5.2D and Table D3). However, the ^{226}Ra activity will have lower associated standard error (Figure 5.3), provided the counting time is sufficient. Figure 5.4A suggests that reported activities of high-TDS brines based on a freshwater standard could be up to ~40% lower than they truly are, when they have not been corrected for attenuation. Conversely, when the daughter products are used for ^{226}Ra activity determination, TDS has a lower effect on the attenuation, as reflected in the α_{TDS} value (Figure 5.2D and Table D3). This activity will have a higher associated standard error (Figure 5.3). In this case however, Figure 5.4B suggests that reported activities could be up to 80% lower than their actual values.

Generally, ^{226}Ra measurements are reported to be more variable than ^{228}Ra measurements. We found that the TDS concentrations did not affect the ^{228}Ra attenuation; and this finding corroborates with the lower variability in ^{228}Ra measurements in the inter-lab study [33]. The radium isotopic ratio, ^{228}Ra/^{226}Ra, is an important tool in fingerprinting oil and gas associated waters. As high-TDS attenuates ^{226}Ra more than ^{228}Ra, it is imperative that the TDS-influenced attenuation is account for when inferences are undertaken based on the radium isotopic ratio.

As the conversation surrounding radium measurements of high-TDS brines and impacted materials continues, it is evident that there is a need for consensus on

methodology, and a consensus on reference standards. Commercial and academic laboratories can improve by considering whether their reference standards are compositionally consistent with the high-TDS samples encountered. Reports on radium measurements should include detailed description on the technique employed for self-attenuation; otherwise, any reported activities and subsequent decisions made

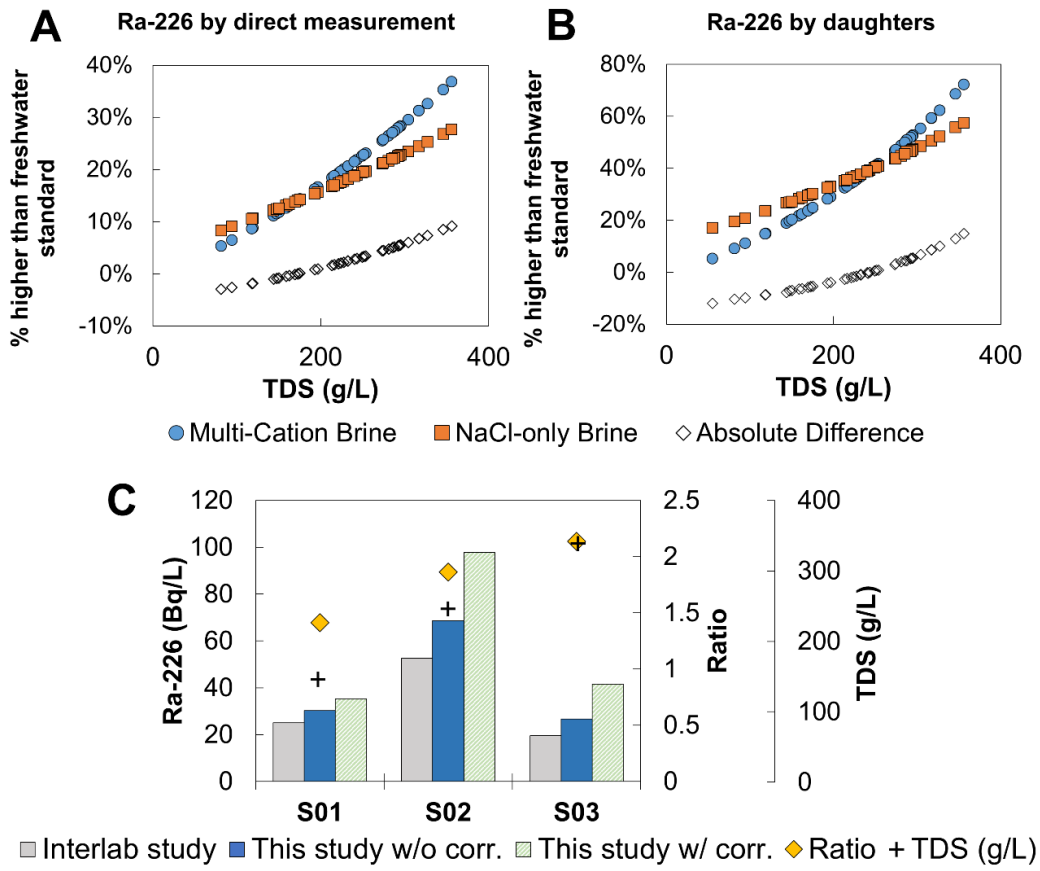

Figure 5.4: **A** and **B.** Radium activities of the 40 produced water samples were determined herein by the freshwater standard, the NaCl-only standard, and the multi-cation standard. The percentage difference between the radium activities when determined by the brines (multi-cation: blue, or NaCl-only: orange) as compared to the activity determined by the freshwater standards: determined by direct Ra measurement at 186 keV (panel **A**), or by the daughter products at 295 keV, 351 keV and 609 keV (panel **B**). Hollow diamonds are the % difference between multi-cation activity and NaCl-only activity. **C.** For representative samples S01,

S02, and S03: radium activities of the samples from the inter-lab study of Tasker *et al.*[33] The radium activities from the study (gray) were compared to the radium activities based on a freshwater standards (i.e. without correction − blue), and based on the multi-cation brine standard (green). The diamond is the ratio of [the activity determined by the multi-cation brine] to [the values from the study]. Higher ratios corresponded to greater TDS concentrations (+) for the samples S01, S02, and S03.

based on such activities remain open to scrutiny. Our results showed that radium and TDS should both be analyzed for Cl-dominated produced waters, especially when these produced waters are reused and recycled. Reuse and recycle will contribute to the TDS concentrations, thus introducing increased likelihood of erroneous radium measurements if attenuation parameters do not include a correction for both the TDS and its cations. For regulators, operators and researchers, it is imperative that TDS, cation, and radium concentrations are accurately determined for the handling, management, and beneficial reuse of O&G produced waters.

5.5 Acknowledgments

This research was funded by a National Science Foundation PFI: AIR-TT #1640634. Further support originated from a Penn State College of Engineering Graduate Excellence Fellowship.

5.6 References

(1) Warner, N. R.; Christie, C. A.; Jackson, R. B.; Vengosh, A. Impacts of Shale Gas Wastewater Disposal on Water Quality in Western Pennsylvania. *Environ. Sci. Technol.* 2013, *47*, 11849−11857.

(2) Ferrar, K. J.; Michanowicz, D. R.; Christen, C. L.; Mulcahy, N.; Malone, S.

L.; Sharma, R. K. Assessment of Effluent Contaminants from Three Facilities Discharging Marcellus Shale Wastewater to Surface Waters in Pennsylvania. *Environ. Sci. Technol.* 2013, *47*, 3472–3481.

(3) Wilson, J. M.; Van Briesen, J. M. Source Water Changes and Energy Extraction Activities in the Monongahela River, 2009–2012. *Environ. Sci. Technol.* 2013, *47* (21), 12575–12582.

(4) Wilson, J. M.; Wang, Y.; VanBriesen, J. M. Sources of High Total Dissolved Solids to Drinking Water Supply in Southwestern Pennsylvania. *J. Environ. Eng.* 2014, *140* (5), B4014003–1 – B4014003–B4014010.

(5) Wilson, J. M.; VanBriesen, J. M. Oil and Gas Produced Water Management and Surface Drinking Water Sources in Pennsylvania. *Environ. Pract.* 2012, *14* (4), 288–300.

(6) Parker, K. M.; Zeng, T.; Harkness, J.; Vengosh, A.; Mitch, W. A. Enhanced Formation of Disinfection Byproducts in Shale Gas Wastewater-Impacted Drinking Water Supplies. *Environ. Sci. Technol.* 2014, *48* (19), 11161–11169.

(7) Rowan, E. L.; Engle, M. A.; Kraemer, T. F.; Schroeder, K. T.; Hammack, R. W.; Doughten, M. W. Geochemical and Isotopic Evolution of Water Produced from Middle Devonian Marcellus Shale Gas Wells, Appalachian Basin, Pennsylvania. *Am. Assoc. Pet. Geol. Bull.* 2015, *99* (2), 181–206.

(8) Hayes, T. *Sampling and Analysis of Water Streams Associated with the Development of Marcellus Shale Gas*; Des Plaines, 2009.

(9) Rowan, E. L.; Engle, M. a.; Kirby, C. S.; Kraemer, T. F. Radium Content of Oil- and Gas-Field Produced Waters in the Northern Appalachian Basin (USA): Summary and Discussion of Data. *USGS Sci. Investig. Rep.* 2011, 38 pp.

(10) Kargbo, D. M.; Wilhelm, R. G.; Campbell, D. J. Natural Gas Plays in the Marcellus Shale: Challenges and Potential Opportunities. *Environ. Sci. Technol.* 2010, *44* (15), 5679–5684.

(11) Zhang, T.; Gregory, K.; Hammack, R. W.; Vidic, R. D. Co-Precipitation of Radium with Barium and Strontium Sulfate and Its Impact on the Fate of

Radium during Treatment of Produced Water from Unconventional Gas Extraction. *Environ. Sci. Technol.* 2014, *48* (8), 4596–4603.

(12) He, C.; Zhang, T.; Zheng, X.; Li, Y.; Vidic, R. D. Management of Marcellus Shale Produced Water in Pennsylvania: A Review of Current Strategies and Perspectives. *Energy Technol.* 2014, *2* (12), 968–976.

(13) Burgos, W. D.; Castillo-Meza, L.; Tasker, T. L.; Geeza, T. J.; Drohan, P. J.; Liu, X.; Landis, J. D.; Blotevogel, J.; McLaughlin, M.; Borch, T.; et al. Watershed-Scale Impacts from Surface Water Disposal of Oil and Gas Wastewater in Western Pennsylvania. *Environ. Sci. Technol.* 2017, *51* (15), 8851–8860.

(14) Harkness, J. S.; Dwyer, G. S.; Warner, N. R.; Parker, K. M.; Mitch, W. A.; Vengosh, A. Iodide, Bromide, and Ammonium in Hydraulic Fracturing and Oil and Gas Wastewaters: Environmental Implications. *Environ. Sci. Technol.* 2015, *49* (3), 1955–1963.

(15) Vengosh, A.; Jackson, R. B.; Warner, N. R.; Darrah, T. H.; Kondash, A. A Critical Review of the Risks to Water Resources from Unconventional Shale Gas Development and Hydraulic Fracturing in the United States. *Environ. Sci. Technol.* 2014, *48* (15), 8334–8348.

(16) Lauer, N. E.; Warner, N. R.; Vengosh, A. Sources of Radium Accumulation in Stream Sediments near Disposal Sites in Pennsylvania: Implications for Disposal of Conventional Oil and Gas Wastewater. *Environ. Sci. Technol.* 2018.

(17) Tasker, T. L.; Burgos, W. D.; Piotrowski, P.; Castillo-Meza, L.; Blewett, T. A.; Ganow, K. B.; Stallworth, A.; Delompré , P. L. M.; Goss, G. G.; Fowler, L. B.; et al. Environmental and Human Health Impacts of Spreading Oil and Gas Wastewater on Roads. *Environ. Sci. Technol.* 2018, *52* (12), 7081–7091.

(18) Veil, J. *U.S. Produced Water Volumes and Management Practices in 2012*; 2015.

(19) Kondash, A. J.; Albright, E.; Vengosh, A. Quantity of Flowback and Produced Waters from Unconventional Oil and Gas Exploration. *Sci. Total*

Environ. 2017, *574*.

(20) Ellsworth, W. L. Injection-Induced Earthquakes. *Science (80-.).* 2013, *341* (6142), 1225942.

(21) Dunne, E. J. *Flowback and Produced Waters*; Dunne, E. J., Ed.; National Academies Press: Washington, D.C., 2017.

(22) U.S. Environmental Protection Agency. *Study of Oil and Gas Extraction Wastewater Management Under the Clean Water Act EPA-821-R19-001*; Washington, D.C., 2019.

(23) U.S. Environmental Protection Agency. *Detailed Study of the Centralized Waste Treatment Point Source Category for Facilities Managing Oil and Gas Extraction Wastes*; Washington, D.C., 2018.

(24) MGX Minerals Inc. (Press Release). MGX Minerals and Eureka Resources Announce Joint Venture to Recover Lithium from Produced Water in Eastern United States https://www.prnewswire.com/news-releases/mgx-minerals-and-eureka-resources-announce-joint-venture-to-recover-lithium-from-produced-water-in-eastern-united-states-300806407.html (accessed May 13, 2019).

(25) Jang, Y.; Chung, E. Adsorption of Lithium from Shale Gas Produced Water Using Titanium Based Adsorbent. *Ind. Eng. Chem. Res.* 2018, *57* (25), 8381–8387.

(26) Jang, Y.; Chung, E. Lithium Adsorptive Properties of H2TiO3 Adsorbent from Shale Gas Produced Water Containing Organic Compounds. *Chemosphere* 2019, *221*, 75–80.

(27) Paranthaman, M. P.; Li, L.; Luo, J.; Hoke, T.; Ucar, H.; Moyer, B. A.; Harrison, S. Recovery of Lithium from Geothermal Brine with Lithium–Aluminum Layered Double Hydroxide Chloride Sorbents. *Environ. Sci. Technol.* 2017, *51* (22), 13481–13486.

(28) Swain, B. Recovery and Recycling of Lithium: A Review. *Sep. Purif. Technol.* 2017, *172*, 388–403.

(29) Schaller, J.; Headley, T.; Prigent, S.; Breuer, R. Potential Mining of Lithium, Beryllium and Strontium from Oilfield Wastewater after Enrichment in Constructed Wetlands and Ponds. 2014.

(30) Dorich, A. Eureka Resources Recovers Vital Resources from Flowback and Production Wastewater. *Energy & Mining International*. 2017.

(31) Nelson, A. W.; May, D.; Knight, A. W.; Eitrheim, E. S.; Mehrhoff, M.; Shannon, R.; Litman, R.; Schultz, M. K. Matrix Complications in the Determination of Radium Levels in Hydraulic Fracturing Flowback Water from Marcellus Shale. *Environ. Sci. Technol. Lett.* 2014, *1* (3), 204–208.

(32) Zhang, T.; Bain, D.; Hammack, R.; Vidic, R. D. Analysis of Radium-226 in High Salinity Wastewater from Unconventional Gas Extraction by Inductively Coupled Plasma-Mass Spectrometry. *Environ. Sci. Technol.* 2015, *49* (5), 2969–2976.

(33) Tasker, T. L.; Burgos, W. D.; Ajemigbitse, M. A.; Lauer, N. E.; Gusa, A. V.; Kuatbek, M.; May, D.; Landis, J. D.; Alessi, D. S.; Johnsen, A. M.; et al. Accuracy of Methods for Reporting Inorganic Element Concentrations and Radioactivity in Oil and Gas Wastewaters from the Appalachian Basin, U.S. Based on an Inter-Laboratory Comparison. *Environ. Sci. Process. Impacts* 2019, *21* (2), 224–241.

(34) Gilmore, G. R. *Practical Gamma-Ray Spectrometry*; John Wiley & Sons, Ltd: Chichester, UK, 2008.

(35) Appleby, P. G.; Richardson, N.; Nolan, P. J. Self-Absorption Corrections for Well-Type Germanium Detectors. *Nucl. Instruments Methods Phys. Res. Sect. B Beam Interact. with Mater. Atoms* 1992, *71* (2), 228–233.

(36) Hubbell, J. H. Photon Mass Attenuation and Energy-Absorption Coefficients. *Int. J. Appl. Radiat. Isot.* 1982, *33* (11), 1269–1290.

(37) Cutshall, N. H.; Larsen, I. L.; Olsen, C. R. Direct Analysis of 210Pb in Sediment Samples: Self-Absorption Corrections. *Nucl. Instruments Andm.* 1983, *206*, 309–312.

(38) Bolivar, J. P.; Garcí a-Leó n, M.; Garcí a-Tenorio, R. On Self-Attenuation

Corrections in Gamma-Ray Spectrometry. *Appl. Radiat. Isot.* 1997, *48* (8), 1125–1126.

(39) Zermeno-Motante, M. I.; Nieto-Delgado, C.; Cannon, F. S.; Cash, C. C.; Wunz, C. C. Chemical Modeling for Precipitation from Hypersaline Hydrofracturing Brines. *Water Res.* 2016, *103*, 233–244.

(40) Harris, D. C. *Quantitative Chemical Analysis*, 9th ed.; Freeman, W.H. & Company, 2015.

(41) Nelson, A. W.; Eitrheim, E. S.; Knight, A. W.; May, D.; Mehrhoff, M. A.; Shannon, R.; Litman, R.; Burnett, W. C.; Forbes, T. Z.; Schultz, M. K. Understanding the Radioactive Ingrowth and Decay of Naturally Occurring Radioactive Materials in the Environment: An Analysis of Produced Fluids from the Marcellus Shale. *Environ. Health Perspect.* 2015, *123* (7), 689–696.

(42) McDevitt, B.; McLaughlin, M.; Cravotta, C. A.; Ajemigbitse, M. A.; Van Sice, K. J.; Blotevogel, J.; Borch, T.; Warner, N. R. Emerging Investigator Series: Radium Accumulation in Carbonate River Sediments at Oil and Gas Produced Water Discharges: Implications for Beneficial Use as Disposal Management. *Environ. Sci. Process. Impacts* 2019, *21* (2), 324–338.

(43) Van Sice, K.; Cravotta, C. A.; McDevitt, B.; Tasker, T. L.; Landis, J. D.; Puhr, J.; Warner, N. R. Radium Attenuation and Mobilization in Stream Sediments Following Oil and Gas Wastewater Disposal in Western Pennsylvania. *Appl. Geochemistry* 2018, *98*, 393–403.

(44) Schubert, M.; Paschke, A.; Lieberman, E.; Burnett, W. C. Air–Water Partitioning of ^{222}Rn and Its Dependence on Water Temperature and Salinity. *Environ. Sci. Technol.* 2012, *46* (7), 3905–3911.

(45) Hamme, R. C.; Emerson, S. R. The Solubility of Neon, Nitrogen and Argon in Distilled Water and Seawater. *Deep Sea Res. Part I Oceanogr. Res. Pap.* 2004, *51* (11), 1517–1528.

(46) Sano, Y.; Takahata, N. Measurement of Noble Gas Solubility in Seawater Using a Quadrupole Mass Spectrometer. *J. Oceanogr.* 2005, *61* (3), 465–473.

Chapter 6

A Rapid Method to Determine ^{226}Ra Concentrations in Oil and Gas Produced Waters using Liquid Scintillation Counting

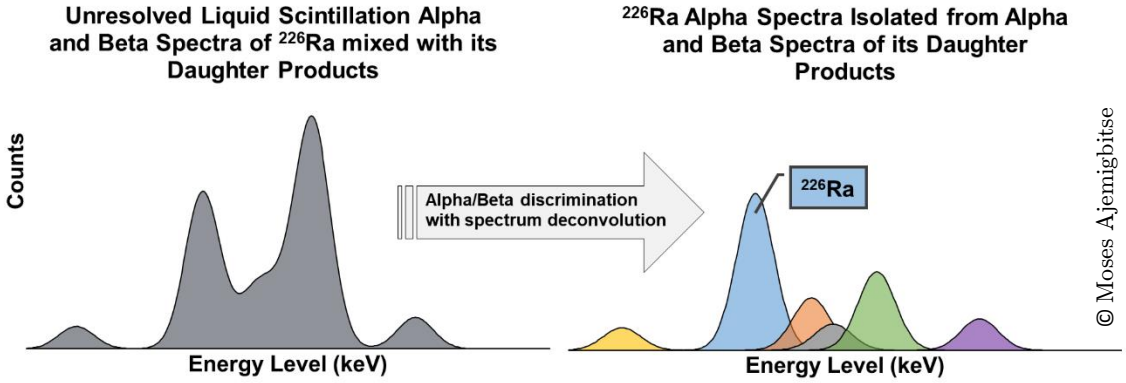

Ajemigbitse MA, Cannon FS, and Warner NR. "A Rapid Method to Determine ^{226}Ra Concentrations in Oil and Gas Produced Waters using Liquid Scintillation Counting and Spectrum Analysis." Manuscript in Preparation.

6.1 Abstract

Concentrations of naturally occurring radioactive material (NORM) in Marcellus Shale produced water presents a challenge for effective management and treatment of the vast volumes produced. With an increased emphasis on beneficial reuse and resource recovery from the produced waters, a rapid, yet reliable, method for quantifying radium in these produced waters is needed. The high total dissolved solids (TDS) concentration introduces difficulties when measuring ^{226}Ra by recommended EPA methods specific to drinking water. While other techniques for measuring radium in these high-TDS fluids have since been developed, these techniques often require extensive and complicated pre-concentration steps which require strong analytical chemistry skills, utilize hazardous chemicals like hydrofluoric acid, require long holding times or measurement times, and high sample volumes. We present a rapid method for ^{226}Ra measurements in high-TDS produced waters by liquid scintillation counting. Prior to one hour counting, samples are prepared for analysis simply by evaporating and re-suspending with acidified distilled deionized water. This protocol produced radium recoveries $\geq$ 93%. The alpha and beta spectra of ^{226}Ra and its daughter are separated by alpha-beta discrimination and spectrum deconvolution. The Minimum Detectable Activity of ^{226}Ra is 0.332 Bq/L (8.97 pCi/L) when the counting time is 60 min and sample volume is 4 mL. Nine Marcellus Shale produced waters of varying TDS and radium concentrations were analyzed by this method and compared with gamma spectroscopy and yielded comparable results with an R^2 of 0.92. The reduced sample preparation steps, low cost, and rapid analysis present this as a method ideal for field appraisal prior to comprehensive radiochemical analysis.

6.2 Introduction

Natural gas production from the Marcellus Shale (mainly in PA, OH, and WV) is accompanied by high volumes of formation produced water [1,2]. This produced water contains naturally occurring radioactive material (NORM) at concentrations orders of magnitude higher than the drinking water or industrial effluent standards [1]; and indeed higher than produced waters from many other US oil and gas producing fields [2–4]. Radium, a major constituent of the NORM, is a carcinogenic element that presents a significant challenge in the handling and management of produced water [5]. Radium can substitute calcium in living organisms, accumulating in and causing damage to living tissue by its ionizing radiation [3]. Radium in produced water occurs mainly as ^{226}Ra (half-life of 1600 y) and ^{228}Ra (half-life of 5.75 y) [3]. However, Marcellus Shale produced waters possess characteristically high ^{226}Ra activities and low ^{228}Ra/^{226}Ra, usually < 0.3 [3,6]. Given its longer life and higher relative activities, ^{226}Ra is the isotope that is routinely monitored in the produced waters. Chemical treatments for radium show no selectivity for the radium isotopes [7]. Herein, we focused on ^{226}Ra for these reasons.

Marcellus Shale produced waters are also characterized by their high total dissolved solids (TDS) concentration – as high as 400,000 mg/L – and high concentrations of Na and alkaline earth metals Mg, Ca, Sr, and Ba [8–11]. The high concentrations of these constituents has also made managing the produced waters challenging [12,13]. Prior treatment and management practices resulted in the degradation of surface water quality through the discharge of partially treated produced waters as elevated levels of salinity, metals and radium have been reported [14–17]. Disposal by injection into Class II underground injection control (UIC) wells is the most common practice nationwide [2]; but is not widely available in the Marcellus Shale

[1]. It is estimated that the large volumes of produced water will soon exhaust the limited capacity of these UIC wells, especially considering that Pennsylvania' s geology has limited the number of UIC wells [18]. As such, recycle and reuse of the produced waters is the prevailing management practice for produced water in Pennsylvania [1]. However, recycle and reuse of produced waters presents several problems that limit its widespread adoption, including downhole scale formation [19] and increased bacterial activity [20], which negatively impact well performance. There has therefore been an increased emphasis on developing alternative uses for produced water [21,22].

Beneficial reuse of produced water through resource recovery has been put forward as one such alternative use [22,23]. NaCl recovered from produced water is currently available commercially [24], and lithium recovery is being researched and attempted [25–29]. Before these practices can be wholly adopted, radium activities in the produced water, treatment products, and recovered materials must be accurately determined.

Methods for determining radium activities in fluids include alpha spectroscopy (EPA Method 903.0) [30], ^{222}Rn emanation (EPA Method 903.1) [31], gamma spectroscopy (EPA Method 901.1) [32], and Inductively Coupled Plasma − Mass Spectroscopy (ICP-MS) [33]. However, there are issues involved with these methods when analyzing the high-TDS produced waters. The EPA Methods 903.0 and 903.1 are specific to drinking water and previous work by Nelson *et al.* showed that these methods are unreliable due to issues with very low radium recoveries (1% - 20%) caused by the high TDS concentrations and ionic strength of the produced waters [34]. Gamma spectroscopy (γ-spec) is the recommended method for measuring radium [34], however, an inter-lab comparison showed that γ-spec radium measurements of

oil and gas produced waters can vary by as much as ±30% for the sample samples analyzed by different labs [35]. This differences could be attributed to calibration/sample preparation issues, radon leakage, or failing to account for gamma photon attenuation [35]. In addition, many applications of γ-spec still include wet-chemical techniques of pre-concentration, chemical separation and purification steps, which have been shown to have low radium recoveries [34]. Zhang *et al.* proposed a new method by ICP-MS [33], however, this method also required chemical separation by ion exchange resin, which can prove difficult given the high concentrations of Ba and Sr in solution. Maxwell *et al.* reported a rapid method for γ-spec [36], but sample preparation was multi-step (and included hydrofluoric acid) and required high sample volumes (400 mL). This method was not tested with real produced waters, leaving its applicability unverified.

In many of the proposed methods, sample preparation was complicated and involved several treatment/separation steps – sometimes with extremely hazardous chemicals – required large sample volumes, and advanced analytical chemical skills, yet produced low radium recoveries because of the challenging chemistry of the produced waters. There is an opportunity for a rapid method that has a simple sample preparation protocol – one that does not use hazardous chemicals – requires little skill, utilizes low sample volumes, yields high radium recoveries, and is robust to the high-TDS concentrations and ionic strength of the produced waters. We propose a method by liquid scintillation counting that fulfils these criteria.

Liquid scintillation counting (LSC) is a well-established technique for radioactivity analyses of alpha and beta decay, such as for ^{14}C, ^{3}H, ^{235}U, ^{232}Th, ^{89}Sr, and $^{90}Sr/^{90}Y$, in groundwater, surface waters, in environmental applications and medical analysis [37–43]. LSC offers several advantages, such as direct measurement of water

samples, low background count rates, and high efficiencies (up to 100% for alpha particles have been reported) [39,41]. Modern LSC instruments are equipped with alpha/beta discrimination capabilities. Alpha/beta discrimination allows for the simultaneous analysis of alpha and beta emitters by pulse shape analysis. Pulse shape analysis enables alpha decay events to be distinguished from beta decay events [39,41,44]. Radium-226 decays by emitting an alpha particle and its subsequent decay series consists of several elements that decay by emitting alpha and beta particles, often with overlapping energies (see Table E1). Following alpha/beta discrimination, the alpha spectra of ^{226}Ra can be isolated by spectrum deconvolution based on multi Gaussian analysis [45]. Techniques that apply alpha/beta discrimination and spectrum analysis for radium analysis exist in literature [44,45], but none are specific for the high-TDS hydraulic fracturing produced waters. Several factors, such as salinity/ionic strength, are known to shift and compress LSC spectra, a phenomenon referred to as "quenching" [46]. However, we note that among the methods that apply LSC for radium analysis in water, none are applied to high-TDS produced waters and none discuss the quenching effect of the high-TDS environment on the LSC spectra.

In this work, we describe a rapid method for ^{226}Ra analysis by LSC. This technique does not require chemical separation of radium, instead alpha/beta discrimination and spectral analysis remove the interference from the other emitting nuclides. The effect of high-TDS on the LSC spectra was evaluated, the first time such an analysis is performed on produced waters. We validated our method by comparing to radium measurements determined by γ-spec.

The objectives of this paper were to i) determine correlations between the TDS concentration, specific gravity, and ionic strength of Marcellus Shale produced

waters, ii) present in detail, a new technique for rapid and accurate ^{226}Ra measurements in high-TDS brines by LSC with alpha/beta discrimination and spectrum analysis, and iii) compare the ^{226}Ra measurements by LSC with γ-spec.

6.3 Materials and Methods

6.3.1 Materials

The radioactivities (LSC and γ-spec) were determined in Wheaton 24 mL high density polyethylene liquid scintillation vials with cone-lined, poly seal, urea caps. Analytical chemicals were ACS reagent grade and supplied by VWR. Ultrapure distilled de-ionized (DDI) water (18.2 $m\Omega$) came from a ThermoScientific Barnstead Nanopure system. Perkin Elmer supplied the liquid scintillation cocktail, Ultima Gold AB, which was specifically designed for alpha/beta counting. The LSC standard set for alpha/beta discrimination were an ^{241}Am and a ^{36}Cl single isotope standards both at 1,167 Bq (100,000 dpm) per vial in Ultima Gold AB; and these standards were provided by Eckert and Ziegler. Liquid scintillation counting was performed on a Pekin Elmer QuantaSmart Tri-Carb 3310TR equipped with alpha/beta discrimination. The LSC calibration standard set consisted of a blank, a ^{14}C, and a ^{3}H standards in Ultima Gold, and were supplied by Perkin Elmer. Nitromethane, for quench comparison with TDS, was provided by Sigma-Aldrich.

6.3.2 Marcellus Shale Produced Water

Nine (9) Marcellus Shale flowback and produced water samples were sourced from across Pennsylvania. Four (4) were flowback samples from two wells in Southwest PA at early (one and two days after production) and later flowback dates (29 and

30 days after production) in conjunction with the Pennsylvania Bureau of Abandoned Mine Reclamation (BAMR) [47]. Three (3) more samples were utilized in a previous study on the practice of spreading of oil and gas produced waters on road [48]. The final two (2) samples came from a fluid processing facility managing produced waters from unconventional wells. Radium-226 activities of these samples were determined by γ-spec on a Canberra ultra-low background, small anode high purity germanium (HPGe) well detector. The ^{226}Ra activities were determined directly at 186.2 keV (^{226}Ra) following deconvolution to remove interference from ^{235}U [49] and self-attenuation corrections [50].

Previously, we have characterized the specific gravity, TDS (g/L), and ionic strength (mol/kg) of forty Appalachian Basin produced waters [50]. Briefly, triplicate 1 mL aliquots of representative filtered samples were weighed and then dried to evaporation at 180 °C. The dry weights were determined after cooling in a desiccator. The specific gravity was determined as the ratio of the sample weight to an equal volume of distilled water. The total dissolved solids was the weight of the dry residue divided by the volume of the sample. The ionic strength was determined by elemental compositions of cations (Na, Mg, Ca, Ba, Sr, and K by inductively coupled plasma-optical emission spectroscopy) and anions (Cl and Br by ion chromatography) and the Lewis-Randall ionic strength equation for non-ideal solutions. Herein, we performed linear regression of specific gravity versus TDS and ionic strength, in order to provide correlations between an easily measured component of produced water, i.e. specific gravity, with one requiring more comprehensive analysis, i.e. ionic strength. These relationships could provide useful approximations of produced water chemistry for operators while appraising radium in these fluids by LSC.

6.3.3 Radium Standard for LSC Efficiency

Synthetic brines at five TDS concentrations (0 g/L, 50 g/L, 100 g/L, 200 g/L, and 300 g/L in ultrapure distilled de-ionized water with 5% v/v nitric acid) were designed to replicate the TDS range encountered in Marcellus Shale produced waters. These brines contained Na, Mg, Ca, Ba, and Sr at the following molar ratios: cations were 75% Na, 15% Ca, 4% Ba, 3% Mg, and 3% Sr; while anions were 100% Cl. This molar distribution was consistent with the mean values of Appalachian Basin produced waters [50] (see Table E2 for the full composition of the synthetic brines). Radium-226 (supplied by National Institute of Standards and Technology (NIST) Gaithersburg, MD) was dosed into the synthetic brines to 185 Bq/L (5,000 pCi/L) activity.

6.3.4 Alpha/Beta Discrimination Calibration

The LSC instrument equipped with alpha/beta discrimination can determine a pulse decay discriminator (PDD) that results in the separation of alpha decay from beta decay events. In order to calibrate the instrument for alpha/beta discrimination, a pure alpha emitter (^{241}Am) and a pure beta emitter (^{36}Cl) standards are required. The optimum PDD setting is automatically determined by counting each standard at varying PDD settings and determining the setting that results in the lowest misclassification of alpha decay in the beta spectrum, and vice-versa [51]. For our instrument, the PDD was determined as 159.

6.3.5 Liquid Scintillation Counting: Sample Preparation and Analysis

When appraising radium concentrations in drinking water by alpha/beta discrimination, sample preparation often includes concentration by evaporation (typically a 10x concentration), followed by dissolution with distilled water at low pH or with

dilute acid solutions (by nitric, hydrochloric or phosphoric acid) [45,52–55]. Evaporation served a second purpose of desorbing radon gas, thereby breaking the secular equilibrium between radium, radon and its short lived daughters (^{218}Po, ^{214}Pb, ^{214}Bi, and ^{214}Po). Following dissolution and cooling, samples were transferred to the measurement vials and the scintillation cocktail was added. (For these high-TDS brines and produced water, a ten-fold concentration could be impractical when the TDS concentrations are close to the saturation concentrations for chloride salts.) Sample volumes for analysis are usually determined by the solution chemistry in order to maintain a homogenous aqueous fluid [56]. For example, sample volumes can be higher when ionic strength is low. When appraising high ionic strength samples, such as produced waters, the sample volumes should be adjusted to ensure cocktail compatibility and stability [56]. Compatibility is achieved when the mixture of cocktail and sample results in a clear fluid (not cloudy or hazy). Stability is achieved when the mixture remains as a single phase mixture without any apparent phase separation leading to an emulsion. Following the tests for compatibility and stability, samples are transferred to the vials for analysis. Scintillation vials can be plastic or glass, however, for radium analysis, plastic vials are recommended because they offer lower background and higher photon transmission [40,46,56]. Finally, counting times ranged from 10 minutes to 300 minutes [45,52–55].

With these considerations, we appraised several approaches to the sample preparation using our radium-dosed synthetic brines at varying TDS concentrations, in order to determine the most suitable sample preparation steps. We decided upon two protocols for sample preparation, namely: i) the Lab Method, which emphasized sample-cocktail compatibility and stability, and ii) the Field Method, which emphasized ease of use and high sample throughput. These are described in the following paragraph.

The raw produced water samples were prepared by filtering with 0.45 μm cellulose acetate syringe filters. Then, the required sample volume was transferred to the scintillation vial. The sample volumes varied from 3.5 mL to 10 mL for the Lab Method, as depicted in Table 6.1, however, for the Field Method, we kept the sample volumes constant at 4mL. The scintillation vials were transferred to a drying oven at 100 − 120 °C; and dried to evaporation for a minimum of 4 hours. This drying time allowed for the short lived daughters to decay to less than 1% of their initial activities [52]. After drying, the samples were allowed to cool for 5 minutes. Then, acidified distilled deionized water (acidified to pH < 2 using hydrochloric acid) was added at volumes equal to the sample volume, i.e. a 1x concentration (see Table 6.1). Then, the vials were capped and agitated using a tube vortexer to completely dissolve the precipitates. Next, the scintillation cocktail, Ultima Gold AB, was added to the vials at their corresponding volumes (see Table 6.1). For the Field Method, the cocktail volume was always 10 mL; while for the Lab Method it ranged from 10 mL to 16.5 mL. The cocktail and sample were thoroughly mixed by overturning the vial a few times over. Each sample was prepared in triplicate. Following these steps, the prepared vials were transferred to the Tri-Carb 3310TR LSC instrument and counted for 60 minutes in the full spectrum (0 keV to 2,000 keV).

The radium recovery of the sample preparation procedure was evaluated by gamma spectroscopy. The 24 mL vials were filled with the synthetic brines at varying TDS concentrations and the radium activities were determined by γ-spec prior to, and after the full sample preparation protocols were performed on the samples.

Table 6.1: Multi-cation brine standards dosed with ^{226}Ra employed in the efficiency determination. The sample and cocktail volumes as well as the dosed ^{226}Ra activity according to the "Lab Method" or "Field Method".

	TDS	Sample Volume (mL)	Cocktail Volume (mL)	Total Volume (mL)	Radium activity (pCi/L)	^{226}Ra Added (pCi)	Expected activity (dpm)
Lab Method	0 g/L	10	10	20	5	50.0	111
	50 g/L	5.5	14.5	20	4.871	26.8	59.47
	100 g/L	5	15	20	5.065	25.3	56.22
	200 g/L	4	16	20	4.87	19.5	43.25
	300 g/L	3.5	16.5	20	4.87	17.0	37.84
Field Method	0 g/L	4	10	14	5	20.0	44.40
	50 g/L	4	10	14	4.871	19.5	43.25
	100 g/L	4	10	14	5.065	20.3	44.98
	200 g/L	4	10	14	4.87	19.5	43.25
	300 g/L	4	10	14	4.87	19.5	43.25

6.3.6 Data and Statistical Analyses

The Tri-Carb 3310TR was equipped with QuantaSmart, a data analytics software package, which provided summary statistics after each analysis. The counts per minute (cpm) in the alpha and beta channels, the associated 95% confidence interval (CI) uncertainties, and quenching factor were reported. Each sample was run in triplicate, and the variance-weighted averages were reported. The level of quench in each sample was quantified by the transformed spectral index of the external standard (tSIE) using a ^{133}Ba source. We also collected the raw alpha spectra (in ASCII format) of each sample for multi-Gaussian analysis. Multi-Gaussian spectrum analyses of the LSC data were performed in MATLAB® using the free signal processing package "*Peakfit*" provided by Professor Tom O' Haver, available for

download from his website (https://terpconnect.umd.edu/~toh/spectrum/). Statistical analyses comparing the ^{226}Ra measurements determined by LSC versus γ-spec were performed using Minitab® 18.

6.4 Results and Discussion

6.4.1 Specififc Gravity as a Proxy for Total Dissolved Solids and Ionic Strength Concentrations of Produced Waters

Applications of LSC for environmental samples requires knowledge of the sample chemistry, such as the salt content, in order to optimize sample-cocktail compatibility [40]. Rapid determinations of metrics such as ionic strength and total dissolved solids can prove beneficial for field applications of LSC. Analysis of the specific gravity, SG, total dissolved solids, TDS, and ionic strength, IS, of forty Appalachian Basin produced waters [50] allowed us to determine regression equations for the TDS and IS versus the SG (Figure 6.1A and 6.1B). The regression of TDS versus SG had an R^2 of 0.97 (Eq. 1), while the regression of IS versus SG had an R^2 of 0.886 (Eq. 2). Parenthetically, the linear regression of IS versus TDS had an R^2 of 0.943 (Figure E1). With these regression equations, it is possible to estimate analytically intensive characteristics of Marcellus Shale produced water, such as the IS and TDS, from an easily measured characteristic, the SG. We measured the TDS and IS of the nine Marcellus Shale produced waters employed in this study and compared it to the estimated TDS and IS from Eq. 6.1 and Eq. 6.2 (Figure 6.1C and 6.1D). This analysis showed that the regression equations produced good agreement with the measured values.

$$\text{TDS (g/L)} = 1704.6 \times \text{SG} - 1737.4 \ (R^2 = 0.97) \tag{6.1}$$

$$\text{IS (mol/kg)} = 31.892 \times \text{SG} - 32.543 \ (R^2 = 0.886) \tag{6.2}$$

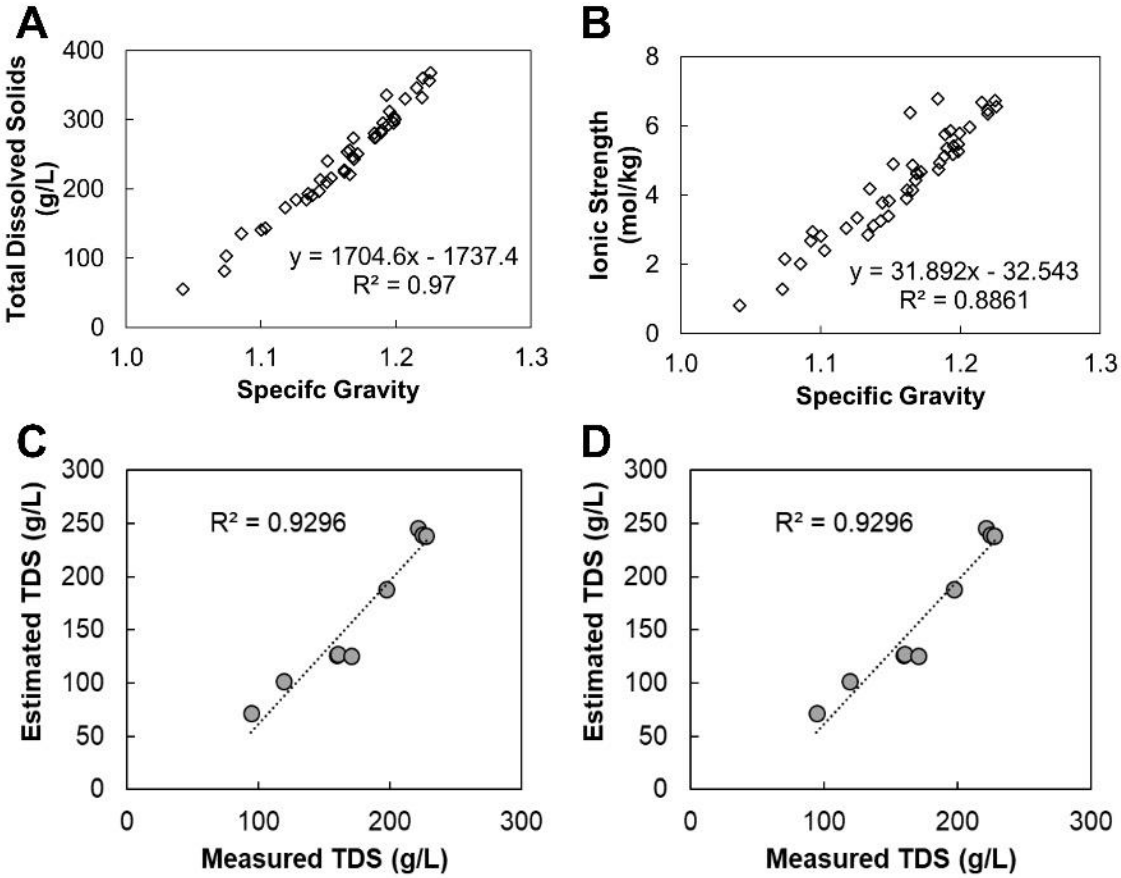

Figure 6.1: Linear regressions of specific gravity versus total dissolved solids (g/L) (**A**) and specific gravity versus ionic strength (mol/kg) (**B**) from forty Appalachian Basin produced water samples. **C.** Total dissolved solids, TDS (g/L), of the nine Marcellus Shale produced waters in estimated by the specific gravity (Eq. 1) versus the measured TDS. **D.** Ionic Strength, IS (mol/kg), of the nine Marcellus Shale produced waters estimated by the specific gravity (Eq. 2) versus the measured IS.

6.4.2 Effect of Total Dissolved Solids Concentration on ^{226}Ra Alpha Spectra

The scintillation cocktails for LSC analysis contain a solvent and photon-emitting fluor molecules. When a sample nucleus undergoes decay, the released energy excites the fluor molecules. As the fluor molecule returns to the ground state, photons are emitted. These photons are detected by a photomultiplier tube and the rate of photon detection is translated to the rate of nuclear decay [46]. A common phenomenon experienced in LSC is the interference in the conversion of nuclear decay energy to photons detected by the LSC photomultiplier; this is known as quenching. Quenching is the result of absorption of nuclear decay energy, or the absorption of the emitted photons by the sample solution [46]. These absorptions can be induced by color, ionization, or chemistry. Herein, we focused on chemical quenching as it is generally the most severe type of quenching [46]. Chemical quenching is attributed to the composition of the sample matrix and can absorb some of the nuclear decay energy, thereby reducing the observed count rate. It can also absorb the photons emitted by the fluor, thereby decreasing the light intensity and pulse height measured by the PMT. Quench correction is therefore important when appraising solutions of varying aqueous chemistries.

The level of quench is usually described by a quenching factor. While there are a variety of methods to determine quenching factors, we utilized the transformed spectral index of the external standard (tSIE) method. The tSIE method utilizes a gamma-emitting standard (^{133}Ba in this study), external to the sample being analyzed but located within the LSC instrument, to irradiate the sample vial from below it. Mathematical transformations of the Compton spectrum produced by the external standard through the sample is compared to a non-quenched standard,

and a value that describes the variation caused by the sample is calculated. The tSIE approach for quench description is very robust and widely utilized [46].

Quench standards for quench correction can be created by adding increasing volumes of a quenching agent, typically nitromethane, to solutions of known radioactivity [46]. The quenching factor, tSIE, and the efficiency are then determined and plotted against each other to create a quench-correction curve. Herein, we investigated the quenching caused by TDS concentrations as they are most relevant to the analysis of high TDS produced waters, such as encountered in the Marcellus Shale, and yet we have found no reference of TDS-influenced quenching in the literature.

A nitromethane standard quench set was created by adding $0 - 230$ µL of nitromethane to the 0 g/L synthetic brine. The alpha spectra and corresponding tSIE values for each standard was collected (Table E3). We also collected the alpha spectra and corresponding tSIE values for the $50 - 300$ g/L synthetic multi-cation brines. When we analyzed the spectra for the nitromethane quench set we observed the degradation of the peak towards lower energy levels. However, the TDS quench set showed peak degradation towards higher energy levels (Figure 6.2), completely opposite to what we observed for nitromethane quench standards. We confirmed this observation with repeated analysis and report this novel finding with great optimism. In addition to this, we again observed an opposite trend for the tSIE values. For the nitromethane quench standards, the tSIE showed an inverse relationship with the centroids of the peak and the quench level. High quench was characterized by low tSIE values and the peak centroid moved towards the lower energy levels.

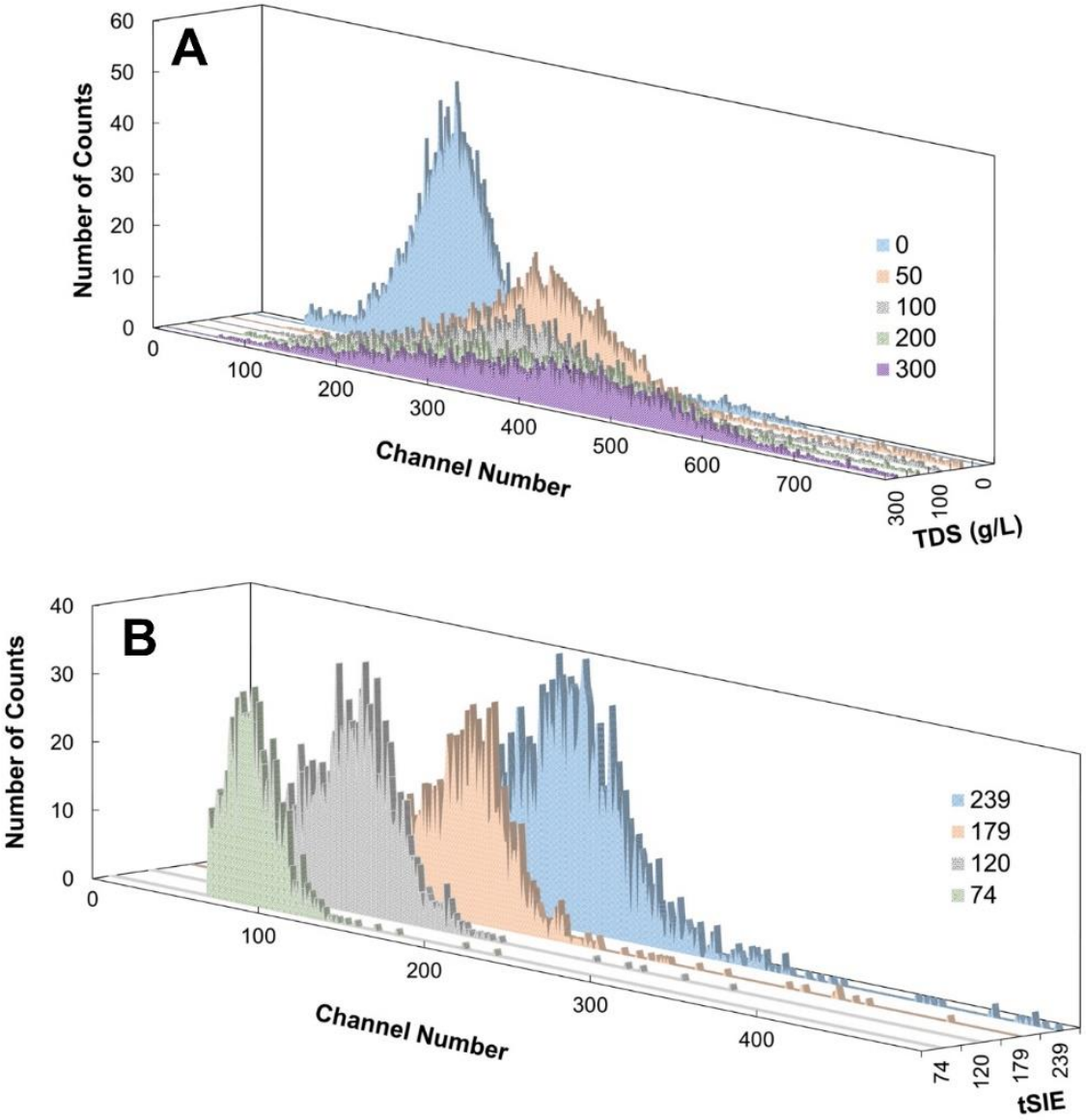

Figure 6.2: **A**. Liquid Scintillation alpha spectra of ^{226}Ra for the synthetic multi-cation brines at varying TDS concentrations. Illustrated is the shift and degradation of the radium spectra as a result of TDS. As TDS concentration increases, the spectra shifted towards higher energy levels. **B**. Liquid Scintillation alpha spectra of ^{226}Ra for nitromethane standards. The spectra shifted to lower energy levels as the level of quench increased, i.e. tSIE value of 239 (low quench) to 74 (high quench).

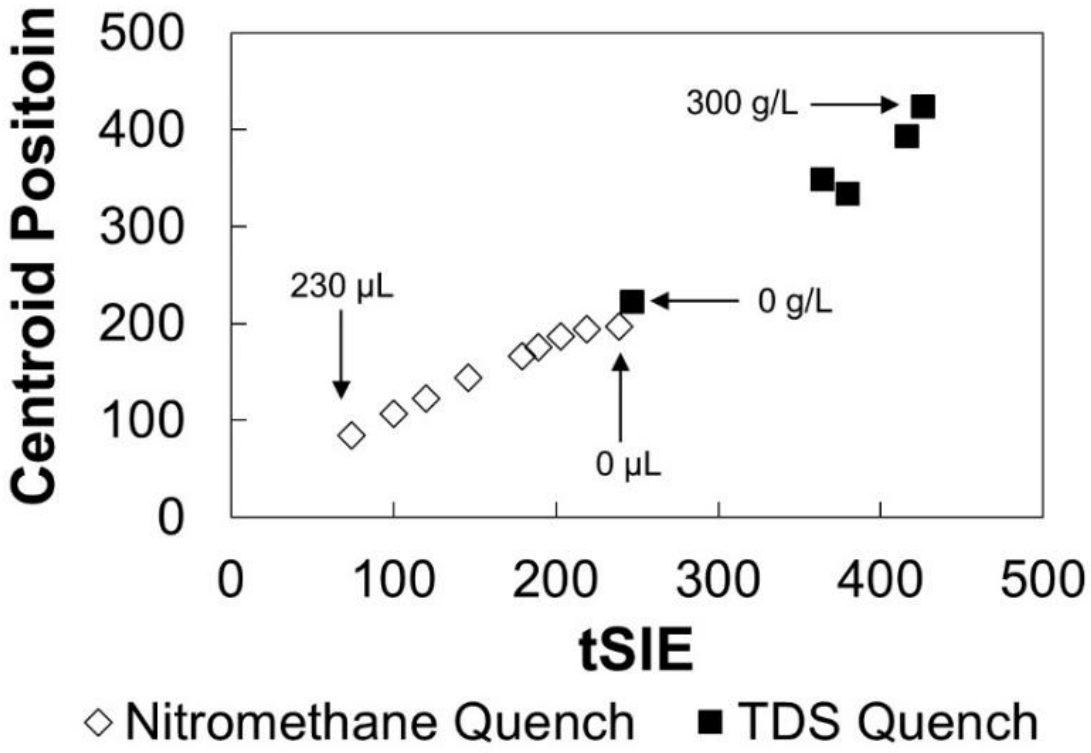

Figure 6.3: The quenching factor, tSIE, versus the fitted Gaussian peak position for the nitromethane quenched standards and the multi-cation standards. The peaks were fitted using Peakfit. For the nitromethane standards, the trend showed that increasing quench moved the peaks to the left, while for the multi-cation standards, quenching by increased TDS concentrations moved the peaks to the right.

However, for the TDS quench standards, high quench was characterized by high tSIE values and the peak centroid moved towards higher energy levels (Figure 6.3). Again, we confirmed this observation with repeated analysis. This anomalous quenching behavior of TDS indicates that the traditional quench correction curve may not be applicable when appraising the radioactivity of high-TDS samples, such

as produced water, by LSC analysis. Therefore, we investigated new quench correction curves, as discussed in the next section.

6.4.3 Determining the ^{226}Ra Efficiencies using the Synthetic Multi-Cation Brines

We have described two protocols for sample preparation – the Lab Method, which emphasizes cocktail-sample compatibility and stability, and hence resulted in cocktail-sample ratios that varied with TDS/IS concentrations (see Table 6.1 and Figure E2); and the Field Method, which emphasizes ease of use and high throughput, and hence utilized a constant sample-cocktail ratios. The radium recoveries of the sample preparation protocol was evaluated by measuring the radium activities prior to, and after the protocol using gamma spectroscopy. The radium recoveries were > 93%, as shown in Table 6.2.

Table 6.2: Radium-226 recovery of the sample preparation step of evaporative drying at the different TDS concentrations of the synthetic multi-cation brine standards. The radium activities were determined by gamma spectroscopy prior to, and after the sample preparation protocol.

Multi-cation brine standards	Initial ^{226}Ra (Bq)	^{226}Ra after sample prep.	^{226}Ra Recovery
0 g/L	4.50	4.54	101%
50 g/L	4.47	4.46	100%
100 g/L	4.61	4.30	93%
200 g/L	4.52	4.33	96%
300 g/L	4.81	5.07	105%

We also present two methods to analyze the LSC data – by Peakfit, which fits Gaussian function to the raw spectra, and by QuantaSmart, which is the instrument-reported data. For data analysis by Peakfit, the radium efficiencies were determined by Eq. 6.3. The radium efficiencies for the analysis by QuantaSmart were determined by Eq. 6.4.

$$\epsilon = \frac{I/T}{A \times 60} \tag{6.3}$$

$$\epsilon = \frac{C}{A \times 60} \tag{6.4}$$

where ϵ is the ^{226}Ra efficiency

I is the integrated peak area, counts

T is the counting time, minutes

A is the dosed ^{226}Ra activity, Bq

C is the reported count rate per minute, cpm

Radium-226 efficiencies were determined for both sample preparation protocols and by both data analysis methods (Table E4 and Figure E3); and ranged from 60% to 98%. Previously, we have discussed the use of quench curves to relate the quench level in a sample to the expected efficiency. As previously mentioned, the quenching effect of TDS on the alpha spectra was different from nitromethane. When we plotted the ^{226}Ra efficiencies against the quench parameter, tSIE, we found no discernable trends (Figure 6.4). Therefore, we concluded that the traditional quench curves of efficiency versus tSIE could not be applied for LSC analysis of high-TDS fluids, such as with oil and gas produced waters.

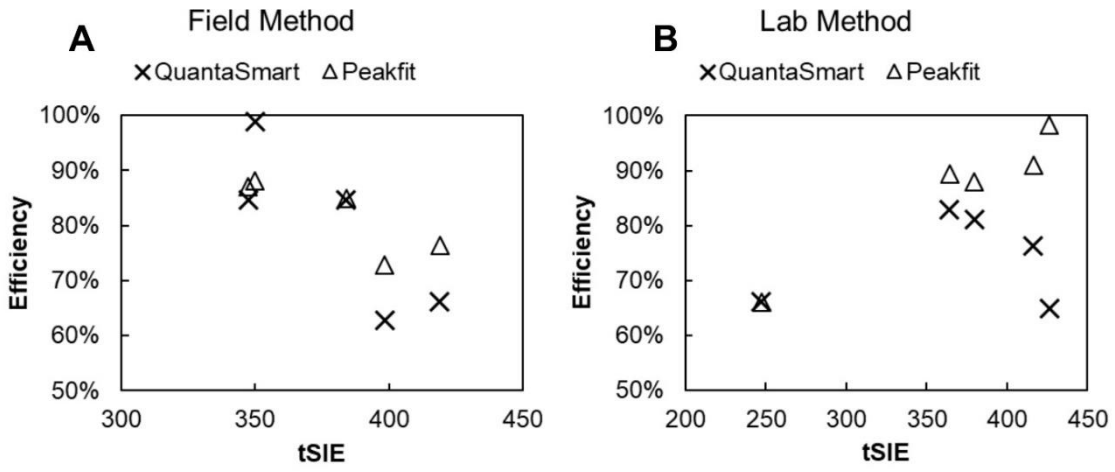

Figure 6.4: The quenching factor, tSIE, versus the ^{226}Ra efficiencies for the Field Method (panel **A**) and the Lab Method (**B**). The traditional quench curve of efficiency versus tSIE could not be applied for the analysis of high-TDS fluids.

In order to determine the relevant efficiency curve for these high-TDS fluids, we performed some data transformations and analyzed the trends with efficiency. First, we define a new variable, R, as the ratio of the sample volume to cocktail volume. Then we observed the trend of the efficiency when plotted against R, SG, TDS, IS, R × SG, R × TDS, R × IS. Second, we defined another variable, R´, as the ratio of the sample volume to the total volume and we performed the same analysis with the efficiency. We performed these analyses for both sample preparation protocols and both data analysis methods giving us 22 sets of curves to compare. From these, we present the three datasets that showed the highest correlations between the efficiency and the transformed data for each sample preparation protocol and data analysis method (Figure 6.5).

For the Field Method, when the LSC data was analyzed by Gaussian analysis, i.e. Peakfit, ^{226}Ra efficiencies correlated with SG, TDS, and IS (Figure 6.5A – 6.5C).

The correlations produced $R^2 > 0.95$ when fitted with linear trendlines. When the data was analyzed based on the instrument output, i.e. QuantaSmart, ^{226}Ra efficiencies also correlated with SG, TDS, and IS (Figure 6.5D – 6.5F). The trendlines, with $R^2 > 0.92$ were logarithmic for SG and IS, while it was exponential for TDS.

For the Lab Method, when the LSC data was analyzed by Peakfit, the ^{226}Ra efficiencies correlated with R × TDS, R × IS, and R´ × IS (Figure 6.5G – 6.5I). The trendlines, with $R^2 > 0.99$, were 2nd order polynomials. When the data was analyzed by QuantaSmart, ^{226}Ra efficiencies correlated with SG, TDS and IS (Figure 6.5D – 6.5F). The trendlines, with $R^2 > 0.99$, were 2nd order polynomials.

The 95% CI uncertainties for the efficiencies ranged from ~2% – ~10% (Figure 6.6 and Table E4). Generally, the lowest uncertainties occurred when the data was analyzed by QuantaSmart, irrespective of the sample preparation protocol.

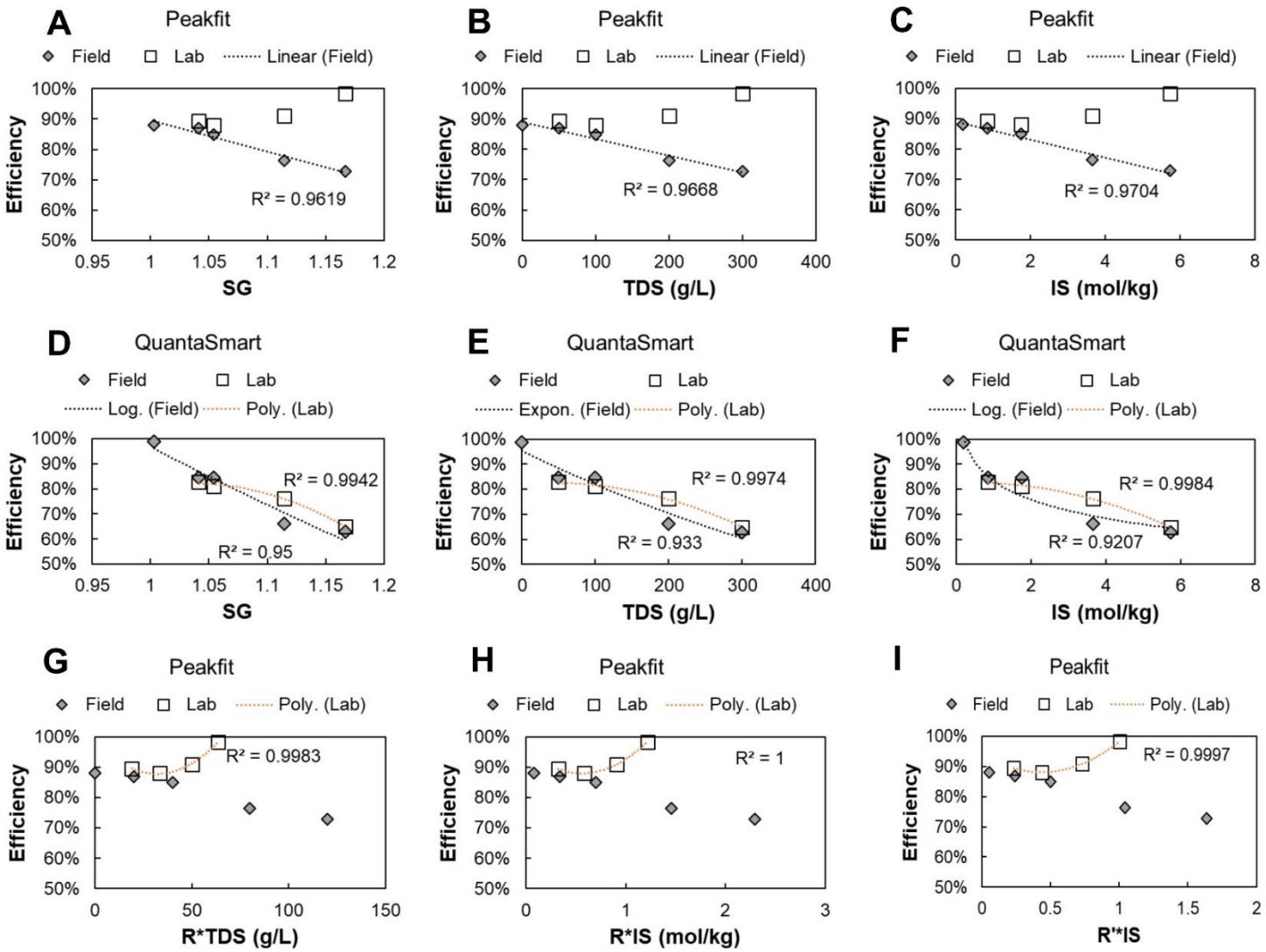

Figure 6.5: Data transformations for the ^{226}Ra efficiency determination by multi-Gaussian analysis (Peakfit) and instrument reported data (QuantaSmart) based on the synthetic multi-cation brines. **A − C**: Efficiencies showed high correlation with specific gravity, SG, total dissolved solids, TDS (g/L), and ionic strength, IS (mol/kg), for the Field Method when the spectra was analyzed by multi-Gaussian analysis (Peakfit). **D − F**: Efficiencies showed high correlation with SG, TDS, and IS for both methods the spectra was analyzed by instrument software (QuantaSmart). **G − I**: Efficiencies showed high correlation with R× TDS, R× IS, and R´× IS, for the Lab Method when the spectra was analyzed by multi-Gaussian analysis (Peakfit). R is the ratio of sample volume to cocktail volume. R´ is the ratio of sample volume to total volume.

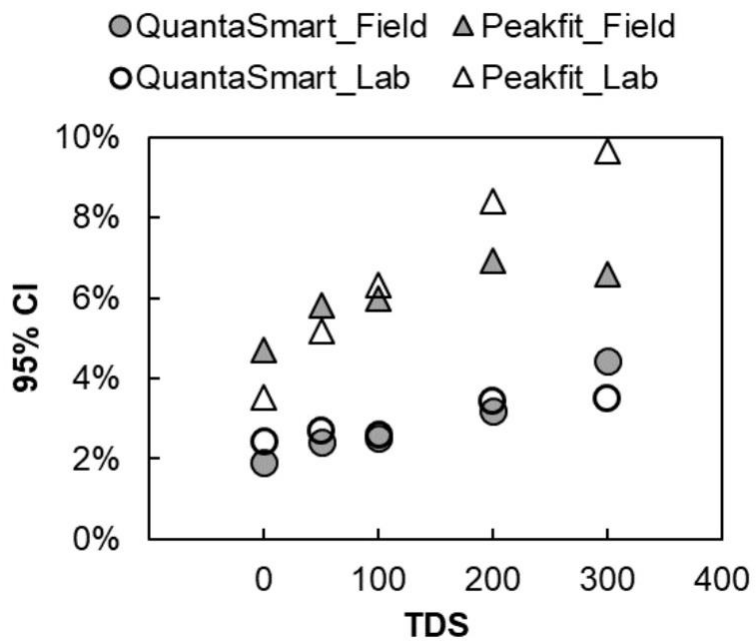

Figure 6.6: The 95% confidence interval (CI) uncertainties of the ^{226}Ra efficiencies versus TDS concentration for the Field and Lab Methods following data analysis by Gaussian spectrum analysis (Peakfit) or by instrument reported data (QuantaSmart).

6.4.4 Analysis of Marcellus Shale Produced Waters

The ^{226}Ra activities of nine Marcellus Shale produced water samples were determined by our proposed LSC method using both the Lab and Field Methods, and the data was analyzed by QuantaSmart and Peakfit (Table E5, Figure E4 and E5). When data was analyzed by Peakfit, the ^{226}Ra activities were determined by Eq. 6.5. When the data was analyzed by QuantaSmart, the activities were determined by Eq. 6.6. The combined uncertainty of the ^{226}Ra activity, σ_A, can be calculated according to Eq. 6.7.

$$^{226}Ra\ [Bq/L] = \frac{I/T}{\epsilon \times 60 \times V} \tag{6.5}$$

$$^{226}Ra[Bq/L] = \frac{C}{\epsilon \times 60 \times V} \tag{6.6}$$

$$\sigma_A = \sqrt{\sigma_R^2 + \sigma_v^2 + \sigma_\epsilon^2} \tag{6.7}$$

where I is the integrated peak area, counts

T is the counting time, minutes

ϵ is the ^{226}Ra efficiency

V is the sample volume, mL

C is the reported count rate per minute, cpm

σ_R is the uncertainty of the count rate from Peakfit or QuantaSmart

σ_v is the uncertainty of measuring the sample volume

σ_ϵ is the uncertainty of the efficiency

We also measured the ^{226}Ra activities of these produced water samples by gamma spectroscopy and performed linear regressions between the two results in order to validate the LSC method. Table 6.3 summarizes the results of the linear regressions.

The LSC methods had R^2 ranging ~0.75 to ~0.92, showing good correlation between the ^{226}Ra activities measured by LSC and to the activities measured by gamma spectroscopy. The Field Method produced higher R^2 than the Lab Method, and data analysis by Peakfit produced higher R^2 than by QuantaSmart, although this was accompanied by higher combined uncertainties (~10 % versus ~4%). The Field Method with data analysis by Peakfit produced the highest R^2 values of ~0.92. Although the regressions showed good agreement with gamma spectroscopy, the

coefficients of the LSC measurements were > 1 for all methods. This indicated that the LSC method underestimated the ^{226}Ra activities of these produced waters. One reason for this could be the additional quenching offered by other aqueous constituents, such as dissolved organic matter, or iron, which we did not account for in the synthetic brines. The presence of organic carbon could have resulted in chemical quenching [46], while the presence of iron could have resulted in color quenching [38]. Furthermore, the constants of the linear were not statistically significant, thereby preventing any inferences from being concluded based on their magnitudes and signs.

Table 6.3: Results of the linear regression of ^{226}Ra activities of the nine Marcellus Shale produced waters measured by gamma spectroscopy versus the ^{226}Ra activity measured by liquid scintillation counting.

Sample Prep and Data Analysis Method	**Data Transformation**	**R^2**	**Coefficient**	**p-value**	**Constant**	**p-value**	**Median 95% CI**
Field Method – Peakfit	SG	93.66%	2.934	0	-1675	0.295	9.6%
	TDS	92.98%	2.996	0	-1848	0.280	
	IS	92.69%	3.097	0	-2036	0.163	
Field Method – QuantaSmart	SG	81.26%	2.36	0.002	-1397	0.666	4.4%
	TDS	83.61%	2.434	0.001	-2716	0.411	
	IS	90.11%	3.134	0	-6026	0.070	
Lab Method – Peakfit	R´ × TDS	87.43%	2.440	0	-1240	0.579	9.8%
	R × IS	87.16%	2.525	0	-1135	0.613	
	R´ × IS	87.27%	2.533	0	-1185	0.597	
Lab Method – QuantaSmart	SG	75.28%	1.58	0.005	2513	0.401	4.1%
	TDS	75.71%	1.669	0.005	2087	0.491	
	IS	75.56%	1.792	0.005	1605	0.607	

6.4.5 Minimum Detectable Activities

The Minimum Detectable Activity, MDA, was calculated by the modified Curie equation [57]:

$$\mathrm{MDA} = \frac{3 + 3.29\sqrt{R_b t_g\left(1 + t_g/t_b\right)}}{\epsilon t_g} \tag{8}$$

where R_b is the background count rate (cpm); 0 cpm were reported in the background alpha channel

t_g is the sample count time; 60 minutes

t_b is the background count time; 180 minutes

ϵ is the efficiency

The MDAs achieved by the two sample preparation protocols and data analysis methods are summarized in Table 6.4. The highest MDA achieved by the LSC method was 0.332 Bq/L (8.97 pCi/L) when the counting time was 60 minutes and sample volume was 4 mL; and this was achieved by Field Method with data analysis by QuantaSmart. Reported MDAs for ^{226}Ra measurement were 0.01 Bq/L [38] (drinking water by LSC), and ~3 Bq/L [34] (gamma spectroscopy), and 3.7 Bq/L [33] (ICP-MS).

Table 6.4: Minimum detectable efficiencies (MDA) for ^{226}Ra calculated for the proposed liquid scintillation counting methods.

Sample Prep and Data Analysis Method	**Minimum Efficiency**	**MDA (dpm)**	**MDA (pCi)**	**MDA (pCi/L)***	**MDA (Bq)**	**MDA (Bq/L)***
Field method – Peakfit	*72.8%*	0.0687	0.0309	7.73	0.00114	0.286
Field method – QuantaSmart	*62.8%*	0.0796	0.0359	8.97	0.00133	0.332
Lab method – Peakfit	*66.0%*	0.0758	0.0341	8.53	0.00126	0.316
Lab method – QuantaSmart	*64.9%*	0.0770	0.0347	8.68	0.00128	0.321

* Assuming a sample volume of 4 mL

6.4.6 Limitations of the Method

In this work, we have focused on the chemical quenching caused by high-TDS concentrations, however, additional quenching could be caused by other constituents of produced water particularly dissolved organic matter and iron. Although iron is found at relatively low concentration in produced waters, median total Fe of ~ 47 mg/L [11], we observed color in some of our Marcellus Shale samples. This color diminished in intensity when the sample was mixed with the cocktail, especially with the Lab Method which had greater cocktail-to-sample ratios. We attempted to account for the presence of organic matter in the produced waters by measuring the chemical oxygen demand (COD) of the samples. However, when the COD values were added to the linear regressions, they did not prove significant.

In order to minimize the interference from the decay products of ^{226}Ra, the sample vials were always counted immediately after the sample protocol was completed. Occasionally, this resulted in high uncertainties for the data reported by QuantaSmart. For these samples, we analyzed the alpha spectrum using Peakfit and found that the count rates were often different; and the difference between the count rate reported by QuantaSmart and Peakfit was related to the uncertainties (Figure E6). Thus, we added the 5 minute cool down period prior to counting. This additional time can result in daughter ingrowth, and thus higher count rates than radium alone [58]. Although the total activity can be corrected based on the elapsed time since sample preparation (Table E6), studies have shown that the efficiencies for other nuclides may not be the same as for ^{226}Ra [38], which is an assumption of this correction. Our sample counting time of 60 minutes was shorter than for other reported methods. We found that the level of uncertainty after 60 minutes was comparable to when the counting time was 5 times longer (Figure E7).

In our analysis herein, we utilized the full LSC spectra from 0 keV to 2000 keV. If the sample is old (>10 − 15 years since production), the ingrowth of the later daughter products could lead to interference in the ^{226}Ra alpha spectra from ^{210}Po (Figure E8). If this is the case, the analyst would need to consider an endpoint that does not include the ^{210}Po spectra, thereby making the analysis more difficult as this endpoint could change depending on the solution chemistry.

Our analysis of produced waters has been focused on ^{226}Ra, however, produced water samples contain ^{228}Ra. Radium-228 decays to other nuclides whose alpha decay spectra could overlap with ^{226}Ra. Such interference would greatly undermine the validity of this method when appraising ^{226}Ra activities of produced waters whose ^{228}Ra/^{226}Ra ratios are close to 1, such as with conventional produced waters. Further study is ongoing on a method to simultaneously determine ^{226}Ra and ^{228}Ra, even at ^{228}Ra/^{226}Ra ratios close to 1.

6.4.7 Implications on ^{226}Ra Measurements of High-TDS Produced Waters

The goal of this study was to propose a new method for appraising ^{226}Ra in produced waters by a rapid method with a simple sample preparation protocol − one that does not use hazardous chemicals − requires little analytical skill, utilizes low sample volumes, yields high radium recoveries, and is robust to the high-TDS concentrations and ionic strength of the produced waters. This method employed a simple sample preparation protocol of evaporative drying, utilized ~4 mL of sample. The method was validated by gamma spectroscopy and yielded high radium recoveries > 90% and R^2 values of > 0.9 when compared to gamma spectroscopy.

As alternative uses of produced waters are being researched and developed, our proposed method could allow for rapid and relatively dependable ^{226}Ra analysis of the produced waters at low costs. This time and cost savings from this could afford entrepreneurs, facility managers, and researchers to more efficiently evaluate the efficacy of their treatments.

6.5 Acknowledgments

This research was funded by a National Science Foundation PFI: AIR-TT #1640634. Further support originated from a Penn State College of Engineering Graduate Excellence Fellowship. The authors would like to thank Prof. Tom O' Haver for providing the MATLAB package for the multi-Gaussian analyses.

6.6 References

(1) Maloney, K. O.; Yoxtheimer, D. A. Production and Disposal of Waste Materials from Gas and Oil Extraction from the Marcellus Shale Play in Pennsylvania. *Environ. Pract.* 2012, *14* (December), 278–287. https://doi.org/10.1017/S146604661200035X.

(2) Veil, J. *U.S. Produced Water Volumes and Management Practices in 2012*; 2015.

(3) Rowan, E. L.; Engle, M. a.; Kirby, C. S.; Kraemer, T. F. Radium Content of Oil- and Gas-Field Produced Waters in the Northern Appalachian Basin (USA): Summary and Discussion of Data. *USGS Sci. Investig. Rep.* 2011, 38 pp.

(4) Jonkers, G.; Hartog, F. A.; Knaepen, W. A. I.; Lancee, P. F. J. Characterisation of NORM in the Oil and Gas Production (E&P) Industry. *Proceedings of the International Symposium on Radiological Problems with Natural Radioactivity in the Non-nuclear Industry, Amsterdam*. 1997.

(5) He, C.; Zhang, T.; Zheng, X.; Li, Y.; Vidic, R. D. Management of Marcellus

Shale Produced Water in Pennsylvania: A Review of Current Strategies and Perspectives. *Energy Technol.* 2014, *2* (12), 968–976. https://doi.org/10.1002/ente.201402060.

(6) Rowan, E. L.; Engle, M. A.; Kraemer, T. F.; Schroeder, K. T.; Hammack, R. W.; Doughten, M. W. Geochemical and Isotopic Evolution of Water Produced from Middle Devonian Marcellus Shale Gas Wells, Appalachian Basin, Pennsylvania. *Am. Assoc. Pet. Geol. Bull.* 2015, *99* (2), 181–206. https://doi.org/10.1306/07071413146.

(7) International Atomic Energy Agency (IAEA). *The Environmental Behaviour of Radium: Revised Edition. Technical Report Series No. 476*; Vienna, 2014.

(8) Hayes, T. *Sampling and Analysis of Water Streams Associated with the Development of Marcellus Shale Gas*; Des Plaines, 2009.

(9) Haluszczak, L. O.; Rose, A. W.; Kump, L. R. Geochemical Evaluation of Flowback Brine from Marcellus Gas Wells in Pennsylvania, USA. *Appl. Geochemistry* 2013, *28*, 55–61. https://doi.org/10.1016/j.apgeochem.2012.10.002.

(10) Stewart, B. W.; Chapman, E. C.; Capo, R. C.; Johnson, J. D.; Graney, J. R.; Kirby, C. S.; Schroeder, K. T. Origin of Brines, Salts and Carbonate from Shales of the Marcellus Formation: Evidence from Geochemical and Sr Isotope Study of Sequentially Extracted Fluids. *Appl. Geochemistry* 2015, *60*, 78–88. https://doi.org/10.1016/j.apgeochem.2015.01.004.

(11) Shih, J.-S.; Saiers, J. E.; Anisfeld, S. C.; Chu, Z.; Muehlenbachs, L. A.; Olmstead, S. M. Characterization and Analysis of Liquid Waste from Marcellus Shale Gas Development. *Environ. Sci. Technol.* 2015, *49* (16), 9557–9565. https://doi.org/10.1021/acs.est.5b01780.

(12) Estrada, J. M.; Bhamidimarri, R. A Review of the Issues and Treatment Options for Wastewater from Shale Gas Extraction by Hydraulic Fracturing. *Fuel* 2016, *182*, 292–303. https://doi.org/10.1016/j.fuel.2016.05.051.

(13) Gregory, K. B.; Vidic, R. D.; Dzombak, D. A. Water Management Challenges Associated with the Production of Shale Gas by Hydraulic Fracturing.

Elements 2011, *7* (3), 181–186. https://doi.org/10.2113/gselements.7.3.181.

(14) Warner, N. R.; Christie, C. A.; Jackson, R. B.; Vengosh, A. Impacts of Shale Gas Wastewater Disposal on Water Quality in Western Pennsylvania. *Environ. Sci. Technol.* 2013, *47*, 11849–11857. https://doi.org/10.1021/es402165b.

(15) Burgos, W. D.; Castillo-Meza, L.; Tasker, T. L.; Geeza, T. J.; Drohan, P. J.; Liu, X.; Landis, J. D.; Blotevogel, J.; McLaughlin, M.; Borch, T.; et al. Watershed-Scale Impacts from Surface Water Disposal of Oil and Gas Wastewater in Western Pennsylvania. *Environ. Sci. Technol.* 2017, *51* (15), 8851–8860. https://doi.org/10.1021/acs.est.7b01696.

(16) Konkel, L. Salting the Earth: The Environmental Impact of Oil and Gas Wastewater Spills. *Environ. Health Perspect.* 2016, *124* (12), A230–A235. https://doi.org/10.1289/ehp.124-A230.

(17) Van Sice, K.; Cravotta, C. A.; McDevitt, B.; Tasker, T. L.; Landis, J. D.; Puhr, J.; Warner, N. R. Radium Attenuation and Mobilization in Stream Sediments Following Oil and Gas Wastewater Disposal in Western Pennsylvania. *Appl. Geochemistry* 2018, *98*, 393–403. https://doi.org/10.1016/j.apgeochem.2018.10.011.

(18) Lutz, B. D.; Lewis, A. N.; Doyle, M. W. Generation, Transport, and Disposal of Wastewater Associated with Marcellus Shale Gas Development. *Water Resour. Res.* 2013, *49* (October 2012), 647–656. https://doi.org/10.1002/wrcr.20096.

(19) Paukert Vankeuren, A. N.; Hakala, J. A.; Jarvis, K.; Moore, J. E. Mineral Reactions in Shale Gas Reservoirs: Barite Scale Formation from Reusing Produced Water As Hydraulic Fracturing Fluid. *Environ. Sci. Technol.* 2017, *51* (16), 9391–9402. https://doi.org/10.1021/acs.est.7b01979.

(20) He, C.; Zhang, T.; Vidic, R. D. Use of Abandoned Mine Drainage for the Development of Unconventional Gas Resources. *Disruptive Sci. Technol.* 2013, *1* (4), 169–176. https://doi.org/10.1089/dst.2013.0014.

(21) U.S. Environmental Protection Agency. *Detailed Study of the Centralized*

Waste Treatment Point Source Category for Facilities Managing Oil and Gas Extraction Wastes; Washington, D.C., 2018.

(22) U.S. Environmental Protection Agency. *Study of Oil and Gas Extraction Wastewater Management Under the Clean Water Act EPA-821-R19-001*; Washington, D.C., 2019.

(23) Rassenfoss, S. Shale Water: Turning Dirty Produced Water Into Fresh Water and Salt To Sell. *J. Pet. Technol.* 2017, *69* (11), 24–31. https://doi.org/10.2118/1117-0024-JPT.

(24) Dorich, A. Eureka Resources Recovers Vital Resources from Flowback and Production Wastewater. *Energy & Mining International*. 2017.

(25) MDN. Eureka to Extract Lithium from Marcellus/Utica Wastewater. *Marcellus Drilling News*. 2019.

(26) Flexer, V.; Fernando Baspineiro, C.; Galli, C. I. Lithium Recovery from Brines: A Vital Raw Material for Green Energies with a Potential Environmental Impact in Its Mining and Processing. *Sci. Total Environ.* 2018, *639*, 1188–1204. https://doi.org/10.1016/j.scitotenv.2018.05.223.

(27) Schaller, J.; Headley, T.; Prigent, S.; Breuer, R. Potential Mining of Lithium, Beryllium and Strontium from Oilfield Wastewater after Enrichment in Constructed Wetlands and Ponds. 2014. https://doi.org/10.1016/j.scitotenv.2014.06.097.

(28) Jang, Y.; Chung, E. Adsorption of Lithium from Shale Gas Produced Water Using Titanium Based Adsorbent. *Ind. Eng. Chem. Res.* 2018, *57* (25), 8381–8387. https://doi.org/10.1021/acs.iecr.8b00805.

(29) Paranthaman, M. P.; Li, L.; Luo, J.; Hoke, T.; Ucar, H.; Moyer, B. A.; Harrison, S. Recovery of Lithium from Geothermal Brine with Lithium–Aluminum Layered Double Hydroxide Chloride Sorbents. *Environ. Sci. Technol.* 2017, *51* (22), 13481–13486. https://doi.org/10.1021/acs.est.7b03464.

(30) United States Environmental Protection Agency. *Method 903.0: Alpha-Emitting Radium Isotopes in Drinking Water*; 1980.

(31) United States Environmental Protection Agency. *Method 903.1: Radium-226 in Drinking Water Radon Emanation Technique*.

(32) United States Environmental Protection Agency. *Method 901.1: Gamma Emitting Radionuclides in Drinking Water*.

(33) Zhang, T.; Bain, D.; Hammack, R.; Vidic, R. D. Analysis of Radium-226 in High Salinity Wastewater from Unconventional Gas Extraction by Inductively Coupled Plasma-Mass Spectrometry. *Environ. Sci. Technol.* 2015, *49* (5), 2969– 2976. https://doi.org/10.1021/es504656q.

(34) Nelson, A. W.; May, D.; Knight, A. W.; Eitrheim, E. S.; Mehrhoff, M.; Shannon, R.; Litman, R.; Schultz, M. K. Matrix Complications in the Determination of Radium Levels in Hydraulic Fracturing Flowback Water from Marcellus Shale. *Environ. Sci. Technol. Lett.* 2014, *1* (3), 204– 208. https://doi.org/10.1021/ez5000379.

(35) Tasker, T. L.; Burgos, W. D.; Ajemigbitse, M. A.; Lauer, N. E.; Gusa, A. V.; Kuatbek, M.; May, D.; Landis, J. D.; Alessi, D. S.; Johnsen, A. M.; et al. Accuracy of Methods for Reporting Inorganic Element Concentrations and Radioactivity in Oil and Gas Wastewaters from the Appalachian Basin, U.S. Based on an Inter-Laboratory Comparison. *Environ. Sci. Process. Impacts* 2019, *21* (2), 224– 241. https://doi.org/10.1039/c8em00359a.

(36) Maxwell, S. L.; Culligan, B. K.; Warren, R. A.; McAlister, D. R. Rapid Method for the Determination of 226Ra in Hydraulic Fracturing Wastewater Samples. *J. Radioanal. Nucl. Chem.* 2016, *309* (3), 1– 8. https://doi.org/10.1007/s10967-016-4745-1.

(37) Hou, X.; Roos, P. Critical Comparison of Radiometric and Mass Spectrometric Methods for the Determination of Radionuclides in Environmental, Biological and Nuclear Waste Samples. *Anal. Chim. Acta* 2008, *608* (2), 105– 139. https://doi.org/10.1016/j.aca.2007.12.012.

(38) Salonen, L. A Rapid Method for Monitoring of Uranium and Radium in Drinking Water. *Sci. Total Environ.* 1993, *130– 131* (C), 23– 35. https://doi.org/10.1016/0048-9697(93)90056-C.

(39) Salonen, L.; Hukkanen, H. Advantages of Low-Background Liquid Scintillation Alpha-Spectrometry and Pulse Shape Analysis in Measuring 222Rn, Uranium and 226 Ra in Groundwater Samples. *J. Radioanal. Nucl. Chem.* 1997, *226*, 67–74.

(40) Salonen, L.; Kaihola, L.; Carter, B.; Cook, G. T.; Passo, C. J. *Environmental Liquid Scintillation Analysis*, Third Edit.; Elsevier, 2013. https://doi.org/10.1016/B978-0-12-384873-4.00009-8.

(41) McKlveen, J. W.; Johnson, W. R. Simultaneous Alpha and Beta Particle Assay Using Liquid Scintillation-Counting with Pulse-Shape Discrimination. *Heal. Phys.* 1975, *28* (1), 5–11.

(42) Chu, L.-C.; Khalique, A. Determination of Radium-226 in Water by Liquid Scintillation Counting. *Trans. Am. Nucl. Soc.* 1990, *61*, 1–5.

(43) Aleissa, K. A.; Almasoud, F. I.; Islam, M. S.; L' Annunziata, M. F. Radium-228 Analysis of Natural Waters by Cherenkov Counting of Actinium-228. *Appl. Radiat. Isot.* 2008, *66* (12), 1954–1963. https://doi.org/10.1016/j.apradiso.2008.05.012.

(44) Cook, M.; Kleinschmidt, R. Simultaneous Determination of 226 Ra and 228 Ra in Water by Liquid Scintillation Spectrometry. 2011, 880–884.

(45) Stamoulis, K. C.; Ioannides, K. G.; Karamanis, D. Deconvolution of Liquid Scintillation Alpha Spectra of Mixtures of Uranium and Radium Isotopes. *Anal. Chim. Acta* 2010, *657* (2), 108–115. https://doi.org/10.1016/j.aca.2009.10.034.

(46) L' Annunziata, M. F.; Kessler, M. J. *Liquid Scintillation Analysis: Principles and Practice*, Third Edit.; Elsevier, 2013. https://doi.org/10.1016/B978-0-12-384873-4.00007-4.

(47) Cavazza, M. Reducing Freshwater Consumption in the Marcellus Shale Play by Recycling Flowback with Abandoned Mine Drainage, The Pennsylvania State University, 2016.

(48) Tasker, T. L.; Burgos, W. D.; Piotrowski, P.; Castillo-Meza, L.; Blewett, T. A.; Ganow, K. B.; Stallworth, A.; Delompré , P. L. M.; Goss, G. G.; Fowler,

L. B.; et al. Environmental and Human Health Impacts of Spreading Oil and Gas Wastewater on Roads. *Environ. Sci. Technol.* 2018, *52* (12), 7081–7091. https://doi.org/10.1021/acs.est.8b00716.

(49) Ajemigbitse, M. A.; Cheng, Y.; Cannon, F. S.; Warner, N. R. Self-Attenuation Corrections for Radium Measurements of Oil and Gas Solids by Gamma Spectroscopy. *Environ. Sci. Technol. Lett.* 2019, Submitted.

(50) Ajemigbitse, M. A.; Tasker, T. L.; Cannon, F. S.; Warner, N. R. Influence of High Total Dissolved Solids Concentration and Ionic Composition on Gamma Spectroscopy Radium Measurements of Oil and Gas Produced Water. *Environ. Sci. Technol.* 2019, Submitted.

(51) Edler, R.; Passo, C. *Basics of α/β-Discriminaton for Liquid Scintillation Counting*; Waltham, 2010.

(52) Fons, J.; Zapata-Garcí a, D.; Tent, J.; Llauradó, M. Simultaneous Determination of Gross Alpha, Gross Beta and 226 Ra in Natural Water by Liquid Scintillation Counting. *J. Environ. Radioact.* 2013, *125*, 56–60. https://doi.org/10.1016/j.jenvrad.2013.01.017.

(53) Abdellah, W. M. Optimization Method to Determine Gross Alpha-Beta in Water Samples Using Liquid Scintillation Counter. *J. Water Resour. Prot.* 2013, No. 5, 900–905. https://doi.org/10.4236/jwarp.2013.59092.

(54) Dias, F. F.; Helena Taddei, M. T.; May Braga Dulley Pontedeiro, E.; Feliciano Jacomino, V. *Total Alpha and Beta Determination by Liquid Scintillation Counting in Water Samples from a Brazilian Intercomparison Exercise*; 2009.

(55) Rusconi, R.; Azzellino, A.; Bellinzona, S.; Forte, M.; Gallini, R.; Sgorbati, G. Assessment of Drinking Water Radioactivity Content by Liquid Scintillation Counting: Set up of High Sensitivity and Emergency Procedures. *Anal. Bioanal. Chem.* 2004, *379* (2), 247–253. https://doi.org/10.1007/s00216-004-2580-7.

(56) Thomson, J. *Sample Preparation Techniques for Liquid Scintillation Analysis*, Third Edit.; Elsevier, 2013. https://doi.org/10.1016/B978-0-12-

384873-4.00008-6.

(57) Strom, D. J.; Stansbury, P. S. Minimum Detectable Activity When Background Is Counted Longer than the Sample. *Health Phys.* 1992, *63* (3), 360–361.

(58) Nelson, A. W.; Eitrheim, E. S.; Knight, A. W.; May, D.; Mehrhoff, M. A.; Shannon, R.; Litman, R.; Burnett, W. C.; Forbes, T. Z.; Schultz, M. K. Understanding the Radioactive Ingrowth and Decay of Naturally Occurring Radioactive Materials in the Environment: An Analysis of Produced Fluids from the Marcellus Shale. *Environ. Health Perspect.* 2015, *123* (7), 689–696. https://doi.org/10.1289/ehp.1408855.

Chapter 7

Conclusions and Recommendations

7.1 Summary

Presented in two parts, this dissertation has presented research aimed at addressing the occurrence of radium in hydraulic fracturing co-products by developing novel treatment and measurement techniques for the co-products, to aid in remediation and the development of new technology for the alternate use of the co-products, while providing rapid and accurate measurements of radium in these co-products.

In Part I of this dissertation, I addressed the opportunity for new treatment technologies that are sustainable in nature. In chapter 2, the recovery of raw materials from otherwise wasted solids was evaluated, and the distribution of radium in the solids was monitored. This work presented evidence there is an opportunity to economically recover reusable proppant sand from the solid co-products that would otherwise be disposed in a landfill. The radium content of the proppant sand is low enough that it would not present considerable concern to the health of workers and consumers. As a result of the treatment, radium was less mobile from the solids, rendering the solids better suited for landfilling. Chapter 3 described research, of an exploratory nature, on the removal of radium from produced water using a synthetic clay, Na-4-mica, that has high affinity for radium. I probed the fundamental nature of radium removal by Na-4-mica and investigated the mechanisms – pH, salinity, and competing ions – that could have an effect on radium removal. Then, I tested radium removal from real produced waters. This work provided key insights into potential radium-specific treatment of the produced waters that could help reduce the volume of radioactive sludge that is produced with the current methods, while allowing for a radioactivity free beneficial reuse of the produced water. While the results showed that Na-4-mica on its own, could not

sufficiently remove radium, it provided key insights into further adjustments that could render it more useful.

The focus of Part II was on developing and describing new considerations for quantifying the radioactivity in the co-products. Specifically, I focused on considerations dependent on the nature of the co-products. For the produced water, discussed in Chapter 5, it was the high concentrations and composition of total dissolved solids; while for the solids of Chapter 4, it was the mineral composition, expressed as the density, of the solids and the volume/mass available for analysis. In both cases, I developed empirical methods to account for the attenuation of gamma rays that occur as a result of these considerations. I showed that, for the liquids, when the consideration of high-total dissolved solids (TDS) is not accounted, radium measurements could be under-reported, by as much as 40%; and for the solid samples, the differences in sample volume/mass and density could affect radium measurement significantly. Finally, Chapter 6 describes a novel rapid method to quantify radium in these high-TDS produced waters using liquid scintillation. This new method would allow for accurate radium measurements at the fraction of the cost of other reliable methods, such as gamma spectroscopy, positioning this new techniques as a more suitable for operators who handle and manage these produced waters.

7.2 Implications and Recommendations

One can argue that the environmentally sustainable energy production is the great challenge of the century. The extensive release of greenhouse gases now threatens our climate, and in response, we are moving away from the carbon-rich fossil fuels to the greener energy sources of solar, wind and in some cases, nuclear power.

However, as the technology for wide-scale application of these greener energy sources is still in development, a bridge-fuel is necessary. Natural gas is positioned to be this bridge-fuel. In 2017 natural gas accounted for 31.8 % of US energy production compared to 19 % a decade earlier (U.S. Energy Information Administration). Economic and expansive natural gas production was made possible by advancements in drilling and completion technology, in the form of directional drilling and hydraulic fracturing. While hydraulic fracturing benefited us with the vast increase in natural gas production, it also challenged us with the handling and management of its co-products.

In moving towards a sustainable future, recycling and reuse of raw materials become more salient than ever. I showed in Chapter 2 that hydroacoustic cavitation presents an opportunity to recover raw materials from solid co-products. Proppant sand continues to be an important commodity in natural gas extraction by hydraulic fracturing, so its recycle and reuse become more necessary. I also show that fine clays can be recovered from this material, however, there is yet to be seen a beneficial reuse of the clays. This work also presented opportunities for radium management by redistributing the radium towards the fine particle portion of the solids. *Together, I provide evidence for the closer consideration of the handling and management of these co-products, mainly to the effect of their relabeling from waste solids to co-products.*

Additionally, the produced waters present a feed stock for several industries. Already, measures are being taken for the beneficial reuse of the produced waters, necessitated by their large volume as well as limited disposal options. One major barrier to adapting the produced waters is the presence of radioactivity, in the form of radium and the daughter products of its decay. Current treatment options generate radioactive sludge that is disposed of as waste, even this waste contains

value, in the form of barite. A treatment that selectively removes radium from solution while allowing for the recovery of other commercially relevant metals is important. This work, while exploratory in nature, is a step towards that reality.

Finally, this work ends by studying the current measurement techniques for radium and suggests ways to improve them. I show that considerations for the nature of these co-products is important, without them, radium measurements are erroneous, which can cause problems when designing and appraising management practices and treatment technologies, especially in light of reuse and resource recovery, whose value are dependent on radium content. I also develop a new method to rapidly assess the radium concentrations of the produced waters, even given their high solids content. This method is crucial to operators who are not privy to sophisticated equipment, nor have the resources to fully benefit from them. Bringing forth such a method to the field level could prove to be a powerful tool in the landscape of the management of the produced water.

7.3 Original Contributions to Science

The research presented in this dissertation provides several original contributions to science summarized below:

- This work is among the first to attempt raw material recovery from residual solid wastes originating from oil and gas development. As such, it is the first to perform a comprehensively evaluate a system, such as hydroacoustic cavitation, for proppant sand recovery.
- Herein, I present a novel management practice for radioacitivity in the residual solids, i.e. by concentrating radium in the finest particle sizes follow-

ing treatment by hydroacoustic cavitation. Herein, the effect of such treatment on the distribution of radium and its potential to leach from the treated solids in a landfill environment are novel.

- This work presents the first characterization of Na-4-mica by quantitative X-ray Diffraction and the determination of the Relative Intensity Ratios (RIR) for the hydrated and anhydrous phases of Na-4-mica. Furthermore, the application of Na-4-mica for radium removal in fluids with high total dissolved solids concentration, such as oil and gas produced water, has not been previously attempted.
- Mass dependent self-attenuation corrections for gamma measurements of solids has been presented previously, however, I present a novel and rapid empirical method that is specific to the solids encountered in oil and gas development.
- I present a novel technique to correct for the interference of ^{235}U at the 186 keV energy level when peforming direct radium measurements.
- Likewise, the mass dependent self-attenuation corrections for gamma measurements of liquids has been previously reported, however, I present a novel and rapid empirical method that is specific to liquids with high total dissolved solids, such as oil and gas produced waters, and show that the use of NaCl as a calibration standard is insufficient for accurate radium measurements. Instead, calibration standard should contain Na, Ca, Mg, Sr, and Ba.
- The development of a rapid liquid scintillation counting method that produces high radium recoveries and comparable results is novel. The effect of total dissolved solids concentration on the liquid scintillation spectra is discussed for the first time in this work.

7.4 Future Work

The material recovery from the solids was focused on raw materials, such as sand and clay. Other potentially useful constituents were not investigated, such as precious metals. Additionally, the application of the novel treatment while performed at pilot scale, was performed in a lab environment. The proposed treatment would need to be appraised at the field scale where its application can be assessed under less than ideal conditions, and with field samples and raw waters.

These co-products are known to possess some organic content, yet a quantitative analysis of the organic compounds is lacking in this work.

The application of Na-4-mica for radium removal was only exploratory, and thus presents many opportunities for future work. The effectiveness of a pre-treatment, the experimental appraisal of the effect of organic compounds, the effect of sonication and cavitation on the adsorption kinetics, are all areas of possible improvement.

Expanding the application of the measurement techniques to more scenarios of produced water and more diversity of samples would afford the opportunity to assess, to a greater degree, the usefulness of these techniques. Appraising the influence of TDS and density with other types of measurement techniques and instruments would allow me to conclude if the effects observed are global and not local.

Appendix A

Supporting Information for Chapter 2

A.1 Supporting Figures and Tables

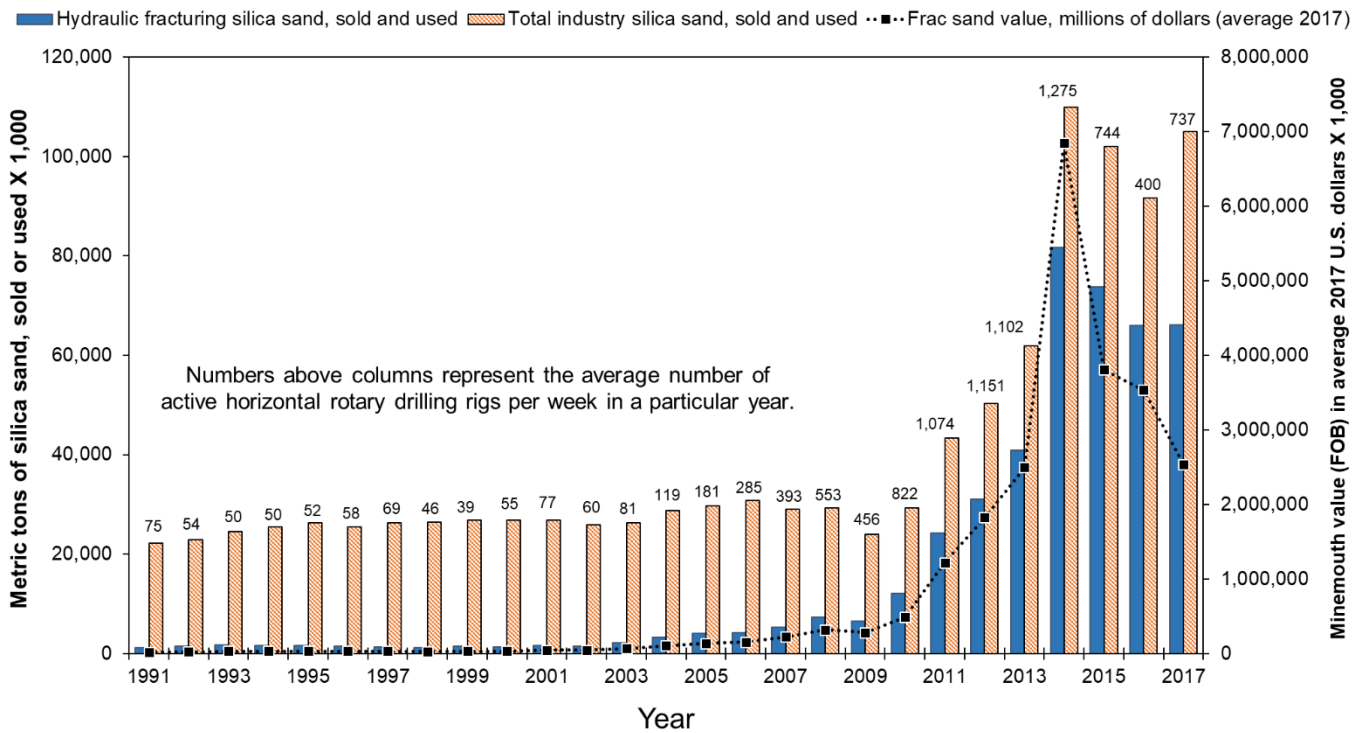

Figure A1: Average weekly US horizontal drill rig count per year, silica sand sales (total industry and hydraulic fracturing), and free on board (FOB) mine values. Dollar values were adjusted to average 2017 U.S. dollars using the U.S. Department of Labor' s U.S. Bureau of Labor Statistics Consumer Price Index. Data from U.S.G.S 1991-2017 [1]; Baker Hughes Inc. [2], after [3].

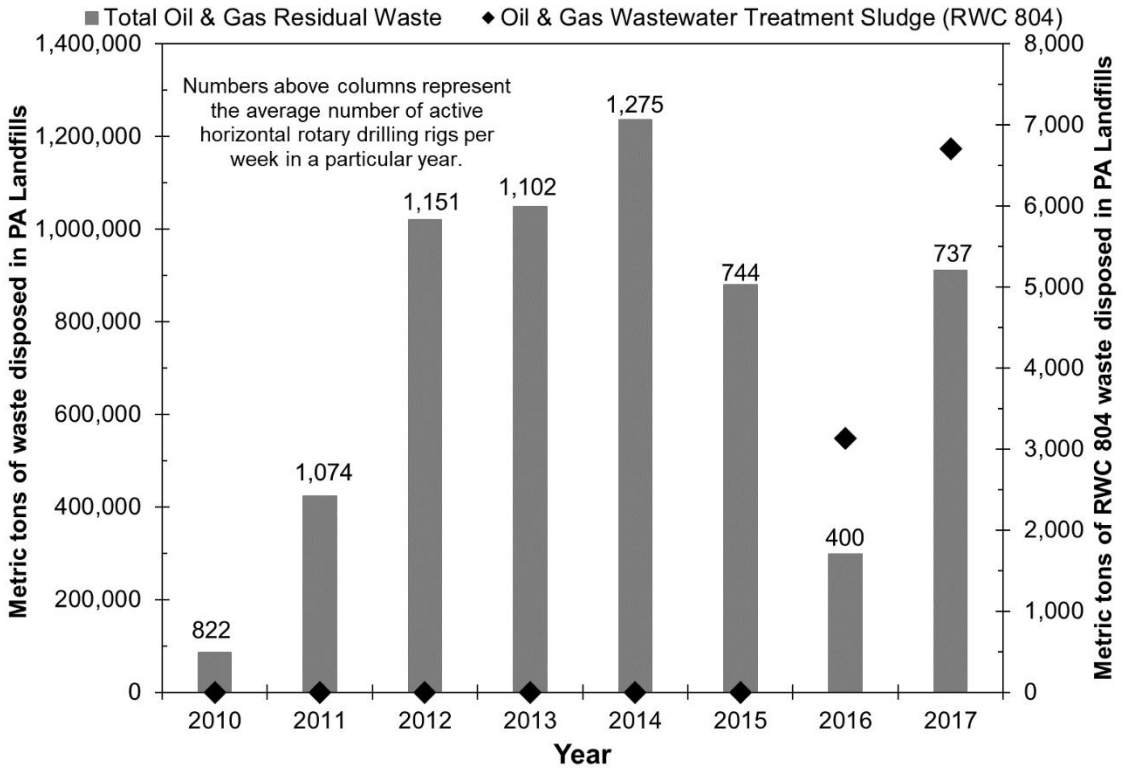

Figure A2: Average weekly horizontal drill rig count per year, total Oil & Gas residual landfill waste, and wastewater treatment sludge disposed in Pennsylvania landfills. Prior to 2015, there were no waste volumes classified as " oil & gas wastewater treatment sludge" in the PA DEP database. Data from PA DEP Oil and Gas Reporting Website [4]. Rig count from Baker Hughes Inc. [2].

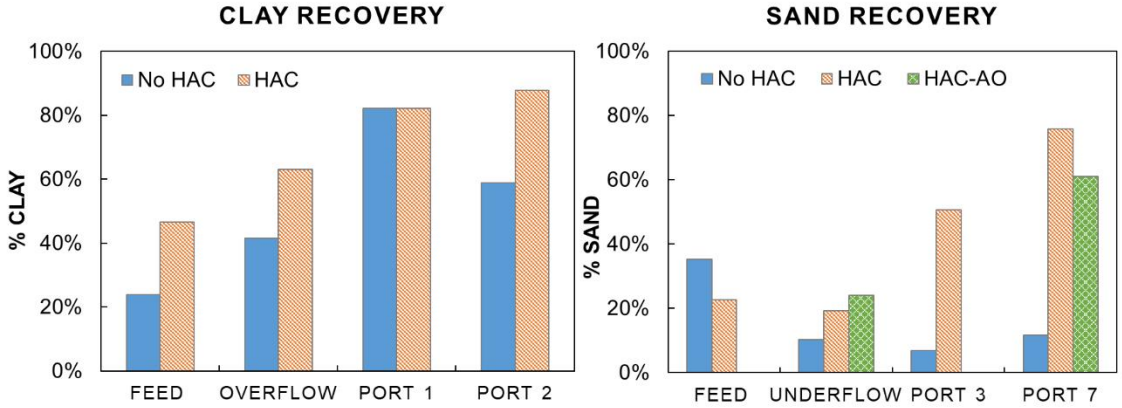

Figure A3: Percent clay and sand at select sampling points for control (No HAC) and treatment (HAC or HAC-AO). The percentage represents how much of the material sampled at each point was clay (<63 μm i.e. #230 mesh), or sand (>210 μm i.e. #70 mesh) relative to the total mass sampled at that point using US mesh sieves per ASTM D6913-04. The combination of HAC treatment and the physical separation devices greatly improved the separation of raw materials.

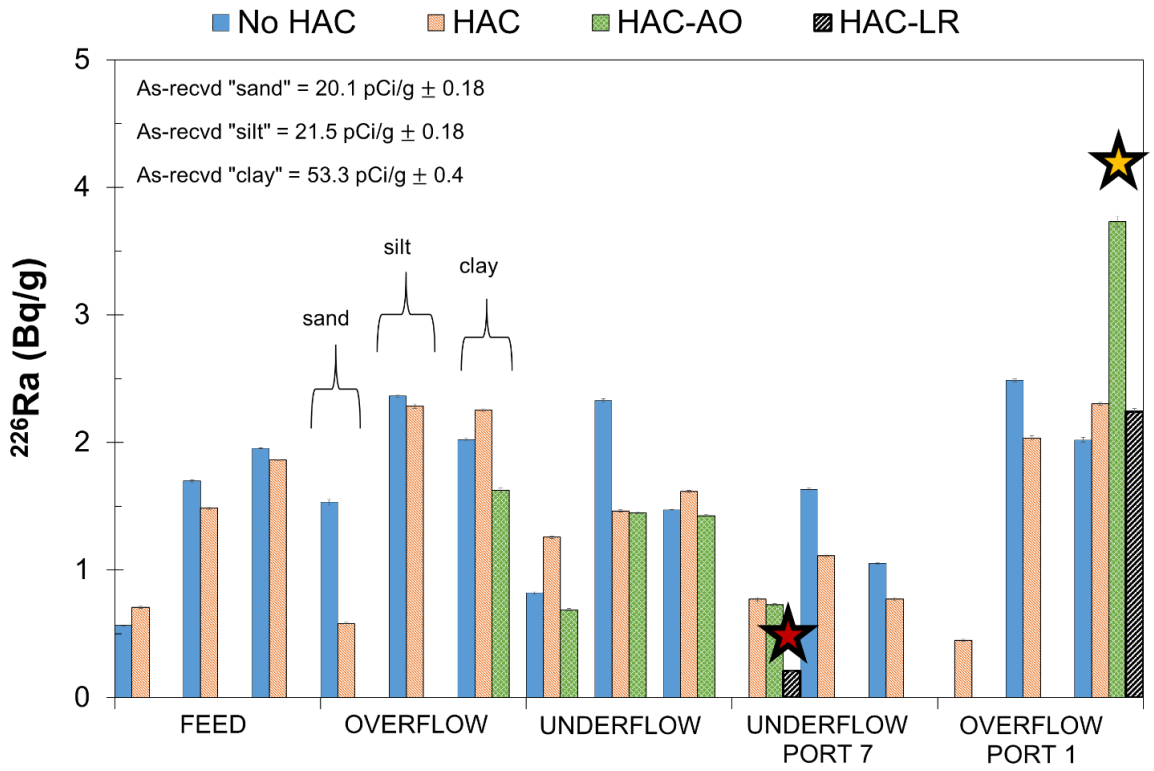

Figure A4: Radium-226 activity on the separated particle sizes showed that treatment led to concentration of radium in the fines while reducing radium on sand grains when treating the dewatered residual waste solids at 5% slurry with municipal tap water. Control run - No HAC. Treatment – HAC; HAC-AO, i.e. HAC with advanced oxidation provided by H_2O_2 and O_3; and HAC-LR, i.e. HAC treatment for an extended period of time (30 minutes cavitation exposure). HAC-LR resulted in reclaimed sand with ^{226}Ra activity of 0.207 Bq/g (5.6 pCi/g) (★), while HAC-AO resulted in reclaimed clay with ^{226}Ra activity of 0.207 Bq/g (100 pCi/g) (★). Size classification using US mesh sieves per ASTM D6913-04: <63 μm is clay (#230 mesh), >210 μm is sand (#70 mesh), and in-between is silt.

Table A1: Sample weights, extraction fluid volume, ^{226}Ra activities and elemental composition of major metals in the extractants for the size-classified solids prior to and following the TCLP extraction.

	SAMPLE NAME	WEIGHT OF SAMPLE (g)	VOLUME OF EXTRACTION FLUID	WEIGHT OF DRIED RESIDUE (g)	Sample mass post extraction	Mass lost (g)	Average 226 Ra before TCLP (Bq/g)	Error (Bq/g)	Average 226 Ra after TCLP (Bq/g)	Error (Bq/g)	Mg (ug/mL)	Ca (ug/mL)	Sr (ug/mL)	Ba (ug/mL)	Na (ug/mL)	K (ug/mL)	Al (ug/mL)	Fe (ug/mL)	Li (ug/mL)	Mn (ug/mL)
	As Recvd (aggregated)	11.61	233	86.9368	10.24	1.37	1.07	0.01	0.96	0.01	106	1,042	183	500	1,037	18.9	0.32	13.8	4.16	27.1
Sand	As Recvd	5.89	119.1	81.69	5.25	0.64	0.74	0.01	1.01	0.01	73.3	676	35.5	81.5	39.3	3.75	0.31	7.05	0.18	16.5
	No HAC Feed	8.933	180.6	84.71	8.37	0.56	0.57	0.01	0.77	0.01	52.7	1,111	8.35	1.09	17.4	2.16	¡0.005	¡0.02	0.02	0.20
	HAC Feed	8.928	180.5	85.17	8.27	0.66	0.71	0.01	0.76	0.01	76.3	1,067	16.3	2.12	36.7	2.17	0.06	¡0.02	0.03	0.15
	No HAC under	5.564	113	81.32	4.47	1.09	0.82	0.01	0.91	0.01	284	1,985	23.9	6.22	180	12.5	¡0.005	0.52	0.25	2.51
	HAC under	8	162	82.98	6.47	1.53	1.26	0.01	1.37	0.01	161	2,319	15.1	2.22	110	5.59	¡0.005	¡0.02	0.23	0.58
	HAC-AO under	8.2651	167	83.81	7.12	1.15	0.69	0.01	0.74	0.01	133	2,099	17.0	1.89	60.7	4.63	¡0.005	0.28	0.44	2.82
	No HAC over	2.1	42	78.41	1.75	0.35	1.53	0.02	1.66	0.02	290	2,087	47.8	3.31	253	7.90	¡0.005	¡0.02	0.78	0.98
	HAC over	0.7	14.2	76.93	0.58	0.12	0.58	0.01	0.62	0.02	386	1,883	52.9	9.37	599	38.1	¡0.005	0.04	0.58	1.67
Silt	As Recvd	8.98	181.6	85.05	8.08	0.90	0.79	0.01	0.68	0.01	62.3	518	24.9	53.0	41.2	3.33	1.37	17.0	0.19	10.8
	No HAC Feed	8.303	167.9	83.94	7.52	0.78	1.70	0.01	2.06	0.01	50.2	1,385	10.9	0.87	70.4	3.27	¡0.005	¡0.02	0.36	¡0.005
	HAC Feed	7.7	155.7	83.39	6.8	0.90	1.49	0.01	1.68	0.02	73.1	1,206	6.88	0.92	64.2	3.50	¡0.005	¡0.02	0.20	¡0.005
	No HAC under	8.973	182	83.38	7.68	1.29	2.33	0.01	2.87	0.04	219	2,240	30.0	2.08	269	7.63	¡0.005	¡0.02	0.88	0.22
	HAC underflow	8.02	162	83.51	6.67	1.35	1.46	0.01	1.64	0.02	165	2,191	11.3	1.26	106	5.28	¡0.005	¡0.02	0.12	0.35
	HAC-AO under	8.44	171	84.48	7.51	0.93	1.45	0.01	1.63	0.02	66.5	1,323	20.1	0.85	312	6.53	¡0.005	¡0.02	0.78	¡0.005
	No HAC over	8.35	169	82.98	7.17	1.18	2.37	0.01	2.89	0.03	201	2,190	29.0	2.06	223	7.00	¡0.005	¡0.02	0.85	0.19
	HAC overflow	7.67	155	83.13	6.59	1.08	2.29	0.02	2.69	0.03	381	1,833	19.3	1.18	151	6.53	¡0.005	¡0.02	0.57	0.62
Clay	As Recvd	9.0899	183.8	82.83	6.3	2.79	1.97	0.01	1.44	0.01	243	1,434	328	739	2,127	40.6	1.09	10.8	7.03	16.6
	No HAC Feed	6.38	129	81.65	5.23	1.15	1.95	0.00	2.69	0.02	29.7	1,989	125	2.63	1,517	35.7	¡0.005	¡0.02	9.13	¡0.005
	HAC Feed	6.7	135	81.29	4.74	1.96	1.86	0.00	2.40	0.02	59.5	1,662	66.5	1.41	963	23.2	¡0.005	¡0.02	0.81	¡0.005
	No HAC under	8.13	164	82.93	6.45	1.68	1.47	0.00	1.98	0.02	240	2,390	64.5	3.68	639	18.3	¡0.005	¡0.02	3.43	0.20
	HAC underflow	8.01	162	83.09	6.65	1.36	1.62	0.01	1.92	0.01	383	2,059	25.7	1.51	347	15.5	¡0.005	¡0.02	1.28	0.37
	HAC-AO under	8	162	83.49	7.12	0.88	1.42	0.01	1.65	0.02	81.5	1,411	22.6	1.01	163	7.40	¡0.005	¡0.02	1.06	¡0.005
	No HAC over	7.55	153	81.72	5.09	2.46	2.02	0.01	3.08	0.03	198	2,985	177	13.4	2,154	48.5	¡0.005	¡0.02	13.5	0.17
	HAC overflow	8.02	162	82.54	6.19	1.83	2.25	0.01	2.86	0.02	387	2,359	92.0	4.23	1,031	26.2	¡0.005	¡0.02	6.66	0.54
	HAC-AO over	5.728	164	80.27	3.76	1.97	1.63	0.02	2.48	0.03	275	2,596	76.7	2.06	535	24.9	¡0.005	¡0.02	4.62	1.12

A.2 Error Propagation for Reporting Error of Measured ^{226}Ra Activities

Radium-226 activities of all solid samples were determined by gamma spectroscopy on a Canberra ultra-low background small anode, high purity germanium (HPGe) well detector, after the incubation period of three weeks. The reported ^{226}Ra activity was the average of the daughter products activities (^{214}Bi at 295.2 keV and 351.9 keV, ^{214}Po at 609.3 keV). The standard errors (in %) reported by the software (Genie 2000) at each energy level were used to calculate the counting error. This counting error was calculated as follows:

$$\epsilon_{counting}[\%] = \sqrt{\left(\frac{1}{3}\right)^2 (\epsilon_{295}^2 + \epsilon_{351}^2 + \epsilon_{609}^2)} \tag{A.1}$$

Where:

ϵ_{295} was the standard error in % at 295.2 keV

ϵ_{351} was the standard error in % at 351.9 keV

ϵ_{609} was the standard error in % at 609.3 keV

The total error included the error from counting, mass measurement and uncertainty of the detector efficiency:

$$\epsilon_{total}\left[\frac{Bq}{g}\right] = \frac{Activity\ [cps]}{mass\ [g] \times eff[\frac{cps}{Bq}]}\sqrt{\epsilon_{counting}{}^2 + \left(\frac{\epsilon_{eff}}{eff}\right)^2 + \left(\frac{\epsilon_{mass}}{mass}\right)^2} \tag{A.2}$$

We found that the error from mass measurement and the uncertainty of the detector efficiency were small compared to the counting error, thus this simplified the total error to:

$$\epsilon_{total}\left[\frac{Bq}{g}\right] = \frac{Activity\ [cps]}{mass\ [g] \times eff[\frac{cps}{Bq}]} \times \epsilon_{counting}[\%] \tag{A.3}$$

A.3 References

(1) U.S. Geological Survey (USGS), Industrial sand and gravel, in Metals and minerals: U.S. Geological Survey Minerals Yearbooks 1991–2017, various pagination, http://minerals.usgs.gov/ minerals/pubs/usbmmyb.html and http://minerals.usgs.gov/ minerals/pubs/commodity/silica/, (accessed 17 February 2018).

(2) Baker-Hughes Inc, Baker-Hughes Rig count: North America Rig Count, http://phx.corporate-ir.net/phoenix.zhtml?c=79687&p=irol-reportsother, (accessed 20 February 2018).

(3) M. E. Benson and A. B. Wilson, Frac Sand in the United States—A Geological and Industry Overview, 2015.

(4) Pennsylvania Department of Environmental Protection (PA DEP), PA DEP Oil and Gas Reporting Website: Statewide Data Downloads by Reporting Period, https:// www.paoilandgasreporting.state.pa.us/ publicreports/ Modules /Welcome/ ProdWasteReports.aspx, (accessed 20 February 2018).

Appendix B

Supporting Information for Chapter 3

B.1 Na-4-mica Synthesis Protocol

$$Na_4Si_4Al_4Mg_6O_{20}F_4 = 854.034 g/mol$$

Na: 22.99 g/mol $\times$ 4 = 91.96 g/mol

Si: 28.09 g/mol $\times 4$ = 112.36 g/mol

Al: 26.98 $\times 4$ = 107.92 g/mol

Mg: 24.31 $\times 6$ = 145.86 g/mol

O: 15.999 g/mol $\times 20$ = 319.98 g/mol

F: 18.998 $\times 4$ = 75.992 g/mol

Total = 854.072 g/mol

<u>Silicic acid method:</u>

$Silicic\ acid$:

$$SiO2 + x\ H2O \rightarrow 60.084\ g/mol + x(18.015)\ g/mol$$

$$(The\ water\ content\ of\ silicic\ acid\ must\ be\ determined)$$

$Boehmite$:

$$AlOOH + x\ H2O \rightarrow 59.9875\ g/mol + x(18.015)\ g\ /mol$$

$$(The\ water\ content\ of\ silicic\ acid\ must\ be\ determined)$$

$MgF2$ = 62.301 g/mol

$NaCl$ = 58.439 g/mol

To make a total of 4 g of Na-4-mica, calculate required amount of chemical by calculating stoichiometric amount required to provide exact molar quantities of each element.

i) Si:

$4g\ Na4mica: MW\ Na4mica = x\ g\ Si : 112.36\ g$

$$x\ g = \frac{4}{854.072} \times 112.36 = 0.52623\ g\ Si\ in\ 4g\ Na4mica$$

$28.09\ g\ Si: 60.084 g\ SiO2\ (assuming\ no\ waters\ of\ hydration)$

$= 0.52623 g\ Si: y\ g\ SiO2$

$$y = \frac{(0.52623 g\ Si)}{28.09 g\ Si} \times 60.084 g\ SiO_2 = 1.1256 g\ SiO_2\ on\ anhydrous\ basis$$

Given a water content of 15.43% in SiO_2. Amount of hydrated SiO_2 required is:

$$\frac{1.1256\ g\ SiO_2}{(1 - 0.1543)} = 1.331 g\ SiO_2$$

ii) Al:

$4 g\ Na4mica: MW\ Na4mica = x\ g\ Al : 107.92\ g\ Al$

$$x\ g = \frac{4}{854.072} \times 107.92 = 0.5055\ g\ Al\ in\ 4 g\ Na4mica$$

$26.98\ g\ Al: 59.9875\ g\ AlOOH\ (assuming\ no\ waters\ of\ hydration)$

$= 0.5055 g\ Al: y\ g\ AlOOH$

$$y = \frac{(0.5055 g\ Al)}{26.98 g\ Al} \times 59.9875 g\ AlOOH = 1.1239 g \quad on\ anhydrous\ basis$$

$Given\ a\ water\ content\ of\ 20.46\ \%\ in\ AlOOH. Amount\ of\ hydrated\ AlOOH\ required\ is:$

$$\frac{(1.1239\ g\ AlOOH)}{(1 - 0.2046)} = 1.4129 g\ AlOOH$$

iii) Mg:

$4 g\ Na4mica: MW\ Na4mica = x\ g\ Mg : 145.86\ g\ Mg$

$$x\ g = \frac{4}{854.072} \times 145.86 = 0.6830\ g\ Mg\ in\ 4 g\ Na4mica$$

$24.31\ g\ Al: 62.301\ g\ MgF_2 = 0.6830 g\ Mg: y\ g\ AlOOH$

$$y = \frac{(0.6830 g\ Mg)}{24.31 g\ Mg} \times 62.301 g\ MgF_2 = 1.7865 g\ MgF_2$$

iv) Na:

Na is provided as an excess in NaCl. Assuming 12M excess then

$4 g\ Na4mica: MW\ Na4mica = x\ g\ Na : 91.96\ g\ Na$

$$x\ g = \frac{4 g}{854.072\ g/mol} \times 22.99\ g/mol \times 12\ M$$

$$= 1.7228\ g\ Na\ in\ 4 g\ Na4mica$$

$22.99\ g\ Na: 58.439\ g\ NaCl\ =\ 1.7228g\ Na: y\ g\ NaCl$

$$y = \frac{(1.7228g\ Na)}{22.99g\ Na} \times\ 58.439g\ NaCl\ = 4.3796g\ NaCl$$

<u>Metakaolin method:</u> Metakaolin has composition $Si_2Al_2O_7$

$Si: 28.085\ g/mol\ \times\ 2\ =\ 56.17\ g/mol$

$Al: 26.982\ g/mol\ \times\ 2\ =\ 53.963\ g/mol$

$O: 15.999\ g/mol\ \times\ 7\ =\ 111.993\ g/mol$

Total $=\ 222.126\ g/mol$

i) Si/Al:

$4g\ Na4mica: MW\ Na4mica\ =\ x\ g\ Si:\ 112.36\ g$

$$x\ g\ = \frac{4}{854.072} \times 112.36\ =\ 0.52623\ g\ Si\ in\ 4g\ Na4mica$$

$56.17\ g\ Si: 222.126g\ \ Si_2Al_2O_7 =\ 0.52623g\ Si: y\ g\ Si_2Al_2O_7$

$$y\ = \frac{(0.52623g\ Si)}{56.17g\ Si} \times 222.126g\ \ Si_2Al_2O_7 = 2.0801g\ \ Si_2Al_2O_7$$

$Kaolinite: Si_2Al_2O_5(OH)_4$

$$Si: 28.085\ g/mol \times 2 = 56.17\frac{g}{mol}$$

$$Al: 26.982\ g/mol \times 2 = 53.963\frac{g}{mol}$$

$$O: 15.999\ g/mol \times 9 = 143.991\frac{g}{mol}$$

$H: 1.0008\ g/mol\ \times 4\ = 4.032\ g/mol$

$Total: 258.156\ g/mol$

$56.17g\ Si\ (from\ metakoalin): 258.156g\ Kaolinite$

$=\ 0.65771\ g\ Si(\ from\ metakaolin):\ y\ g\ kaolinite$

$$y\ g\ = \frac{0.65771g}{56.17g/mol}\ \times\ 258.156\ g/mol\ kaolinite = 3.0228\ g\ kaolinite$$

Stoichiometry Calculations of Na4mica synthesis

Silicic Acid Method:

$Na_4Si_4Al_4Mg_6O_{20}F_4$

MW = 854.02881g

Components	MW	Water Content/Purity		
Silicic Acid	60.084	21.321%	%	
Boehmite	59.988	20.459%	%	
MgF2	62.302	98	%	
NaCl	58.443	X	16	mole of NaCl

Amount of Na4mica you wish to prepare

6 g

9

Si		
Amount of Si in desired amount of Na4mica	0.78924738	
Amount of SiO2 to add on anhydrous basis	1.68849479	
Amount of SiO2 to add on hydrated basis	1.6921	g of Silicic Acid

Al		
Amount of Al in desired amount of Na4mica	0.75823777	
Amount of AlOOH to add on anhydrous bas	1.68579684	
Amount of AlOOH to add on hydrated basis	1.68925	g of Boehmite

Mg		
Amount of Mg in desired amount of Na4mic	1.02453218	
Amount of MgF2 to add on anhydrous basi	2.67981	g of MgF2

16 mole Na		
Amount of Na in desired amount of Na4mic	2.58424282	
Amount of NaCl to add on anhydrous basis	6.56946	g of NaCl

Water content of Silicic Acid and Boehmite

Kaolinite method: From Metakaolin Si2Al2O7

$Na_4Si_4Al_4Mg_6O_{20}F_4$

MW = 854.02881g

Components	MW
Metakaolin	60.0843
Kaolinite	59.9883
MgF2	62.3018
NaCl	58.4428

Amount of Na4mica you wish to prepare

6 g

Si (Al)		
Amount of Si in desired amount of Na4mica	0.7892474	
Amount of Metakaolin to add on anhydrous basis	3.1211	g of metakaolin
Amount of Kaolinite to form metakaolin on anhydrous basis	3.62736	g of kaolinite

Mg		
Amount of Mg in desired amount of Na4mica	1.0245322	
Amount of MgF2 to add on anhydrous basis	2.67981	g of MgF2

16 mole Na		
Amount of Na in desired amount of Na4mica	2.5842428	
Amount of NaCl to add on anhydrous basis	6.56946	g of NaCl

Figure B1: Excel worksheet that automatically calculates the required amounts of the constituent chemicals for Na-4-mica synthesis. Input variables shown in green shade and output mass (grams) in red ink.

B.2 Cation Exchage Capacity Protocol

Place the sample in a centrifuge tube.

Part 1: Sodium Acetate Wash (4 times) pH of about 8.2

Step 1: Add 33 ml of Sodium Acetate to the tube. Cap the tube and shake vigorously.

Step 2: Attach the tube to the rotating shaker and shake it for 5 minutes.

Step 3: Centrifuge the tube at 1000 RCF for 5 mins or until the supernatant is clear. Centrifuge settings: SS-34, 5 mins, 1000 RCF 20 C.

Step 4: Decant the supernatant liquid from the tube into the collection bucket.

Repeat for a total of 4 times.

Part 2: Ethanol Wash (3 times)

Step 1: Add 33 ml of Ethanol to the tube. Cap the tube and shake vigorously.

Step 2: Attach the tube to the rotating shaker and shake it for 5 minutes.

Step 3: Centrifuge the tube at 1000 RCF for 5 mins. Centrifuge settings: SS-34, 5 mins, 1000 RCF 20 C.

Step 4: Decant the supernatant liquid from the tube into the collection bucket.

Repeat for a total of 3 times.

Part 3: Ammonium Acetate Wash (3 times) pH 7 (use acetic acid or ammonium hydroxide for pH adjustments)

Step 1: Add 33 ml of Ammonium Acetate to the tube. Cap the tube and shake vigorously.

Step 2: Attach the tube to the rotating shaker and shake it for 5 minutes.

Step 3: Centrifuge the tube at 1000 RCF for 5 mins. Centrifuge settings: SS-34, 5 mins, 1000 RCF 20 C.

Step 4: Collect the supernatant liquid from the tube into a beaker.

Repeat for a total of 3 times.

Collect all 3 rinses into the beaker and mix them using a glass stirring rod.

The final volume should be 100 ml.

Pour 45 ml of the supernatant into a clean centrifuge tube and label the tube.

Add a few drops of conc. Nitric acid to pH¡2 and invert the tube to mix.

Calculation:

$$CEC\ [meq/100\ g]\ = \frac{(Na.conc.of\ extract\ in\ meqL^{-1} \times 10)}{(sample\ weight\ in\ g)}$$

B.3 X-ray Diffraction Patterns

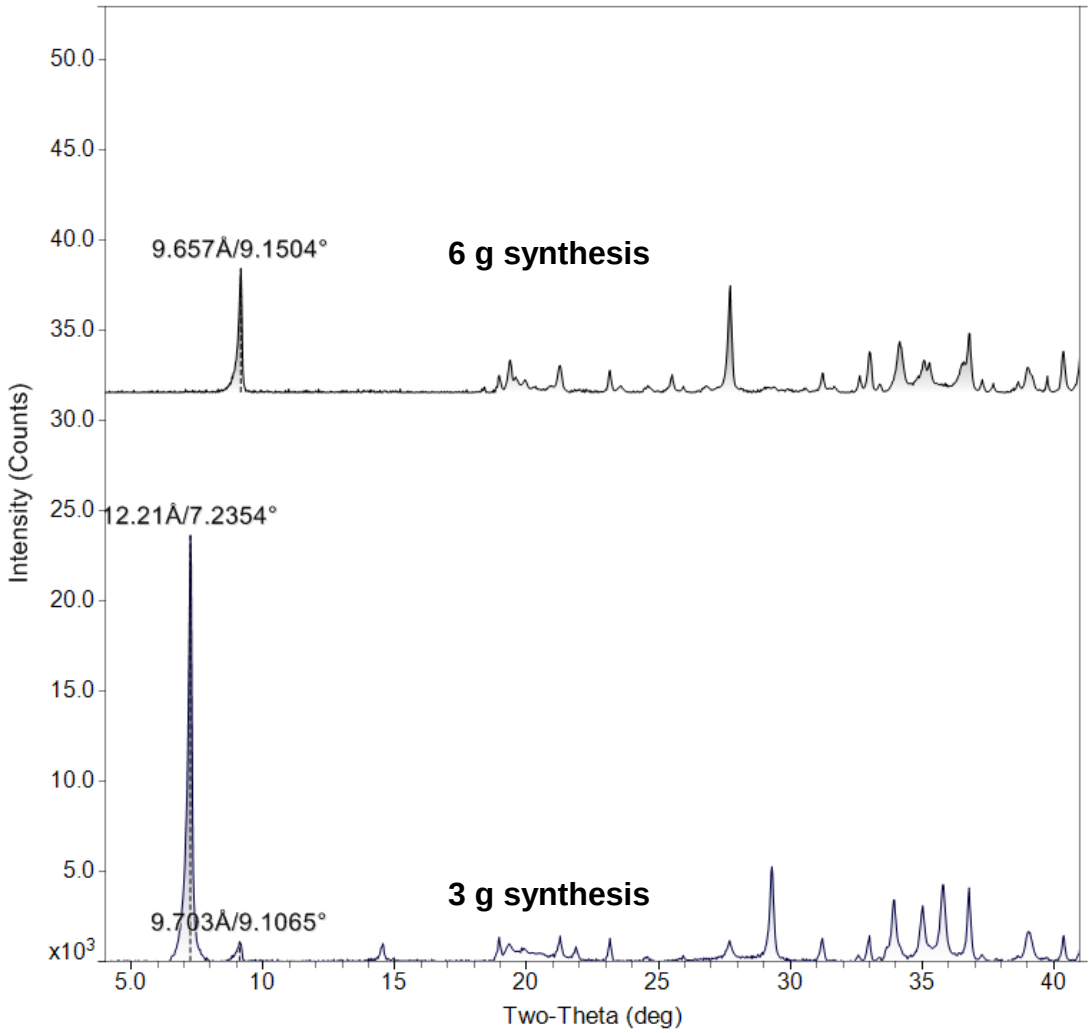

Figure B2: X-ray diffraction patterns of Na-4-mica synthesized from method II (meta-kaolinite) in platinum crucible at 900 flC for 5 hours. The synthesis attempted a 3 g batch and a 6 g batch. The 3 g batch had high purity compared to the 6 g batch.

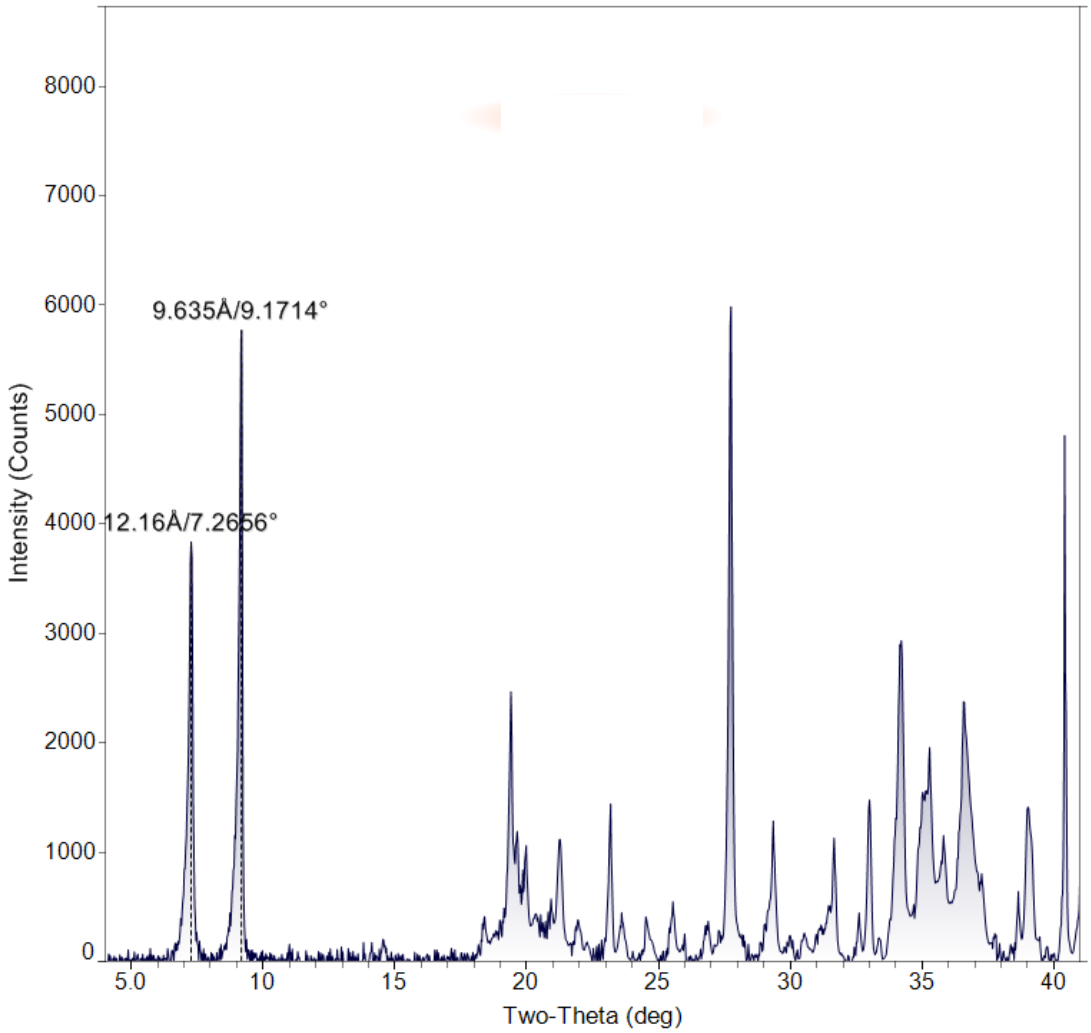

Figure B3: X-ray diffraction pattern of Na-4-mica synthesized from method I (silicic acid and boehmite) in platinum crucible at 900 flC for 5 hours. The synthesis attempted a 4 g batch that produced a mixture of the hydrated and anhydrous phases.

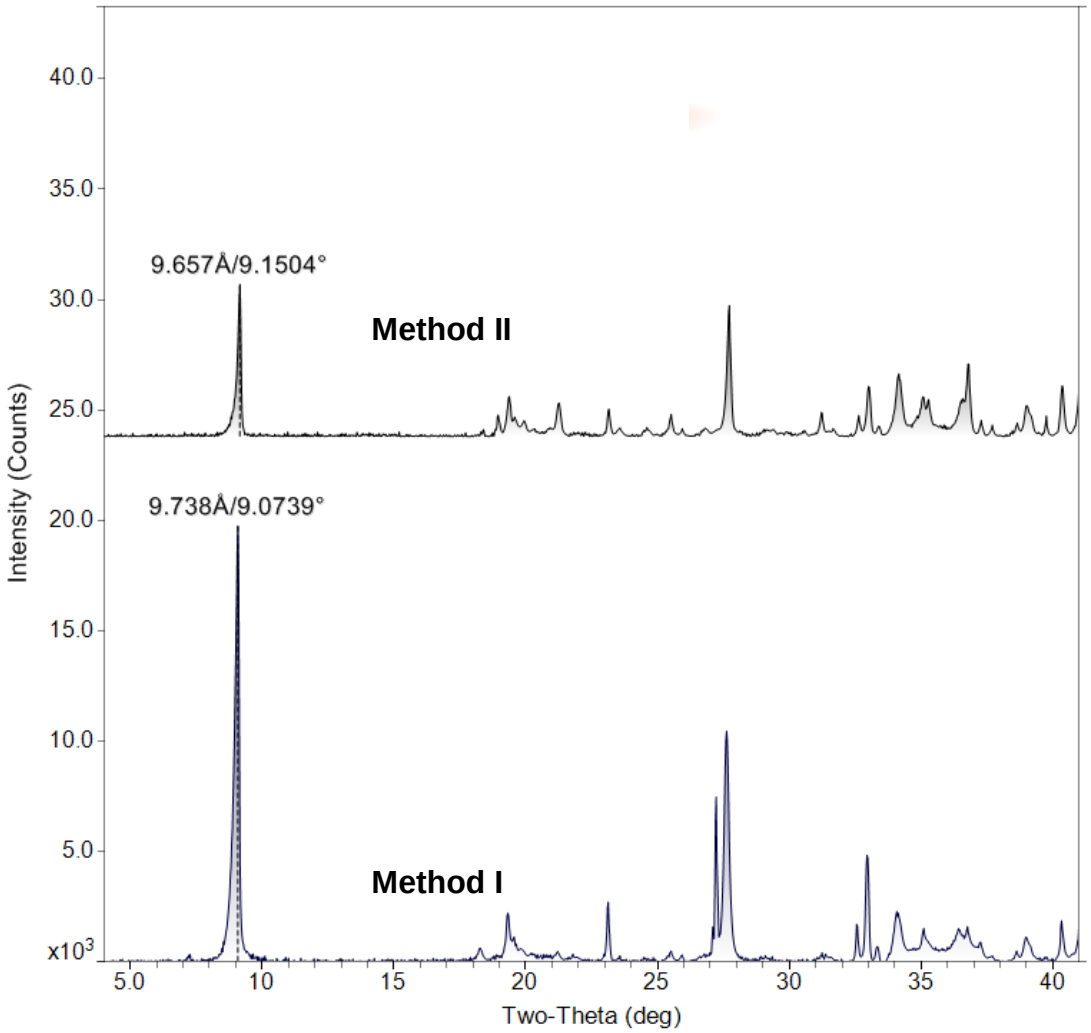

Figure B4: X-ray diffraction patterns of Na-4-mica synthesized from method I (silicic acid and boehmite) and method II (meta-kaolinite) in platinum crucible at 900 flC for 5 hours. The syntheses attempted a 6 g batch that produced the anhydrous phases.

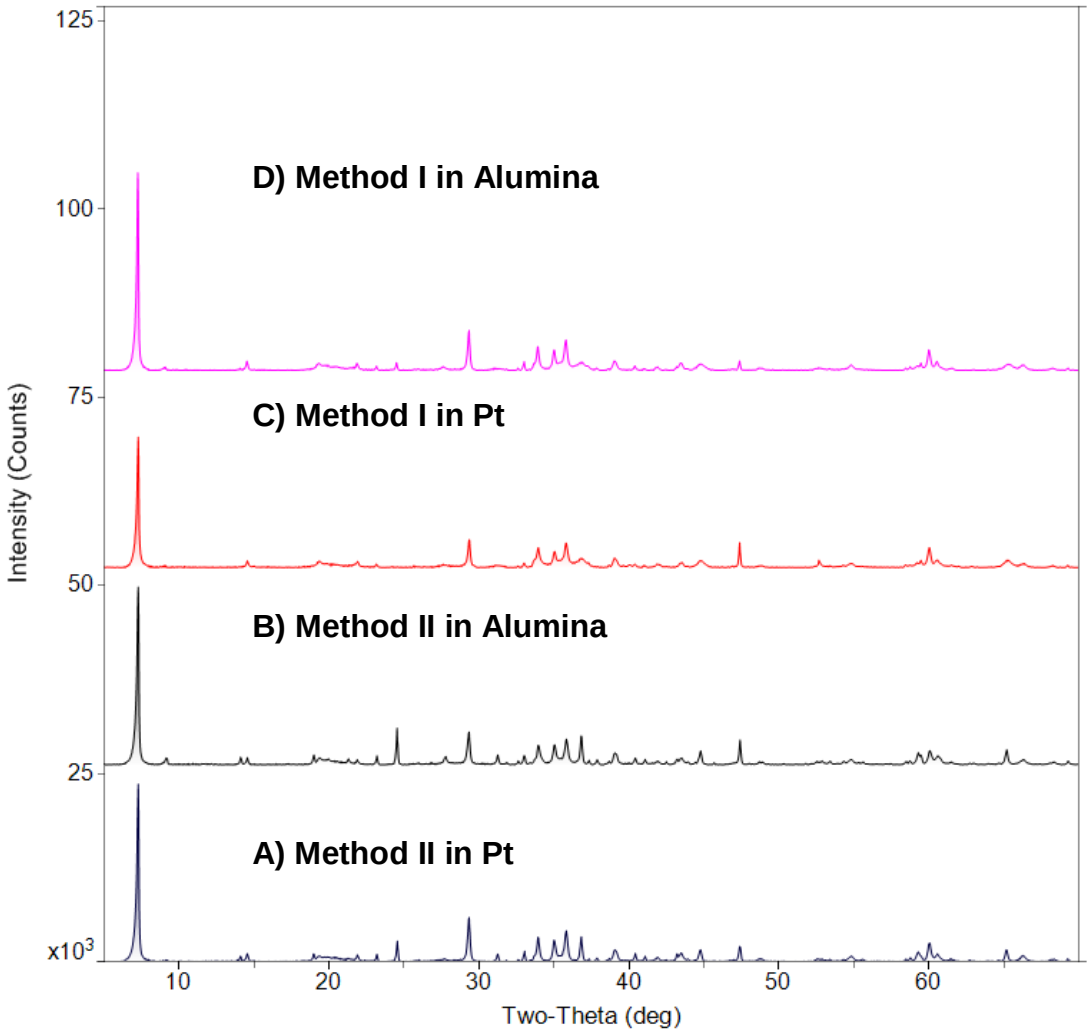

Figure B5: X-ray diffraction patterns of Na-4-mica synthesized from several methods that produced high purity: **A**. Method II (meta-kaolinite) in platinum crucible at 900 flC for 5 hours. **B**. Method II (meta-kaolinite) in alumina crucible at 900 flC for 5 hours. **C**. Method I (silicic acid and boehmite) in platinum crucible at 900 flC for 5 hours. **D**. Method II (meta-kaolinite) in alumina crucible at 900 flC for 5 hours. The syntheses attempted a 2 g batch.

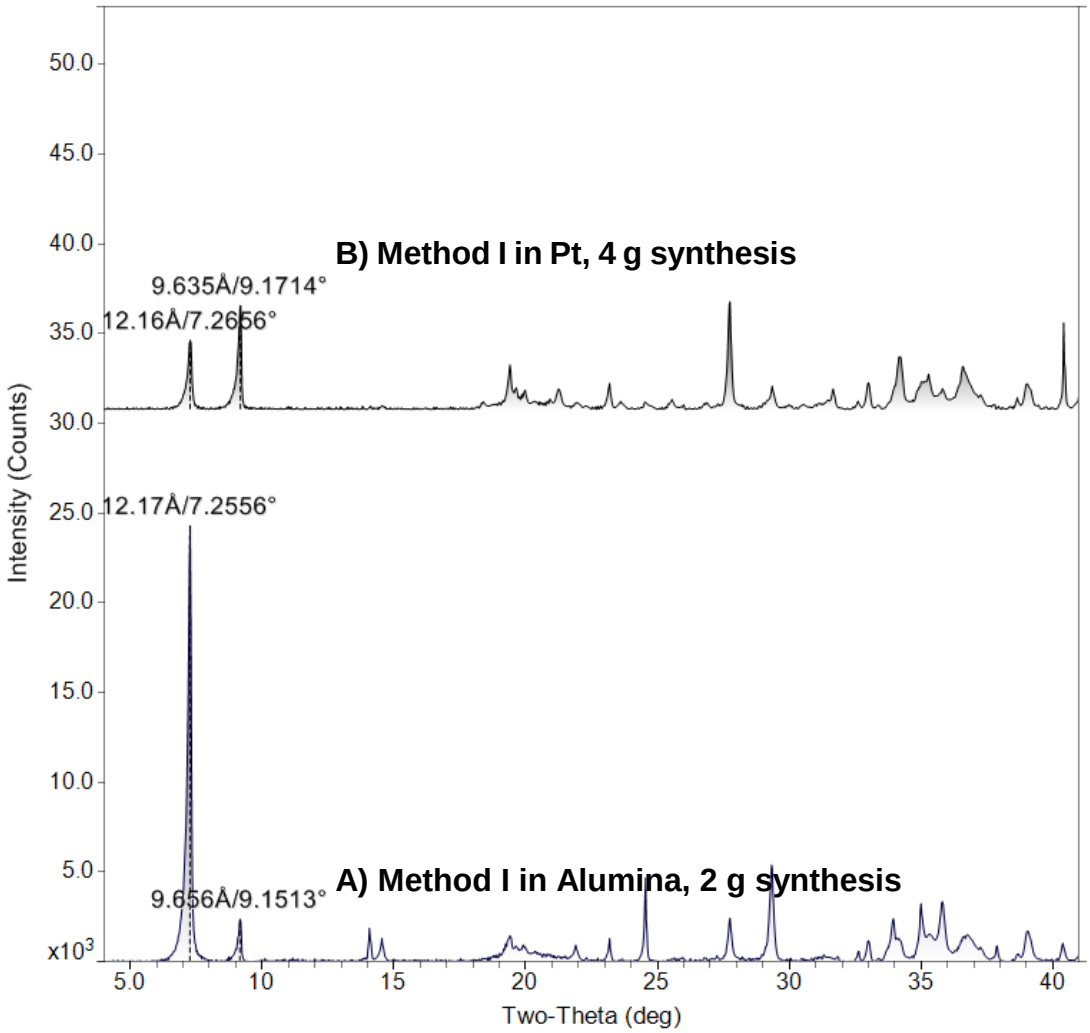

Figure B6: **A**. X-ray diffraction patterns of Na-4-mica synthesized from method I (silicic acid and boehmite) in alumina crucible at 900 flC for 5 hours. The syntheses attempted a 2 g batch that produced a mixture of the hydrated and anhydrous phases. **B**. X-ray diffraction patterns of Na-4-mica synthesized from method I (silicic acid and boehmite) in platinum crucible at 900 flC for 5 hours. The syntheses attempted a 4 g batch that produced a mixture of the hydrated and anhydrous phases.

B.4 Scanning Electron Microscopy Micrographs

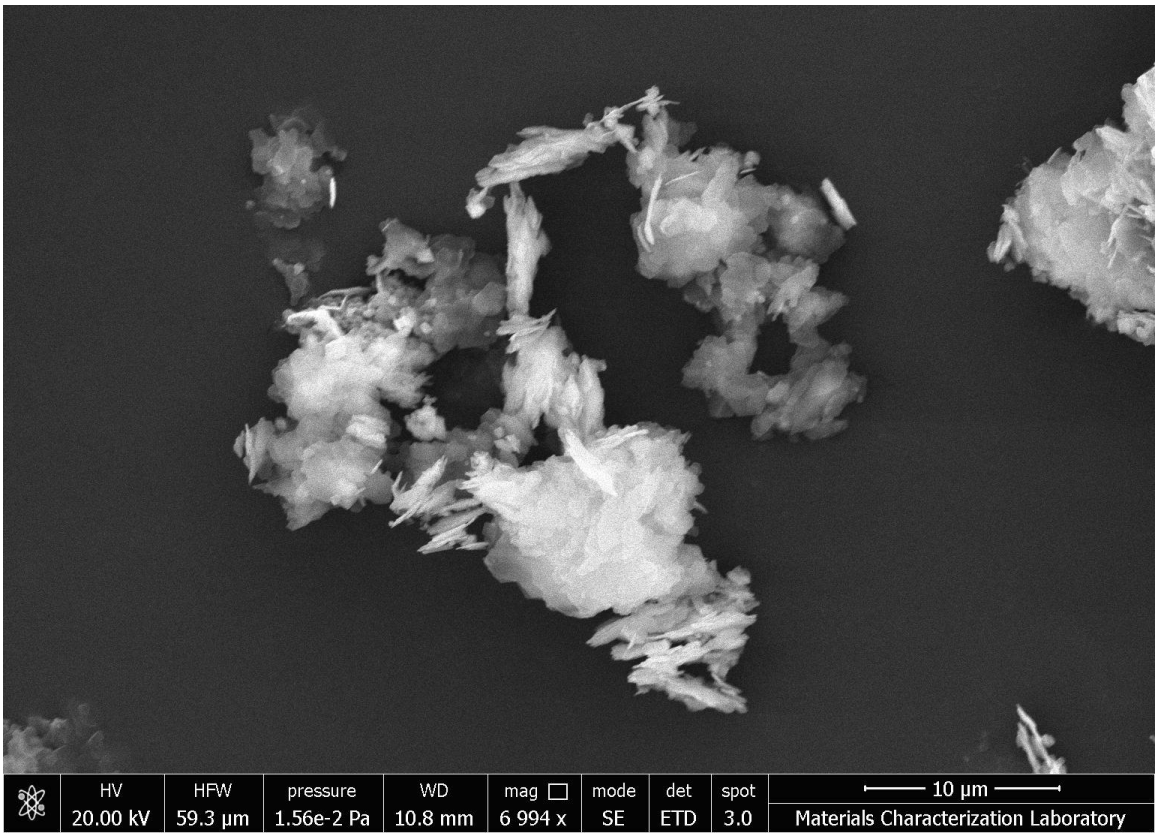

Figure B7: Scanning electron microscopy micrographs of Na-4-mica synthesized from method II (meta-kaolinite) in platinum crucible at 900 flC for 5 hours. The synthesis attempted a 2 g batch.

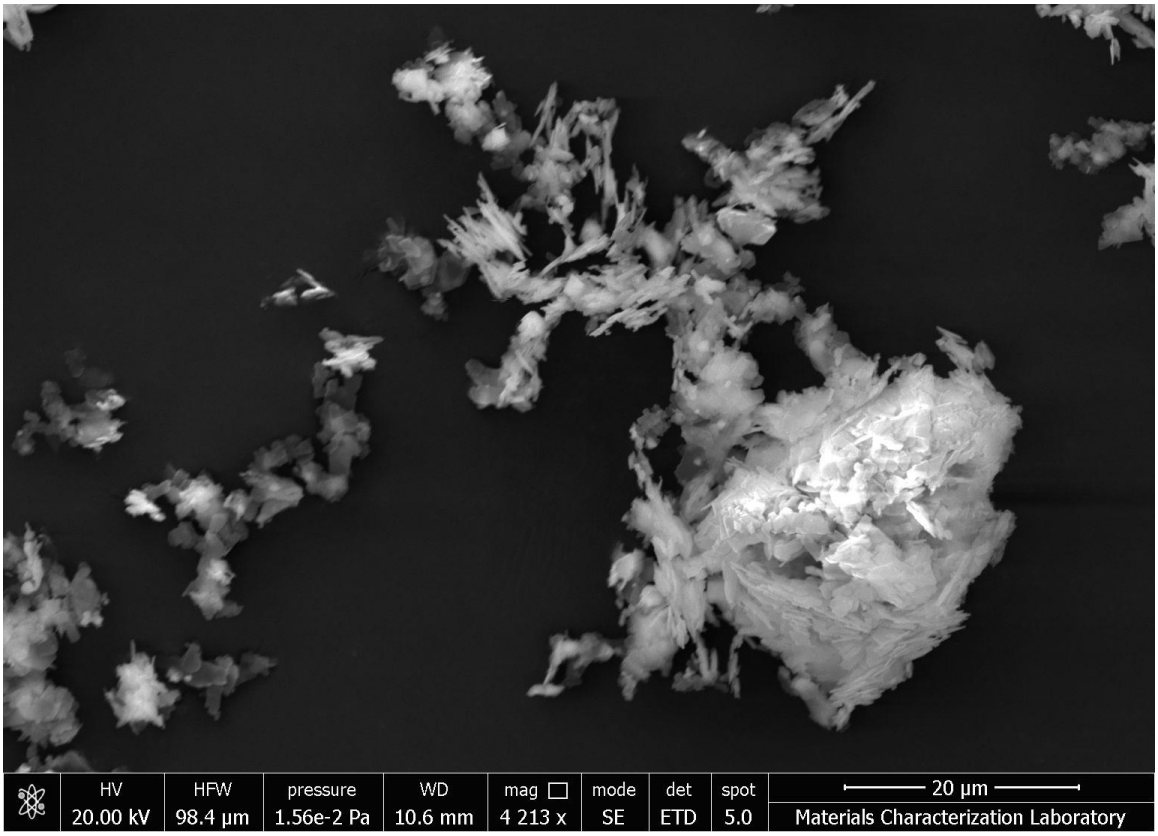

Figure B8: Scanning electron microscopy micrographs of Na-4-mica synthesized from method II (meta-kaolinite) in platinum crucible at 900 flC for 5 hours. The synthesis attempted a 3 g batch.

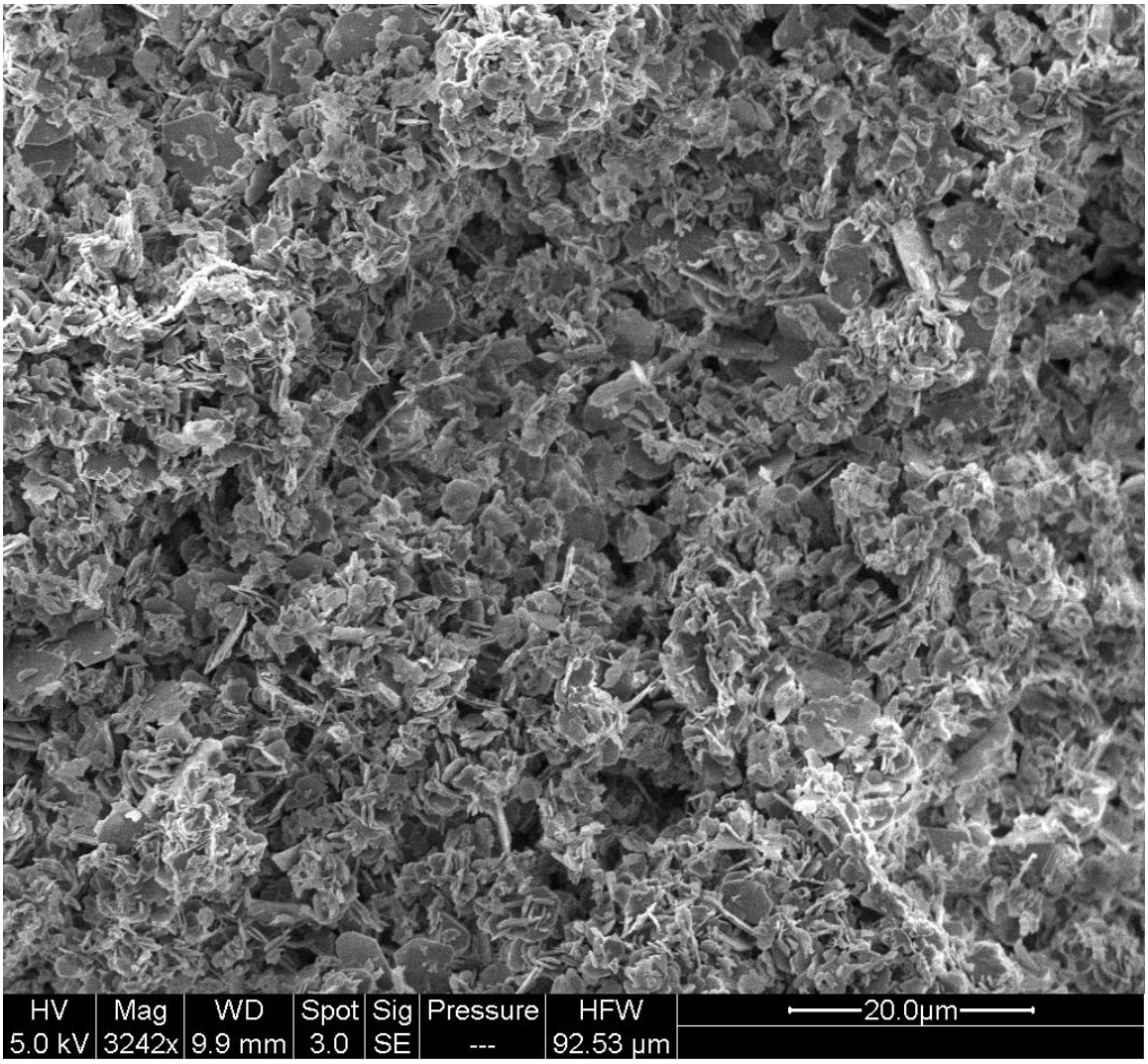

Figure B9: Scanning electron microscopy micrographs of Na-4-mica synthesized from method II (meta-kaolinite) in platinum crucible at 900 flC for 5 hours. The synthesis attempted a 6 g batch.

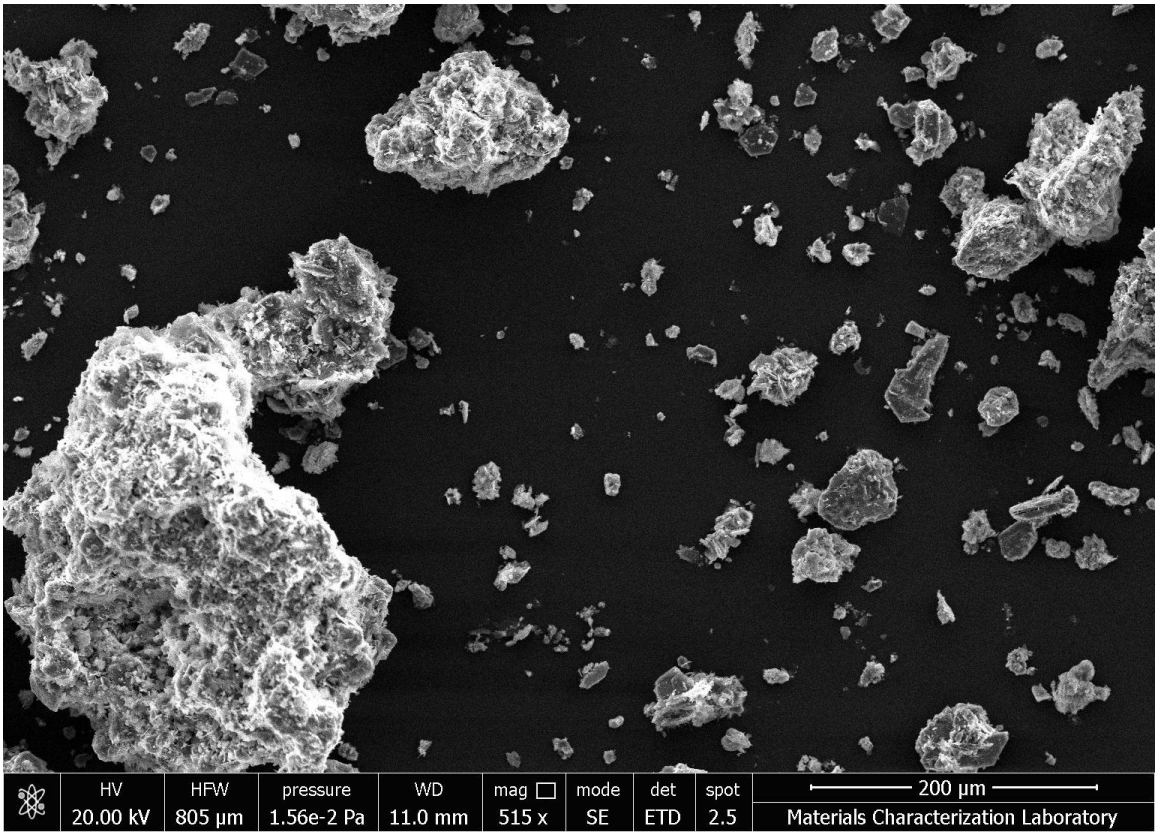

Figure B10: Scanning electron microscopy micrographs of Na-4-mica synthesized from method I (silicic acid and boehmite) in platinum crucible at 900 flC for 5 hours. The synthesis attempted an 8 g batch.

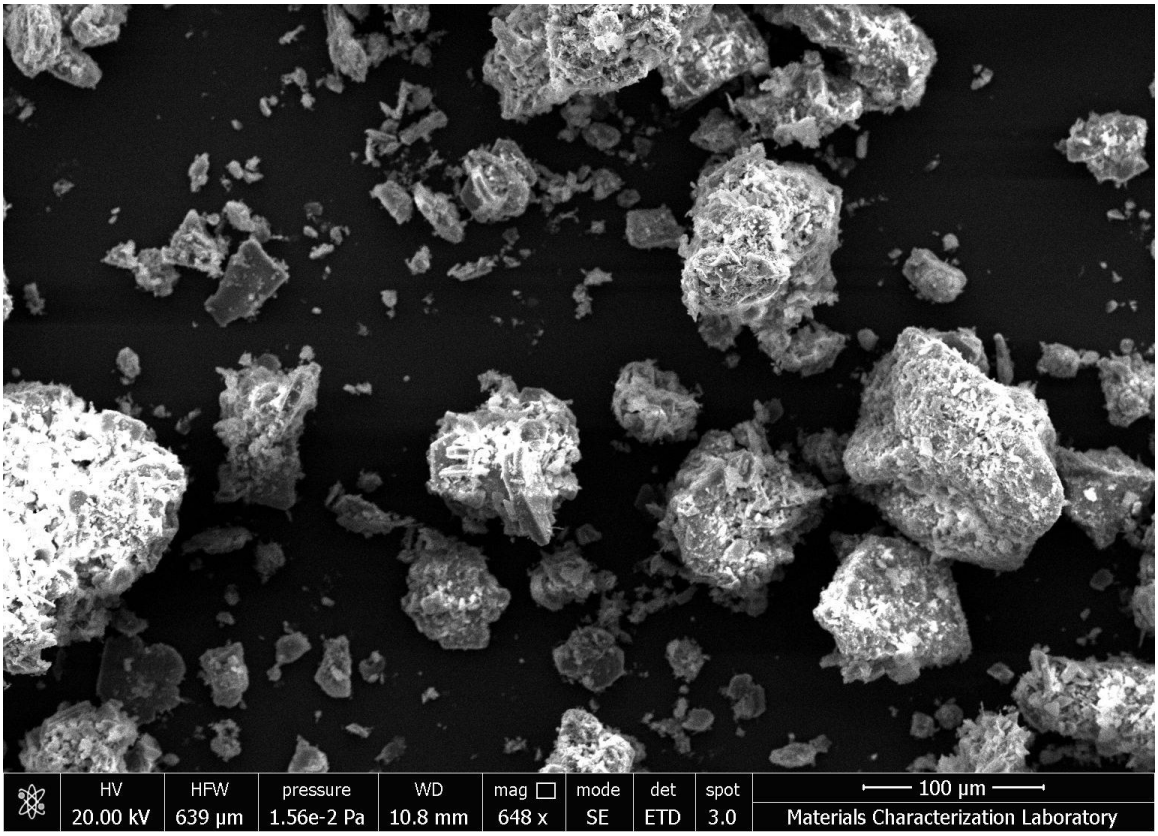

Figure B11: Scanning electron microscopy micrographs of Na-4-mica synthesized from method I (silicic acid and boehmite) in platinum crucible at 900 flC for 5 hours. The synthesis attempted an 8 g batch.

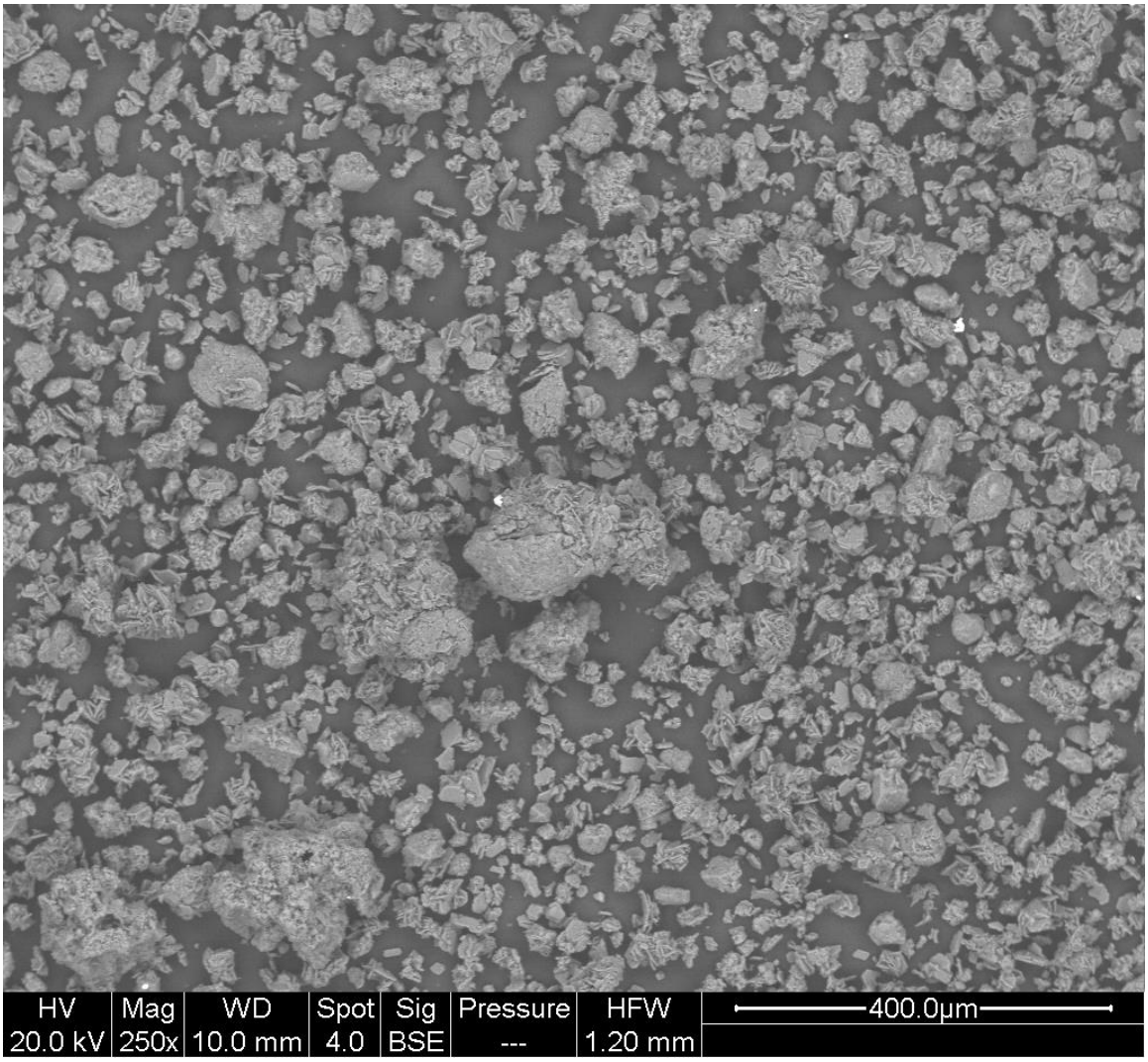

Figure B12: Scanning electron microscopy micrographs of Na-4-mica synthesized from method I (silicic acid and boehmite) in platinum crucible at 900 flC for 5 hours. The synthesis attempted an 8 g batch.

B.5 Reactive Transport Model (CrunchFlow)

```
TITLE
Final Project: Radium Entrapment and Immobilization from High TDS Water
onto Clays (Montmorillonite, surrogate for Na-4-mica) through Cation Exchange
END

RUNTIME
time˙units minutes
timestep˙max 0.1
timestep˙init 1.0E-10
time˙tolerance 0.001
speciate˙only false
database database.dbs
graphics kaleidagraph
density˙module temperature
database˙sweep false
END

OUTPUT
time˙units minutes
spatial˙profile 720.0
time˙series˙interval 1
time˙series TimeSeries.out 1 1 1
time˙series˙print Ra++
END

INITIAL˙CONDITIONS
initial 1-1
END
DISCRETIZATION
! This is a reactor with 1 m * 1 m * 0.0005 m = 0.0005 m3 = 0.5 liter = 500 cm3
distance˙units meters
```

```
xzones 1 0.0005
END

PRIMARY˙SPECIES
H+
CO2(aq)
Ba++
Sr++
Ca++
Mg++
Na+
ClSiO2(aq)
Ra++
BrSO4--
Acetic˙acid(aq)
Al+++
! Although SiO2(aq) and Al+++ are not in the given water recipe, we need to
include
! these species so the code recognize the mineral Montmor-Na, because these spe-
cies are
! included in the Montmor-Na dissolution reaction. Acetic Acid is the surrogate
for
! organic matter complexation with Radium
END

SECONDARY˙SPECIES
! We can potentially put some here however here we focus on ion exchange
! and not considering much of aqueous complexation here yet.
Acetate
Ba(CH3COO)2(aq)
BaCH3COO+
BaCl+
BaOH+
HCO3-
```

Ca(CH3COO)2(aq)
CaCH3COO+
CaCl+
CaCl2(aq)
CaOH+
CaSO4(aq)
H2SO4(aq)
H4(H2SiO4)4----
H6(H2SiO4)4--
HCl(aq)
HSO4-
Mg(CH3COO)2(aq)
Mg4(OH)4++++
MgCH3COO+
MgCl+
MgSO4(aq)
Na(CH3COO)2-
NaCH3COO(aq)
OHRa(CH3COO)2(aq)
RaCH3COO+
Sr(CH3COO)2(aq)
SrCH3COO+
SrCl+
SrOH+
SrSO4(aq)
BaCO3(aq)
CO3--
CaCO3(aq)
CaHCO3+
MgCO3(aq)
Mg(OH)+
MgHCO3+
NaCO3-

```
NaHCO3(aq)
SrCO3(aq)
END
GASES
CO2(g)
END

ION˙EXCHANGE
exchange XMont- on Montmor-Na
convention Gaines-Thomas
END

MINERALS
Montmor-Na -label default
-rate -14.7
Barite        -label default
-rate   -7.26
Calcite       -label default
-rate   -3.30
Calcite       -label h+
-rate   -0.05
Calcite       -label co2
-rate   -6.19
Celestite     -label default
-rate   -6.36
END

CONDITION initial
! The volume fraction of Montmor-Na is 0.3%
! We have Montmor-Na grains with total volume of 2 cmˆ3 in the batch reactor
! This is an open system with partial pressure of CO2 being 0.03 bar so the
CO2(aq) is set
! to equilibrate with CO2 gas in the air
```

```
units ppm
temperature 25.0
pH 7.00
CO2(aq) CO2(g) 3.15E-4
Ba++ 2000.0
Sr++ 1700.0
Ca++ 7000.0
Mg++ 600.0
Na+ 50000.0
Cl- 50000.0
SiO2(aq) 1E-14
Ra++ 1E-03
Br- charge
SO4-- 1E-14
Acetic˙acid(aq) 1E-14
Al+++ 1E-14
! The following two lines means that ion exchange sites are on Montmor-Na with
! volume fraction of 0.4 %
! (=500 cmˆ3 * 0.003 = 2 cmˆ3) specific surface area of 15 mˆ2/g, a CEC value
of
! 1.00E-03 eq/g. This is equivalent  to .100 eq/100g, 100.0 meq/100g, and 1000
meq/kg
XMont- -cec 1.0E-03
Barite 1E-24
Calcite 1E-24
Celestite 1E-24
Montmor-Na 0.003
specific˙surface˙area 700
END
```

Table B1: Water Chemistry conditions for the RTM. Data from Barbot *et al.* 2013 [1].

	Minimum	**Maximum**	**Average**
TDS (mg/L)	680	345,000	*106,390*
COD (mg/L)	195	36,600	*15,358*
pH	5.1	8.42	*6.56*
SO_4 (mg/L)	0	763	*71*
Cl (mg/L)	64.2	196,000	*57,447*
Br (mg/L)	0.2	1,990	*511*
Na (mg/L)	69.2	117,000	*24,123*
Ca (mg/L)	37.8	41,000	*7,220*
Mg (mg/L)	17.3	2,550	*632*
Ba (mg/L)	0.24	13,800	*2,224*
Sr (mg/L)	0.59	8,460	*1,695*
Total Ra (pCi/L)	2.75	10,640	*743*

Table B2: Selectivity Coefficient for Ion exchange on Kaolinite. Data from Li *et al.* 2010 [2] and Appelo and Postma 1993 [3]. (** Radium was assumed to be the same as Strontium)

Ion exchange reaction	**log K**
$NaX \Leftrightarrow Na_{+} + X_{-}$	0.0
$KX \Leftrightarrow K_{+} + X_{-}$	-0.69
$CaX_2 \Leftrightarrow Ca_{2+} + 2X_{-}$	-0.39
$MgX_2 \Leftrightarrow Mg_{2+} + 2X_{-}$	-0.30
$BaX_2 \Leftrightarrow Ba_{2+} + 2X_{-}$	-0.45
$SrX_2 \Leftrightarrow Sr_{2+} + 2X_{-}$	-0.45
$RaX_2 \Leftrightarrow Ra_{2+} + 2X_{-}$	-0.45**

Table B3: Selectivity Coefficient for Ion exchange on Montmorillonite. Data from Shao *et al.* 2009 [4].

Ion exchange reaction	log K
$NaX \Leftrightarrow Na_{+} + X_{-}$	0.0
$KX \Leftrightarrow K_{+} + X_{-}$	1.03
$CaX_2 \Leftrightarrow Ca_{2+} + 2X_{-}$	1.11
$MgX_2 \Leftrightarrow Mg_{2+} + 2X_{-}$	1.03
$BaX_2 \Leftrightarrow Ba_{2+} + 2X_{-}$	1.11
$SrX_2 \Leftrightarrow Sr_{2+} + 2X_{-}$	1.11
$RaX_2 \Leftrightarrow Ra_{2+} + 2X_{-}$	1.11

Table B4: Properties of clay minerals modeled by the RTM

	Kaolinite	**Montmorillonite**
SSA (m_2/g)	15	700
CEC (meq/100g)	468	100
Molar Volume (cm_3/mol)	99.5	156.16
MW (g/mol)	258	549.07

Table B5: Summary of the conditions tested.

	Base Case	**Case 1**	**Case 2**
Solid Conc.	10 g/L	100 g/L	500 g/L
TDS	50,000 ppm	1,000 ppm	100,000 ppm
pH	7	4	10
Sulfate	0 ppm	70 ppm	700 ppm
Organic Matter	0 ppm	1,000 ppm	30, 000 ppm

Table B6: Summary of Results for Montmorillonite (Na-4-mica surrogate).

		K_d ($L\ g^{-1}$)	% Removal	Distribution factor
Base Case		**2.62E-06**	**0.00%**	**1**
OM	1000 ppm	2.64E-06	0.00%	1.01
	30,000 ppm	3.52E-06	0.00%	1.34
pH	4	2.62E-06	0.00%	1.00
	10	8.05E-07	0.00%	0.31
Sulfate	70 ppm	2.59E-06	0.00%	0.99
	700 ppm	2.35E-06	0.00%	0.90
TDS	1,000 ppm	1.13E-03	0.23%	431.38
	100,000 ppm	5.14E-07	0.00%	0.20
Volume fraction	100 g/L	2.62E-06	0.01%	1.00
	500 g/L	2.62E-06	0.03%	1.00

Table B7: Summary of Results for Kaolinite.

		K_d ($L\ g^{-1}$)	% Removal	Distribution factor
Base Case		**4.09E-04**	**0.43%**	**1**
OM	1000 ppm	4.14E-04	0.42%	1.01
	30,000 ppm	5.75E-04	0.29%	1.41
pH	4	4.09E-04	0.43%	1.00
	10	1.63E-04	0.45%	0.40
Sulfate	70 ppm	4.06E-04	0.43%	0.99
	700 ppm	3.78E-04	0.43%	0.92
TDS	1,000 ppm	8.94E-03	9.35%	21.84
	100,000 ppm	8.59E-05	0.09%	0.21
Volume fraction	100 g/L	4.09E-04	4.44%	1.00
	500 g/L	4.09E-04	26.65%	1.00

B.6 References

(1) Quality Parameters of Produced Waters from Devonian-Age Shale Follwoing Hydraulic Fracturing. Environ. Sci. Technol. 2013, 47, 2562−2569.

(2) Li, L.; Steefel, C. I.; Kowalsky, M. B.; Englert, A.; Hubbard, S. S. Effects of Physical and Geochemical Heterogeneities on Mineral Transformation and Biomass Accumulation during Biostimulation Experiments at Rifle, Colorado. J. Contam. Hydrol. 2010, 112 (1−4), 45−63. https://doi.org/10.1016/J.JCONHYD.2009.10.006.

(3) Appelo, C. A. J.; Postma, D. Geochemistry, Groundwater and Pollution; Balkema, 2005.

(4) Shao, H.; Kulik, D. A.; Berner, U.; Kosakowski, G.; Kolditz, O. Modeling the Competition between Solid Solution Formation and Cation Exchange on the Retardation of Aqueous Radium in an Idealized Bentonite Column. Geochem. J. 2009, 43 (6). https://doi.org/10.2343/geochemj.1.0069.

Appendix C

Supporting Information for Chapter 4

C.1 Supporting Figures and Tables

Table C1: Certified Compositions of the UTS-2, UTS-3 and UTS-4 Canadian Certified Reference Materials[1].

		Mass %						µg/g				Bq/g						
Constituent	**Density (g/mL)**	**Fe (total)**	**Ti**	**Al**	**Ca**	**S (total)**	**Sulfate**	**Ba**	**U**	**Th**	**As**	**Th-230**	**Ra-226**	**Pb-210**	**Po-210**	**Th-232**	**Ra-228**	**Th-228**
UTS-2	1.81	3.2	0.18	2.71	0.42	3.23	0.84	464	56	174		4.4	5.6	4.55	4.4	0.88	1	0.92
UTS-3	1.83	3.25	0.23	5.8	4.03	0.23		212	513	10		11.3	13.3	12.6	11.8			
UTS-4	1.42	2.62	0.24	6.29	1.75	1.8	5.21	65	1010	15.4	38	22.9	38.6	32.4	30.8			

Table C2: Sample mix, vial fill height, densities and masses at various fill heights, and height-to-mass slope of each sample utilized in creating the regression.

Masses		Mix	Height (cm)	Density (g/mL)	Full Mass (g)	6 cm	3.5 cm	3 cm	2 cm	1 cm	H/M slope (cm/g)
UTS-2	Density: Bentonite	0:100	6	0.998	*23.940*	*23.940*	*13.859*	*11.879*	*7.919*	*3.960*	*0.2514*
		10:90	6	1.063	*25.519*	*25.519*	*14.773*	*12.663*	*8.442*	*4.221*	*0.2359*
		40:60	6	1.266	*30.382*	*30.382*	*17.588*	*15.076*	*10.050*	*5.025*	*0.1981*
		80:20	6	1.533	*36.802*	*36.802*	*21.305*	*18.261*	*12.174*	*6.087*	*0.1636*
	Density: Aluminum oxide	0:100	6	1.114	*26.732*	*26.732*	*15.475*	*13.265*	*8.843*	*4.422*	*0.2252*
		10:90	6	1.243	*29.828*	*29.828*	*17.268*	*14.801*	*9.867*	*4.934*	*0.2018*
		40:60	6	1.538	*36.923*	*36.923*	*21.375*	*18.321*	*12.214*	*6.107*	*0.1630*
		70:30	6	1.698	*40.747*	*40.747*	*23.589*	*20.219*	*13.479*	*6.740*	*0.1477*
	Height	100:0	6	1.809	*43.411*	*43.411*	*24.864*	*21.540*	*15.136*	*8.560*	*0.1379*
		100:0	3.5	1.809	*24.864*	-	*24.864*	-			-
		100:0	2	1.809	*15.136*	-	-	-	*15.136*	-	-
		100:0	1	1.809	*8.560*	-	-	-	-	*8.560*	-
UTS-3	Density: Aluminum oxide	0:100	6	1.114	*26.732*	*26.732*	*15.475*	*13.265*	*8.843*	*4.422*	*0.2252*
		10:90	6	1.356	*32.546*	*32.546*	*18.841*	*16.150*	*10.766*	*5.383*	*0.1849*
		40:60	6	1.549	*37.182*	*37.182*	*21.525*	*18.450*	*12.300*	*6.150*	*0.1619*
		80:20	6	1.710	*41.036*	*41.036*	*23.756*	*20.362*	*13.575*	*6.787*	*0.1467*
	Height	100:0	6	1.830	*43.911*	*43.911*	*25.420*	*20.671*	*14.526*	*7.035*	*0.1381*
		100:0	3	1.830	*20.671*	-	-	*20.671*	-	-	-
		100:0	1	1.830	*7.035*	-	-	-	-	*7.035*	-

Table C3: Sample mix, vial fill heights, CRM mass added, bentonite/aluminum oxide mass added, and total radium activities used for efficiency determination in the 19 mixtures of the CRMS UTS-2 and UTS-3 with bentonite and aluminum oxide

Radium activities (Bq)		Mix	Height (cm)	CRM mass (g)	Bentonite mass (g)	Aluminum oxide mass (g)	^{226}Ra from CRM (Bq)	^{226}Ra from bentonite (Bq)	Total ^{226}Ra (Bq)
UTS-2	Density: Bentonite	0:100	6	0	23.94	-	0	4.573	4.57
		10:90	6	2.55	22.97	-	14.291	4.387	18.68
		40:60	6	12.15	18.23	-	68.06	3.482	71.534
		80:20	6	29.44	7.36	-	164.87	1.406	166.28
	Density: Aluminum oxide	0:100	6	0	-	26.73	0	-	0
		10:90	6	2.98	-	27.00	16.70	-	16.70
		40:60	6	14.61	-	22.41	81.80	-	81.8
		70:30	6	29.21	-	12.81	159.73	-	159.73
	Height	100:0	6	43.41	-	-	243.1	-	243.1
		100:0	3.5	24.86	-	-	139.24	-	139.24
		100:0	2	15.14	-	-	84.76	-	84.76
		100:0	1	8.56	-	-	47.94	-	47.94
UTS-3	Density: Aluminum oxide	0:100	6	0	-	26.73	0	-	0
		10:90	6	3.25	-	36.01	43.29	-	43.29
		40:60	6	14.87	-	24.00	197.81	-	197.81
		80:20	6	31.98	-	8.00	425.27	-	425.27
	Height	100:0	6	43.91	-	-	584.02	-	584.02
		100:0	3	20.67	-	-	274.93	-	274.93
		100:0	1	7.03	-	-	93.56	-	93.56

Table C4: Interference Correction for ^{226}Ra relative to ^{235}U at 186 keV Energy Level by Peak Deconvolution for the CRMs at full fill height.

	^{226}Ra (Bq/g)	U (`g/g)	$\frac{R_{63\,keV}}{R_{186\,keV}}$ (%)	$\frac{R_{U-235}}{R_{Ra-226}}$ (%)	With deconvolution (Bq/g)	Without deconvolution (Bq/g)
UTS-2	5.6	56	12	8.5	5.75	6.26
UTS-3	13.3	513	40	28	13.95	19.19
UTS-4	38.6	1010	30	22	36.06	45.3

R is the background corrected count rate (cps) at the given energy level

Table C5: Average Elemental Compositions of Sediment Cores Sampled from Streams Impacted by Oil and Gas Produced Water Disposal [2]

Fe %	Ti %	Al %	Ca %	S %	Ba ppm	U ppm	Th ppm
7.92	0.004	2.96	0.2	0.37	176	1.89	3.4
8.63	0.004	1.53	0.13	0.34	147.5	1.29	2.95
1.76	0.004	0.43	3.67	0.37	226	0.283	1.26

C.2 Density Determination Based on Mass and Sample Volume

In some cases the available sample mass could be so little that it would not fill the sample vial. This could happen, for example, when appraising environmentally impacted samples or engineered samples when small bench-scale studies are performed and minimal masses are available.

A relationship between the fill height and the mass of the sample can be derived. It becomes independent of the density of the sample when the mass at any fill height is divided by the mass required to fully fill the vial. We refer to this as the mass ratio (Eq. S1):

$$mass\ ratio = \frac{mass\ at\ given\ height}{mass\ at\ full\ height} \tag{S1}$$

The relationship between the mass ratio and the height (Figure S1A) was derived from ten samples where the CRMs UTS-2, UTS-3, and UTS-4, were packed into the vials and filled to various heights. This relationship was linear over the range of heights:

$$mass\ ratio = 0.1654 \times Height\ (cm) \tag{S2}$$

Using Eq. (S2), we derived the masses required to fill any vial to a given height, provided the mass at the full fill height was known. Then, we performed linear regressions of fill height versus sample mass (Table C2) to obtain height-mass slopes at each density. The relationship between density and the height-mass slope is shown in Figure C1B; and it was best described by a power law (Eq. S3) over the range of values. From Eq. (S3), the density of any sample can be determined from the mass and the fill height:

$$Density\ [g/mL] = 0.2504\ \left(\frac{Height\ [cm]}{Mass\ [g]}\right)^{-1.00113} \tag{S3}$$

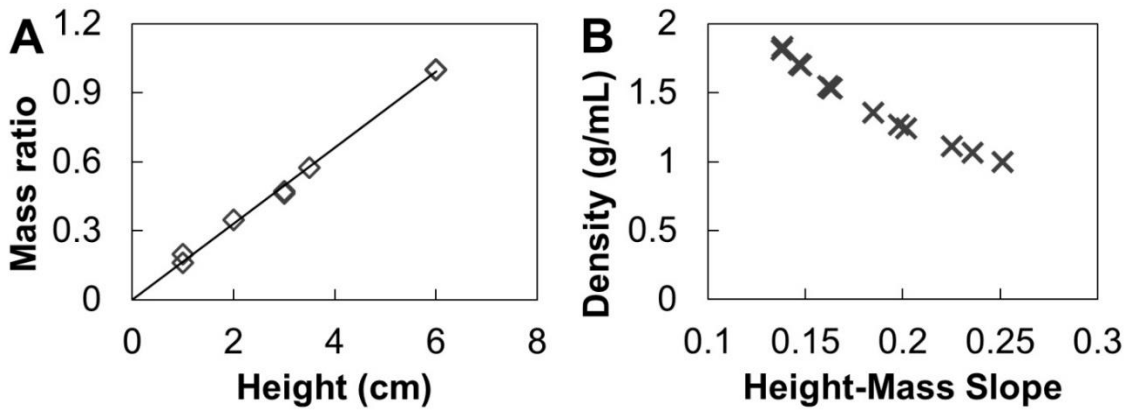

Figure C1: **A.** Mass ratio, Eq. (S2), vs. Height (cm) for ten samples originating from mixtures of bentonite or aluminum oxide with UTS-2, UTS-3 or UTS-4 CRMs. **B.** Density (g/mL) of mixed sediments versus the slope of the height-mass regressions for various proportions of UTS-2, or UTS-3, to bentonite or aluminum oxide. For the mixtures of these two sediments, the slope exhibited a trend described by Eq. (S3).

For a cylindrical body, the density is defined as follows::

$$Density = \frac{Mass}{Volume} = \frac{Mass}{\pi R^2 Height} \tag{S4}$$

The scintillation vials have outer dimensions of 2.8 cm diameter and 6.1 cm height, giving an outer volume of 37.6 mL. Herein, we used a nominal inner volume of 24 mL. Therefore, the theoretical definition for the density at any given height reduces:

$$D = \frac{Mass/Height}{\pi(1.4)^2\left(\frac{24}{37.6}\right)} = 0.2544\left(\frac{Height}{Mass}\right)^{-1} \tag{S5}$$

This empirical determination for the density showed good agreement to the theoretical definition (Eq. S3 and S5), and hence we decided to use the theoretical definition moving forward.

C.3 MATLAB Code

```
% Moses Ajemigbitse
% Civil and Environmental Engineering, The Pennsylvania State
University
% November 28th 2018
% Density and Height Correction Script
% This script uses the density correction derived by UTS-2
and bentonite,
% UTS-2 and corundum, and UTS-3 and corundum mass dilutions
to derive an
% approximate density value for samples of unknown density.
% This corrected density is then used in the efficiency
% correction to calculate a new efficiency that corrects for
the difference
% in densities of the sample and the standard.

clear
clc
format short

filename = 'Mass and Height.xlsx';
MassnHeight = xlsread(filename);

x = MassnHeight(:,1);   % i.e. mass
y = MassnHeight(:,2); % i.e. height
 dmin  = 0.9975;  % set the min density
 dmax  = 1.82964;  % set the min density

for i=1:length(y);
    if i == length(y) + 1
    end

slope(i) = y(i)/x(i);
density (i) = 0.25036*slope(i)^-1.00113;

if y (i) < 6
    density (i) = density (i) / 0.995;
else
    density (i) = density (i) / 1.0034;
end

if slope(i) > 0.25143
```

```
    density (i) = dmin;
elseif slope(i) < 0.13794
    density (i) = dmax;
end

eff_186 (i) = 0.02415739592 - 0.00134526998 * y (i) -
0.00348095505 * density (i);
eff_295 (i) = 0.08156105618 - 0.00436885267 * y (i) -
0.01218736403 * density (i);
eff_351 (i) = 0.13595292376 - 0.00720004489 * y (i) -
0.02034647892 * density (i);
eff_609 (i) = 0.04647643134 - 0.00167370913 * y (i) -
0.00617686638 * density (i);
end

densitycorr_cells=num2cell(density');      %Convert data to
cell array
eff = [eff_186; eff_295; eff_351; eff_609];
eff_table = num2cell(eff');

Mass_cells = num2cell(x);
Height_cells = num2cell(y);

col_header={'Mass','Height','Density','186 Eff', '295 Eff',
'351 Eff', '609 Eff'};    %Row cell array (for column labels)
output_matrix=[col_header; Mass_cells Height_cells densi-
tycorr_cells eff_table];     %Join cell arrays
xlswrite('Density Correction Output.xls',output_matrix);
%Write data and both headers
```

C.4 References

(1) Canadian Certified ReerenceMaterials Project (CCRMP). UTS-1 to UTS-4 Certificate of Analysis — Natural Resources Canada https://www.nrcan.gc.ca/mining-materials/certified-reference-materials/certificate-price-list/8127 (accessed Mar 30, 2019).

(2) Burgos, W. D.; Castillo-Meza, L.; Tasker, T. L.; Geeza, T. J.; Drohan, P. J.; Liu, X.; Landis, J. D.; Blotevogel, J.; McLaughlin, M.; Borch, T.; et al. Watershed-Scale Impacts from Surface Water Disposal of Oil and Gas Wastewater in Western Pennsylvania. Environ. Sci. Technol. 2017, 51 (15), 8851−8860. https://doi.org/10.1021/acs.est.7b01696.

Appendix D

Supporting Information for Chapter 5

D.1 Supporting Figures and Tables

Table D1: Elemental composition of the mixed-cation synthetic brines. The amount of each salt added to 1 L of Distilled-Deionized Water to create the brine at each given TDS concentration.

Salt mass added (g) to create 1 L of mixed-cation synthetic brines				
	50 g/L	**100 g/L**	**200 g/L**	**300 g/L**
NaCl	28.68	57.36	114.71	172.07
$CaCl_2$	10.89	21.78	43.57	65.35
$BaCl_2$	5.45	10.90	21.80	32.70
$MgCl_2$	1.87	3.74	7.48	11.21
$SrCl_2$	3.11	6.22	12.45	18.67

Table D2: Elemental composition of Appalachian oil and gas produced water. [1]

Source		TDS (mg/L)	Cl (mg/L)	Na (mg/L)	Ca (mg/L)	Sr (mg/L)	Ba (mg/L)	^{226}Ra (pCi/L)	^{228}Ra (pCi/L)	228 / 226
Produced Appala-chian Basin	Mean	189,410	112,081	42,987	20,076	782	507	881	1,127	1.28
	Median	186,600	112,572	42,550	17,600	727	230	480	500	1.04
	Count	1,965	1,867	1,800	1,841	1,072	592	95	72	
Produced Marcellus	Mean	91,888	51,714	26,527	7,023	1,449	1,076	3,976	425	0.11
	Median	59,750	34,000	18,000	4,360	953	297	1,042	201	0.19
	Count	110	103	100	129	165	110	31	31	

Table D3: Results of the linear regression of efficiency versus TDS for the NaCl-only synthetic brine and the multi-cation synthetic brine. The TDS-influenced attenuation factor, α_{TDS}, its 95 % CI and p-values at each energy level are presented.

Energy Level (keV)		186	295	351	609	911	1120	1764
Multi-cat-ion	$\alpha_{TDS} \times 10^{-4}$	-2.57	-1.66	-1.46	-0.523	0.0255	-0.3	-0.36
	95%CI $\times 10^{-6}$	2	12	14	8	6	16	30
	p-value	0.025	0.013	0.005	0.011	0.821	0.035	0.098
NaCl-only	$\alpha_{TDS} \times 10^{-4}$	-1.56	-1.27	-1.07	-0.375	-0.177	-0.24	-0.28
	95%CI $\times 10^{-6}$	0	4	10	2	4	16	32
	p-value	0.001	0.002	0.004	0.001	0.132	0.059	0.182

Table D4: Validation of the linear regressions of efficiency against TDS. The empirically calculated efficiency was divided by the efficiency predicted by the regression equation for each energy level and at each TDS level. These are the column values. Then the averages and 95% CI of these values were calculated, shaded in grey. Finally, the averages and 95% CI of all data points at all the energy levels was calculated, bolded and italicized.

	Multi-Cation Synthetic brine					
	TDS (g/L)	**186 keV**	**295 keV**	**351 keV**	**609 keV**	**911 keV**
	0	99%	105%	103%	105%	103%
	50	98%	99%	101%	100%	97%
	100	101%	93%	94%	92%	99%
	200	101%	98%	97%	100%	101%
	300	99%	105%	104%	104%	100%
Ave	***100%***	99.7%	100%	100%	100%	100%
95 CI	***7.01%***	2.4%	10.8%	8.35%	10.1%	5.17%

	NaCl-only Synthetic brine					
	TDS (g/L)	**186 keV**	**295 keV**	**351 keV**	**609 keV**	**911 keV**
	0	101%	101%	103%	102%	103%
	50	101%	100%	98%	99%	98%
	100	99%	99%	98%	99%	100%
	200	101%	97%	98%	99%	99%
	300	100%	103%	103%	102%	102%
Ave	***100%***	100%	100%	100%	100%	100%
95 CI	***2.85%***	1.62%	4.68%	5.22%	3.15%	4.18%

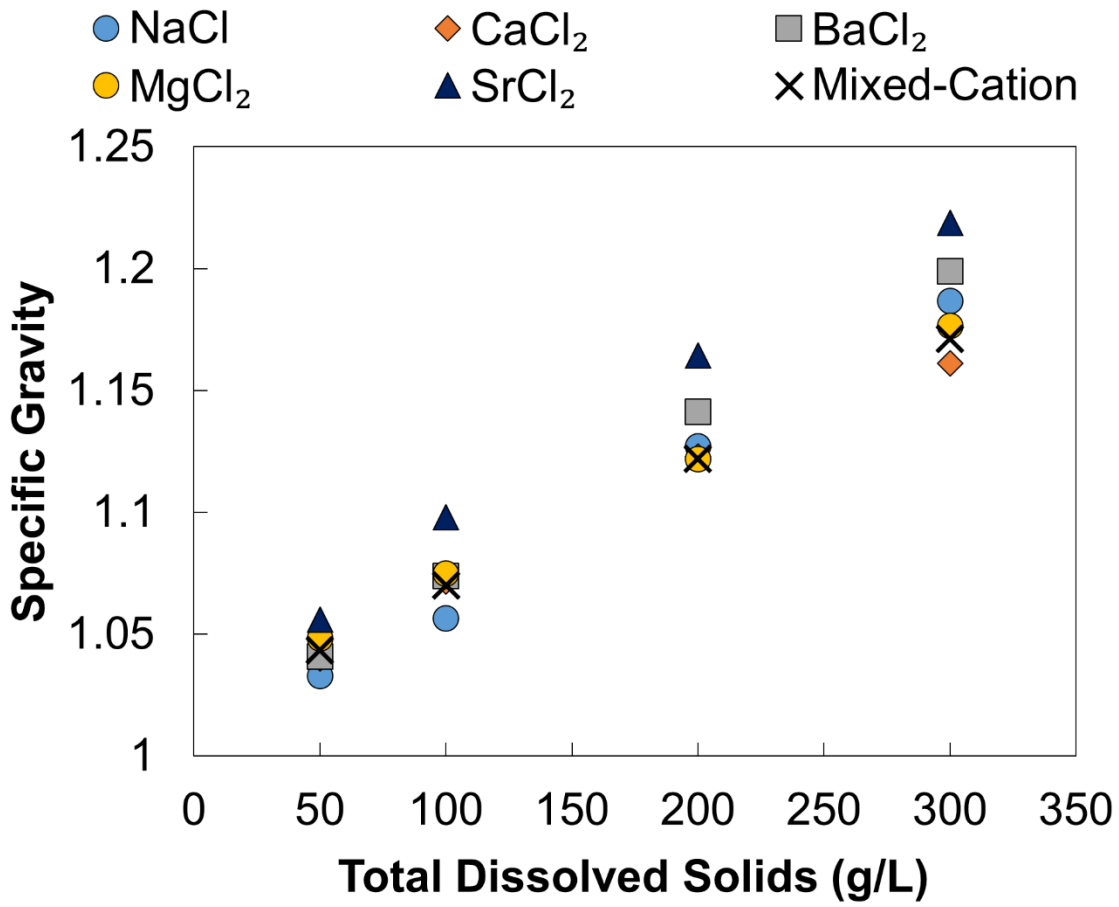

Figure D1: The TDS and specific gravities of NaCl, $CaCl_2$, $BaCl_2$, $MgCl_2$, $SrCl_2$, and mixed Na-Ca-Mg-Sr-Cl brine solutions.

D.2 Calculating the attenuation factor by the theoretical approach of Appleby *et al.* 1992 [2] and Hubbell 1981 [3]

Appleby *et al.* in their paper put forth a theoretical model to calculate the self-adsorption factor for a well-detector γ-spec. In their paper, they introduce a geometric parameter, k shown in Eq. (D1) and (D2), which characterizes the dimensions of the well detector/sample holder. This parameter was defined theoretically and then determined empirically. For a gamma ray beam of incident intensity I_0, they derive the attenuation factor I/I_0, as being dependent on sample mass and the mass attenuation coefficient, μ. The mass attenuation coefficients can be obtained from Hubbell' s work, provided the exact elemental composition of the sample is known.

Herein, we attempt to derive the attenuation coefficient for the 300 g/L mixed-cation synthetic brine based on the theoretical work of Appleby and Hubbell.

$$k_t = \frac{1}{\lambda \pi a L} \tag{D.1}$$

$$k_e = \frac{0.133}{a^2}(\lambda L/a)^{-0.687} \tag{D.2}$$

$$0 < \lambda \leq 1 \tag{D.3}$$

$$\frac{I}{I_0} = f(m) \begin{cases} e^{-k\mu m} & \text{for} \quad k\mu m < 0.28 \\ \left(1 + \frac{(k\mu m)^2}{4}\right) e^{-k\mu m} & \text{for} \quad 0.28 < k\mu m < 1.15 \end{cases} \tag{D.4}$$

Where,

k_t is the theoretical derivation for the geometric parameter

k_e is the empirical derivation for the geometric parameter

λ describes the depth to which the sample holder has been filled

a is the radius of the sample holder

L is the depth of the sample holder

μ is the mass attenuation coefficient

m is the sample mass

Table D5: The dimensional characteristics of our well detector and the geometric parameter based on theoretical or empirical relationships of Eq. (D.1) & Eq. (D.2).

Parameter	**Value**	k_t	k_e
a	1.675 cm	0.0469	0.0258
L	4.05 cm		
λ	1		

Table D6: The sample mass attenuation factor, μm, for the 300 g/L mixed-cation synthetic brine at 150 keV and at 200 keV.

Element	m	μ **(cm²/g)**		μm **(cm²)**	
	grams	150 keV	200 keV	150 keV	200 keV
Na	1.45	*0.1335*	*0.1199*	*0.193*	*0.174*
Ba	0.0356	*0.7827*	*0.4045*	*0.0279*	*0.0144*
Mg	0.103	*0.1393*	*0.1245*	*0.0143*	*0.0128*
Ca	0.877	*0.1671*	*0.1374*	*0.147*	*0.1205*
Sr (Br*)	0.113	*0.2889**	*0.1834**	*0.0325*	*0.0207*
K	0.0129	*0.1579*	*0.1318*	*0.00204*	*0.00170*
Cl	4.42	*0.1479*	*0.1265*	*0.655*	*0.560*
H_20	20.4	*0.1504*	*0.1370*	*3.07*	*2.79*
Plastic Container	8.5	*0.1534*	*0.1401*	*1.304*	*1.191*
			Total	***4.14***	***3.70***

*Sr data was not provided. Bromine data was used instead as it was the closest atomic number.

Table D7: The self-adsorption factor at 150 keV and 200 keV for the 300 g/L mixed-cation synthetic brine calculated for the theoretical and empirical derivations of the geometric parameter. The empirical derivations predicted $9 - 10\%$ attenuation while the theoretical derivation predicted $20 - 22$ % attenuation in the $150 - 200$ keV range. Our TDS-influenced attenuation factor predicted ~23 % at 186 keV, placing it within range of the empirical values.

	$k\mu m$		I/I_0		$(1 - I/I_0)\%$	
	150 keV	200 keV	150 keV	200 keV	150 keV	200 keV
k_t	*0.254*	*0.228*	*0.776*	*0.796*	**22%**	**20%**
k_e	*0.140*	*0.1256*	*0.870*	*0.882*	**13%**	**12%**

D.3 References

(1) Geeza, T. J.; Gillikin, D. P.; McDevitt, B.; Van Sice, K.; Warner, N. R. Accumulation of Marcellus Formation Oil and Gas Wastewater Metals in Freshwater Mussel Shells. Environ. Sci. Technol. 2018, 52 (18), 10883–10892.

(2) Appleby, P. G.; Richardson, N.; Nolan, P. J. Self-Absorption Corrections for Well-Type Germanium Detectors. Nucl. Instruments Methods Phys. Res. Sect. B Beam Interact. with Mater. Atoms 1992, 71 (2), 228–233. https://doi.org/10.1016/0168-583X(92)95328-O.

(3) Hubbell, J. H. Photon Mass Attenuation and Energy-Absorption Coefficients. Int. J. Appl. Radiat. Isot. 1982, 33 (11), 1269–1290. https://doi.org/10.1016/0020-708X(82)90248-4.

Appendix E

Supporting Information for Chapter 6

E.1 Supporting Figures and Tables

Table E1: Radium-226 and radium-228 decay chains showing half-lives, alpha and beta decay energy. [1]

Parent	Daughter	Half life	Alpha Decay Energy (keV)	Beta Decay Energy (keV)
226 Radium	222 Radon	1602 y	4784	-
222 Radon	218 Polonium	3.8 d	5489	-
218 Polonium	214 lead	3.1 min	6002	-
214 Lead	214 Bismuth	26.8min	-	1030
214 Bismuth	214 Polonium	20 min	-	3270
214 Polonium	210 Lead	0.1643 sec	7686	-
210 Lead	210 Bismuth	22.3 y	-	63.49
210 Bismuth	210 Polonium	5d	-	1161
210 Polonium	206 Lead	138 d	5304	-
228 Radium	228 Actinium	5.75 y	-	10.04
228 Actinium	228 Thorium	6.15 h	-	609.7, 385
228 Thorium	224 Radium	1.9116 y	5423, 5340	-
224 Radium	220 Radon	3.6319 d	5685	-
220 Radon	216 Polonium	55.6 s	6288	-
216 Polonium	212 Lead	0.145 s	6778	-
212 Lead	212 Bismuth	10.64 h	-	171.7, 93.5
212 Bismuth	212 Polonium	60.55 m	6050	834
(64.06%) 212 Polonium	208 Lead	0.299 s	8784	-
(35.94%) 208 Thallium	208 Lead	3.053 m	-	649

Table E2: Elemental composition of the mixed-cation synthetic brines. The amount of each salt added to 1 L of distilled-deionized water to create the brine at each given TDS concentration.

Salt mass added (g) to create 1 L of mixed-cation synthetic brines				
	50 g/L	**100 g/L**	**200 g/L**	**300 g/L**
NaCl	28.68	57.36	114.71	172.07
$CaCl_2$	10.89	21.78	43.57	65.35
$BaCl_2$	5.45	10.90	21.80	32.70
$MgCl_2$	1.87	3.74	7.48	11.21
$SrCl_2$	3.11	6.22	12.45	18.67

Table E3: Volume of nitromethane added in to 0 g/L synthetic brine and quench factor for each quench level (tSIE). [2]

Quench Level	**Volume Added (mL)**	**tSIE**
1	0	239
2	5	219
3	10	229
4	15	203
5	26	189
6	45	179
7	70	146
8	110	120
9	150	100
10	230	74

Table E4: Sample volumes, dosed ^{226}Ra activities, sample chemistries, quench level, and ^{226}Ra efficiencies for the synthetic multi-cation brines employed in both methods of liquid scintillation counting analysis.

																					QuantaSmart		Peakfit	
Method	Sample	Sample Volume (mL)	Cocktail Volume (mL)	Total Vial Volume (mL)	Radium activity (pCi/L)	Ra-226 Added (pCi)	Expected alpha activity (dpm)	R	R'	SG	TDS	IS	R * SG	R' * SG	R * TDS	R' * TDS	R * IS	R' * IS	Av. tSIE	**Radium Efficiency**	**95% CI**	**Radium Efficiency**	**95% CI**
Field	0 g/L	4	10	14	5	20.0	44.40	0.4	0.286	1.003	0	0.20	0.40	0.29	0	0	0.08	0.06	350.0	*98.8%*	*2.4%*	*88.1%*	*4.7%*
	50 g/L	4	10	14	4.871	19.5	43.25	0.4	0.286	1.041	50	0.85	0.42	0.30	20	14.3	0.34	0.24	347.4	*84.6%*	*2.7%*	*87.0%*	*5.8%*
	100 g/L	4	10	14	5.065	20.3	44.98	0.4	0.286	1.054	100	1.75	0.42	0.30	40	28.6	0.70	0.50	384.0	*84.5%*	*2.6%*	*85.0%*	*6.0%*
	200 g/L	4	10	14	4.87	19.5	43.25	0.4	0.286	1.115	200	3.65	0.45	0.32	80	57.1	1.46	1.04	419.1	*66.1%*	*3.4%*	*76.4%*	*6.9%*
	300 g/L	4	10	14	4.87	19.5	43.25	0.4	0.286	1.167	300	5.73	0.47	0.33	120	85.7	2.29	1.64	398.5	*62.8%*	*3.5%*	*72.8%*	*6.6%*
Lab	0 g/L	10	10	20	5	50.0	111	1	0.500	1.003	0	0.20	1.00	0.50	0	0	0.20	0.10	247.2	*66.1%*	*1.9%*	*66.0%*	*3.5%*
	50 g/L	5.5	14.5	20	4.871	26.8	59.47	0.379	0.275	1.041	50	0.85	0.40	0.29	19	13.8	0.32	0.23	364.2	*82.8%*	*2.4%*	*89.4%*	*5.2%*
	100 g/L	5	15	20	5.065	25.3	56.22	0.333	0.250	1.054	100	1.75	0.35	0.26	33	25.0	0.58	0.44	379.7	*81.1%*	*2.5%*	*88.0%*	*6.3%*
	200 g/L	4	16	20	4.87	19.5	43.25	0.250	0.200	1.115	200	3.65	0.28	0.22	50	40.0	0.91	0.73	416.3	*76.3%*	*3.2%*	*91.0%*	*8.4%*
	300 g/L	3.5	16.5	20	4.87	17.0	37.84	0.212	0.175	1.167	300	5.73	0.25	0.20	64	52.5	1.22	1.00	426.2	*64.9%*	*4.4%*	*98.3%*	*9.7%*

KEY: R – ratio of sample volume to cocktail volume, R´ - ratio of sample volume to total volume, SG – specific gravity, TDS – total dissolved solids, and IS – ionic strength

Table E5: Radium-226 activities determined by liquid scintillation counting for both the Field and Lab Methods with 95% CI uncertainties following data analysis by multi-Gaussian analysis (Peakfit) or instrument reported data (QuantaSmart). For each sample preparation protocol and data analysis method, ^{226}Ra efficiencies were determined by the data transformations illustrated in Figure S4. 95% CI uncertainties are the combined uncertainties.

								Field Method - Peakfit				Field Method - QuantaSmart				Lab Method - Peakfit				Lab Method - QuantaSmart			
COD (mg/L)	Weight	Sample	S.G	Measured TDS	Measured IS	Ra-226 gamma (pCi/L)	% error 186 keV	F_SG_PF	F_TDS_PF	F_IS_PF	95% CI_F_PF	F_SG_QS	F_TDS_QS	F_IS_QS	95% CI_F_QS	L_R'*TDS_PF	L_R*IS_PF	L_R'*IS_PF	95% CI_L_PF	L_SG_QS	L_TDS_QS	L_IS_QS	95% CI_L_QS
7575	0.01183	#1	1.061	94	1.645	11451	2.47	*4414*	*4410*	*4369*	8.8%	*4464*	*4654*	*4716*	4.7%	*4697*	*4600*	*4594*	8.4%	*4303*	*4315*	*4297*	4.2%
9105	0.00184	#2	1.079	119	1.845	14550	2.26	*5314*	*5290*	*5184*	8.9%	*6144*	*6411*	*6279*	4.4%	*6246*	*6081*	*6075*	8.7%	*5689*	*5698*	*5621*	4.1%
5775	0.01183	#3	1.093	159	2.713	12133	2.28	*4946*	*4979*	*4887*	9.5%	*5470*	*5926*	*5666*	4.8%	*5598*	*5364*	*5372*	9.8%	*5571*	*5657*	*5545*	4.2%
7500	0.00617	#4	1.130	197	3.174	22718	1.98	*7673*	*7575*	*7348*	9.6%	*9295*	*9710*	*8809*	4.2%	*9693*	*9320*	*9310*	9.4%	*12236*	*12054*	*11528*	3.7%
12600	0.00222	#5	1.163	221.2	4.145	11789	2.57	*4916*	*4721*	*4663*	10.1%	*6782*	*6648*	*5990*	4.7%	*5629*	*5227*	*5249*	10.2%	*7872*	*7209*	*7013*	4.1%
7710	0.00125	#6	1.160	224.2	4.151	3980	4.97	*1133*	*1096*	*1081*	11.2%	ND	ND	ND	3.7%	*1645*	*1530*	*1536*	13.1%	ND	ND	ND	3.3%
11505	0.00022	#7	1.159	227.2	3.903	17237	1.93	*6647*	*6452*	*6283*	10.1%	*8874*	*8932*	*7877*	4.4%	*6576*	*6214*	*6229*	10.3%	*8487*	*7972*	*7570*	4.2%
13605	0.00034	#8	1.094	160	2.941	9445	3.54	*3922*	*3947*	*3904*	9.7%	*5035*	*5455*	*5267*	4.7%	*4725*	*4487*	*4502*	9.6%	*5421*	*5504*	*5438*	4.0%
13665	0.00054	#9	1.093	170	2.686	8653	4.2	*4116*	*4179*	*4064*	8.9%	*5036*	*5582*	*5213*	4.4%	*5750*	*5562*	*5552*	10.3%	*6062*	*6227*	*6030*	4.1%

KEY: F – Field Method, PF – Peakfit (i.e. multi-Gaussian analysis), QS – QuantaSmart (i.e. instrument reported data), L – Lab Method, SG – specific gravity, TDS – total dissolved solids, IS – ionic strength, R – ratio of sample volume to cocktail volume, and R´ - ratio of sample volume to total volume.

Table E6: Ingrowth multiplier when appraising ^{226}Ra by alpha spectrometry following radium separation by $BaSO_4$ co-precipitation. [3]

Hours since separation	Ingrowth multiplier
0	1.00
1	1.02
2	1.04
3	1.06
6	1.12
24	1.49

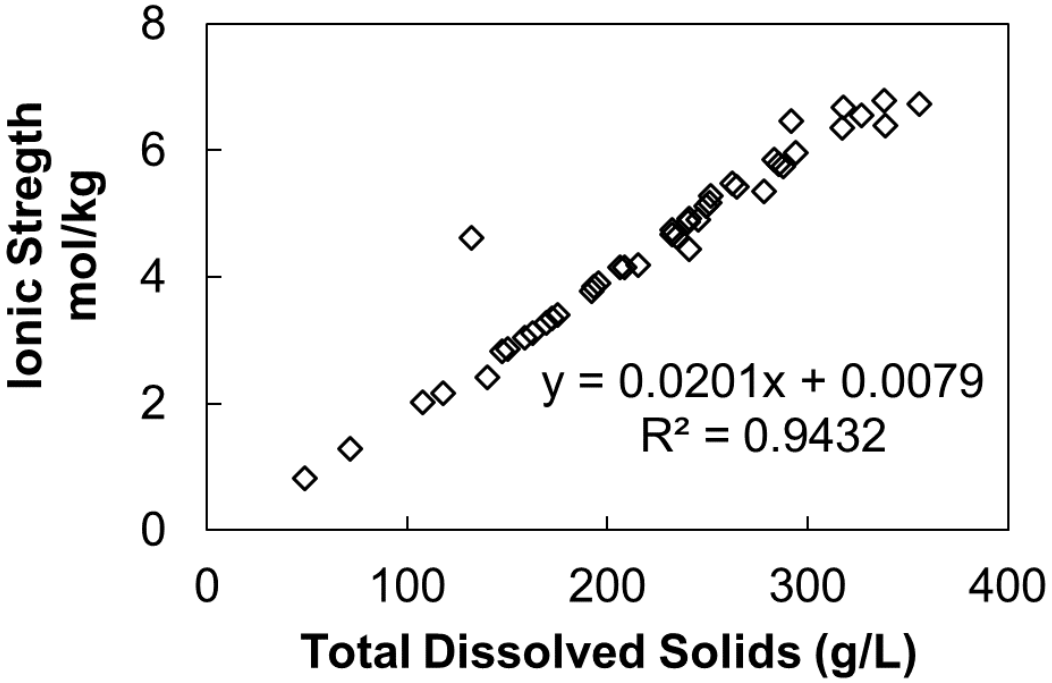

Figure E1: Linear regression of total dissolved solids (g/L) versus ionic strength (mol/kg) from forty Appalachian Basin produced waters.

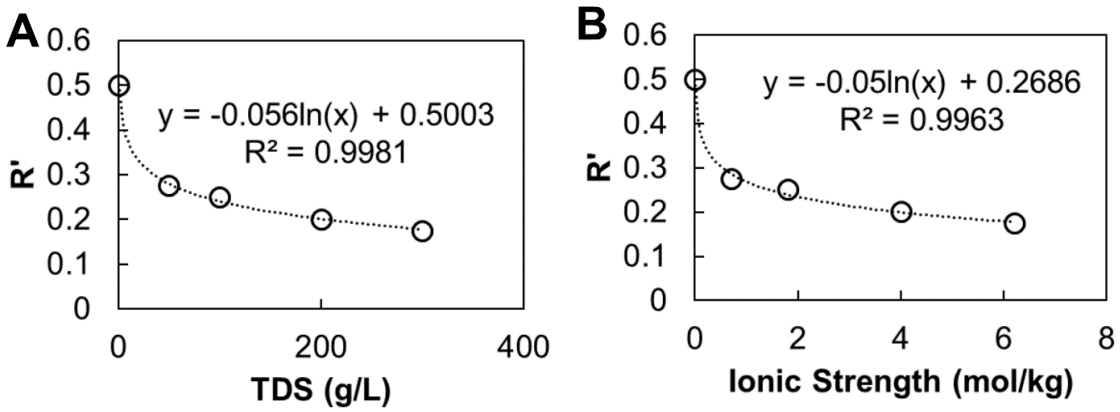

Figure E2: Ratio of sample volume to total volume (R´) plotted against the total dissolved solids (g/L) (panel **A**) and ionic strength (mol/kg) (panel **B**) for the optimal sample-cocktail compatibility and stability (i.e. the Lab Method).

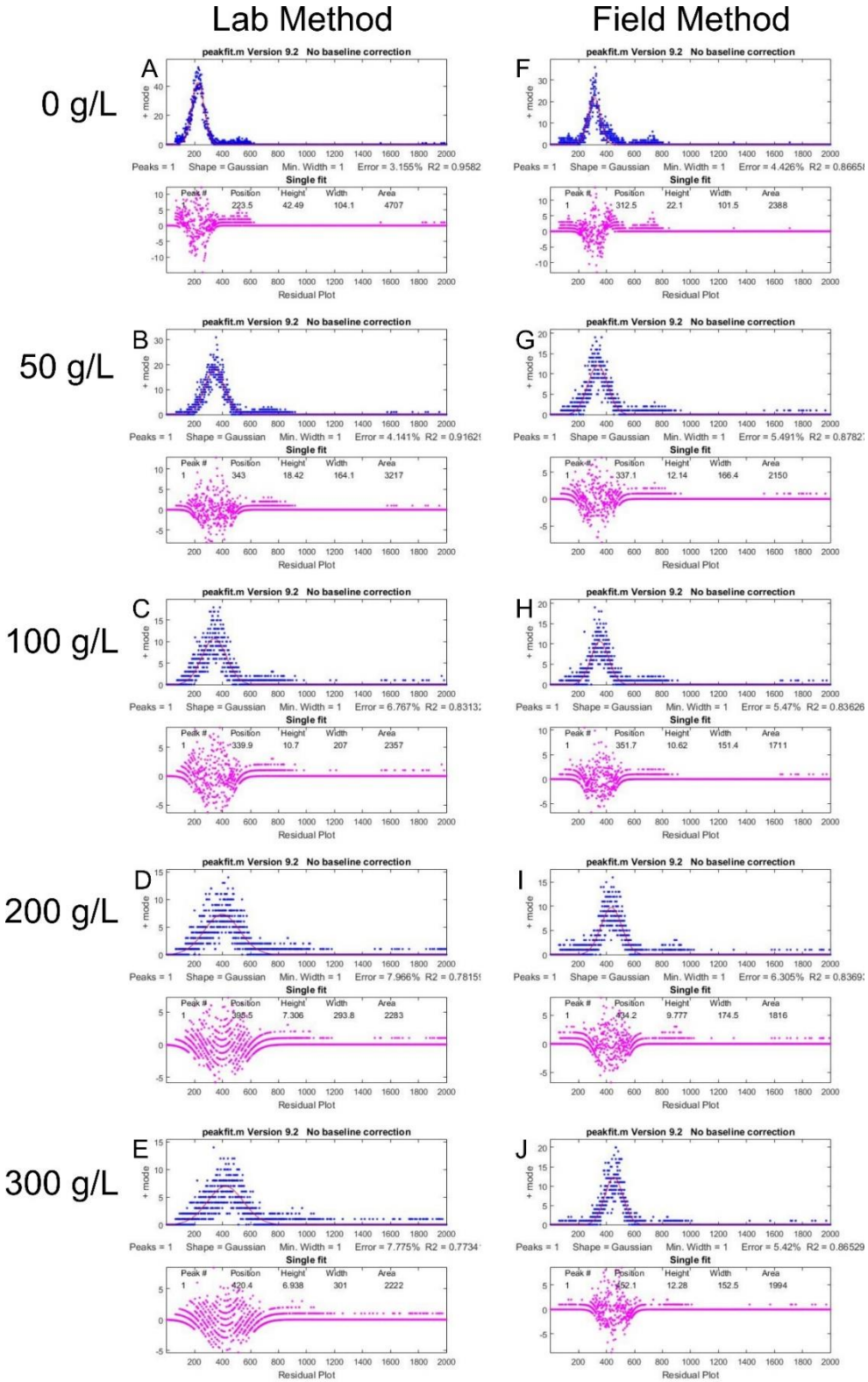

Figure E3: Fitted Gaussian spectra for the mixed-cation radium-dosed brines for the Lab Method (left, **A - E**) and the Field Method (right, **F - J**).

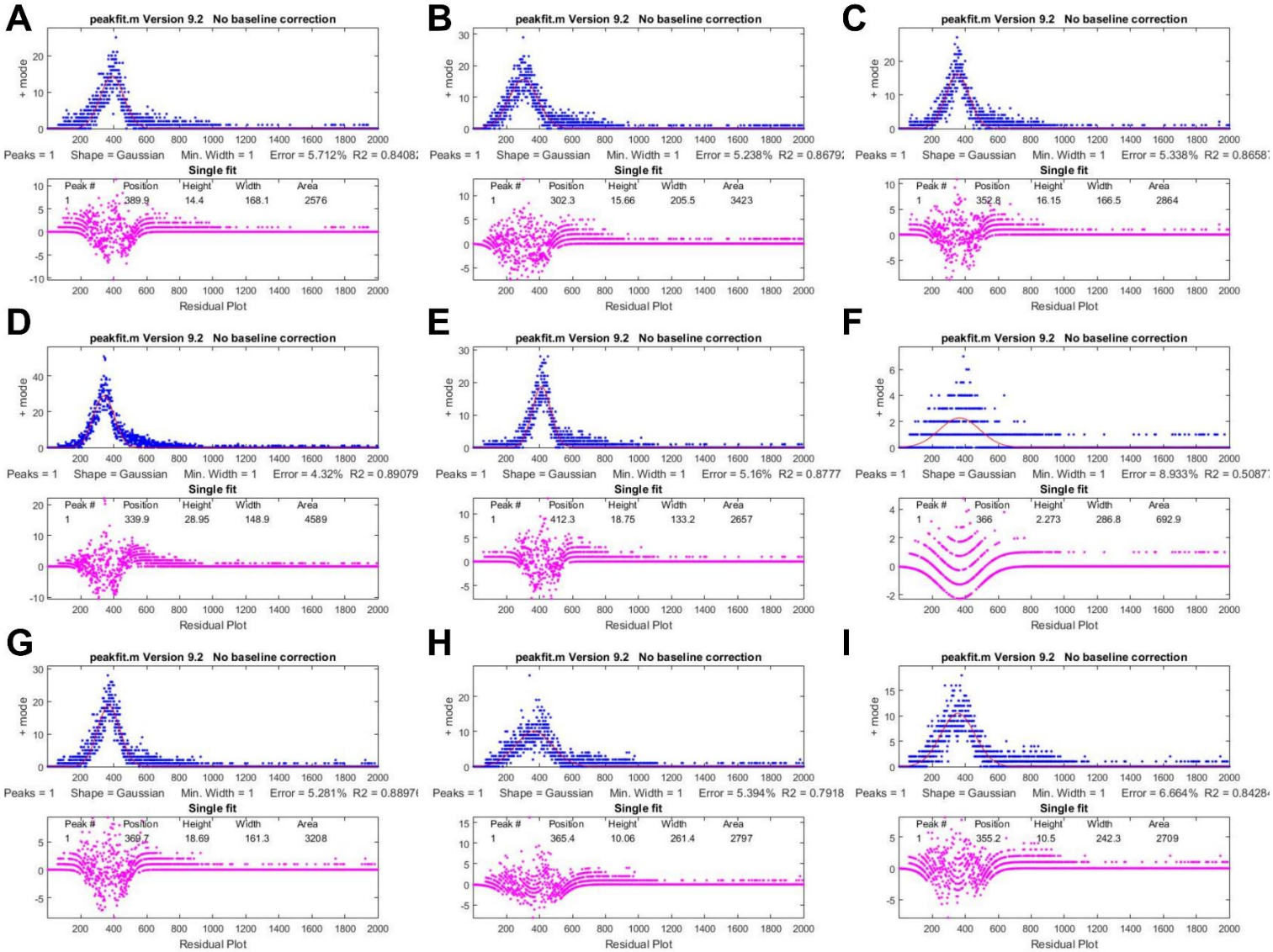

Figure E4: Fitted Gaussian spectra for the nine Marcellus brines for the Lab Method.

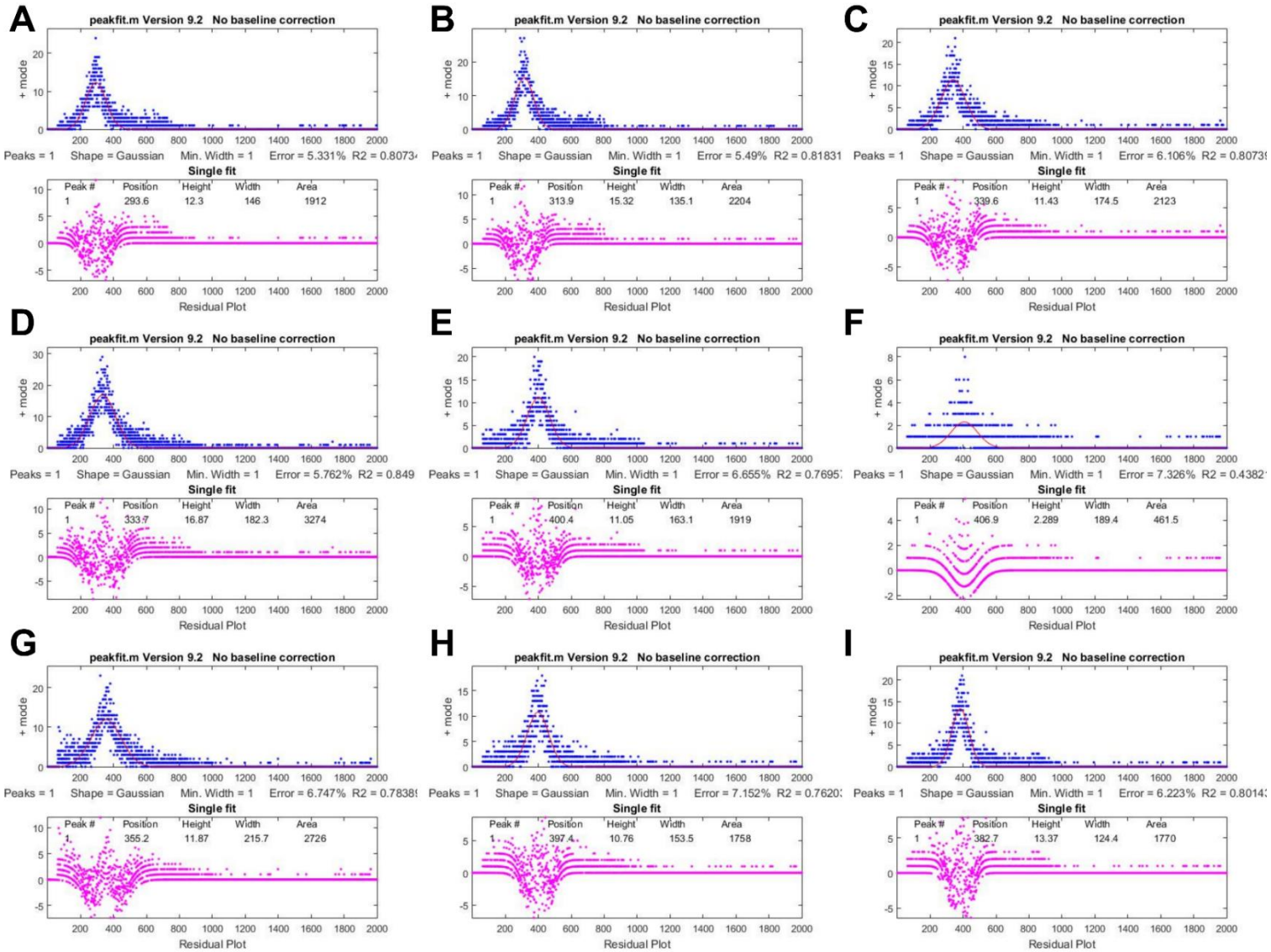

Figure E5: Fitted Gaussian spectra for the nine Marcellus brines for the Field Method.

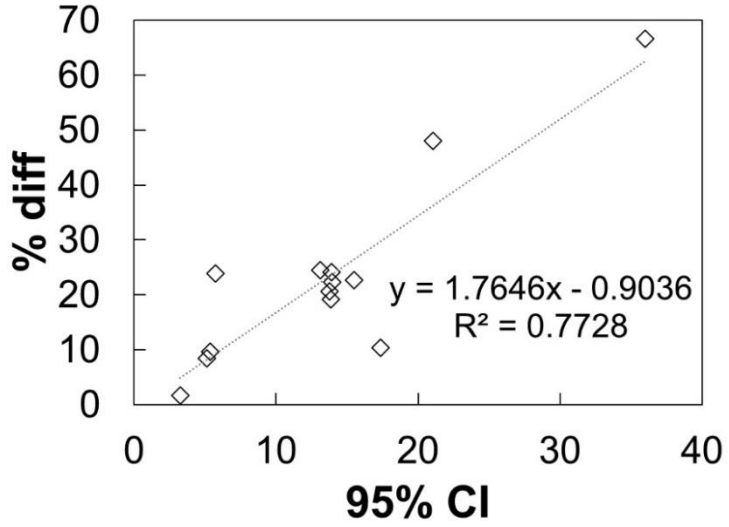

Figure E6: The difference between the counts per minute reported by QuantaSmart and the multi-Gaussian analysis with Peakfit against the 95% confidence interval (CI) uncertainties reported by QuantaSmart. Data with greater uncertainties showed a bigger difference between the counts determined by the two methods.

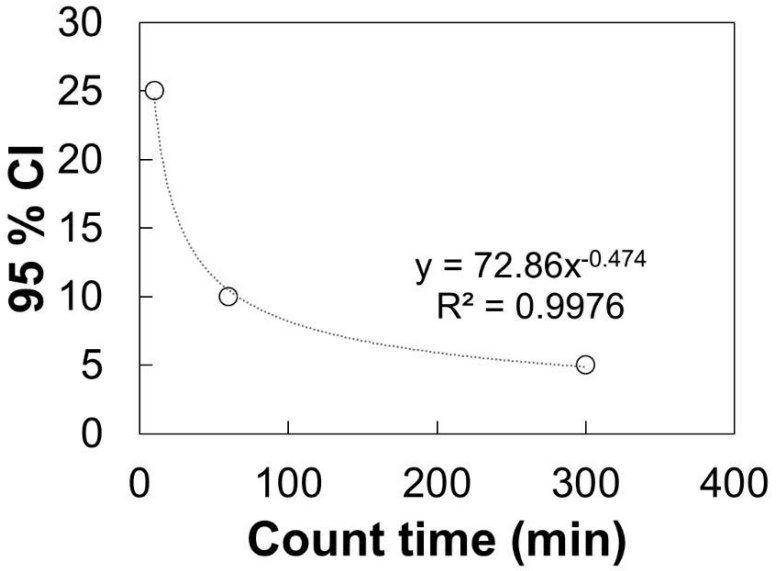

Figure E7: The count time for liquid scintillation counting versus the 95% confidence interval. Longer counting time resulted in lower uncertainty.

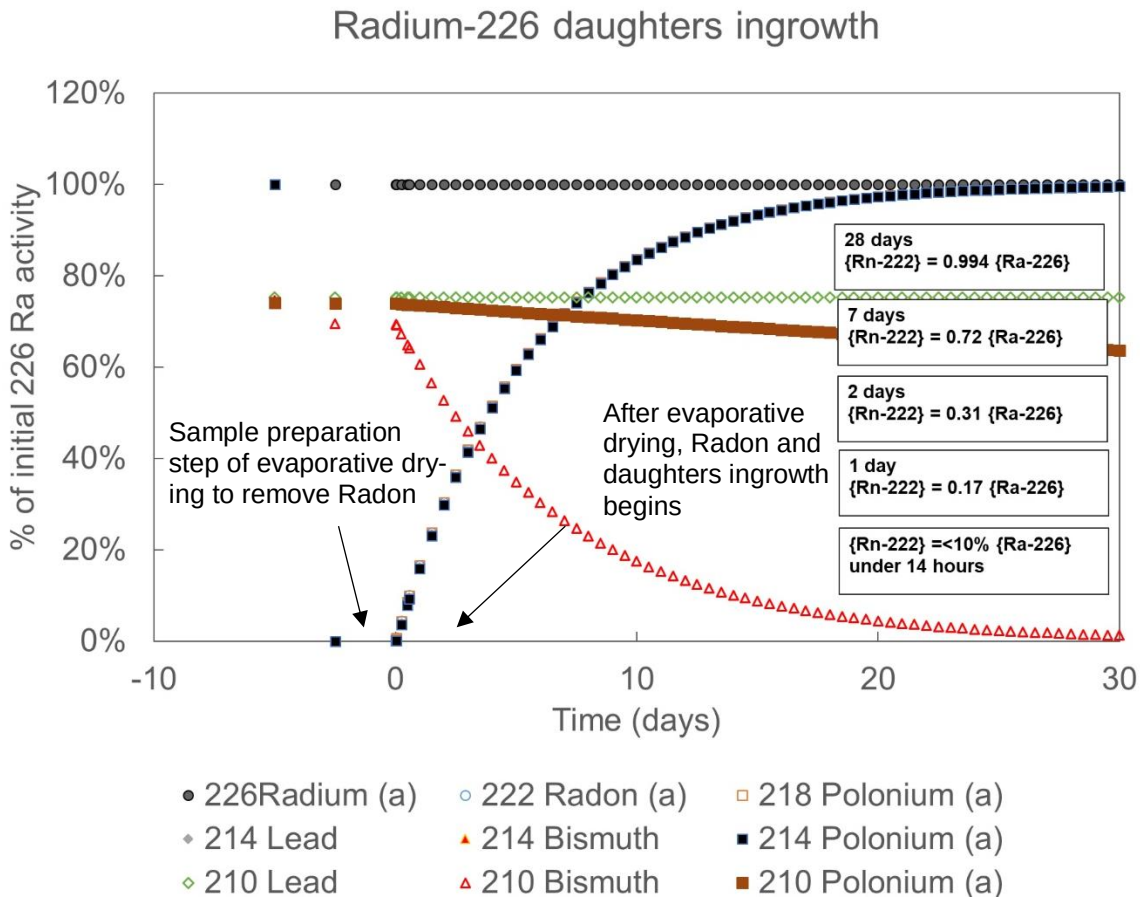

Figure E8: Radium-226 and the ingrowth of its daughters following the evaporative sample preparation for liquid scintillation counting. Daughter ingrowth calculated using the Bateman equations [4]. The ^{226}Ra standard had a reference date of 4/27/1975, providing enough time for the ingrowth of ^{210}Pb (green diamond), ^{210}Bi (red triangle) and ^{210}Po (brown square).

E.2 References

(1) National Nuclear Data Center. NuDat 2.7. Brookhaven National Lab: Upton.

(2) Thomson, J. *Sample Preparation Techniques for Liquid Scintillation Analysis*, Third Edit.; Elsevier, 2013. https://doi.org/10.1016/B978-0-12-384873-4.00008-6.

(3) United States Environmental Protection Agency. *Method 903.0: Alpha-Emitting Radium Isotopes in Drinking Water*; 1980.

(4) Bateman, H. The Solution of a System of Differential Equations Occuring in the Theory of Radio-Acive Transformations. *Cambridge Pilos. Soc.* 1910, *15* (1908– 10), 423– 42.

VITA

Moses A. Ajemigbitse

EDUCATION

Ph.D., Environmental Engineering
Department of Civil and Environmental Engineering
Pennsylvania State University, University Park PA
August 2014 – August 2019

B.S., Petroleum and Natural Gas Engineering
Department of Petroleum and Natural Gas Engineering
West Virginia University, Morgantown WV
August 2010 – May 2014

PUBLICATIONS

Ajemigbitse MA, Cannon FS, Klima M, Furness JC, and Warner NR. **2019**. "Raw Material Recovery from Oil and Gas Residual Waste with Implications for Sustainability and Radioactive Waste Disposal." *Environ Sci.: Processes Impacts.* 21(2), 308-323.

Zhang XYS, **Ajemigbitse MA**, Cannon FS, Hooper AE, Allara DL, Paulsen PD, and Furness JC. **2018**. "Hydrogen Peroxide-Generated Gases at Asphalt-Glass Interface: Effect on Surface Cleaning and Analysis by Nanoscale Surface Imaging Spectroscopy". *Environ Eng Sci.*, 35(4), 300-310.

Ouyang B, Renock DJ, **Ajemigbitse MA**, Van Sice K, Warner NR, Landis JD, and Feng X. **2019**. "Radium in hydraulic fracturing wastewater: distribution in suspended solids and implications to its treatment by sulfate co-precipitation". *Environ Sci.: Processes Impacts,* 21(2), 339-351.

Tasker TL, Burgos WD, **Ajemigbitse MA,** Lauer NE, Gusa A, Kuatbek M, May D, Landis JD, Alessi DS, Johnsen AM, Kaste J, Headrick K, Wilke FDH, McNeal M, Engle M, Jubb A, Vidic R, Vengosh A, and Warner NR. **2019**. "Accuracy of methods for reporting inorganic element concentrations and radioactivity in oil and gas wastewaters from the Appalachian Basin, U.S based on an inter-lab comparison." *Environ Sci.: Processes Impacts,* 21(2), 224-241.

McDevitt B, McLauglin M, Cravotta III C, **Ajemigbitse MA**, Van Sice KL, Blotevogel J, Borch T, Warner NR. **2019**. "Radium Accumulation in Carbonate River Sediments at Oil and Gas Produced Water Discharges: Implications for Beneficial Use as Disposal Management."*Environ Sci.: Processes Impacts,* 21(2), 324-338.

AWARDS

Alumni Dissertation Award and Distinguished Doctoral Scholar Medal	**2019**
Chevron Corporation Scholarship in Environmental Engineering	**2018 & 2019**